RECONFIGURABLE LASER MICRO-PROCESSING SYSTEMS: DEVELOPMENT OF GENERIC SYSTEM-LEVEL TOOLS FOR IMPLEMENTING MODULAR LASER MICRO-MANUFACTORING PLATFORMS

by

PAVEL NEDYALKOV PENCHEV

A thesis submitted to
The University of Birmingham
for the degree of
DOCTOR OF PHILOSOPHY

School of Engineering
Department of Mechanical Engineering
University of Birmingham
February 2016

UNIVERSITYOF
BIRMINGHAM

University of Birmingham Research Archive

e-theses repository

ABSTRACT

Laser micromachining (LMM) is an attractive manufacturing technology for the fabrication of a wide range of micro-components due to its intrinsic processing attributes for : (i) non-contact machining that can be used to structure/process a wide range of materials; (ii) producing complex free-form (3D) structures that incorporate multi-length scale features with complex geometrical designs; and (ii) in-situ selective functionalization of free-form surfaces. In addition, LMM can be integrated in hybrid manufacturing platforms and/or process chains and thus to combine LMM with other complementary processes for the cost effective fabrication of a broader range of miniaturised products for various industrial sectors, e.g. micro-electromechanical systems, micro-sensor systems, microelectronics, smart communication systems and biomedical devices. Nevertheless, the broader industrial uptake of LMM both as standalone fabrication solutions and also as a constituent processing technology in hybrid manufacturing routes and process chains is still to come due to system-level issues in designing and implementing LMM systems, which affect adversely the LMM process predictability and reliability.

In this context, the research reported in this thesis aims at improving the system-level performance of reconfigurable LMM platforms and thus to create the necessary pre-requisites for achieving a much better machining accuracy, repeatability and reproducibility (ARR) in different processing configurations. First, a systematic approach for assessing and characterizing the manufacturing capabilities of LMM platforms in terms of machining accuracy, repeatability and reproducibility (ARR) is proposed and thus to quantify the contributions of their key component technologies towards the resulting overall machining performance. The results from the quantitative evaluations of the ARR capabilities of LMM systems' key component technologies imply that state-of-art LMM systems do not have the technology maturity level of well-established micromachining processes, e.g. milling, and thus further system-level developments are required in order to improve the overall machining ARR of LMM platforms, especially when optical axes are employed during the laser processing operations.

Motivated by the results of the systematic quantitative study, the development of generic integration tools for improving the system-level performance of reconfigurable LMM

platforms in terms of manufacturing flexibility and reliability both as stand-alone machine tool configurations and also as component technologies in multi-process manufacturing solutions is presented. In particular, the research presents two generic integration tools: (i) a modular workpiece holding device that allows different LMM configurations to be realised, e.g. the machining of complex prismatic and axis-symmetric parts, while delivering positional ARR better than +/- 1 μm, respectively and (ii) an automated workpiece setting up routine that can be applied for the LMM of complex free-from parts without the use of datum marks, while delivering alignment ARR better than +/- 4 μm, respectively.

Next, generic software tools are developed and validated for improving the manufacturing capabilities of LMM systems for realizing complex multi-axis laser processing strategies with a closed-loop manufacturing control and thus to produce multi length-scale functional features with the required level of ARR. More specifically, the research presents two generic software tools, which can substantially improve the manufacturing capabilities of reconfigurable LMM systems in terms of machining throughput and complexity of the laser manufacturing operations. The two generic software solutions are: (i) a software tool to counteract the negative dynamic effects of optical scanning head systems and thus to improve significantly the laser machining accuracy, quality and efficiency of LMM platforms and (ii) an automated strategy for multi-axis LMM with rotary stages for performing demanding complex machining routines with machining ARR better than +/- 6.5 μm, respectively. The achieved manufacturing improvements with the developed software tools are achieved by implementing ''adaptive'' postprocessors as stand-alone software solutions and thus users can benefit from the two software tools regardless of their knowledge and experience with any given LMM systems.

Finally, the research demonstrates that the utilization of the developed tools and techniques leads to improved system-level machining performance of LMM systems in terms of manufacturing flexibility, robustness, operability and reliability and thus they create sufficient laser processing capabilities for the fabrication of miniaturised products with complex geometrical designs and multi-length scale functional features, e.g. Terahertz technology devices.

ACKNOWLEDGEMENTS

I would like to express my sincere gratitude to my supervisor, Prof. Stefan S. Dimov for accepting me as his PhD student and for his invaluable guidance and supervision throughout this study.

Also, I would like to thank my second supervisor, Dr Sein Leung Soo, for his valued support during my research.

I would also like to thank, Dr Xiaobang Shang, Dr Debajyoti Bhaduri, Prof. Michael J. Lancaster and Mr Pooria Ghavam for their assistance and constructive advice in the course of my postgraduate studies.

I am also grateful to the University of Birmingham for providing me with the opportunity and financial support to pursue my postgraduate studies.

My deepest gratitude goes to my family, especially to my mother Darina and to my girlfriend, Jeni for their constant support, encouragement and love.

TABLE OF CONTENTS

LIST OF FIGURES

LIST OF TABLES

ABBREVIATIONS

Abbreviations

1D	One dimensional
2D	Two dimensional
3D	Three dimensional
AM	Additive manufacturing
ARR	Accuracy, repeatability and reproducibility
BCS	Laser Beam coordinate system
CAD	Computer aided design
CAM	Computer aided manufacturing
CL	Cutter location
CNC	Computer numerical control
CST MWS	Computer Simulation Technology Microwave Studio
CW	continuous wave
DC	Direct current
DFM	Design focusing module
DM	Design for manufacture
DoE	Design of experiment
DoF	Depth of focus
DRIE	Deep Reactive Ion Etching
EDM	Electrical discharge machining
FCS	Focus variation probe coordinate system
FV	Focus variation
IR	Infrared
GUI	Graphical user interface
HAZ	Heat affected zone
HCS	Workpiece Holding device coordinate system
HALAR	High accuracy linear and rotary
IF	Infinite focus
ISO	International organization for standardization
LIGA	German acronym for Lithography, Electroplating and Moulding
LIPSS	Laser induced periodic surface structures
LMM	Laser micromachining
MCS	Machine tool coordinate system
MEMS	Microelectromechanical system
MMP	Micro manufacturing process

MOPA	Master Oscillation power amplifier
MRR	Material removal rate
NC	Numerical control
PID	Proportional integral derivative
PMMA	Polymethyl methacrylate
PP	Polypropylene
PSO	Position synchronized output
RPM	revolutions per minute
SEM	Scanning Electron Microscopy
THz	Terahertz
WCS	Workpiece coordinate system

NOMENCLATURES

Symbol	Parameter definition	Units
$\%_{PO}$	Pulse overlap Percentage	%
λ	Laser wavelength	nm
E	Laser pulse energy	J
D_0	Input beam diameter to the focusing lens	mm
f	Laser pulse frequency/repetition rate	Hz
F	Fluence/ Energy density	J/cm^2
F_0	Peak fluence	J/cm^2
F_{th}	Abalation threshold fluence	J/cm^2
F_r	Fluence at a distance r from the laser beam centre	J/cm^2
FL	Focal length of the focusing lens	mm
k	Uncertainty coverage factor	%
M^2	Beam quality factor	-
N	Number of incident laser pulses	-
P	Average power	W
P_{peak}	Peak power	W
r	Distance from the laser beam centre	mm
R_a	Profile surface roughness parameter	µm
S	Material incubation coefficient	-
S_a	Areal surface roughness parameter	µm
sd	Standard deviation	µm
τ	Laser pulse duration	fs/ps/ns
U_A	Type A uncertainty	µm
U_B	Type B uncertainty	µm
U_C	Combined uncertainty	µm
U_T	Total uncertainty	µm
V_{scan}	Scanning speed	mm/s
w_0	Laser beam spot radius at the focal plane	µm
w_z	Laser beam diameter at any plane along the axis of the laser beam propagation	µm
z	Distance from the focal plane along laser propagation axis	mm
z_R	Rayleigh length	mm

LIST OF PUBLICATIONS

Journal Publications (Published)

1. Bhaduri D, **Penchev P**, Dimov S and Soo SL. Investigation of accuracy, repeatability and reproducibility of laser micromachining platforms. *Measurement*, published online: March 2016, DOI: 10.1016/j.measurement.2016.03.033.
2. **Penchev P**, Shang X, Dimov S and Lancaster M. Novel manufacturing route for scale up production of Terahertz technology devices. *ASME Journal of Micro- and Nano-Manufacturing*, published online: February 2016, DOI: 10.1115/1.4032688.
3. **Penchev P**, Dimov S and Bhaduri D. Experimental investigation of 3D scanheads for laser micro-processing. *Optics & Laser Technology 2016*; Volume 81: 55–59.
4. **Penchev P**, Dimov S, Bhaduri D and Soo SL. Generic integration tools for reconfigurable laser micromachining systems. *Journal of Manufacturing Systems 2016*; Volume 38: 27–45.
5. Deng S, **Penchev P**, Liu J, Wang Y, Jiang K, Dimov S, Zhang Z, Liu Y, Leng J, Butt H. Laser directed writing of flat lenses on buckypaper. *Nanoscale*, published online: August 2015, DOI: 10.1039/c5nr02481a.
6. **Penchev P**, Dimov S, Bhaduri D, Soo SL and Crickboom B. Generic software tool for counteracting the dynamics effects of optical beam delivery systems. *IMechE Part B: Journal of Engineering Manufacture*, published online: February 2015, DOI: 10.1177/0954405414565379.

Journal Publications (Submitted and In preparation)

7. Shang X, **Penchev P**, Lancaster M and Dimov S. W-band Waveguide Filters Fabricated by Laser Micromachining and 3-D Printing, *IEEE Transactions on Microwave Theory and Techniques*, Submitted: December 2015.
8. **Penchev P,** Bhaduri D, Dimov S. Laser polishing of free form 3D printed Stainless Steel and Titanium parts, In preparation.

Conference Publications

9. **Penchev P**, Nasrollahi V and Dimov S. Novel laser micromachining strategy for high aspect ratio features. In: *11th International Conference on Micro Manufacturing (ICOMM 2016)*, Orange County, California, USA, March 2016.

10. **Penchev P**, Shang X, Dimov S and Lancaster M. Novel manufacturing route for scale up production of Terahertz technology devices. In: Proceedigns of the *4M/ICOMM 2015 Conference*, Milan, Italy, 31 March-2 April 2015, pp. 605-608.

11. Bhaduri D, **Penchev P**, Dimov S, Soo SL. Improving the surface integrity of 3D printed Stainless Steel parts by laser polishin. In: Proceedigns of the *4M/ICOMM 2015 Conference*, Milan, Italy, 31 March-2 April 2015, pp. 593-596.

12. Bhaduri D, **Penchev P**, Dimov S, Soo SL. On comparative evaluation of accuracy, repeatability and reproducibility of laser micromachining systems. In: Proceedigns of the *4M/ICOMM 2015 Conference*, Milan, Italy, 31 March-2 April 2015, pp. 597-600.

13. Shang X, **Penchev P**, Lancaster M and Dimov S. Design of Terahertz waveguide filters for hybrid manufacturing based on CNC milling and laser micromachining. In: Proceedigns of the *4M/ICOMM 2015 Conference*, Milan, Italy, 31 March-2 April 2015, pp. 378-381.

14. Harris C, Dearn KD, **Penchev P** and Dimov S. Improving the tribological performance of Poly-ether-ether-ketone (PEEK) in Boundary/mixed Lubrication regimes by laser surface texturing . In: Proceedigns of the *4M/ICOMM 2015 Conference*, Milan, Italy, 31 March-2 April 2015, pp. 522-525.

15. **Penchev P**, Bhaduri D, Dimov S, and Soo SL. Novel manufacturing platform for scale up production of miniaturized components. In: *Proceedings of the 9th International Workshop on Microfactories*, Honolulu, USA, 5-8 October 2014, pp.231-238.

16. Pavey J, **Penchev P**, Dimov S, Chang I, Petkov P and Kolew A. Laser machining of Zr-based bulk metallic glass with nano-second laser. In: *Proceedigns of the 10th International Conference on Multi-Material Micro Manufacture (4M 2013)*, San Sebastian, Spain, 8-10 October 2013, pp. 157-151.

CHAPTER 1
INTRODUCTION

1.1 Motivation

Design for manufacturing is a product development philosophy, which postulates that industrial products designs are governed by manufacturing systems' capabilities [1] and thus their processing limitations define the boundaries of engineering ingenuity, implemented in new products designs. Technological advances across different application areas, e.g. micro-electromechanical systems, micro-sensor systems, microelectronics, smart communication systems and biomedical devices, have driven the demands for product miniaturization, increased accuracy and precision of products while satisfying constantly growing requirements for production efficiency and reliability and improved environmental footprint [2 - 4]. To address both product and process development requirements underpinning the product miniaturisation trends, considerable research efforts are focused on increasing the capabilities of various manufacturing processes such as milling, forming, additive manufacturing and laser processing. Also, this includes the development of hybrid manufacturing platforms and process chains that combine innovatively the capabilities of complementary processes and thus to exploit the advantages offered by their standalone solutions while overcoming some of their shortcomings [2].

Laser micromachining (LMM) is a research and development area that has been attracting a significant interest both from research communities and industry due to its appealing intrinsic machining characteristics such as non-contact processing, capabilities to machine complex free-form (3D) surfaces in a wide range of materials. In addition, its possible integration in hybrid manufacturing platforms and process chains and thus to combine LMM with other complementary processes and address a broader range of application/product specific requirements is even more commercially attractive for industry. Other important reasons for the consistently growing interest in LMM are the advances in the laser processing technology. In particular, these advances allows LMM to meet manufacturing requirements for increased throughput and quality of miniaturised products that incorporate functional features across

different length scales and geometrical complexity while extending the process capabilities for in-situ selective surface treatment and functionalization [5,6]. However, as it is disclosed in more detail in Chapter 2, the broader industrial uptake of this attractive manufacturing technology both as a standalone fabrication system and also as a component in hybrid manufacturing solutions and process chains is still to come due to various open issues related to the process fundamental characteristics, process predictability and process reliability [7, 8].

1.2   Research aims and objectives

The research aim and objectives of the work reported in this thesis are driven by the necessity to address a number of system-level issues in the design for implementation of LMM systems, which could broaden their manufacturing capabilities. Thus, engineering ingenuity will be encouraged by increasing laser process flexibility and reliability in fabricating different products regardless of their design complexity. The overall aim of this research is to improve the system-level performance of reconfigurable LMM platforms and thus to create the necessary pre-requisites for increasing their machining accuracy, repeatability and reproducibility (ARR) in different processing configurations. The development and validation of such reconfigurable LMM platforms is important:

a. to capitalise on the latest advances in LMM component technologies, i.e. high dynamic optical beam delivery system, ultrafast (pico and femto second) laser sources with high repetition rates (MHz);

b. to broaden the application areas of standalone LMM systems;

c. to create capabilities for integrating LMM modules in multi-process production lines and thus to extend the capabilities of industrially proven conventional manufacturing routes such as micro milling for the cost effective fabrication of high-value miniaturized products that incorporate complex multi length-scale (micro-and meso-scale) functional features.

To realise this overall aim, open research issues were identified (Chapter 2) that provided the motivation for defining the following main objectives of the research reported in this thesis:

- **Objective 1**: To develop and implement a systematic approach for assessing and characterizing the manufacturing capabilities of LMM platforms in terms of machining accuracy, repeatability and reproducibility (ARR);

Objective 1 has driven the research efforts to address *Key Research issue 1* identified in Chapter 2:

Lack of sufficient knowledge about the manufacturing capabilities of LMM systems in terms of machining accuracy, repeatability and reproducibility (ARR). Even though two studies have reported qualitative evaluations of the technological maturity levels of LMM systems [100, 123], there is not a comprehensive analysis of their ARR capabilities yet, which can clearly quantify the contributions of the integrated component technologies to the observed overall machining performance. Thus, comprehensive quantitative studies focused on LMM systems ARR capabilities are of high importance for identifying critical performance issues associated with their components technologies and thus to improve their overall manufacturing capabilities. In addition, such comprehensive quantitative studies could also provide valuable information for identifying system-level integration issues in state-of-art LMM platforms, which impair the synergistic functioning of their integrated component technologies.

- **Objective 2**: To design, implement and validate generic integration tools for reconfigurable LMM platforms which can improve their system-level machining performance in terms of manufacturing flexibility and reliability both as stand-alone machine tool configurations and also as constituent manufacturing technologies in multi-process production lines;

Objective 2 has driven the efforts to address *Key Research Issue 2* identified in Chapter 2:

Lack of generic integration tools, which can enhance the reconfigurability, modularity and reliability of laser micro-processing platforms. In particular, such integration tools should offer capabilities for automated geometrical registration of a workpiece in LMM systems prior to executing the machining operations, because the accurate alignment of parts is of critical importance for achieving the required level of machining ARR. In addition, the integration tools should create capabilities: (i) to enable highly accurate and precise positioning of workpieces in LMM platforms; (ii) to provide sufficient flexibility for realizing various LMM configurations; (iii) to provide the required modularity in integrating LMM modules with different primary shaping, processing and inspection stages in multi-process manufacturing platforms.

- **Objective 3**: To design, implement and validate generic software tools for reconfigurable LMM modules that create the capabilities for realizing complex multi-axis laser processing strategies with a closed-loop manufacturing control and thus to enable a flexible and robust LMM technology for the fabrication of multi length-scale functional features with the required level of ARR;

Objective 3 has driven the research efforts to address *Key Research issue 3* identified in Chapter 2:

Lack of generic software tools to address the open-loop control issues of LMM systems and at the same time to increase their manufacturing flexibility by creating capabilities for realizing complex multi-axis laser processing strategies. In particular, such tools should be designed and implemented: (i) to improve the laser micro processing throughput; (ii) to improve the closed-loop manufacturing control of LMM systems; (iii) to improve ARR in various multi-axis LMM configurations.

Objective 4: To develop and demonstrate novel multi-process manufacturing platforms that integrate LMM technology as a key product enabler and thus to extend the capabilities of industrially proven conventional manufacturing processes such as micro milling for producing high-value miniaturised products like Terahertz (THz) technological devices which have complex and challenging-to-fabricate functional features and overall geometrical designs.

Objective 4 has driven the research efforts to address *Key Research issue 4* identified in Chapter 2:

Lack of sufficient implementation strategies of the laser micro-processing as a modular technology that can be seamlessly integrated in multi-process manufacturing platforms and thus to provide the required manufacturing complementarity to other micro-scale processing technologies for the fabrication of complex products with multi-length scale functional features.

1.3　Thesis organization

The thesis consists of seven interconnected chapters in order to ensure that the research objectives are achieved. The links among the chapters in the thesis are illustrated in Figure 1.1.
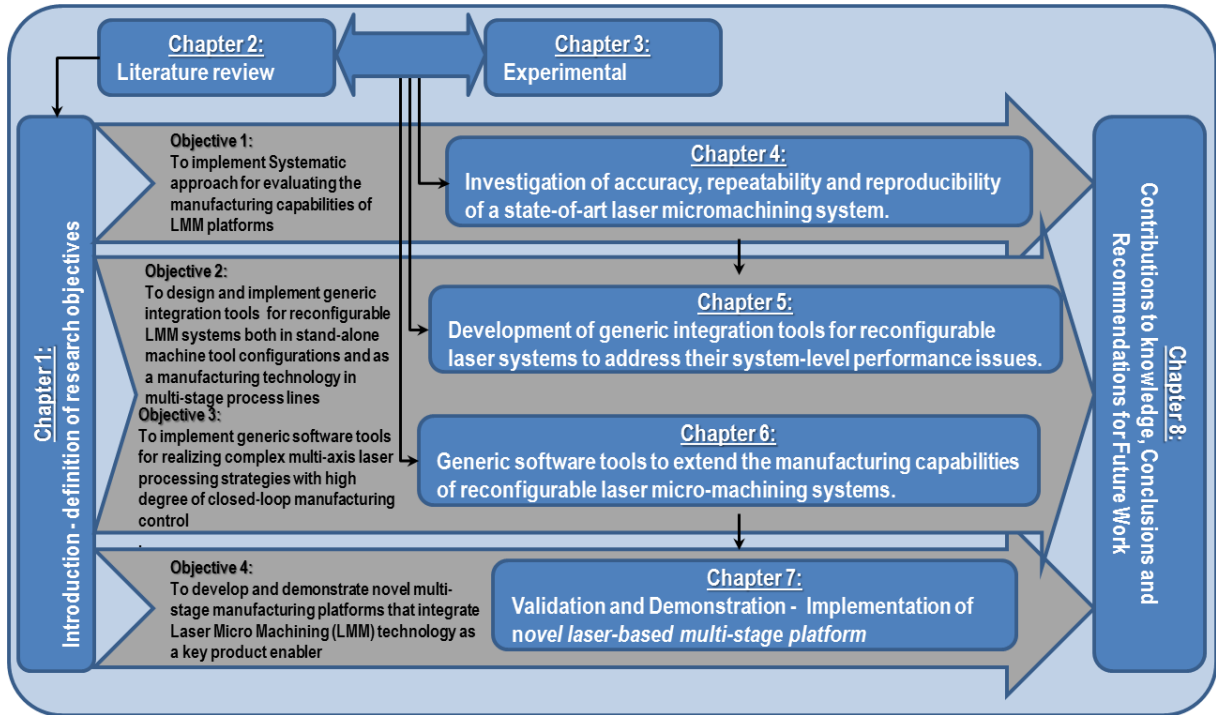
Figure 1.1 Overall structure of the research and the links between the chapters in the thesis

The research findings that led to the claimed contributions to knowledge are reported in Chapters 4 to 7. The current Chapter introduces the research objectives of the work, Chapter 2 reports the carried out literature review and Chapter 3 describes the experimental equipment and methods utilized in the research. Chapter 8 summarizes the contributions to knowledge, main conclusions and suggests direction for future research work. More detailed description of the contents of each chapter is provided below.

Chapter 2 presents a literature review of the laser manufacturing technology in order to identify key machine tool performance issues of LMM platforms that are the focus of the research reported in the thesis.

Chapter 3 provides a detailed description of the equipment, which has been used to perform the experimental work and also introduces generic experimental methods used to achieve the research objectives.

Chapter 4 reports a systematic quantitative study that investigates the effects of key component technologies on manufacturing capabilities of state-of-art LMM systems in

regards to their machining ARR. In addition, the chapter introduces an experimental method that can be used to quantify the dynamic capabilities of z-modules and thus to judge about their negative effects in LMM of complex free-form (3D) surfaces.

Chapter 5 is dedicated to the development of generic integration tools, which address system-level issues of LMM platforms that has negative impact on their machining performance in terms of process operability and robustness both in the stand-alone machine tool configurations and also as an integrated manufacturing sub-system in multi-process production platforms.

Chapter 6 is focused on the development of generic software tools, which can substantially improve the manufacturing capabilities of LMM systems in terms of machining throughput and complexity of the laser manufacturing operations and thus to provide the necessary level of reconfigurability in addressing challenging technological requirements of micro-scale products across different application areas.

Chapter 7 demonstrates the capabilities of the proposed generic system-level tools and techniques reported in Chapters 4 and 5 to enhance the machine tool performance of LMM systems in regards their process reliability, robustness, reconfigurability and flexibility. In addition, this chapter reports a pilot implementation of a LMM system as a modular manufacturing technology. In particular, a pilot system that can be seamlessly integrated in multi-process manufacturing system and thus to extend the capabilities of well proven conventional manufacturing routes, i.e. mechanical machining, and also to provide the required manufacturing capabilities for producing complex products with multi-length scale (micro-and meso-scale) functional features, i.e. Terahertz technology devices.

Chapter 8 summarises the main contributions to knowledge and conclusions of the research, and also proposes some recommendations for further research work that can improve the technological maturity level of LMM platforms.

CHAPTER 2

LITERATURE REVIEW

Outline of the chapter

This chapter presents a literature review of the laser manufacturing technology. In particular, the carried out literature review was focussed on (i) investigation of the fundamental laser-material interaction phenomena (ii) review of both well-established and potential industrial applications of the laser processing technology, (iii) review of laser processing platform implementations and their key machine tool performance issues and (iv) investigation of critical system-level requirements for laser micro-processing platforms both in stand-alone machine tool configurations and also as an integrated component technology in multi-process manufacturing solutions. Finally, the chapter concludes with a summary of open research issues, which provide motivations for the work reported in the rest of the thesis.

2.1 Laser machining process

2.1.1 Fundamentals of pulse laser-material interaction

Classifications of advanced machining processes reveal that laser machining is a non-conventional thermoelectric manufacturing process [9], which utilizes a highly collimated, monochromatic and coherent laser light beam to remove matter from a material substrate [10, 11]. When a laser beam is irradiated on material surface, the physical phenomena of the laser material interaction region can be categorized as reflection, absorption, scattering and transmission [12]. However, induction of any effect in the workpiece is only possible through the absorbed energy portion of the laser beam, while the other portions of the irradiated energy (reflection, scattering and transmission) do not contribute to the laser material interactions [12]. In particular, absorption of a high energy density laser beam in a material workpiece surface leads to heating of the material and transforming it into a molten, vaporized or chemically changed state that is removed from the substrate [13]. The material removal process is explained with excitation of material electrons by laser photons followed by heating of the electron subsystem and transferring of the heat to the material lattice due to electron-electron excitation and electron-hole recombination (Auger process) [14]. The material

electron excitation and de-excitation process occurs over a very short time span and thus the laser–matter interaction within the near surface region achieves extreme heating and cooling rates ($10^3 – 10^{10}$ K s^{-1}), while the bulk of the substrate is not affected [14]. Important parameters which influence the laser machining process are related both to laser source characteristics and material optical and thermal properties [15]. In particular, significant laser source parameters include wavelength, pulse energy and pulse duration, while significant material properties include thermal conductivity, thermal diffusivity and absorptivity [12, 16]. Depending on the heat diffusion time of the material and the pulse duration of the laser source, two laser material interaction mechanisms can be distinguished: photothermal process, characterized with short pulse durations (ns and longer) that are longer than the material thermalization time (material characteristic time for electrons and phonons to reach equilibrium) and photochemical process, characterized with ultrashort pulse durations (ps and fs) that are shorter than the material thermalization time [16-18]. The photothermal laser process is usually explained with the classical linear light absorption theory, namely the Beer-Lambert law, which states that the absorption of a specific wavelength of light transmitted through a material is a function of the material path length, and is independent of incident intensity [19, 20]. Thus, in the nanosecond laser processing regime, the material is firstly melted and then evaporated from liquid state [21]. Due to its thermal nature, laser processing with short pulses (ns and longer) have important machining drawbacks such as the existence of heat-affected zone (HAZ), the formation of recast layer around processed area, the existence of micro cracks and shock wave induced surface damages as shown in Figure 2.1a [12, 14, 15, 22].

In contrast, the photochemical laser process is characterized with non-linear absorption phenomena due to the extremely high energy intensities of the ultrashort laser pulses [15, 18, 23, 24]. Two material removal mechanisms are existent in the photochemical laser process, namely the avalanche ionization and multiphoton absorption with the multiphoton ionization being the dominant process [25]. In avalanche ionization, the ionization of bound electrons is achieved through their collision with highly excited free (seed) electrons, leading to two free electrons, which in turn absorb more photons of light, gain kinetic energy and collide with other bound electrons, that lead to a large number of electrons in the conduction band [26, 27]. In multiphoton absorption, the bound electrons of the material can be directly freed from the valence band by absorbing multiple photons [28, 29]. The direct ionization and the

formation of dense electron-hole plasma lead to athermal material transformations – bond breaking and explosive disintegration of the lattice through electron repulsion (Coloumb explosion), which makes it possible to process any material including transparent substrates such as glass [30]. Thus, at sufficiently high energy intensities, laser ablation with ultrashort pulses is characterized by phase explosion, in particular collective transition from solid phase directly to a gaseous phase (sublimation) and thus suppressing the melting phase from the laser ablation which allows obtaining a very high precision and clean manufacturing process [31]. Due to its non-thermal nature, advantages of laser processing with ultrashort pulses (ps and fs) include very minimized thermal damage in the processed materials, a nearly melt free ablation process, capability to process optically transparent materials, highly localized ablation process, minimum HAZ and absence of recast layer as shown in Figure 2.1b [32, 33]. For example, in a study dedicated on the comparison of heat-affected zones in materials processed with nanosecond and femtosecond laser pulses, it was demonstrated that by employing a femtosecond laser source the thermal effects were significantly reduced, i.e. the width of the HAZ was reduced to less than 2 μm in comparison to the 40 μm wide HAZ observed with the nanosecond laser pulses [34]. Figure 2.1 depicts the characteristic differences in the laser ablation mechanisms with short pulses (ns and longer) and ultrashort pulses (ps and fs). In particular, Figure 2.1a shows that the HAZ is significantly more pronounced in the photothermal process in comparison to the HAZ in the photochemical process (Figure 2.1b).
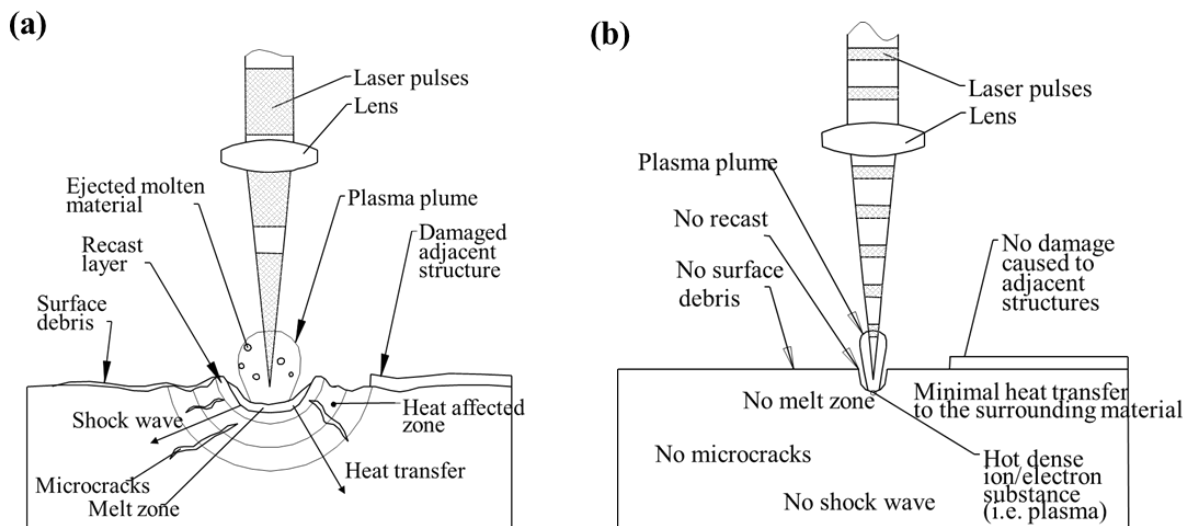
Figure 2.1 Laser ablation mechanism with (a) short pulses (ns) and (b) ultrashort pulses (ps and fs) [15]

Taking into account the fundamental physical processes behind pulsed laser material processing, it can be observed that the attractiveness of this manufacturing process is embedded in its flexible intrinsic characteristics to address diverse material-specific manufacturing requirements such as laser processing of optically transparent, hard and brittle materials and thus the industrial uptake of this technology can be considered very attractive for a wide range of micro applications.

2.1.2 Applications

A global market report on laser applications by segments reveals that the industrial uptake of lasers include diverse application areas such as military, optical storage, instrumentation and sensors, medical, lithography, communication, displays, printing, lithography and material processing [35]. Market growth rates are especially impressive for laser micro processing, because it is becoming a key enabling product manufacturing technology due to its capabilities to address the growing demands for products miniaturization across different industries like mobile communication, healthcare and transportation [36]. In 2012, financial reports put a total market value of € 7.9 billion for laser materials processing systems, which represents a twentyfold increase within the past 20 years and accounts for no less than 12 % of the worldwide machine tool market [36-38]. Main application areas of laser micro processing could be summarized as topographic surface laser modifications [14, 16], laser micro-drilling [27, 32], laser transmission micro-joining and 3D LMM [39-41].

Important application examples in the field of topographic surface laser modifications include localized laser micro-polishing through remelting [42], surface texturing for tribological performance improvements [43] and generation of self-organized laser induced periodic surface structures (LIPSS) for optical and wetting properties functionalization of materials surfaces[44].

Localized micro-polishing through remelting has been successfully reported for diverse range of materials like metals [45] , glasses and thermoplastics [42], but it is applicable to surface with low initial surface roughness, i.e. surface structures with lateral dimensions of up to 40μm [42]. Typical polishing rates are in the range between 0.005 and 0.1 cm^2/sec [42], while improvements in surface topography are strongly dependent on the initial surface roughness, the laser pulse duration, the spatial laser beam intensity distribution and the employed laser beam movement strategies [46]. For example, 72% improvement in average surface roughness of micro end milled Ti6Al4V is reported through careful optimization of the nano-

second laser micro-polishing process [47]. Figure 2.2 also shows that a reduction in surface roughness of over 90% (from ~2.4 to ~0.24 µm Sa) could be obtained on 3D printed stainless steel (SS316L) specimens, when the optimum laser process settings were applied [Publication 11 from the List of Publications].
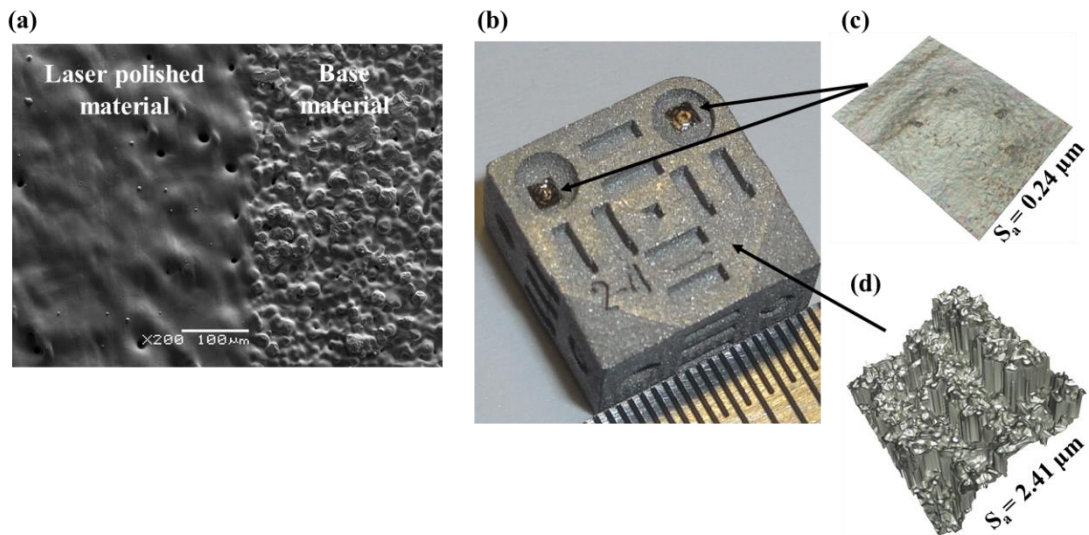
Figure 2.2 (a) SEM micrographs of laser polished stainless steel surface, (b) Laser polished regions on 3D printed stainless steel part, (c) Surface roughness (Sa) on the laser polished regions and (d) on the base material [Publication 11 from the List]

Laser surface texturing for tribological improvements represents the process of generating geometries (i.e dimples with diameter in the range of 50-300 µm and depth in the range of 5-80 µm) on materials surfaces both in static and dynamic surface contact regimes, where key parameters for friction improvements are the dimple density, diameter and depth [43]. In dynamic contact applications, the produced micro-dimples can serve as a micro-hydrodynamic bearing in cases of full or mixed lubrication, a micro-reservoir for lubricant in cases of starved lubrication conditions, and a micro-trap for wear debris in either lubricated or dry sliding regimes [48]. In static surface contact applications, the micro-dimples are used to increase the hydrostatic pressure between stationary (non-moving) mated surfaces [49] and thus to improve the adhesion between the mated surfaces. Well-known industrial applications of laser surface texturing include reduction of friction through laser texturing of cylinder liner, piston rings and thrust bearings in automotive industry [50, 51], laser texturing of mechanical seals for improving their reliability at petrochemical refinery plants [52, 53] and laser texturing of cutting tools for wear improvements and built-up edge stabilization in conventional turning operations [54]. Figure 2.3 demonstrates that the laser texturing of piston rings could reduce the friction forces in automotive engines and thus to improve their fuel

economy. In particular, Figure 2.3b shows that the laser textured piston rings (shown in Figure 2.3a) exhibited about 25% lower friction in comparison to non-textured piston rings [51].
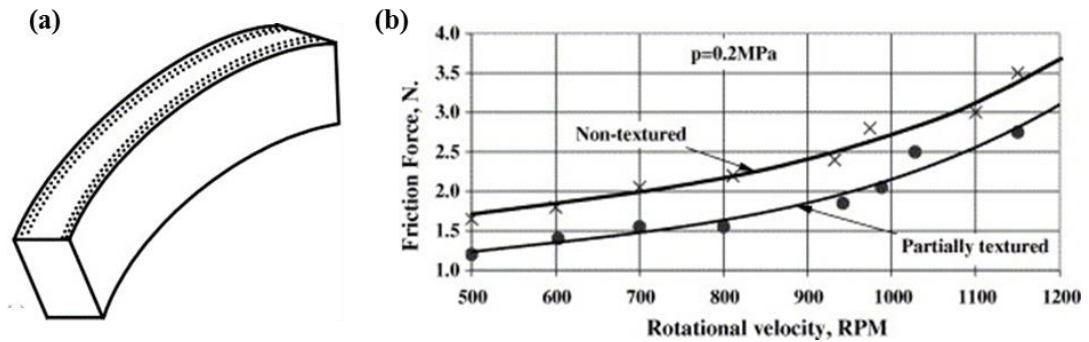
Figure 2.3 (a) Schematics of a partial laser textured engine piston ring segment and (b) measurement of the average friction force versus crank rotational velocity for non-textured piston rings and for the partially textured piston rings [51]

LIPSS or ripples are low spatial frequency and high spatial frequency laser-induced surface structures that can appear on various metallic, ceramic, semiconductor and glass surfaces when they are irradiated with ultrashort pulses at fluences (energy density) near the material ablation threshold [27,33].Even though formation of LIPSS is not completely understood and its fundamental physical explanation is still under debate [27, 33], experimental investigations have reported that their formation on material surfaces is highly dependent on laser irradiation dose (accumulated energy in the material), polarization and wavelength of the incident laser beam [55]. In particular, the laser energy dose controls the geometry and size of the LIPSS [55, 56], while the polarization and the wavelength of the laser beam determine their orientation and periodicity, respectively [55, 57]. Utilization of LIPSS for functionalization of the wetting and adhesive properties of materials surfaces have been reported for a number of application areas such as self-cleaning products [33], increased corrosion resistance of metallic products [58, 59], cutting tools with improved anti-adhesive properties [60], biomaterial surfaces with enhanced cell adhesion properties [61], improved adhesion of medical implants surfaces [33], and Li-ion batteries with significantly improved capacity retention [62]. For example, Figure 2.4 exemplifies that generation of LIPSS on cutting tools significantly improves the anti-adhesiveness at the tool chip interface (as shown in Figure 2.4 c and d), which can potentially reduce the breakages of cutting tools [60]. A well-known industrial example of LIPSS for functionalizing the optical properties of material surfaces is their application for improving the efficiency of photovoltaic cells by enhancing the light

trepanning properties of silicon [63]. Other interesting applications of LIPSS are their utilizations on glass substrates as micro-fluidic and nano-fluidic channels [64].
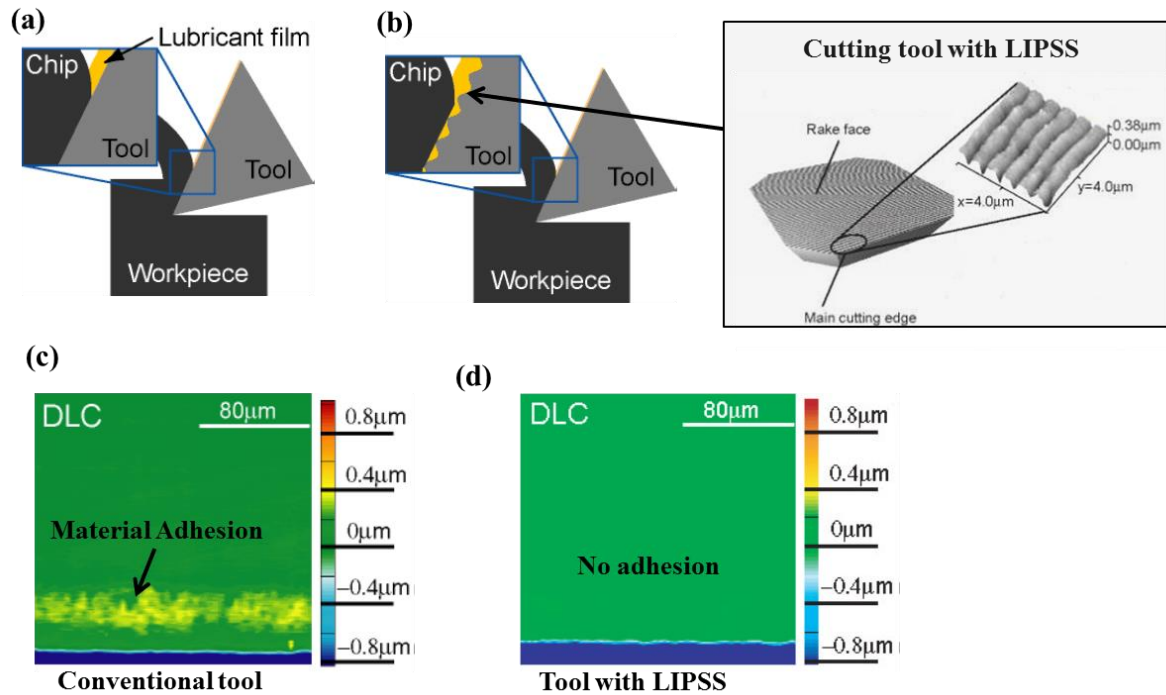
Figure 2.4 Schematic illustrations of a cutting tool: (a) Conventional cutting tool, (b) Cutting tool with LIPSS; The tool rake after cutting for 1800 m of (c) conventional cutting tool and (d) cutting tool with LIPSS [60]

Laser micro drilling is the process of producing blind or through micro holes on variety of materials such as metals [65], ceramics [66], glasses [67] and polymers [68], where critical hole parameters such as hole taper, precision and throughput can be controlled very accurately to address technical requirements for different industrial products [14]. The high flexibility of laser drilling in addressing holes with different geometrical requirements is ensured through the employment of different drilling techniques such as single shot and percussion drilling [69], helical drilling [70] and trepanning [71]. Major application areas of laser micro-drilling are in aeronautic, automobile, semiconductor and biomedical industries [72]. Specific industrial laser drilling application examples include drilling of large numbers (~100000) of closely spaced cooling holes in turbine engine components such as airfoils, nozzle guide vanes and combustion chambers [73], laser drilling of microvia holes and channels in silicon wafers for microelectronic devices [74], inkjet printer nozzle drilling (shown in Figure 2.5 a and b) [75] and multiple hole drilling of drug delivery catheters (shown in Figure 2.5 c and d) [75, 76].
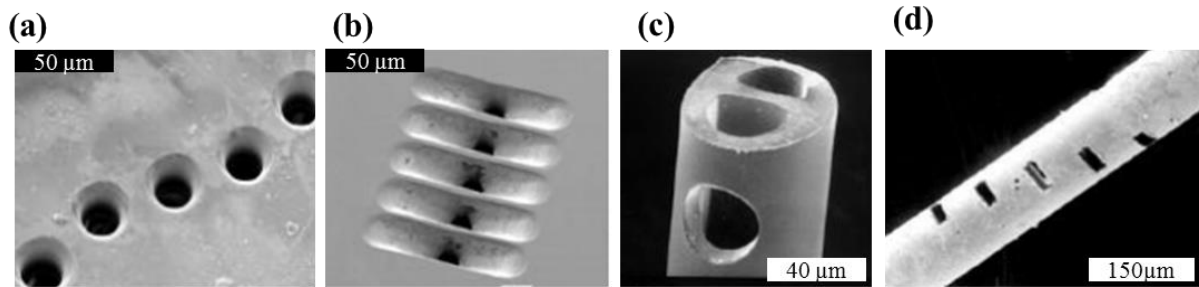
Figure 2.5 (a) Array of 30μm diameter ink jet printer nozzles drilled in polyimide, (b) Array of nonlinear tapered nozzles aiding laminar fluid flow, (c) Hole in the side of a bilumen catheter for monitoring blood in prematurely borne babies and (d) Rectangular 50x20μm holes drilled in 100μm fibers for PaO2 & PaCO2-sensors [75]

Laser transmission micro-joining is the process of welding two stacked substrates (top substrate is partly transparent to the laser radiation while the bottom absorbs it) by irradiating a laser beam at their interface where due to heat conduction processes and melting of the bottom substrate the adjacent transparent part is also heated up and melted and thus the material within the contact area is mixed up before it solidifies [39]. Figure 2.6a shows the working principle of laser transmission micro-joining. Important functional parameters that determine the strength of the weld are contact pressure between the two substrates, their surface roughness and their optical and thermal properties, wavelength of the laser beam and laser radiation intensity [39, 77, 78]. The laser transmission micro-welding has been successfully reported for a number of material combinations such as glass on glass (B270 glass on silver nanoparticles composite glass) [79], glass on silicon (borosilicate glass on boron doped silicon) [80] and polymer on polymer (Plexiglas PMMA with Polypropylene PP) [81]. Well-known industrial applications of laser transmission micro-joining process are welding of polymers for packaging of disposable microfluidic-biochips with near-infrared fiber lasers (as shown in Figure 2.6 b) [81] and welding of glass on silicon for packaging of microsystems [80].
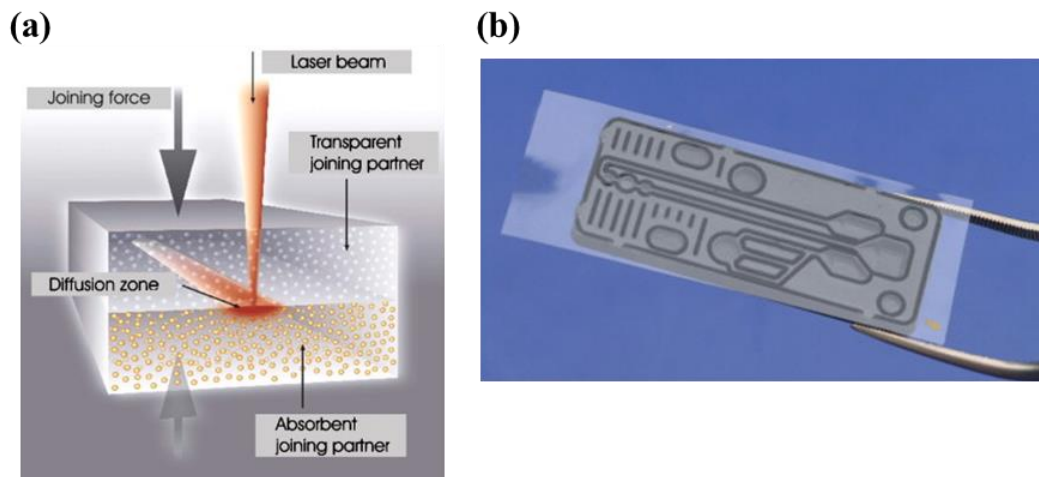
Figure 2.6 (a) Principle of laser micro-joining and (b) PMMA microfluidic device sealed with a transparent cover foil [81]

In its broadest definition, LMM is the process of controlled non-contact removal of material with extremely high precision in order to address the fabrication of complex 3D miniaturized structures for various industries like biotechnology, microelectronics, telecommunication, microelectromechanical systems (MEMS), biomedical applications and fine mechanics. [10, 11, 12-15, 27, 31, 33, 36, 82, 83]. With the advent of different laser sources, that operate at short and ultrashort laser pulse durations and have wavelengths from UV to the far-infrared regions of the electromagnetic spectrum, there are no limitations on material choice for the LMM process [14, 84]. A list of selected application examples include LMM of ultrafine biodegradable medical implants such as stents (as shown in Figure 2.7a)[85, 86], ophthalmic lenses [87], and biomaterial scaffolds for improved cell proliferation in tissue engineering[88], LMM of ceramic MEMS platforms working under harsh environmental conditions for semiconductor and thermocatalytic sensors of combustible gases, gas fire detectors, and electrochemical sensors of oxygen [89], laser fabrication of waveguides and microfluidic channels for optofluidic Lab-on-Chip devices used for the sensing and manipulation of biomolecules and cells confined in micro channels [90, 91] and laser production of complex injection moulding replication masters with micro- and nano-scale features on innovative bulk metallic glass materials (as shown in Figure 2.7b) [92]. Other interesting application examples of LMM can be found in the field of biomimetic [93], jewellery [94] and fine mechanics [75]. It should be noted that the literature review on application areas of LMM reveals that there are trends are towards lasers with ultrashort pulses and shorter wavelengths due to their capabilities for cold material processing, which

allows the precise fabrication of intricate 3D structures with sub-diffraction dimensions. Thus, ultrashort laser processing can be applied to fabricate of features as small as 20 nm [95-97].
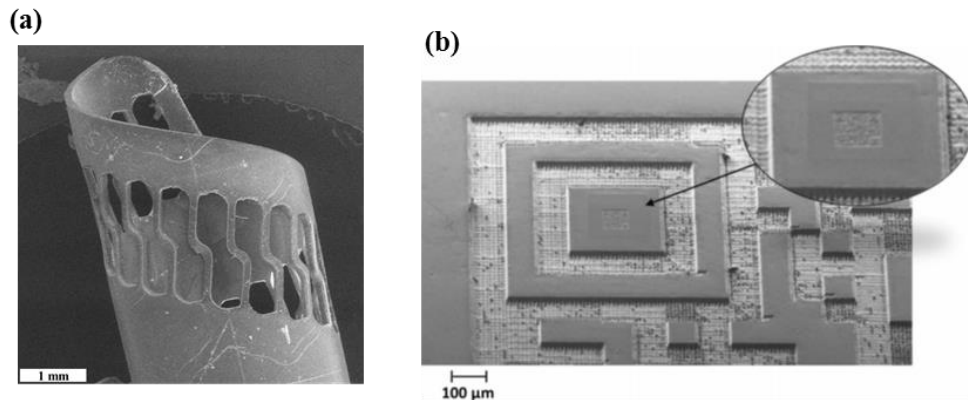
Figure 2.7 Picosecond laser micromachining of (a) coronary stents [86] and (b) replication master with micro- and nano- scale features [92]

2.2 Laser micromachining platforms

To benefit from the intrinsic appealing characteristics of lasers, they have to be integrated in complex micro-processing platforms and thus to fulfil the requirements of different industrial applications (presented in Section 2.1.2). Main deterministic factors, which drive the designs and implementations of such LMM platforms, are the length scale of features and the geometrical complexity of the parts to be processed together with their technical requirements for accuracy, precision and surface topography [98]. The following subsections will attempt to provide a snap shot of the state-of-art in LMM platforms in terms of their machine tool performance related to the manufacturing robustness, reliability and complexity (Section 2.2.1). In addition, requirements for laser micro-processing configurations both in stand-alone systems (Section 2.2.2) and also as an integrated manufacturing technology in multi-process fabrication platforms (Section 2.2.3) will be discussed. Thus, key issues in LMM platforms, which hinder the overall process reliability and flexibility can be identified to motivate the system-level development work reported in Chapters 4 and 5 of the thesis.

2.2.1 Key performance issues of laser processing platforms

As communicated in Section 2.1 above, laser micro-processing is a research and development manufacturing area that has been attracting a significant interest both from the research community and industry (discussed in Section 2.1.2) due to its appealing capabilities (presented in Section 2.1.1) such as non-contact processing, machining of complex free-form (3D) surfaces in a wide range of materials and high machining quality with minimum thermal

damage in and around the laser-material interaction zone. Nevertheless, the literature review on the applications of laser processing (Section 2.1.2) reveals that even though some commercial LMM platforms for specific application areas are available, the broader uptake of this attractive manufacturing technology is still at its infancy and thus the utilization of the laser processing technology both as an established stand-alone fabrication route and also as an integrated component manufacturing technology in multi-process manufacturing solutions is still to come [7, 99]. A detailed qualitative capability maturity model, which evaluates the maturity levels of various micro- and nano- manufacturing processes, e.g. micro-milling, focus-ion beam, micro injection moulding, electroforming and hot embossing, shows that in comparison to micro-milling, which is ranked as a mature process and is widely used across different industrial sectors, laser micro processing is considered not sufficiently mature due to various open issues related to its process fundamental characteristics as well as to its process predictability and reliability [100]. The processes maturity evaluation methodology was based on in-depth qualitative characterization from process experts of 32 key process capability parameters, which are grouped in 6 key process capability areas, namely Quality (surface roughness, edge definition of produced featutrs) and Accuracy(the dimensional deviations from nominal values), Part Size (overall part dimensions) and Complexity(the range of multi-length scale geometrical and dimensional features), Materials, Efficiency(cost and throughput of the manufacturing process), Processing (overall manufacturing capabilities of the process), and Fixturing and Setup(tools that are used to hold and align the parts prior the machining process) [100]. The capability maturity model reveals that laser micro-processing systems lack the required level of manufacturing flexibility and reconfigurability to address the constantly evolving geometrical complexity of micro-scale industrial products, which makes the laser processing technology highly vulnerable to products design changes. More specifically, the capability maturity model identifies that the laser technology has a very empirical processing nature, i.e. process optimization trials are needed to accommodate new product designs [100], which adversely affects the overall performance reliability and predictability of laser micro-processing systems in the machine tool context. Other factors, which could contribute to the lack of process adaptability of laser systems, include the insufficiently flexible workpiece fixturing devices and the non-standardized manual datum setup strategies, which are critical for the achieving the required level of machining ARR in any manufacturing system. For example, in a study reporting the application of LMM for

producing a complex ceramic microsurgical tool with features on two opposite sides of the component, a sequence of manual operations (fixing, repositioning and alignment in a single machining setup) were required to manufacture the microsurgical tool as shown in Figure 2.8 due to the lack of flexible workpiece fixturing devices and automated workpiece referencing strategy. This lead to sufficiently big machining errors in the produced parts and thus the target products dimensional tolerances could not be met [101].
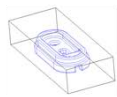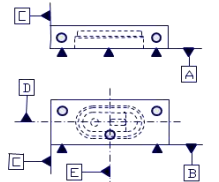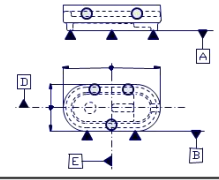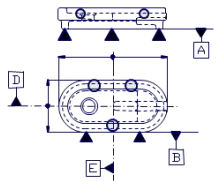
	Operation	Set-up diagram	Geometry after laser milling
Sequence of operations for producing the ceramic microsurgical tool	Blank with the component centred within it.		
	Milling of the first cavity and the outer contour.		
	Milling of the second cavity.		
	Milling of the through hole and the slot.		

Figure 2.8 A sequence of operations for LMM of a ceramic microsurgical tool with features on two opposite sides of the component [101]

The system-level technology gaps of state-of-art laser micro-processing platforms in the machine tool context have also been recognized in other studies, which state that in comparison to the closed-loop control of high precision CNC milling systems [102], the laser systems are predominantly characterized with open-loop control, which makes their machining results not sufficiently reliable for achieving the required level of machining accuracy and precision of various micro-scale application areas [102, 103]. In conventional precision CNC systems, the closed-loop control can be established via real-time signals, i.e. torque, drift force, feed force, cutting speed, feed rate, which can be directly linked with the machining results due to the contact machining approach (the cutting tool is always in contact

with the material substrate undergoing processing) [104]. However, the establishment of closed-loop control in LLM systems with the well formulated techniques reported for conventional manufacturing systems is more challenging due to the non-contact machining approach of LMM. Thus, LMM platforms are predominantly characterized with open-loop control [103].[103]. Nevertheless, researchers have attempted to improve the open-loop laser process control for specific laser processing applications like laser micro-spot welding by utilizing high-speed pyrometer systems and thus to judge about the laser processing progress status by monitoring the material temperature evolution [104]. Figure 2.9 shows the arrangements of components in the developed setup [104].
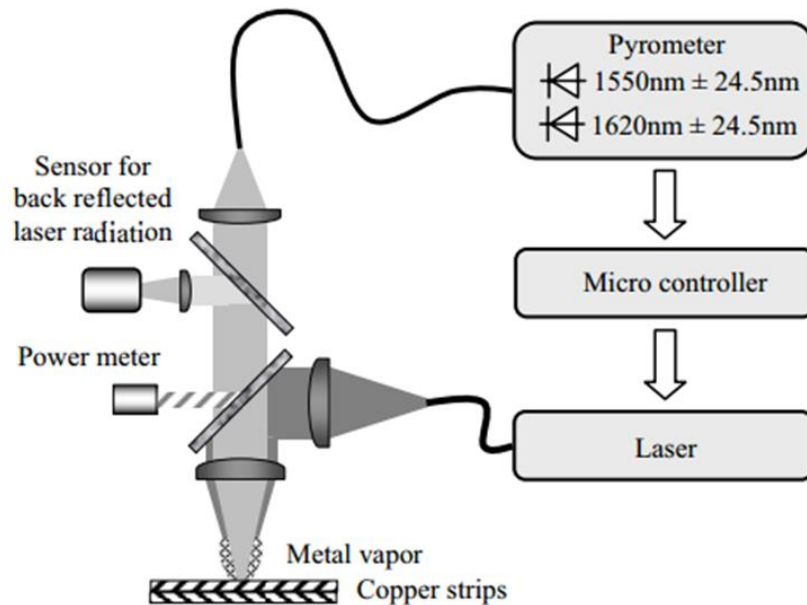
Figure 2.9 The establishment of closed-loop control by utilizing high-speed pyrometer systems in laser micro-spot welding [104]

In addition, the establishment of closed-loop control in ultrafast laser milling process has also been attempted by utilizing a CCD camera for monitoring the brightness of the derived light from the laser triggered plasma and thus to use it as an indicator to adjust the relative distance between the laser beam focal plane and the material substrate for efficient machining operations [103]. Even though, such methods can improve the laser process control to a certain extend for specific laser processing operations, they cannot be considered sufficiently generic due to their highly conditional nature, i.e. laser triggered plasma [103] and temperature gradient [104] must be present during the laser processing operations. In spite of the necessity of system-level tools for improving the closed-loop control of LMM platforms,

they have not been on the forefront of the laser technology research agenda. In particular, the laser technology literature review shows that in the last two decades the research efforts were mainly focussed on investigating laser-material interactions [6, 105], process modelling [12, 106] and empirical process optimization [107, 108] to address specific manufacturing requirements, such as surface integrity and processing time, while not paying sufficient attention to the development of generic system-level tools and techniques for extending the LMM capabilities both as standalone machine tools or as a component technology in multi-process manufacturing platforms. More specifically, the research on improving the performance and reliability of LMM platforms as machine tools was mostly limited to:

- Advances in control algorithms of optical beam deflection systems for synchronizing laser pulse firing events with the movements of scanning mirrors (shown in Figure 2.10a) [109];

- Optimization of closed-loop control of optical beam deflection systems for enhanced rotary movement accuracy and precision of the scanning mirrors [110, 111];

- Development of strategies for the simultaneous use of optical beam deflection systems with mechanical stages for high-speed wide area laser processing [112];

- Design optimizations of focusing lens to account better for optical machining field distortions and thus to improve the laser beam positioning accuracy during the manufacturing operations [113];

- Beam-path generation software tools (shown in Figure 2.10b) based on commercially available CAD/CAM systems for creating NC part programmes for machining components with high geometrical complexity [114-116];

- Development of strategies for the automated identification of the laser beam focal plane on material substrates [117];

- Implementation of high-sensitive thermal cameras for monitoring the temperature build-up in the material during the laser process and for corresponding adjustments of the laser power based on the collected temperature data to avoid overheating of the processed substrates [103, 104, 117].
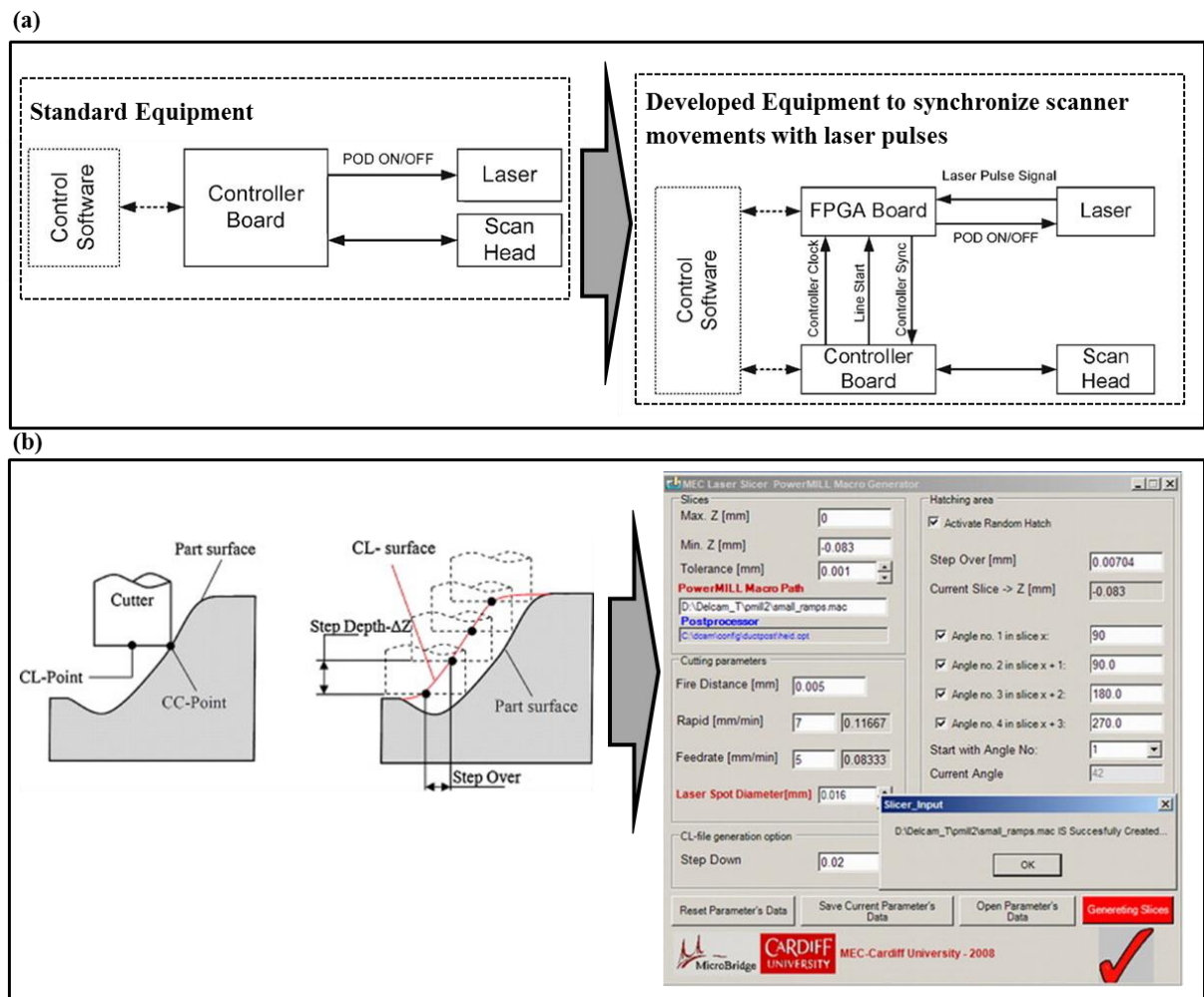
Figure 2.10 (a) Example of advances in control algorithms of optical beam deflection systems for synchronizing laser pulse firing events with the movements of scanning mirrors [111] and (b) Example of a beam-path generation software tool for creating NC-part programmes [114]

At the same time there are significant advances in LMM systems component technologies, e.g. the growing number of short and ultrashort laser sources with constantly increasing maximum pulse energies and repetition rates [118], decreasing pulse durations and shorter wavelengths [119], ultra-high speed variable focus elements for advance beam delivery [120], high dynamic optical beam deflection systems with integrated digital scanner motor control electronics [121], linear and rotary mechanical axes with a repeatable positioning resolution of less than 0.1 μm and less than 30 μrad, respectively [122]. Nevertheless, the advances in these laser systems component technologies do not immediately translate into improvements of the LMM machine tool performance at the system level in terms of machining ARR unless adequate integration tools and techniques are used to achieve the necessary level of components' synergy without compromising their individual performance. The importance of

integration tools and techniques in LMM installations is exemplified in a comparative study of three different LMM systems that have comparable component technologies with very similar specifications, but in spite of this, their ARR results were significantly different and far away from the stated specifications of the equipment manufacturers [123]. For example, the comparative study revealed that the overall machining accuracy is 12 μm, 15 μm and 70 μm for laser system 1, 2, and 3, respectively [123]. Even though the study does not quantify the individual contribution of the integrated component technologies to the overall machining errors in each of the three evaluated systems, it still clearly outlines the state-of-art laser systems reliability issues in the machine tool performance context. Thus, these findings reiterate the importance of developing and validating critical system-level integration tools and techniques for LMM platforms and thus to improve the closed-loop performance of laser systems and to bring the technology to a maturity level of well-established manufacturing processes such as micro-milling. Such system-level research and development efforts are necessary to underpin both the standalone use of LMM systems and also their integration in hybrid manufacturing platforms and process chains for different application contexts.

2.2.2   Requirements for stand-alone laser micromachining configurations

In LMM, the critical demands for ARR are addressed through the integration of a wide range of laser sources in highly controllable direct-writing micromachining platforms to realise the beam-workpiece relative movements [124, 125]. There are three main machine configurations in designing and implementing LMM platforms: (A) moving workpiece and stationary beam; (B) stationary workpiece and moving beam; and (C) combination of both. In Configuration A, the workpiece is mounted on precise linear stages that move the workpiece and determine the machining envelop under a stationary focused laser beam as shown in Figure 2.11a. Complex beam paths can be executed by controlling the stages' movements, in particular Computer Numerical Control (CNC) part programs are generated prior to the machining operations which contain programmed stages movements commands in accordance to the parts contours [126, 127]. Mechanical stages are widely used in many different manufacturing systems where relative movements between workpieces and processing tools have to be performed. Thus, mechanical stages are used both in conventional manufacturing systems, e.g. milling, turning, and in non-conventional manufacturing systems, e.g. laser micro processing, electron beam machining, wire electrical discharge machining (EDM) and electro chemical machining (ECM). For example, implementation of mechanical stages in three-axis and five-axis

machining centres is so well established and commercialized in conventional milling industry that it is covered by variety of machine tool ISO standards, i.e. ISO-230-2:2014. [128]. Therefore, it is not surprising that linear stages as a key component technology in their realisation were widely studied and had attracted a significant research and development interest both from industry and research groups.
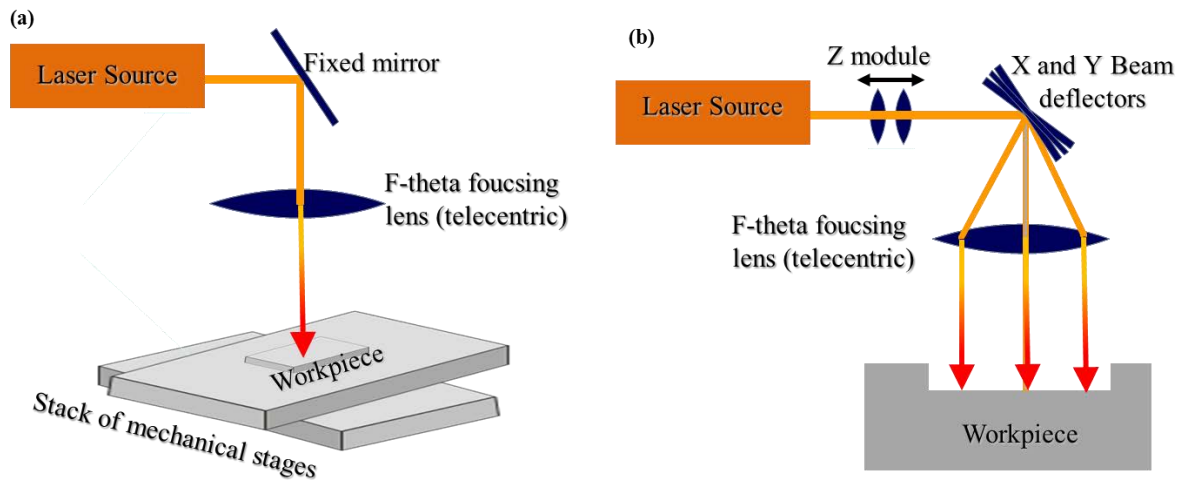
Figure 2.11 (a) Configuration A LMM and (b) Configuration B LMM

The stages' performance both in regards to their ARR and dynamic capabilities has undergone through continuous improvements in the last two decades to deliver repeatable ultra-precise positioning [129, 130]. In extreme cases, they can accommodate movement increments of tens of nanometres and thus to realise a very reliable machining in terms of ARR. Furthermore, linear stages' drivers provide advanced solutions for integrating laser sources in Configuration A LMM systems, in particular for achieving a precise synchronization of laser pulse firing events with the stages' movements across the whole machining envelop. Such solutions for LMM platforms are commercially available and incorporate an advanced control tool for Positioned Synchronized Output (PSO) that controls the laser firing events in order to deliver a consistent pulse distance in the laser processed regions (the spacing between the laser pulses) regardless of the workpiece velocity along the machining paths [109]. Nevertheless, an important shortcoming of mechanical stages is their relatively low machining speed, typically it does not exceed 500 mm/s. [130]. This relatively low speed is a major limiting factor for integrating the latest generation of high frequency laser sources in Configuration A LMM systems and therefore they are usually implemented for a higher ARR machining in expense of relatively high processing time.

Figure 2.11b presents schematically a Configuration B LMM where the workpiece is stationary while the beam moves along the machining path. A key component technology in such LMM platforms is the scanning galvanometer mirrors system, generally referred to as an optical deflection system that realizes the CNC controlled movements of the laser beam along the machining path. Due to their low mass, optical deflection systems do not have the dynamic limitations of mechanical stages and thus can easily achieve significantly higher processing speeds. Therefore, Configurations B and C LMM can benefit from the highest addressable laser pulse firing rates of the integrated laser sources. However, the higher dynamic performance of the optical deflection systems in comparison to that of linear stages is in expense of a relatively lower processing ARR. Furthermore, the working envelop of Configuration B systems is limited by the field of view of the integrated focusing lens system, which typically does not exceed a 50 mm x 50 mm working area (telecentric lens focal length=100) , and therefore such LMM platforms are mostly utilized for the fabrication of components with relatively small overall dimensions [131].

Finally, laser micro processing systems are also realized employing Configuration C platform design that integrates a CNC controlled movement of both the workpiece and the laser beam as shown in Figure 2.12a. This LMM configuration benefits from the advantages of both Configurations A and B systems and thus can be employed either for addressing higher ARR processing by utilizing the highly accurate and precise positioning capabilities of the linear stages or the high speed machining capabilities of the optical beam deflection systems (as shown in Figure 2.12b. The development of Configuration C LMM systems that can perform laser processing with simultaneous synchronized movements of both the optical scan head and the linear stages were already reported [112]. The main objective in implementing Configuration C LMM systems is the realization of high speed machining of workpieces requiring a bigger working envelop realized by the stages [112]. Such a configuration can significantly extend the processing capabilities of LMM systems, because it can be used for a higher speed processing of bigger components without the constraints of the used focusing lens system. However, ARR of such LMM platforms is still determined by the optical beam deflection system because of its ultimate control of the laser beam movements. Therefore, improvements of the ARR capabilities of optical beam deflection systems are essential in order to benefit fully from their high speed processing capabilities in Configurations' B and C LMM systems.
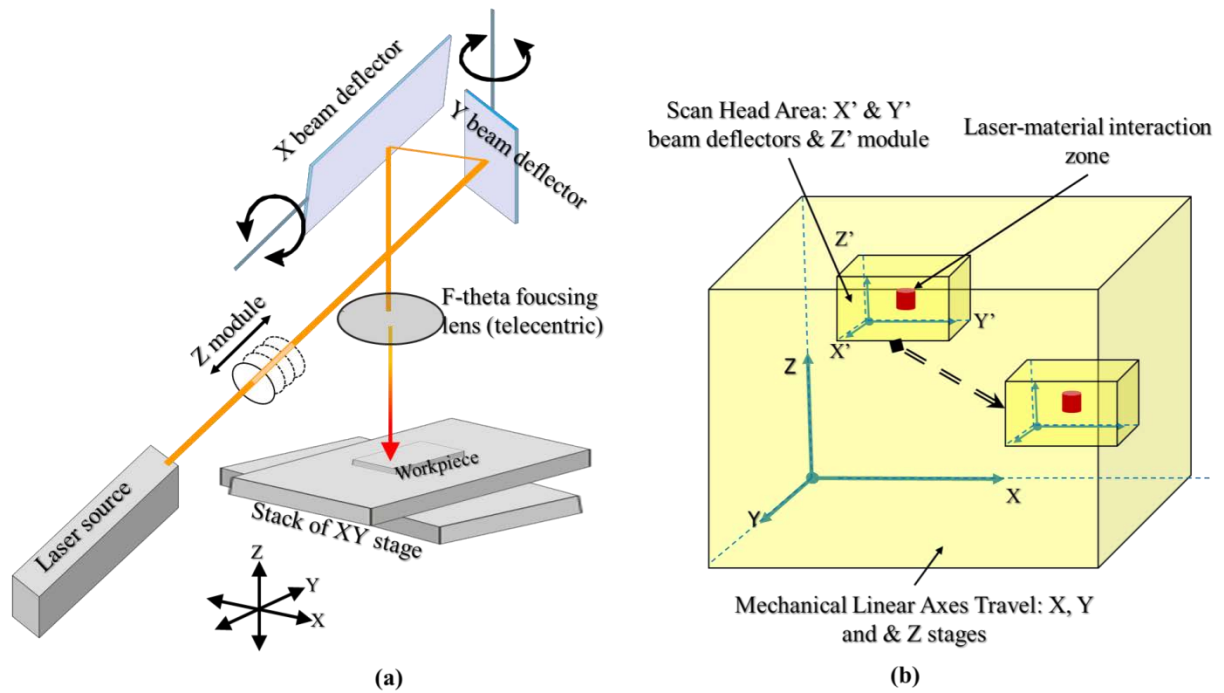
Figure 2.12 Configuration C LMM: (a) schematic representation; (b) beam processing envelops of optical and mechanical axes

2.2.3 Requirements for laser micromachining enabled multi-process manufacturing solutions

Research and developments in micro machining processes (MMP) such as milling [132], forming [133], additive manufacturing [134] and laser micro processing [14] are constantly advancing the manufacturing technologies capabilities in an attempt to address the wide range of industrial requirements for complex product designs with increased technological functionalities. In particular, MMPs research efforts are focused on finding flexible manufacturing solutions for the production of components that incorporate different length scale functional features down to submicron sizes and functionalised surfaces while cost efficiency, products' life cycle characteristics and environmental impact are major considerations in the process designs and implementations [99, 135].However, when MMPs are individually employed they often fail to deliver products that meet all their technical requirements concerning accuracy, geometrical complexity, surface integrity and manufacturing costs due to the intrinsic technological limitations of individual manufacturing processes as well as due to their cost effective processing windows in regards to the length scale of features and materials that can be processed. For example, such critical technological constraints of induvial MMPs include:

- The shapes and sizes of cutting tools in micro-milling introduce constraints in regards to the length scale and the geometrical complexity of features which can be fabricated at the micro scale, i.e. internal vertical edges have corner radius and thus the edge sharpness is greatly determined by the tool diameter [109]. At the same time, reduction of tools diameters adversely affect the milling process reliability and significantly increases manufacturing costs due to micro cutters' wear and breakages, spindles thermal growth, requirements for specialized machining strategies and implementation of complex tool control monitoring systems [136];

- Additive manufacturing (AM) processes can produce complex geometrical features, but built parts have a rough and ribbed surface finish due to the "stair-step" effect and also due to plastic beads or large-sized powder particles that are stacked on top of each other [137].

- The requirements for high-precision handling of sheet-metals in micro-forming of features with dimensions in the submillimetre range (sheet-metals positioning accuracy better than 1 μm) limits the micro-forming process production rates and reliability [133]. In addition, limited materials' formability and springback effect confines the development of micro-forming processes [138].

- LMM is usually viable only when small volumes of material have to be removed due to relatively low material removal rates [14].

Taking into account the inherent technological constraints of individual MMPs, the cost effective manufacturing of miniaturised parts that incorporate different length scale functional features necessitate complementary processing technologies to be integrated into hybrid manufacturing platforms and process chains, i.e. multi-process manufacturing solutions, and thus to overcome the limitations of single processing routes. Such hybrid manufacturing platforms and process chains combine complementary processes to form flexible fabrication solutions which exploits the advantages of a process technology in order to overcome shortcomings of another [139]. In the context of hybrid manufacturing, the combinations of machining processes and/or operations are generally considered to be realized in a single manufacturing system (as shown in Figure 2.13a) [140], while in the context of process chains, the combinations of manufacturing processes are realized through the sequential utilization of multiple machine setups (as shown in Figure 2.13b) [100]. Furthermore, in order to provide a clear definition for hybrid manufacturing, the International Academy for

Production Engineering- CIRP has proposed the following two classifications for hybrid processes, which are now widely adopted in literature [139-141]:

- "Open definition: A hybrid manufacturing process combines two or more established manufacturing processes into a new combined set-up whereby the advantages of each discrete process can be exploited synergistically;"

- "Narrow definition: Hybrid processes comprise a simultaneous acting of different (chemical, physical, controlled) processing principles on the same processing zone."
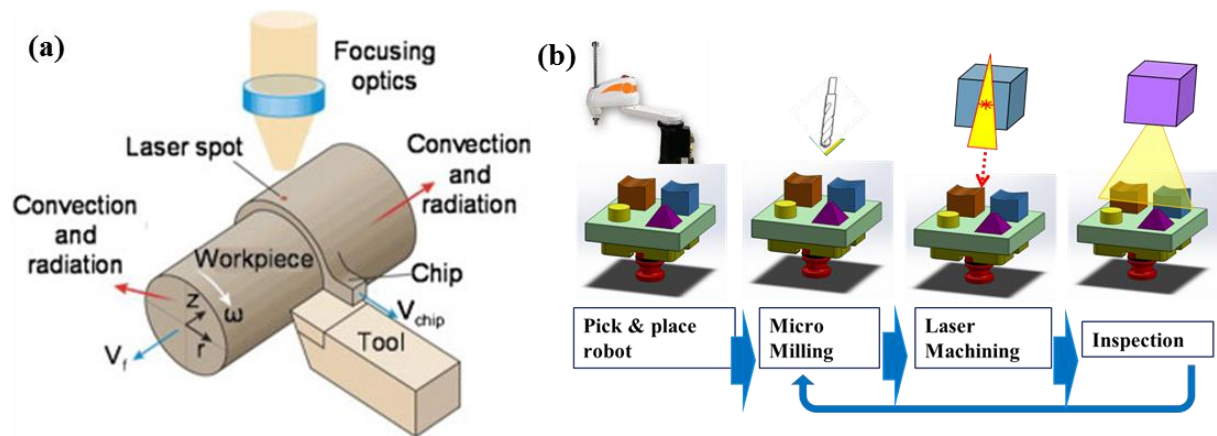
Figure 2.13 (a) Principle of hybrid manufacturing system (laser assisted turning [146]); (b) Principle of process chain

Research efforts both in the context of hybrid manufacturing and process chain fabrication at micro and nano scale are focused on combining different manufacturing processes with the objectives to improve surface integrity, products' accuracy and processing efficiency and also to reduce tool wear and production times [139-143]. For example, a combination of additive manufacturing and milling can significantly reduce manufacturing time and cost by employing additive manufacturing for the near-net shape fabrication of parts while their high quality and accuracy is achieved by employing milling as a finishing step [144]. In another example, a combination of electrical discharge machining (EDM) with grinding for the machining of single-crystal silicate carbide (SiC) allowed to achieve both high efficiency and surface integrity, while the tool wear was also reduced [145]. An in-depth literature review of the various reported hybrid manufacturing processes and process chains together with their reported industrial applications is provided in [139-141, 146]. However, the literature also reveals that a key issue in state-of-art hybrid manufacturing processes and process chains is the fact that they are product specific, which makes their fabrication capabilities highly dependent on products' specific technical requirements and also vulnerable to design changes

even within their respective application areas [139]. This is exemplified by the fact that their processes designs are mainly focused on extending particular capabilities of well-established conventional manufacturing processes, e.g. milling is the most frequently used micro scale hybrid manufacturing process [139]. In attempt to address current limitations of hybrid manufacturing processes and process chains, the LMM is envisaged as a key enabling processing technology for the realization of novel and more flexible hybrid manufacturing solutions and process chains for a diverse range of application areas as shown in Figure 2.14 [139]. This is due to the fact that the laser technology can address the identified future trends and objectives of hybrid and process chain manufacturing in regards to their capabilities to accommodate the following characteristics: three-dimensional features; multiple workpiece materials; multi-scale and multi-functional structures for achieving structural, mechanical, electrical, magnetic, optical, and/or bio-functionalities; tuneable materials for improving properties of materials; ultra-precision [139]. The manufacturing flexibility of innovative laser-based hybrid process solutions and process chains have already been demonstrated in a number of researches, where the laser technology is utilized both as an assistive process to enhance the manufacturing performance of well-established conventional machining process and also as a complimentary machining step in multi-process manufacturing solutions [139-141, 143 , 146]. For example, the integrations of laser technology with mechanical machining processes such as turning, milling and grinding have been reported to significantly enhance the processing of difficult-to-machine brittle and hard materials, which lead to increase in material removal rate and productivity [147]. In particular, this is due to the localized heating of the material with the laser beam, which softens the material in front of the cutting tools and as a result, the yield strength, hardness and strain hardening of the workpiece reduce and deformation behaviour of the hard-to-machine materials (especially ceramics) changes from brittle to ductile [147].
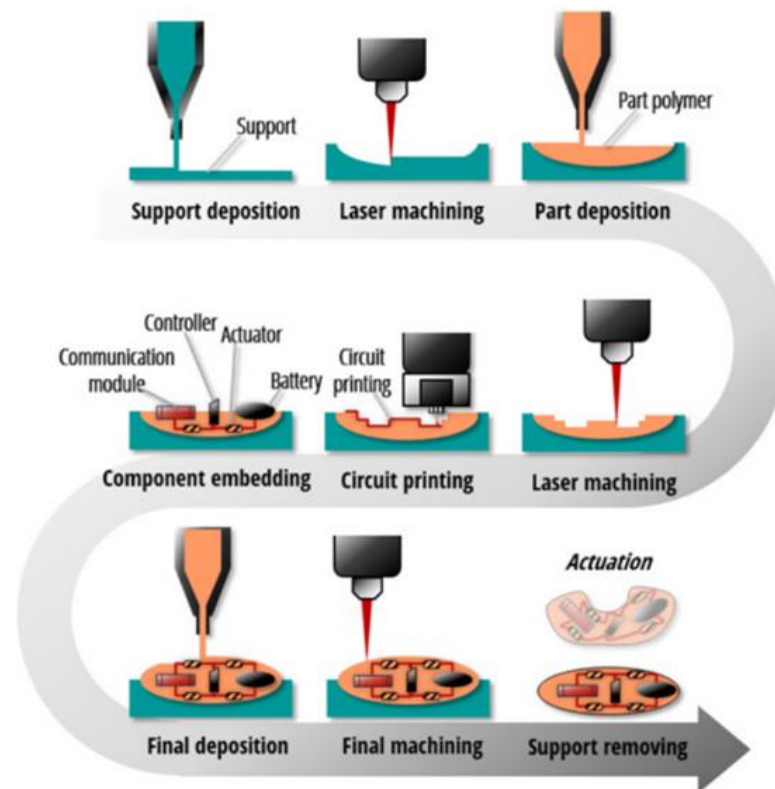
Figure 2.14 Envisaging of LMM as a key enabling processing technology in novel hybrid manufacturing solutions and process chains [139]

Examples from literature, which report about the integration of laser micro-processing as a complimentary subtractive process in hybrid manufacturing platforms and process chains include:

- A combination of micro-milling with LMM was reported to produce complex biotechnology products with feature sizes smaller than the cutting tool diameter without compromising machining time and thus the proposed manufacturing platform benefits from the complementary capabilities of its component manufacturing technologies for a higher removal rates and higher machining resolution, respectively [148];

- A combination of additive manufacturing with laser micro-structuring and micro-polishing for the production of high quality medical implants (hip stem prostheses). In particular, due to higher productivity of the additive manufacturing process, it was employed for the near-net shape fabrication of the medical implant, while the laser micro-structuring and polishing was applied both for the customized functionalizing of the surfaces and also as a post-processing step to improve the surface quality of the implants [149].

- A combination of EDM with LMM to improve the efficiency of drilling micro holes with a diameter of 140 μm in diesel fuel injection nozzles [150]. In addition, micro grooves and complex 3D structures have also been fabricated using this hybrid machining process, where the nano-second laser regime was utilized for the machining of the rough structures prior to the high-precision micro EDM operations, which significantly reduces the tool wear of the electrode [151].

- More examples of other laser-based hybrid manufacturing processes that report on the combination of laser micro-processing with ECM, water-jet, and high-speed abrasive jet machining for the high precision manufacturing of difficult- to-machine prismatic parts could be found in [152].

Despite the capabilities of the laser processing technology to bring a high level of manufacturing complementarity to other MMPs for the formulation of flexible and reconfigurable novel hybrid processes and process chains, the state-of-art laser based hybrid and multi-process manufacturing solutions are not mature enough to fully utilize the manufacturing capabilities of the laser processing technology due to various system-level integration issues both on a local level within the induvial laser systems (discussed in Section 2.2.2) and also on a global level when interfacing the laser process with other complimentary processes in hybrid manufacturing platforms and process chains [100]. It should be noted here that the integration issues in process chains are also recognized in other sequential multi-process fabrication solutions and thus are not limited only to laser-based hybrid manufacturing routes and process chains. For example, the hybrid process designs requiring a sequential combination of manufacturing processes in a single machine set-up could be very challenging due to some dissimilar machining requirements of the integrated processes such as the clamping of the workpieces, the necessary machining workspace, the physical characteristics of the process and also safety considerations [153, 154]. This is demonstrated in a process combination of additive manufacturing with milling, where the proposed hybrid process has to accommodate different manufacturing requirements in a single machining set-up.In particular, the additive manufacturing creates requirements for well controlled environment in order to build parts in layer by layer fashion from powder, while the follow-up subtractive machining introduces specific fixturing requirements to resists the cutting forces and also to protect the machined parts from occasional spatter during the additive manufacturing process [153]. In the context of process chains, a critical interface requirement

is the need for accurate and precise repositioning and referencing of the workpiece in the different machine set-ups of the process chain as this has a direct impact on the overall products' ARR [100, 139, 155]. This is especially important for multi-process manufacturing platforms that integrate laser micro processing, because the lateral machining area defined by the laser beam diameter at the focal plane is often in the range of a few tens of micrometres while the depth of cut from a few microns down to sub-microns [148]. The necessity for the development of flexible interface tools which facilitate the evolution of laser micro-processing into a modular manufacturing technology that can be seamlessly integrated in multi-process manufacturing systems for ''zero-defect'' fabrication of highly complex miniaturized products is on the forefront of the manufacturing technology research agenda, as stipulated in the latest ''H2020 factory of the future'' call for action from the European manufacturing research commission [156]. In particular, special attention is paid to the development of software and hardware integration tools, which enhance the machine tool performance of laser systems and thus to make possible their integration in various multi-process processing solutions for addressing the manufacturing demands for diverse micro-scale application areas [156]. This will enable the scale-up production of miniaturised parts with high ARR that at the same time incorporate different micro-scale functional features.

2.3   Summary of open research issues

Laser micro-processing is attractive manufacturing technology that can address the constantly growing requirements for product miniaturization in many application areas due to the laser technology intrinsic processing characteristics such as: capabilities to process any material, including glasses, ceramics, metals, polymers and composites; and capabilities for high manufacturing flexibility and thus to realize different in-situ processing operations including subtractive, joining and post-processing operations. Nevertheless, the carried out literature review reveals that state-of-art laser micro-processing platforms do not have sufficient technological maturity to provide the required level of machine tool performance in terms of process reliability, predictability, flexibility and robustness. Thus, in compassion to the closed-loop process control of well-established conventional machining technologies, e.g. milling, the laser systems have open-loop control, which impairs their manufacturing capabilities to deliver the required level of machining ARR both in the standalone laser systems and also as an integrated manufacturing technology in hybrid manufacturing platforms and processing chains. Specific open research issues that have to be addressed in

regards to the LMM system' performance as a robust machine tool are summarized as follows:

- *Key Research Issue 1:* Lack of sufficient knowledge about the manufacturing capabilities of LMM systems in terms of machining accuracy, repeatability and reproducibility (ARR). Even though two studies have reported qualitative evaluations of the technological maturity levels of LMM systems [100. 123], there is not a comprehensive analysis of their ARR capabilities yet, which can clearly quantify the contributions of the integrated component technologies to the observed overall machining performance. Thus, comprehensive quantitative studies focused on LMM systems ARR capabilities are of high importance for identifying critical performance issues associated with their components technologies and thus to improve their overall manufacturing capabilities. In addition, such comprehensive quantitative studies could also provide valuable information for identifying system-level integration issues in state-of-art LMM platforms, which impair the synergistic functioning of their integrated component technologies.

- *Key Research Issue 2:* Lack of generic integration tools, which can enhance the reconfigurability, modularity and reliability of laser micro-processing platforms. In particular, such integration tools should offer capabilities for automated geometrical registration of a workpiece in LMM systems prior to executing the machining operations, because the accurate alignment of parts is of critical importance for achieving the required level of machining ARR. In addition, the integration tools should create capabilities: (i) to enable highly accurate and precise positioning of workpieces in LMM platforms; (ii) to provide sufficient flexibility for realizing various LMM configurations; (iii) to provide the required modularity in integrating LMM modules with different primary shaping, processing and inspection stages in process chains.

- *Key Research Issue 3:* Lack of generic software tools to address the open-loop control issues of LMM systems and at the same time to increase their manufacturing flexibility by creating capabilities for realizing complex multi-axis laser processing strategies. In particular, such tools should be designed and implemented: (i) to improve the laser micro processing throughput; (ii) to improve the closed-loop manufacturing control of LMM systems; (iii) to improve ARR in various multi-axis LMM configurations.

- *Key Research Issue 4:* Lack of sufficient implementation strategies of the laser micro-processing as a modular technology that can be seamlessly integrated in multi-process

manufacturing solutions and thus to provide the required manufacturing complementarity to other micro-scale processing technologies for the fabrication of complex products with multi-length scale functional features.

CHAPTER 3
EXPERIMENTAL

Outline of the chapter

This chapter provides detailed description of the equipment, which has been used to perform the experimental work of the research reported in the thesis. In addition, it also introduces generic experimental methods, which are related both to the design and optimization of laser machining operations/routines and also to the analyses of machining results.

3.1 Experimental Equipment

3.1.1 Laser micro-processing system

The laser micro-processing platform employed in this research is schematically shown in Figure 3.1. It integrates complimentary laser system component technologies in order to achieve the required level of reconfigurability for realizing different laser processing operations such as micro-structuring, drilling, texturing and micro-welding and polishing/remelting on a wide range of materials. The next subsections provide a detailed description of the component technologies integrated in the laser processing system employed in this research.
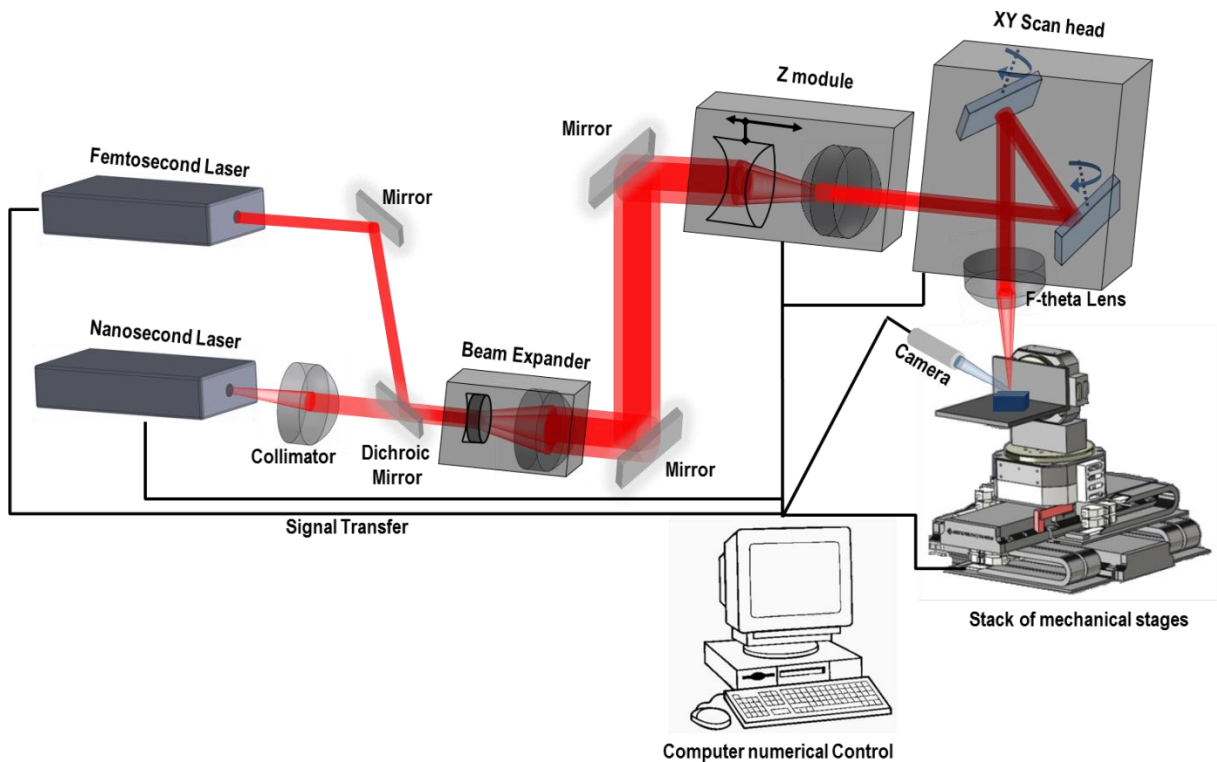
Figure 3.1 Schematic representation of the laser micro-processing platform

3.1.1.1 Laser sources

The LMM platform integrates two laser sources – a short-pulsed (nanosecond) laser source and an ultrashort (femtosecond laser source). The short-pulsed laser source is a SPI redENERGY G4 S-type 50 W nanosecond (ns) fibre laser that operates at a central wavelength of 1060 nm, supports repetitions rates of up to 1 MHz and has varying pulse durations (waveforms) in the range from 15ns to 220ns [157]. The laser architecture is based on the Master Oscillation Power Amplifier (MOPA) configuration, which consists of a master laser (seed laser) and an optical amplifier to boost the output power [158]. In particular, the laser is a DC-powered module based around a dual-stage Yb GTWaveTM fibre amplifier system with an optical seed pulse generated by a single-mode semi-conductor (master-oscillator) laser diode [159]. The laser source also possesses the capability to operate in continuous wave (CW) mode with modulation. It is equipped with a beam delivery collimator attached to the laser source fibre exit to provide a highly collimated beam with a nominal beam diameter of 3 mm [159]. Detailed specifications of the laser source are provided in Table 3-1.

Table 3-1 Detailed specification of the SPI G4 S-type nanosecond laser source

Parameter	Units	Value
Average Output Power	W	50
Output power variation	%	1.4
Maximum Pulse Energy	mJ	0.71
Maximum Peak Power	kW	15
Central Emission wavelength	nm	1060
Emission Bandwidth	nm	<10
Pulse Width (duration) range	ns	15-220
Beam Quality (M^2)	-	<1.3
Astigmatism	1/Rayleigh length	<0.3
Full-angle divergence (collimator)	mrad	0.5
Circularity	%	90
Beam diameter (collimator)	mm	3
Degree of Polarization	%	<20

The ultrashort laser source is an Amplitude system Satsuma Ytterbium-doped fibre laser that has a maximum average power of 5W, operates at a central wavelength of 1030 nm, has a maximum repetition rate of 2 MHz and provides pulse duration of less than 400 fs [160]. The laser architecture is based on mode-locking laser configuration [161], which employs the Chirped-pulse Amplification principle [162]. The technical specification of the fs laser source is provided in Table 3-2.

Table 3-2 The technical specification of the Amplitude Systems Satsuma laser source

Parameter	Units	Value
Average Output Power	W	5.4
Output power variation	%	2
Maximum Pulse Energy	μJ	10.8
Maximum Peak Power	MW	33.5
Central Emission wavelength	nm	1030
Emission Bandwidth	nm	7.5
Pulse Width (duration)	fs	310
Beam Quality (M^2)	-	<1.3
Astigmatism	1/Rayleigh length	<0.5
Full-angle divergence	mrad	2
Circularity	%	87
Beam diameter	mm	2
Polarization Type	-	Linear (S-type)

3.1.1.2 Mechanical stages

The LMM platform used in this research integrates five mechanical axes, in particular three linear stages (X, Y and Z axes) with maximum travel of 300 mm and two rotary axes (A – rotations around X axis and C- rotations around Z axis) with no limits on rotational travel.

The XY table includes two direct-drive Aerotech linear stages, in particular a PRO165LM-0300 stage mounted on a PRO225LM-0300 stage [163, 164]. The combined XY positioning accuracy of the XY table is +/-4μm. The Z stage, PRO115-300 [165], is used to perform accurate and repeatable positioning of the workpieces at the right focal distance for the laser machining operations with positioning accuracy of 10 μm. The maximum speed of the three linear stages taking into account their load capacities is 300mm/s [163-165]. The assembly of two high precision rotary axes are mounted onto the XY table and are Aerotech ADRS-150, which provide rotational positioning accuracy of 48 μm and have maximum rotational speed of 600 rpm [166]. All mechanical stages are equipped with High Accuracy Linear And Rotary (HALAR) Aerotech option, which provides interferometer calibration and error mapping of an individual axis where micron level linear errors are analysed and the resulting calibration information is included as a look-up table to perform movements with extremely high accuracy and repeatability [167].

3.1.1.3 Optical axes

The LMM platform also integrates a state-of-art Newson 3D optical beam deflection system in order to realize beam spot movements with high dynamic. The dynamic capabilities of the X and Y scanning mirrors are 25 rad/s., their maximum angular excursion is 800 mrad, their positioning repeatability is better than 15 μrad and their tracking error is 110 μs [168].

3.1.1.4 Focusing lenses

The system is equipped with two exchangeable telecentric lenses with focal lengths of 100 mm and 160 mm, respectively in order to focus the laser beam on a flat field and with a perpendicular angle of incidence and with the desired spatial laser beam characteristics. Both lenses are made of fused silica and are optimised for high performance with ultrashort pulse lasers that operate at the near-infrared electromagnetic spectrum (1030-1060 nm) [169]. Based on the specifications of the 3D optical scanning head, the 3D working envelopes of the optical axes are 35mm (X) x 35 mm (Y) x 6 mm (Z) and 60mm (X) x 60 mm (Y) x 10 mm (Z) with the 100 mm focal length lens and 160 mm focal length lens, respectively. Furthermore, the focal beam spot diameters are 30 μm and 60 μm with the 100 mm and 160 mm lens, respectively.

3.1.1.5   Beam delivery path components

Figure 3.2 provides a detailed schematics layout of the laser system optical beam delivery path from the laser sources exits to the laser material interaction working envelope defined by the telecentric lens and the 3D optical scanning head system. The optical beam delivery path is situated on a granite frame structure with a passive isolation to limit disturbances from the surrounding environment and also to facilitate integration of optical components in the beam delivery path. In particular, the beam path integrates the following optical components:

- Mirrors to guide the beam from the laser source to the optical scanning head. The mirrors are made of fused silica, have dual coating for the fundamental (1064 nm) and the second harmonic (532 nm) wavelengths of the laser sources and have reflectivity efficiency higher than 99% for minimum losses when guiding the laser beam [170].

- A Dichroic mirror ensures that the two laser sources can share the same beam delivery path, in particular the SPI laser beam is transmitted through the dichroic mirror, while the Satsuma laser beam is reflected from it [177].

- Two laser beam polarizer units are available to obtain the desired beam polarization. In particular, a quarter-wave plate is used to convert the linearly polarized beam into circularly polarized beam, while a half-wave plate is used to obtain either s- or p- type linear beam polarizations depending on the initial polarization state of the laser beam. Both beam polarizers are zero-order wave plates for minimum retardance sensitivity on temperature and incident beam angle. The wave plates are made of crystalline quartz and have reflectivity losses lower than 1% [171].

- A variable beam expander is utilized for spatial laser beam conditioning in order to achieve the desired focal beam spot diameter and depth of focus. The expansion range of the beam expander is X2-X8, while its transmission efficiency is better than 97% [172].
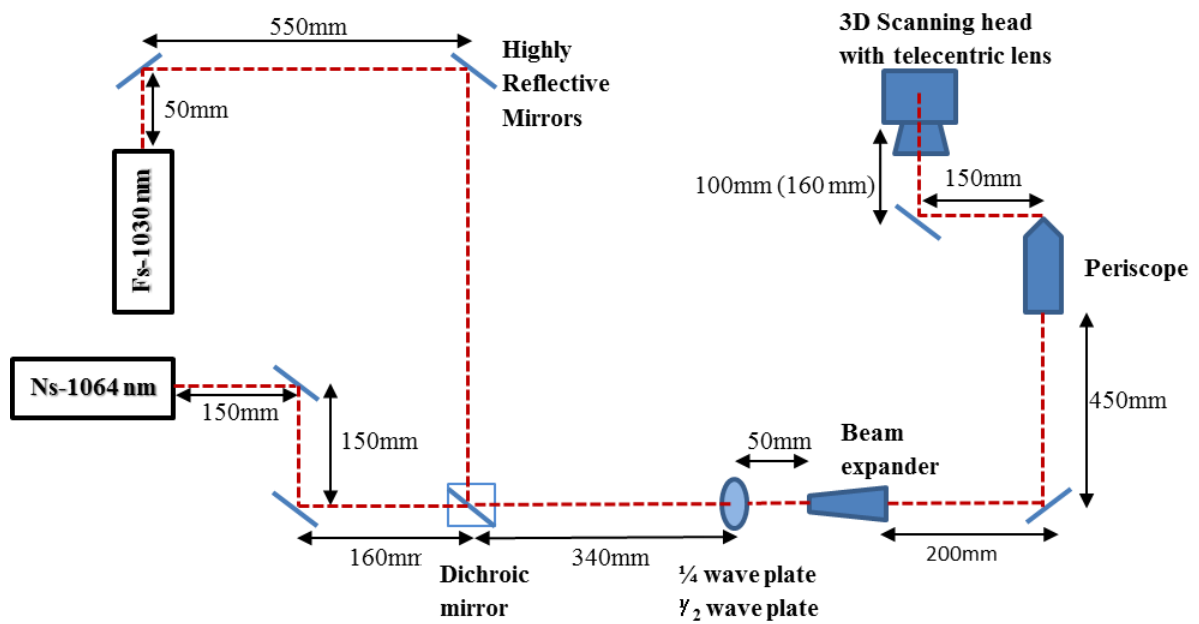
Figure 3.2 Detailed schematics of the components layout in the optical beam delivery path of the laser system

3.1.1.6 Auxiliary components

In order to meet the British Standards for Health and Safety regulations of laser products, the platform is equipped with fume extractor to remove material particles from the system during the ablation process and also protective window is installed to shield direct exposure of human beings to laser radiation [173]. Furthermore, the laser system integrates high resolution optical camera [174] and a confocal microscope [175] to facilitate the calibration of the focusing lens and the manual setting up of workpieces in the workstation.

3.1.2 Analytical equipment

3.1.2.1 Focus Variation optical microscope

Characterization of machining results in terms of accuracy, repeatability and reproducibility is performed with Focus Variation (FV) technology optical microscope, namely Alicona InfiniteFocus (IF) G5 [176]. It has x5, x10, x20, x50 objective and x100 lenses that provide lateral resolution of 3.52 μm, 1.76 μm, 0.88 μm, 0.64 μm and 0.44 μm and vertical resolution of 0.41 μm, 0.1 μm, 0.05 μm, 0.02 μm and 0.01 μm, respectively [176]. The system is equipped with three mechanical axes with travel range of 100 mm in X, Y and Z axes for measurement envelopes bigger than the field of view of the objective lenses. The measurement repeatability of the system is 0.12 μm, 0.03 μm, 0.01 μm, 0.003 μm and 0.001 μm for x5, x10, x20, x50 and x100 objective lenses, respectively. The system also has a set of

software tools (MeasureSuite), which allow analyses of measurement data both in terms of form and surface topography [178]. All analyses conform to the relevant ISO standards: profile roughness and surface texture analyses conform to ISO 4287/4288 [179] and 3D form analyses conform to the ISO 1101 [180].

3.1.2.2 Laser spatial beam analyser and laser pulse power meter

A scanning slit beam profiler, shown in Figure 3.3(a) is utilized to perform real-time measurements of the laser beam spatial profile at any plane along its axis of beam propagation. It employs Si detector and measurement resolution and accuracy are 0.1 μm and 0.5 μm, respectively [181]. The beam analyser is capable of measuring tightly focused laser beams (down to 2 μm in dimeter) with the Knife- Edge mode [181]. Measurements of the spatial beam profile parameters such as beam divergence, beam diameter, and Rayleigh length conform to the ISO 11146-2 [182].

In addition, a laser pulse power meter, shown in Figure 3.3(b), is utilized to record the pulse average power.
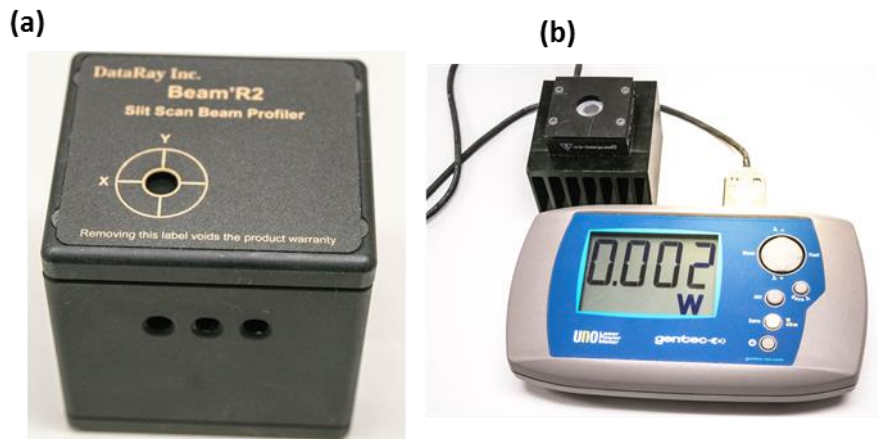
Figure 3.3 (a) A scanning slit beam profiler and (b) a laser pulse average power meter

3.2 Experimental methods

3.2.1 Fundamental laser processing parameters

This subsection introduces fundamental theoretical relations for deriving important laser machining parameters. Equations 3.1, 3.2, 3.3 and 3.4 are used to calculate Peak Power (P_{peak}), Laser pulse energy (E), Maximum pulse energy intensity or Peak fluence (F_0) and Spatial Fluence profile (F_r), respectively.

$$P_{peak} = \frac{P}{\tau}$$
(Equation 3.1)

$$E = \frac{P}{f} \qquad \text{(Equation 3.2)}$$

$$F_0 = \frac{2E}{\pi w_0^2} \qquad \text{(Equation 3.3)}$$

$$F_r = F_0 e^{\frac{-2r^2}{w_0^2}} \qquad \text{(Equation 3.4)}$$

where P is average power, τ is laser pulse duration, f is pulse frequency, w_0 is laser beam radius ($1/e^2$ clipping level) and r is the distance from the beam centre.

Figure 3.4 also introduces important optics parameters, which determine the spatial characteristics of a focused Gaussian laser beam.

w₀ – beam spot radius at focal plane
z_R – Rayleigh length
Θ_d – full divergence angle
DOF – depth of focus
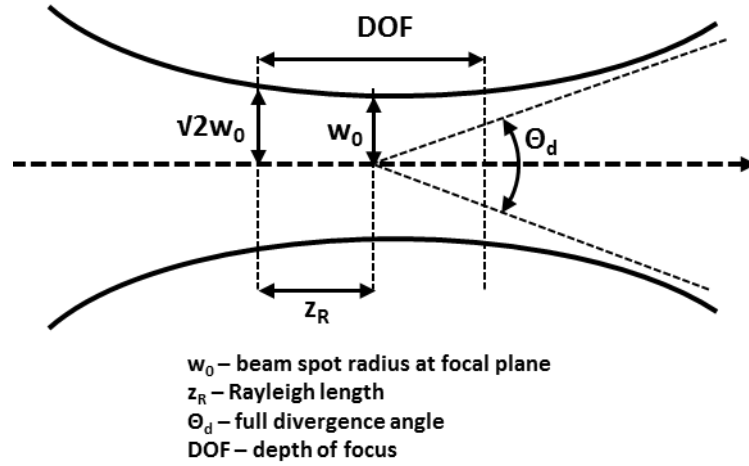
Figure 3.4 Spatial Parameters of a focused Gaussian laser beam

The theory of Gaussian beam optics explains in details the laser beam propagation through the methods of wave optics [183]. Equations 3.5, 3.6, 3.7, and 3.8 can be used to calculate the laser beam diameter at the focal plane ($2w_0$), laser beam diameter at any plane along the axis of the laser beam propagation ($2w_z$), Rayleigh length (z_R), and the depth of focus of the laser beam (DOF), respectively.

$$2w_0 = \frac{4M^2\lambda(FL)}{\pi D_0} \qquad \text{(Equation 3.5)}$$

$$2w_z = 2w_0\sqrt{1 + \left(\frac{z}{z_R}\right)^2} \qquad \text{(Equation 3.6)}$$

$$z_R = \frac{\pi \times w_0^2}{\lambda \times M^2} \qquad \text{(Equation 3.7)}$$

$$DOF = \frac{8M^2\lambda(FL)^2}{\pi D_0^2} \qquad \text{(Equation 3.8)}$$

where M^2 is Gaussian beam quality factor, λ is the laser wavelength, FL is the focal length of the focusing lens, z is an arbitrary distance from the focal the focal plane along the axis of laser beam propagation and D_0 is the input beam diameter to the focusing lens.

Laser machining strategy has a strong influence both on resulting surface topography and machining throughput and therefore different removal strategies are applied to meet the manufacturing requirements [184]. The parameters used in designing machining strategies are hatch distance, which represents the distance between neighbouring laser beam tracks and pulse distance, which determines the distribution of laser pulses along a laser beam track. Equations 3.9 and 3.10 calculate the pulse distance (*PD*) and percentage pulse overlap *(%PO)*, respectively.

$$PD = \frac{V_{scan}}{f}$$ (Equation 3.9)

$$\%_{PO} = \left[1 - \frac{V_{scan}}{2w_0 f}\right] \times 100$$ (Equation 3.10)

where V_{scan} is the scanning speed of the laser beam.

3.2.2 Ablation Threshold

Determination of the single-shot ablation threshold intensity for the materials, which have been under investigation in this research, is performed in accordance to the Liu's experimental method, which relates the diameter of the ablated area (D_{abl}) to the ablation threshold fluence (F_{th}) [185]. Equation 3.11 formulates this relation.

$$D_{abl}^2 = 2w_0^2 \ln\left(\frac{F_0}{F_{th}}\right)$$ (Equation 3.11)

Furthermore, reduction of material ablation threshold fluence is evident in multi-shot laser ablation scenario due to the existence of incubation effects [186]. The incubation effects affect the material response in multi-shot laser processing and can be explained with the increase in energy coupling efficiency, which is responsible for the reduction of the material reflectance after the first laser pulses are irradiated on the material substrate [187]. Thus, the multi-shot ablation threshold fluence can be calculated with Equation 3.12.

$$F_{th}(N) = F_{th}(1) \times N^{S-1}$$ (Equation 3.12)

where *N* is the number of incident laser pulses and *S* is material incubation coefficient.

The experimental method that can be used to determine the ablation threshold fluence of a material can be summarized as follows:

- Step 1: Create single- (multi-) shot pulse craters with incrementing laser pulse energies.
- Step 2: Characterize the diameter of the ablated craters.

- Step 3: Plot the squared diameters of the ablated craters versus natural logarithm of the pulse energies (D_{abl}^2 vs $ln(E)$).
- Step 4: Derive a best straight line fit on the plotted data.
- Step 5: The gradient (slope) of the fitted straight line gives the w_0^2.
- Step 6: Apply Equation 3.3 to replace pulse energy (E) with laser fluence (F_0).
- Step 7: Derive the x-intercept of the best straight line fit to find the material ablation threshold fluence.

Figure 3.5 also provides a graphical description of the methodology that is used to determine the ablation threshold of a material. The material that has been used to demonstrate the methodology in Figure 3.5 is silicon.

STEP 1: Lines of single-shot craters with incrementing laser pulse energies.
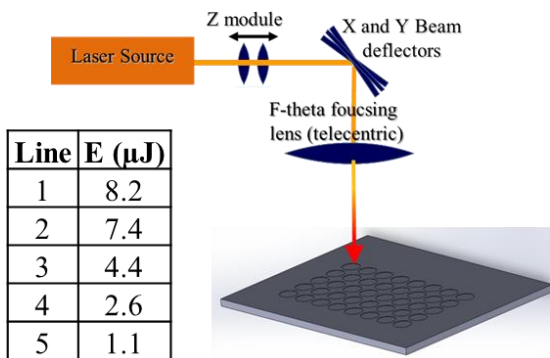
STEP 2: Measure the radius/diameter of the ablated craters.

Line	E (μJ)
1	8.2
2	7.4
3	4.4
4	2.6
5	1.1

w_0=3.7μm w_0=7.8μm w_0=9.1μm w_0=9.5μm w_0=10 μm
E=1.1μJ E=2.6μJ E=4.4μJ E=7.4μJ E=8.2μJ
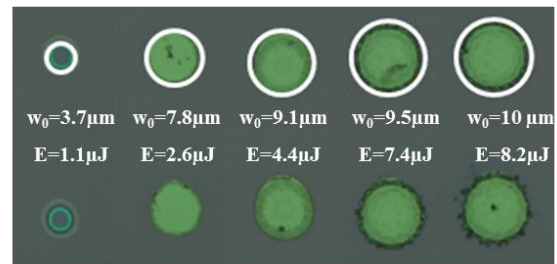
STEP 3 -7: Plot the squared diameters of the ablated craters versus natural logarithm of the laser fluence and obtain the laser beam spot diameter and the material ablation threshold fluence

$y = 160.79x + 216.79$
$R^2 = 0.9622$
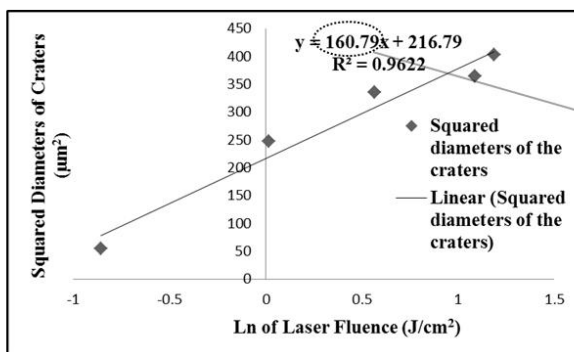
$w_0^2 = 160.79$ um^2 → w_0= 12.7um

$0=160.79(ln(F_{th})+216.79$ → $ln(F_{th}) = -1.348$

$F_{th} = 0.26$ J/cm^2

Figure 3.5 A graphical demonstration of the application of the methodology to determine the ablation threshold of silicon

3.2.3   Accuracy, Repeatability and Reproducibility

According to ISO 5725-1, accuracy is the closeness of a measurement result to a pre-defined reference (nominal) value [188]. On the other hand, repeatability and reproducibility refer to the precision of the measurement results, where ISO 5723-1 defines precision as the closeness of agreement between independent test results obtained under stipulated conditions. In order to differentiate between the two precision terms, ISO 5723-1 provides the following definitions for the repeatability and reproducibility [188]:

- Repeatability is the precision obtained, under the identical conditions, when independent test results are obtained with the same method, on identical test items, in the same laboratory, by the same operator, using the same equipment, and within short intervals of time. Thus, repeatability leads to an estimate of the minimum value of precision.

- Reproducibility is the precision obtained, under changing conditions, when independent test results are obtained with the same method, on different test items, or in different laboratories by different operators. Thus, reproducibility leads to an estimate of the maximum value of precision.

Figue 3.6 also provides graphical definitions for accuracy, repeatability and reproducibility. In particular, Figure 3.6a shows that Result 1(green dot) is more accurate than Result 2 (red dot), because it is closer to the target value (black dot). Figure 3.6b shows that Set 1 (green dots) has higher repeatability than Set 2 (red dots), because the spread of results in Set 1 is less than that in Set 2. Figure 3.6c shows that Set 3 has higher reproducibility than Set 4, because the spread of results in Set 3 is less than that in Set 4. Finally, in order to differentiate between repeatability and reproducibility, it is worth mentioning that both measurands quantify precision, but reproducibility defines the precision under changing conditions, e.g. on a number of different samples, over longer intervals of time.
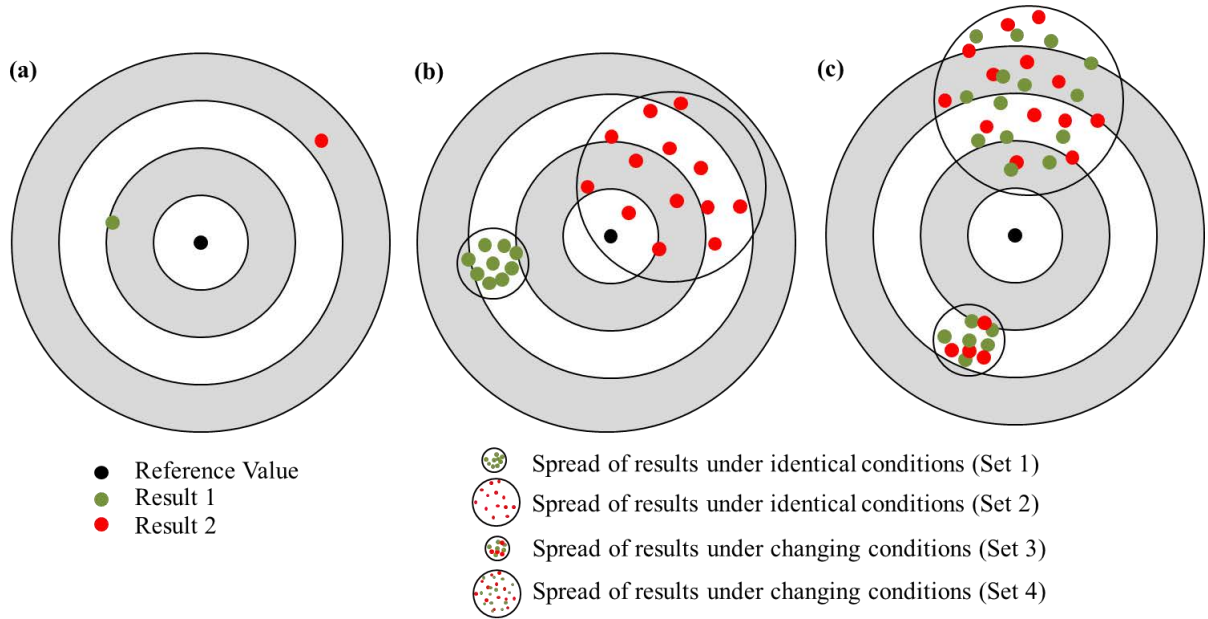
Figure 3.6 Graphical definitions for (a) Accuracy, (b) Repeatability and (c) Reproducibility

3.2.4 Evaluation of the total measurement uncertainty

Evaluation of measurement uncertainty in this thesis was performed in accordance to the guidelines of the United Kingdom Accreditation Service (UKAS) Publication M 3003 [189], the European co-operation for Accreditation (EA) publication EA-4/02 [190] and the National Physical Laboratory Guide No. 11 (Issue 2) [191]. In order to perform comprehensive evaluation of the measurement uncertainty, both Type A and Type B uncertainty were characterized, where:

- Type A uncertainty (U_A) - evaluation of uncertainty is carried out using statistical analysis of a series of observations [189-191]

- Type B uncertainty (U_B) – evaluation of uncertainty using methods and information other than statistical analysis. This could be information from past experience of the measurements, from calibration certificates, manufacturer's specifications, from calculations, from published information, and from common sense [189-191].

The Type A uncertainty (U_A) was calculated according to Equations 3.13-2.15:

$$\bar{x} = \frac{\sum_{i=1}^{n} y_i}{n} \qquad \text{(Equation 3.13)}$$

$$sd = \sqrt{\frac{\sum_{i=1}^{n}(x_i - \bar{x})^2}{(n-1)}} \qquad \text{(Equation 2.14)}$$

$$U_A = \frac{sd}{\sqrt{n}} \qquad \text{(Equation 2.15)}$$

45

where sd is the standard deviation of the data set, x_i is the result of the ith measurement, n is the total number of measurements, and $\overline{x}$ is the arithmetic mean of the n results considered.

It should be mentioned that Type A uncertainty calculations in this thesis were achieved based on at least 10 repetitive measurements based on guidelines in [189-191] unless otherwise stated in the respective analytical sections of the thesis.

After Type A and Type B uncertainties were obtained, the combined uncertainty (U_C) was calculated in accordance to Equation 3.16 by treating the uncertainties as uncorrelated:

$$U_C = \sqrt{(U_A{}^2 + U_B{}^2)}$$ (Equation 3.16)

It is also worth mentioning that Equation 3.16 was also applied to calculated overall Type B uncertainty, when it contains more than one uncertainty components at the same time from different sources of information like calibration certificate and manufacturer's specifications.

Finally, the total uncertainty (U_T) can be found by Equation 3.17, in particular multiplying the expanded uncertainty with a coverage factor (k), which accounts for the ''level of confidence'' [189-191].

$$U_T = k \times U_C$$ (Equation 3.17)

Detailed explanations for the different coverage factors with various data distribution types can be found in [189]. Nevertheless, for normal data distribution some cover factors are:

- k=1 for a confidence level of 68 %;
- k=1.64 for a confidence level of 90 %;
- k=2 for a confidence level of 95%;
- k=3 for a confidence level of 99.7%.

Since the total uncertainty is given most commonly at the 95% confidence level [191], the scaling factor used for calculating the total uncertainties in this thesis is k=2.

Figure 3.7 also presents the step-wise procedure, which was used for evaluating the total uncertainty of measurands in this thesis.

Step 1:
Determine the measurand.

Step 2:
Carry out the measurements of the machined geometries and perform measurement analysis procedures

Step 3:
Determine the mean of the measurand and calculate Type A uncertainty of the measurand mean.

Step 6:
Express the total uncertainty in terms of a coverage factor and state a level of confidence.

Step 5:
Calculate the expanded uncertainty.

Step 4:
 Estimate other contributing sources of uncertainty:
• Calibration certificate
• Equipment technical specifications
• Prior knowledge for the uncertainties of the measurement procedures

Figure 3.7 Step-wise procedure for evaluating the total uncertainty of measurands

CHAPTER 4

INVESTIGATION OF ACCURACY, REPEATABILITY AND REPRODUCIBILITY OF STATE-OF-ART LASER MICROMACHINING PLATFORMS

Outline of the chapter

This chapter reports a systematic quantitative study for evaluating the accuracy, repeatability and reproducibility (ARR) of a state-of-art LMM system in an attempt to address *Research Issue 1* discussed in Chapter 2. The proposed study evaluates the effects of key component technologies on ARR capabilities of LMM systems. In particular, the ARR capabilities of the optical and mechanical axes are investigated when they are utilised separately or in combination and thus to quantify the individual contributions of the integrated component technologies to the overall laser machining errors. The study was performed on four different LMM platform implementations and thus to provide a reliable and objective ''snapshot'' of current ARR capabilities of state-of-art LMM systems. In addition, the chapter also introduces a specialized experimental technique for quantifying the dynamic capabilities of z-modules and thus to judge better about their negative effects in the laser micro-processing of complex free-form (3D) surfaces.

The research reported in this Chapter refers to Publications 1 and 3 from the List of Publications.

4.1 Introduction- Machine specifications of the investigated laser systems

The carried out literature review in Chapter 2, revealed that there is a clear lack of reliable and objective information about the manufacturing capabilities of state-of-art LMM systems in terms of their machining ARR. In an attempt to address this gap of knowledge, an empirical investigation of ARR of state-of-art LMM platforms is presented in this chapter. An important consideration for the objectivity of the performed study was the requirement to characterize the representative ARR capabilities of state-of-art LMM systems on more general level rather than commenting on the subjective manufacturing capabilities of an individual laser platform

implementation. Therefore, four LMM systems (denoted as Systems A, B, C and D in this research), which were implemented by different laser system integrators, were investigated in the study. In addition, the systems were located at different locations and were operated by different machine operators. In this way, the study attempted to objectively identify laser machining ARR shortcomings in the LMM implementations on a more general level rather than reporting findings related to either a specific laser system integrator or particular LMM system. The technical specifications of the component technologies of the four investigated LMM systems are provided in Table 4-1.

Table 4-1 Technical specifications of component technologies (as provided be vendors)

Laser System	A		B		C	D	
Optical axes							
XY scanning head							
Max scanner speed (XY)	25 rad/s		25 rad/s		2 m/s with 160 mm focusing lens	2.5 m/s with 163 mm focusing lens	
Pos. resolution [µrad]	<12		< 12		10	<8	
Thermal drift [µrad]	< +/-12		< +/-12		<25	<20	
Tracking error [µs]	110		110		110	<20	
Focusing lens system							
Focal length [mm]	100	160	100	160	160	100	163
Focusing field [mm]	35×35	60×60	35×35	80×80	100×100	35×35	80×80
Beam spot size [µm]	30	60	20 - 56	20 - 90	40	20-56	40-90
Z-module							
Focusing range [mm]	6	10	6	10	-	10	
Max. speed	NA		NA		NA	NA	
Mechanical axes							
XY axes/stage							
Travel [mm]	300		300×300		160	600×450	
Max.travel speed [mm/s]	500		500		300	500	
Resolution [µm]	0.25		0.25		0.01	1.0	
Accuracy per axis [µm]	+/- 2		+/- 2		+/- 0.75	+/- 0.5	
XY Accuracy (2D) [µm]	+/- 4		+/- 4		-	+/- 1.0	
Z axis/stage							
Travel [mm]	300		300		300	200	
Max.travel speed [mm/s]	50		50		10	220	
Resolution [µm]	0.5		0.5		0.1	1.0	
Accuracy per axis [µm]	+/- 1		+/- 1		+/- 0.75	+/- 1.0	
XY Accuracy (complete 2D travel) [µm]	+/- 10		+/- 10		-	+/- 10	

4.2 Quantitative investigation of LMM systems' machining capabilities

4.2.1 Planning of machine performance evaluation tests

A sequence of six tests, described in Table 4-2, was planned in order to assess the ARR capabilities of optical and mechanical axes of laser machining platforms when they were utilised separately or in combination. Figure 4.1 shows the test geometry in Tests 1, 2, 4 and 5, Figure 4.2 shows the test geometry in Test 3 and Figure 4.3 shows the test geometry in Test 6. In addition, Appendix 1 provides detailed engineering drawings of the six tests. Unless otherwise stated in the induvial test descriptions, the following laser parameter settings were used for producing the test geometries: Satsuma femtosecond laser source, laser energy of 8 µJ, scanning speed (optical axes) of 1000 mm/s, and scanning speed (mechanical stages) of 100 mm/s.
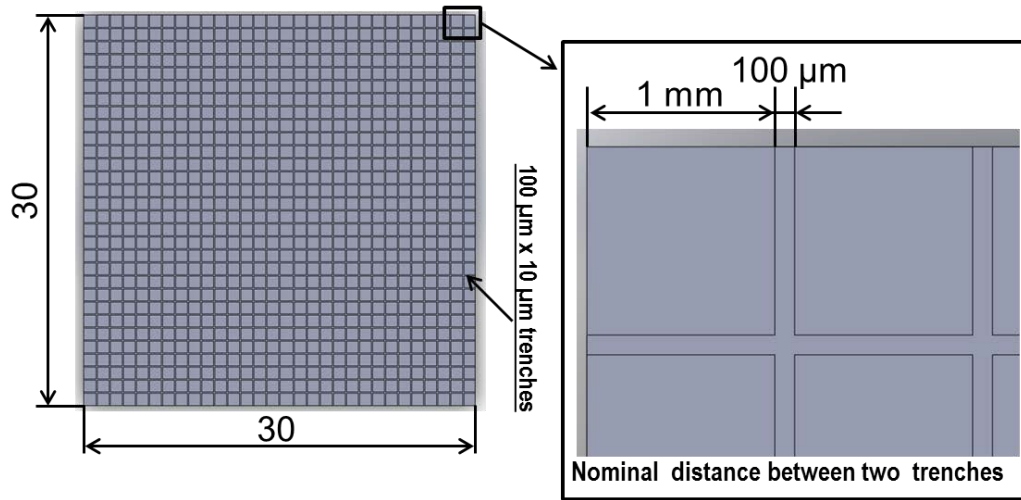
Figure 4.1 Arrangement of the laser ablated trenches in the test geometry for tests 1, 2, 4 and 5 of the quantitative study
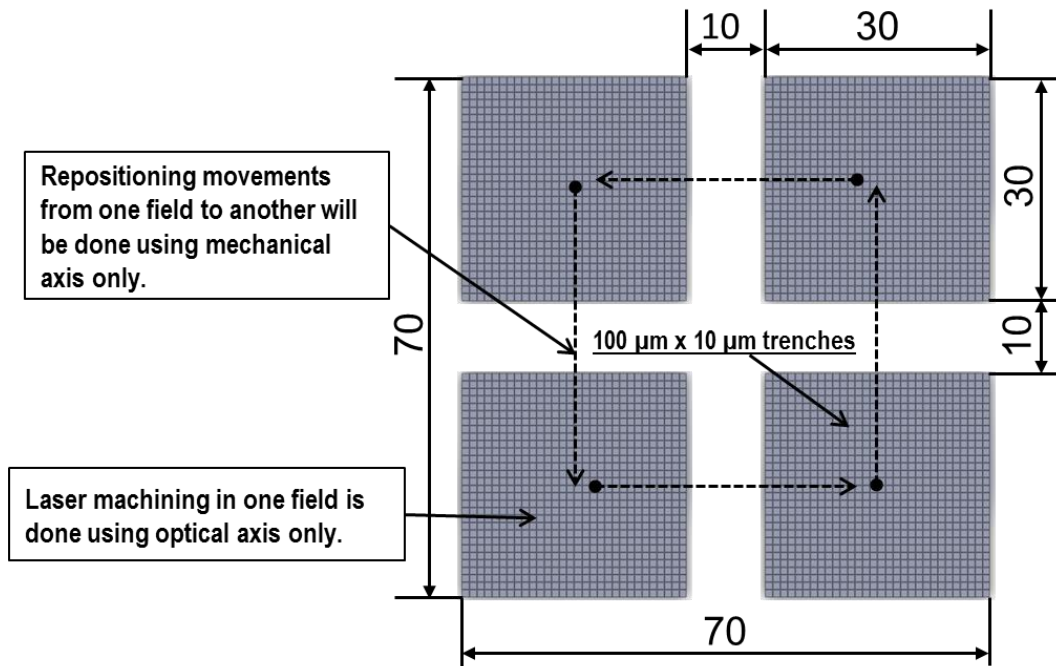
Figure 4.2 Test geometry in test 3 of the quantitative study

Table 4-2 Test plan of the proposed quantitative study

Test No.	Test description	Component technologies
1.	Machining of 30×30 mm fields with perpendicular intersecting trenches to structure stainless steel (SS304) plates. The nominal width and depth of the trenches are 100 and 10 μm, respectively while they are 1 mm apart along the X and Y axes. The test quantifies the machining accuracy of X-Y scan heads.	1) X and Y beam deflectors 2) Focusing lens
2.	The same perpendicular intersecting trenches as in Test 1 are produced on SS304 plates with a stationary beam and moving mechanical axes. The test assesses the accuracy of the X-Y mechanical stages.	1) X and Y mechanical stages 2) Focusing lens
3.	Four 30×30 mm fields with perpendicularly intersecting trenches as in Test 1 are machined on a 70×70 mm area of SS304 plates. The structuring is carried out using the optical axes only, whereas the repositioning between the fields is carried out using the mechanical axes only. The test is intended to quantify the machining ARR when both XY scan heads and XY mechanical stages are used in combination.	1) X and Y beam deflectors 2) X and Y stages 3) Focusing lens
4.	Test 1 is repeated after adjusting the beam spot diameter at the focal plane using a beam expander and then calibrating the scan head. The test quantified the effectiveness of the calibration routines after conditioning the beam diameters.	1) X and Y deflectors 2) Beam expander 3) Calibration routine 4) Focusing lens

5.	Machining of 30×30 mm fields with perpendicular intersecting trenches is performed with different scanning speeds (100, 500 and 1500 mm/s) on stainless steel SS304 plates tilted at 9° along either X or Y axes. The test is carried out using the optical axes and the Z module of the scan heads. The test quantifies the combined effect of optical axes and Z-module on ARR when laser processing 3D surfaces.	1) X and Y deflectors 2) Z-module 3) Focusing lens
6.	Producing arrays of separated dimples on SS304 plates that are normal and tilted (at 0°, 5°, 10°, 15° and 20° along Y-axis) in regards to the beam. Each dimple is produced with a sequence of 20 pulses (SPI laser source was used) on the "fly" (20 passes of the bean) with five scanning speed settings (100, 500, 1000, 1500 and 2000 mm/s) and thus to qualitatively assess the effects of the dynamic capabilities of Z-module on machining ARR.	1) X and Y beam deflectors 2) Z-module 3) Focusing lens

The test geometries produced on the four LMM systems are given in Table 4-3.
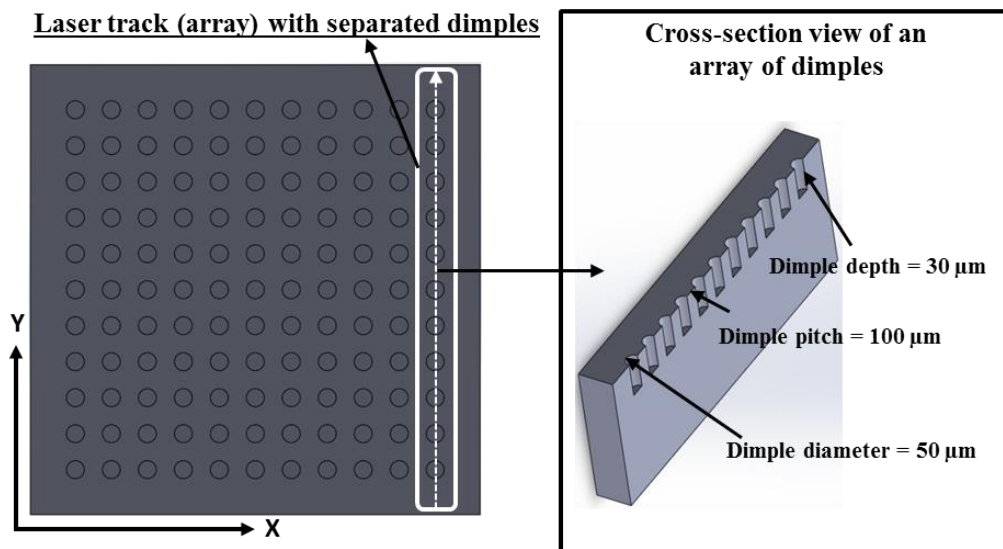
Figure 4.3 Test geometry in test 6 of the quantitative study

Table 4-3 Test geometries produced on the four LMM systems

Laser system	Test No.					
	1	2	3	4	5	6
A	x	x	x		x	x
B	x	x		x		
C	x		x	x		
D	x	x	x	x		

4.2.2 Measurement procedures

4.2.2.1 General measurement considerations and uncertainty

An important consideration in designing the measurement procedures for Test 1 to 5 was the requirement to minimize the contributions of laser material interactions in investigation the

systems' ARR and thus to obtain objective information only for the ARR capabilities of optical and mechanical axes. This was achieved by measuring only the relative distances between the trenches, while their widths, depths and resulting surface quality were not considered as shown in Figure 4.4, which depicts representative measurements between two trenches from the produced test geometries in Tests 1 to 5.
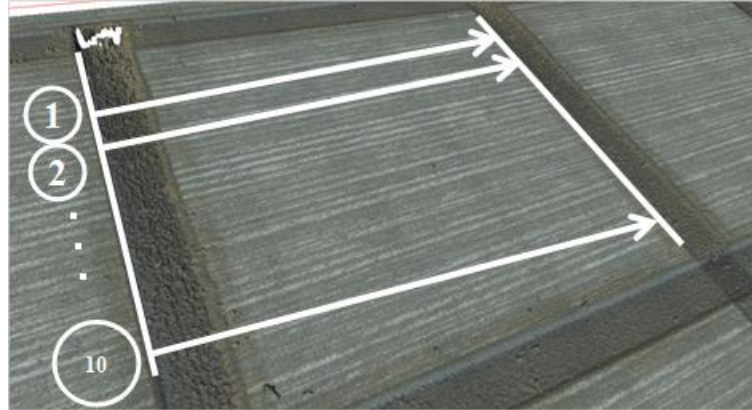
Figure 4.4 Representative measurements between two corresponding trenches from the produced test geometries in Tests 1 to 5 of the quantitative study

In contrast, since Test 6 attempts to qualitatively assess the effects of the dynamic capabilities of Z-module on machining ARR, the measurement procedure in Test 6 takes into consideration the laser material interaction effects. In particular, by analysing the volumetric changes of the dimples in the produced laser tracks at different speeds and tilt angles, it was possible to extract information for the geometrical consistency of dimples in terms of their depths and dimeters and thus to judge about the effects of Z-module on machining ARR. More specifically, any inconsistency of the volumetric morphologies of dimples along a laser track produced at a specified scanning speed and tilt angle could be attributed to the dynamic limitations of the Z-module, exemplified by its inability of dynamically preserving the focal plane of the laser beam on the tilted workpiece surface within the laser track. Figure 4.5 shows a representative measurement in Test 6, which assess the volumetric characteristics of a dimple in a laser track.
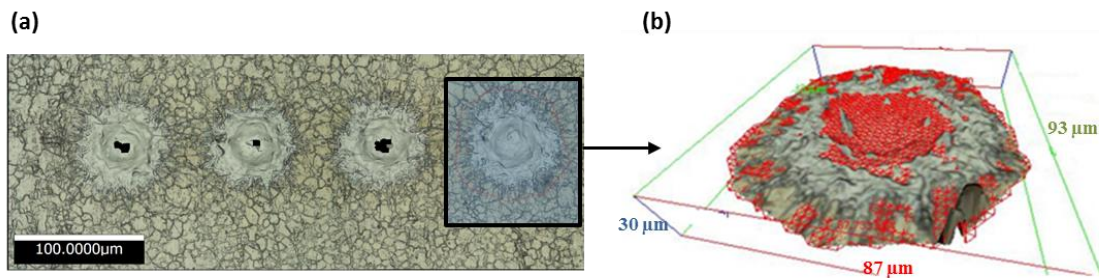
Figure 4.5 A representative volumetric analyses of a dimple in a laser track in Test 6: (a) an array of laser dimples produced at a specified scanning speed and tilt angle and (b) evaluating volumetric characteristics of a dimple in regards to its depth and diameter

The measurements on laser structured surfaces were carried out using the FV technology Alicona G5 IF microscope. The x20 lens, which provides lateral and vertical resolution of 0.88 μm 0.05 μm, respectively, was used for the measurement of laser produced geometries in Tests 1, 3, 4, 5 and 6. The x50 lens with lateral resolution and vertical resolution of 0.44 μm 0.02 μm, respectively, was used in Test 2. Furthermore, the total uncertainty of the measurement procedures with the x20 lens and x50 was calculated (based on the measurement uncertainty evaluation procedure presented in Chapter 2) to be 1.1 μm and 0.2 μm at a confidence level of 95%, respectively. Appendix 2 also provides comprehensive calculations for the total uncertainty of the measurement procedures both with the x20 lens and with the x50 objective lenses.

The following subsections provide detailed descriptions of the analytical steps used for evaluating the machining ARR in the performed tests.

4.2.2.2 Evaluation of LMM systems ARR capabilities with the proposed tests

For Tests 1, 2, 4 and 5, the measurements were carried out at the two diagonally opposite corners of the structured fields as the lowest accuracy of the beam deflectors were expected there while the highest in the centre of the scan fields. In particular, the 20X magnification was used to scan the areas between the 1st and 11th trenches in Tests 1, 4 and 5 and also to measure the distances between 1st and 3rd, 1st and 5th, 1st and 7th, 1st and 9th and 1st and 11th trenches along both horizontal (X-axis) and vertical directions (Y-axis). A similar measurement procedure was applied in Test 2, however only the distances from 1st to 2nd, 3rd, 4th and 5th trenches were measured due to the large size of the scan data generated with the 50X objective. The schematic diagrams of the measured regions in Tests 1, 2, 4 and 5 are depicted in Figure 4.6(a) and (b). The machining accuracies of the beam deflectors and the

stages of the four LMM systems analysed in this comparative study were then determined by comparing the nominal values with the measurement results.
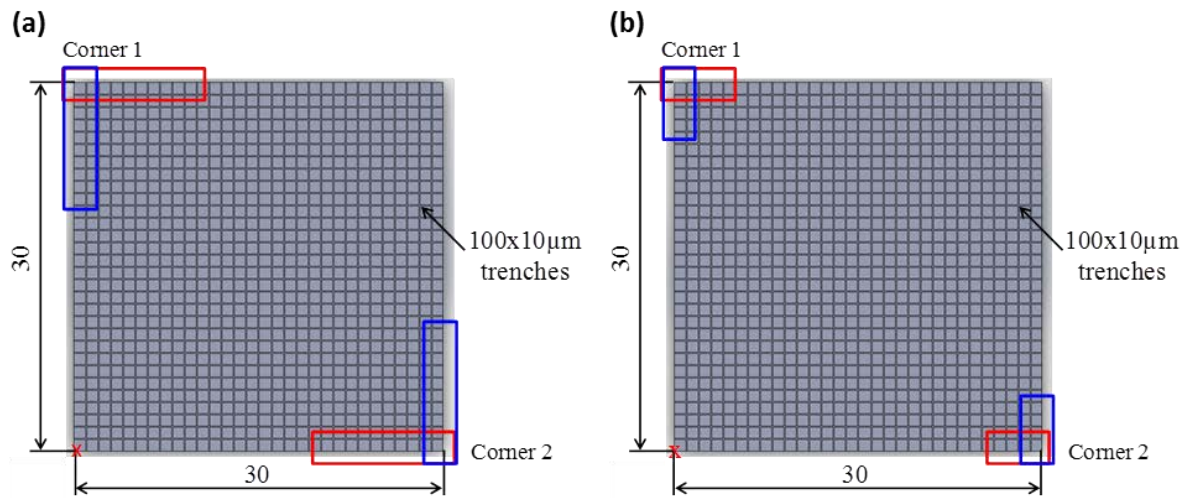
Figure 4.6 (a) Scanned regions for (a) Tests 1, 4 and 5, (b) Test 2

A representative 3D image of a scanned region on a Test 1 specimen is shown in Figure 4.7(a) while the top view together with the measurements of relative distance between trenches is shown in Figure 4.7(b). The point data from the scans were analysed using the 'Profile form measurement' tool available in the Alicona software. The data were treated with 'form' removal operation prior to measuring the distances between trenches. The edge of the 1st trench in Tests 1, 4 and 5 was used as a datum for measuring the distances to the corresponding edges of the 3rd and similarly 5th, 7th, 9th and 11th trenches using the software tool. Ten lateral measurements were taken for each scanned area as illustrated in Figure 4.7 (a) and (b) and the average values were calculated.
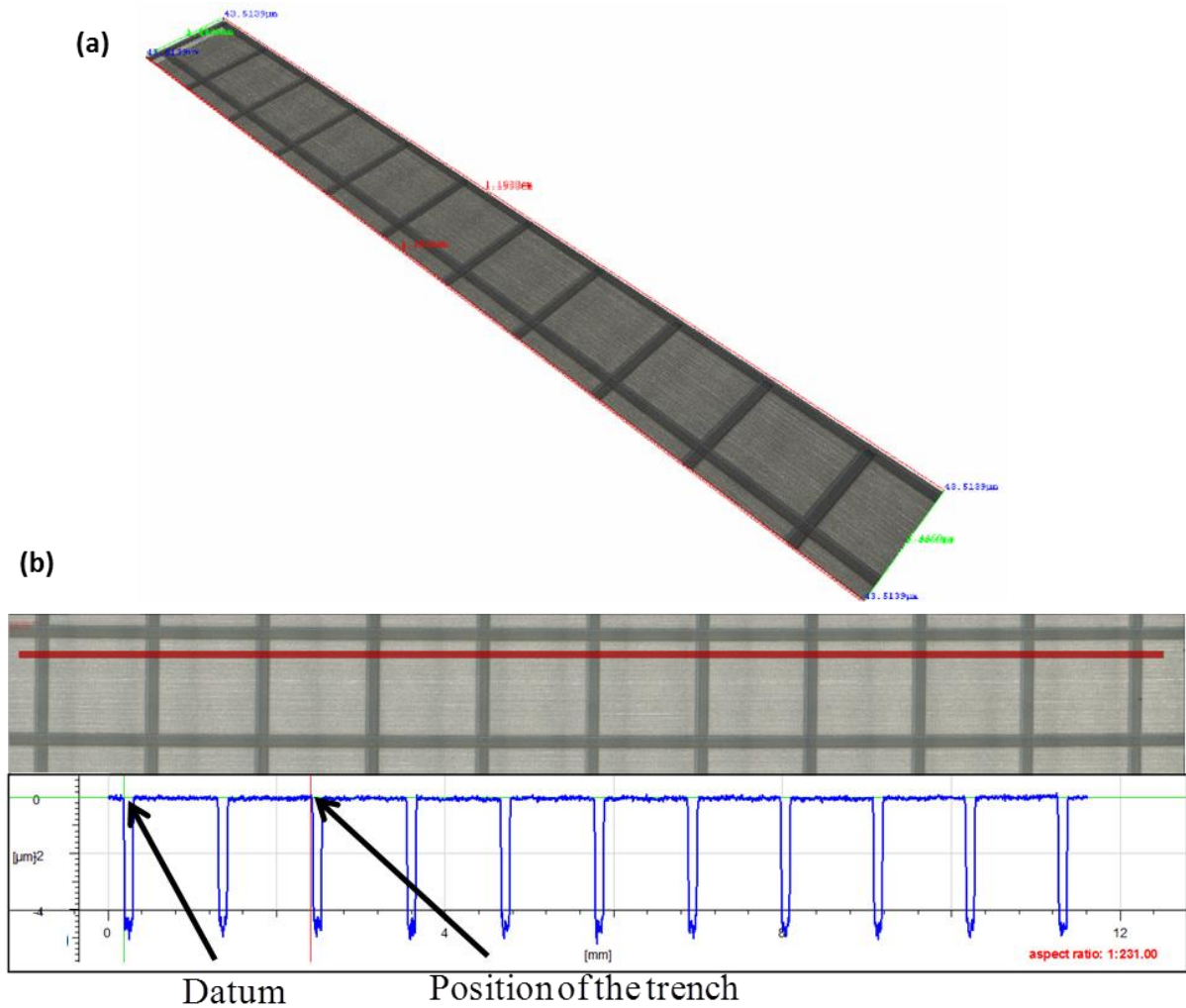
Figure 4.7 (a) A representative 3D scanned area showing 1st to 11th trenches of a laser structured field, (b) Top view of the scanned data and measurement of distances between the trenches using 'Profile form measurement' tool

The measurements in Test 3 were carried out along the horizontal (X) and vertical (Y) axes at the stitching junction of the laser scanned fields as it is schematically shown in Figure 4.8(a). The procedure is detailed in Figure 4.8(b) that included measuring the distances from 1st to 2nd, 3rd, 4th and 5th trenches. The D_1 and D_2 measurements provide information about the accuracy of the beam deflectors when structuring Field 1 while D_4-D_3 renders equivalent information about Field 2. At the same time, D_3-D_2 provides information about the accuracy of the stage as the mechanical axes were used to reposition the laser processed areas from Field 1 to Field 2. Furthermore, D_2-D_1 and D_4-D_3 measurements provide information about the pseudo-repeatability of laser structuring operation carried out only with the beam deflectors, while D_2 and the distance from the 1st to 3rd trenches in Test 1 exhibit

reproducibility of structuring operations, i.e. the machining precision obtained with the optical beam deflectors.
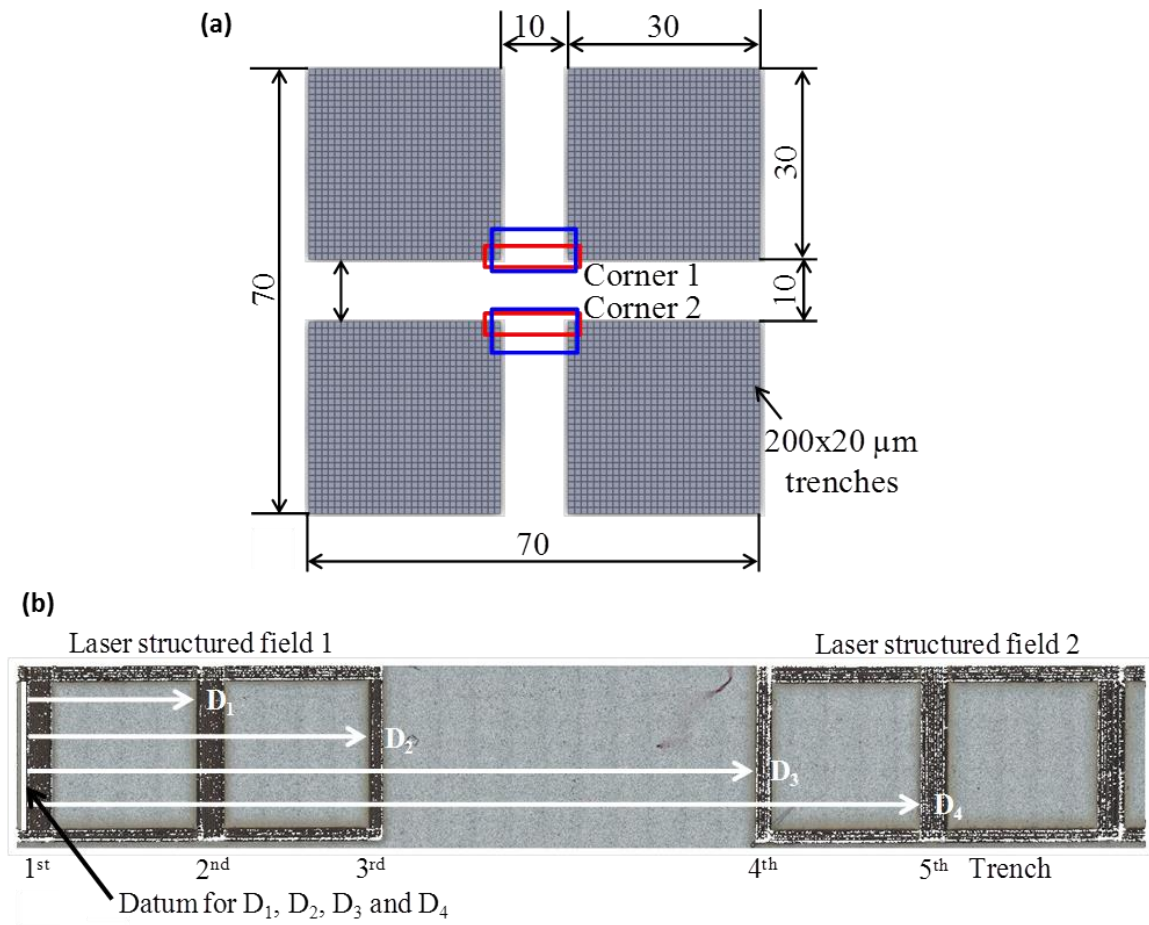
Figure 4.8 (a) Schematic diagram of the four structured fields in Test 3, (b) Measurement procedure in Test 3

Test 6 involved measuring the depths and diameters of the dimples produced at various scanning speeds using the 'Profile form measurement tool'. A representative scanned area of the dimples together with the measured depth and diameter is shown in Figure 4.9.

Figure 4.9 A scanned area containing several dimples created at various scanning speeds together with the measured depth and diameter of one of them

4.3 Results and discussions

4.3.1 Machining accuracy of X-Y optical beam deflection systems

The results obtained in Test 1, i.e. by using the X-axis beam deflectors, are shown in Figure 4.10. The machining accuracy typically decreased with the increase of the distance from the 1st trench. System A achieved the best accuracy amongst the four systems with values between 0.8to 12.8μm while the majority of data was within the technical specification for the optical axes, i.e. ±10 μm, whereas machining errors of the other three micromachining set-ups was much higher. System C exhibited the worst results, i.e. deviations up to ~300 μm, followed by the System B and System D. The machining accuracy between the corners 1 and 2 of Systems B and D was in the range from 2 to 40 μm.

Figure 4.10 Machining accuracy of beam deflectors along the X-axis in Test 1

The graph in Figure 4.11 shows that the accuracy of System A along the Y-axis was again the best amongst all four systems, however with a marginally higher deviation, up to 15.7 µm, in comparison to that along the X-axis. Conversely, System B exhibited greater deviation in X, up to 120 µm, compared to that in Y axis, up to -65 µm. The results obtained with System C were the worst among all set-ups with values gradually increasing from the 1st to 11th trenches and this can be attributed to a systematic error, e.g. calibration errors, in carrying out the laser machining operations. The accuracy of System D's optical axes was similar along both axes.
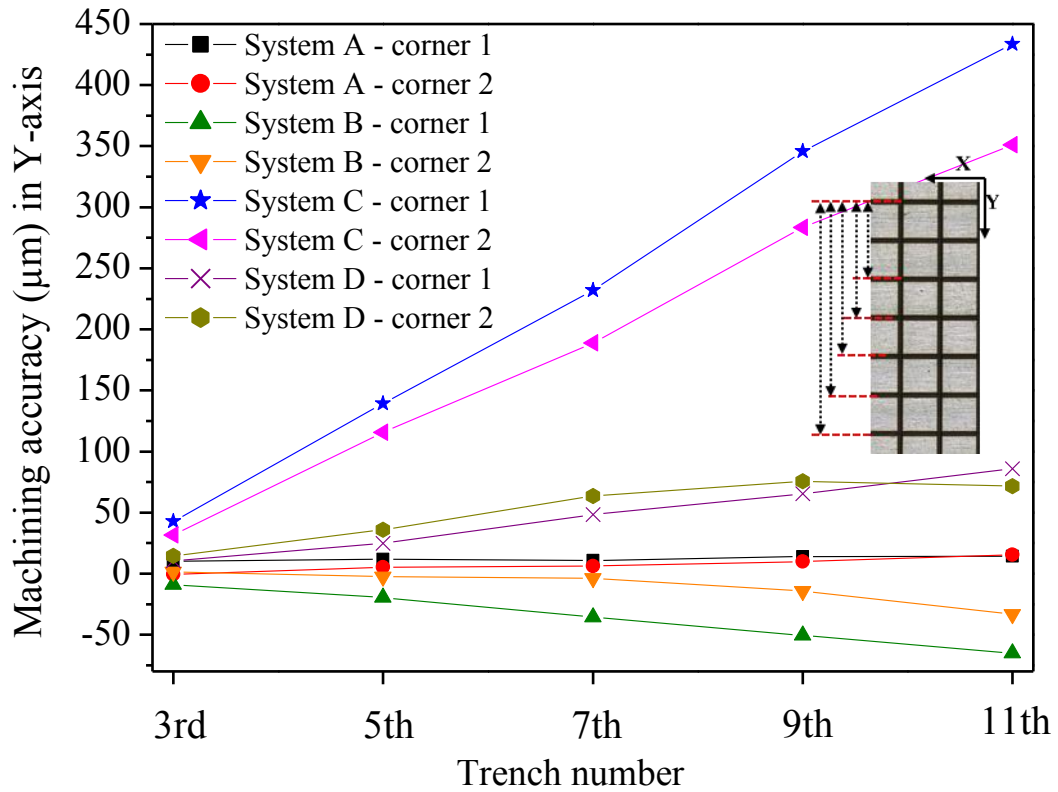
Figure 4.11 Machining accuracy of beam deflectors along the Y-axis in Test 1

The machining accuracy of the beam delivery systems improved typically when the systems were calibrated after using the beam expanders. Machining accuracy of System D improved by ~75-85%, with values from 53.2 to 11.3 μm along X (Figure 4.12), and ~35-45% in Y (Figure 4.13). Thus, regular calibrations of the beam delivery systems are very important, especially if accurate and precise laser machining operations have to be performed. Typically, a positive systematic error was noted for System D in X as opposed to a negative along Y. Systems B and C however did not show any significant improvements, possibly due to the errors in the calibration methodologies associated with both machines, although the accuracy in X was marginally better for System C.
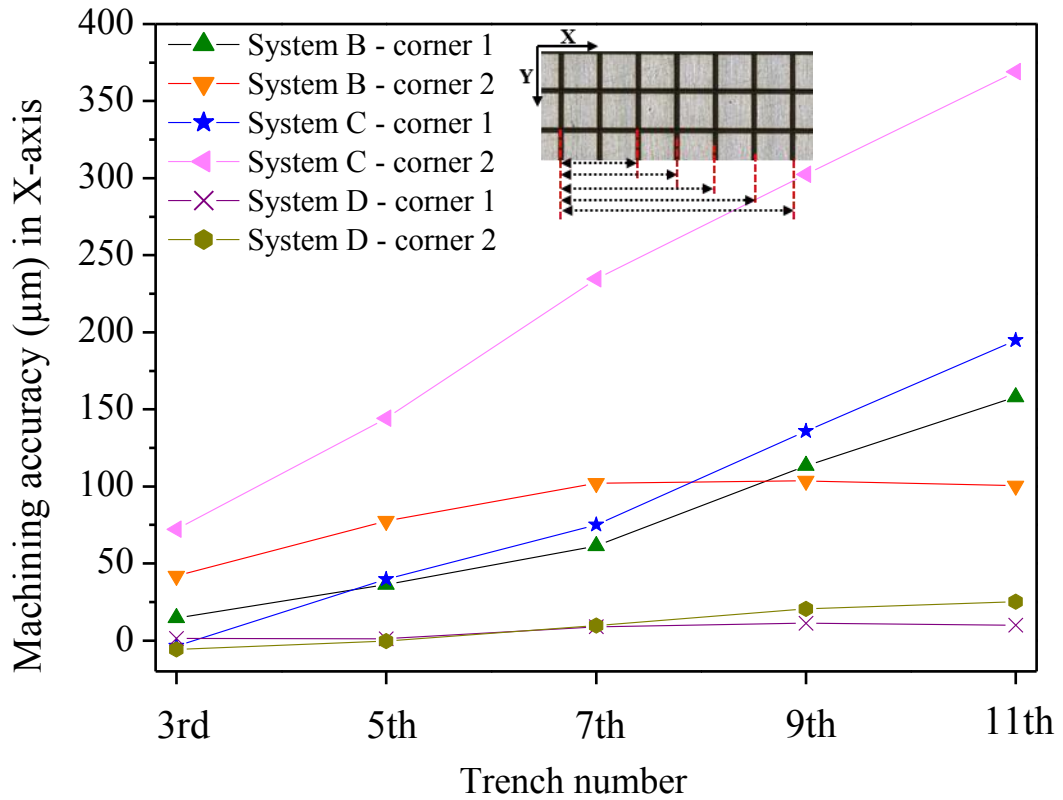
Figure 4.12 Machining accuracy of beam deflectors along the X-axis in Test 4
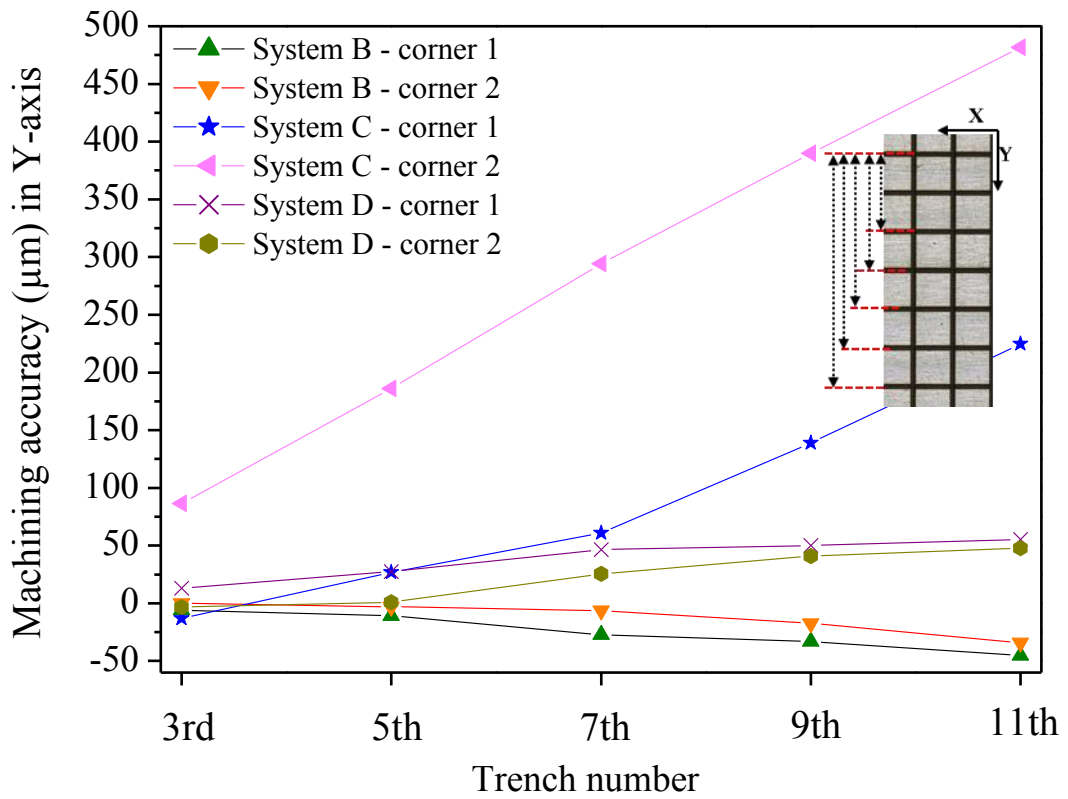
Figure 4.13 Machining accuracy of beam deflectors along the Y-axis in Test 4

4.3.2 Machining accuracy of mechanical stages

As expected, the accuracy of the mechanical stages was much better, typically in the range of ± 2 to 4 µm, than their optical counterpart. This is due partly to the much lower processing speed, typically less than 100 mm/s, compared to the optical axes, which operate at speeds higher than 1 m/s when laser texturing/structuring operations are performed. The deviation from the nominal value generally increased with the distance from the 1st trench as shown in Figure 4.14. Systems A and B performed better in X than in Y; while for System D the accuracy was comparable in both directions as depicted in Figure 4.15.
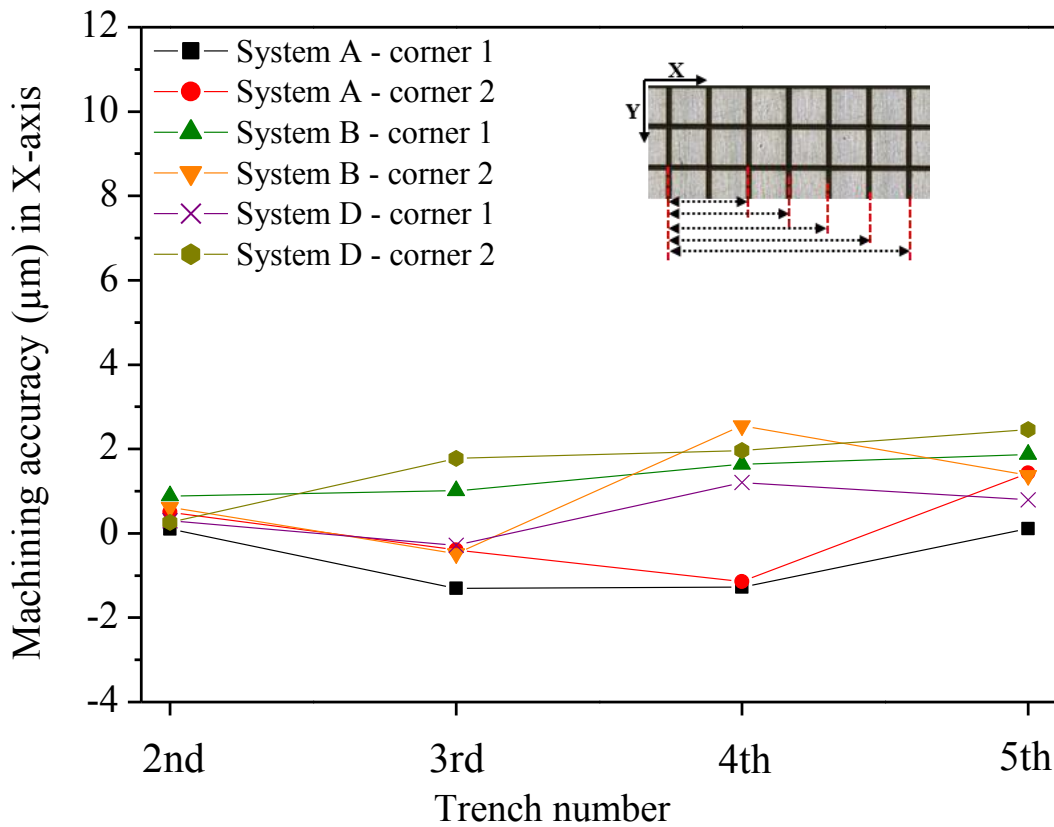
Figure 4.14 Machining accuracy of mechanical axes along the X -axis in Test 2
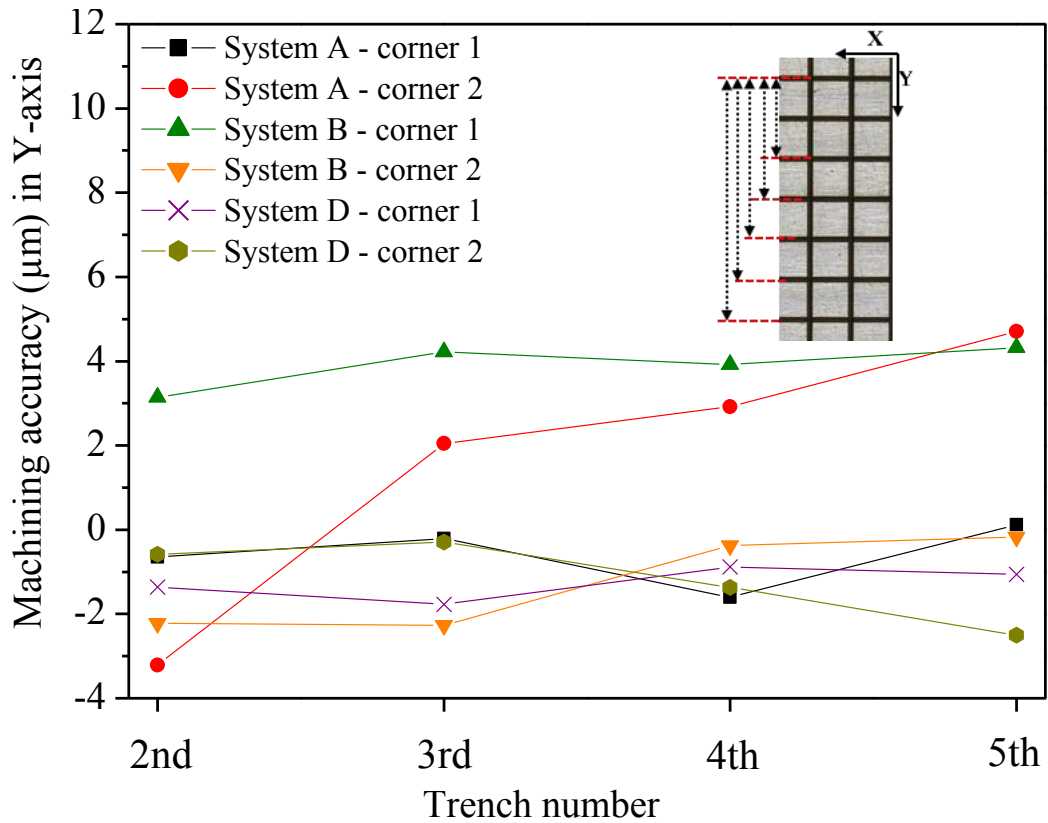
Figure 4.15 Machining accuracy of mechanical axes along the Y-axis in Test 2

4.3.3 Machining accuracy with combined used of mechanical and optical axes

The position accuracy of the System A's beam deflector along the X-axis varied from 2.84 to -5.81 μm as shown in Table 4-4 while that of mechanical axes was within -1.02 to -1.91 μm; however, both were within the system's technical specifications of ±10 and ±4 μm, respectively. Conversely, the deviations of the scanners were much higher for Systems C and D. As it was already mentioned, this was possibly due to calibration issues for both set-ups. Although the accuracy of the mechanical axes of both systems at Corner 1 was 2.72 and -2.02 μm respectively, that at Corner 2 was much lower, i.e. -15.08 and 14.70 μm for Systems C and D, respectively. The deviations of the mechanical stages were still typically lower than that of the scanners, which can be explained with the scanners' much higher processing speeds.

The stitching accuracy of the machined fields along the Y-axis was measured only for System A. Better stitching accuracy was observed at Corner 1 compared to that at Corner 2 with values ranging from 0.7 μm to 2.6 μm and -6.5 μm to -11.1 μm, respectively as shown in Table 4-5.

Table 4-4 Machining accuracies of the scan heads and mechanical stages along X in Test 3

Systems	Corner	Field 1 (D_2-D_1) (μm)	Field 2 (D_4-D_3) (μm)	Mechanical axes (D_3-D_2) (μm)
A	1	-4.74	3.17	-1.91
	2	-5.81	2.84	-1.02
C	1	63.74	69.92	2.72
	2	58.62	71.96	-15.08
D	1	12.46	54.06	-2.20
	2	11.78	51.74	14.70

Table 4-5 Stitching accuracy along the Y-axis in Test 3

System A	Stitching accuracy (μm)				
	1st trench	2nd trench	3rd trench	4th trench	5th trench
Corner 1	0.70	3.52	2.42	2.64	2.64
Corner 2	-6.46	-8.12	-8.32	-8.94	-11.0

4.3.4 Machining accuracy of dynamic focusing modules

The machining accuracies of System A's scan head when structuring inclined surfaces either along X or Y-axis are shown in Figs. 4.16 to 4.19. The deviation from the nominal values in X-axis greatly increased from 14 to 108 μm when the surface was inclined along the same axis, whereas machining accuracy along the Y varied only from ~5 to 32 μm. Similar results were also observed when the workpiece was inclined along Y-axis. In this case, the accuracy along the X-axis was within 1.5 to 10 μm while that along Y varied from ~30 to 190 μm. It was further noticed that the accuracy of X-axis was typically better compared to that of Y. This was in line with the observation from Test 1 on System A's scan head accuracy.

The accuracy deterioration in Test 5 can be attributed to 3D calibration errors. For example, greater errors were observed in Figures 4.16 and 4.17 along the inclined X-axis, where each of the trenches was produced with a constant Z- module focusing settings. This is illustrated in Figure 4.20, where no programmed movements occurred in the Z direction; thus the dynamic capabilities of the Z-module should not affect the trenches' machining accuracy. Similarly, bigger machining errors were observed in Figures 4.18 and 4.19 along the inclined Y-axis, where trenches were again produced without any movements along the Z-axis. Although Figures 4.17 and 4.19 exhibit that the accuracy slightly deteriorated with the increase of laser scanning speed for the trenches requiring programmed movements along the

Z-axis, this does not provide any conclusive evidences regarding the Z-module's performance in comparison to the X and Y beam deflectors.

Figure 4.16 Machining accuracies along X-axis in Test 5 (workpiece inclined along X-axis)
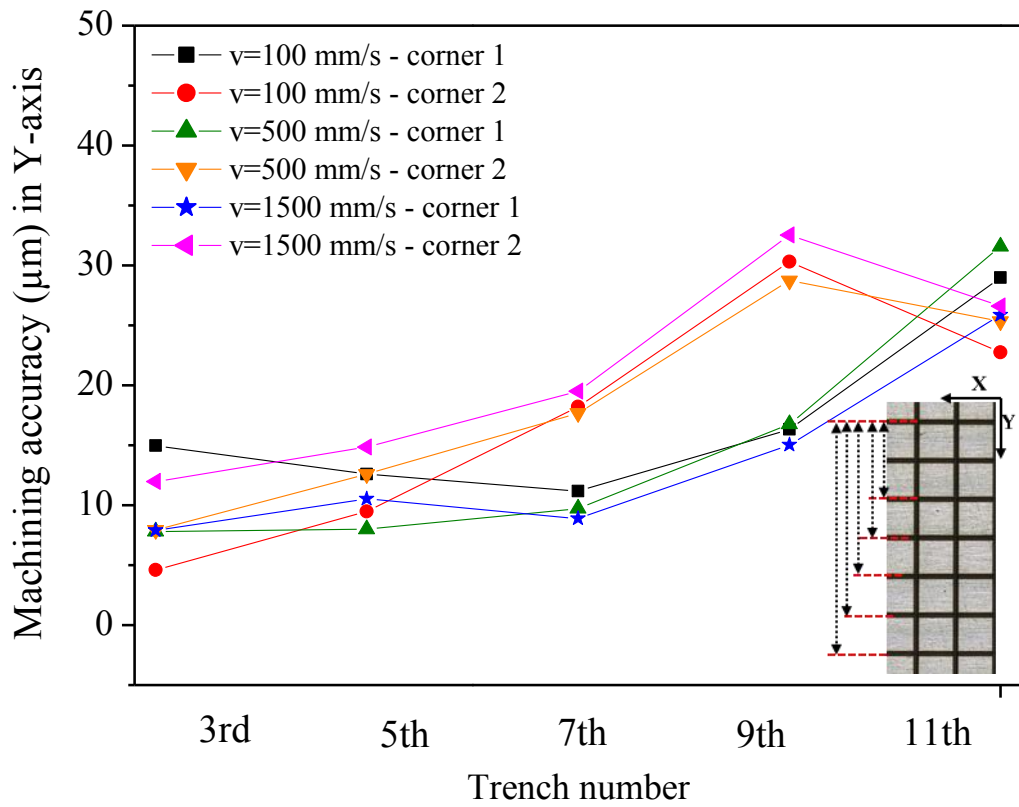
Figure 4.17 Machining accuracies along Y-axis in Test 5(workpiece inclined along X-axis)
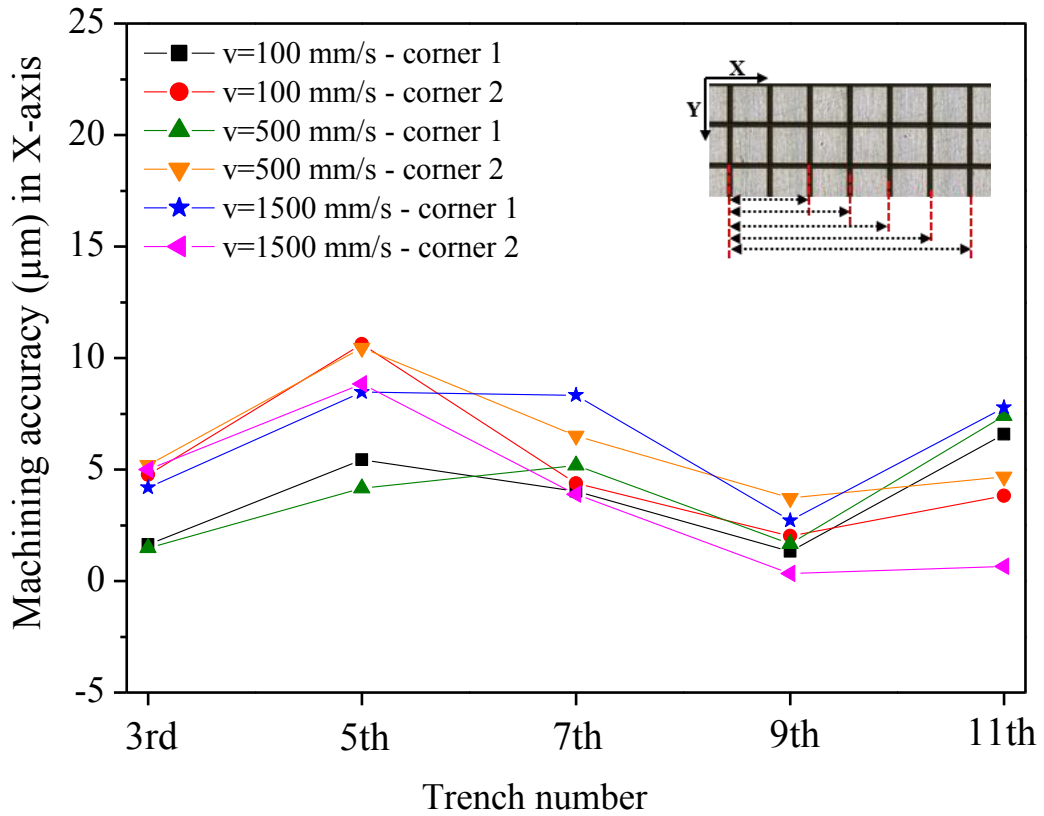
Figure 4.18 Machining accuracies along X-axis in Test 5 (workpiece inclined along Y-axis)
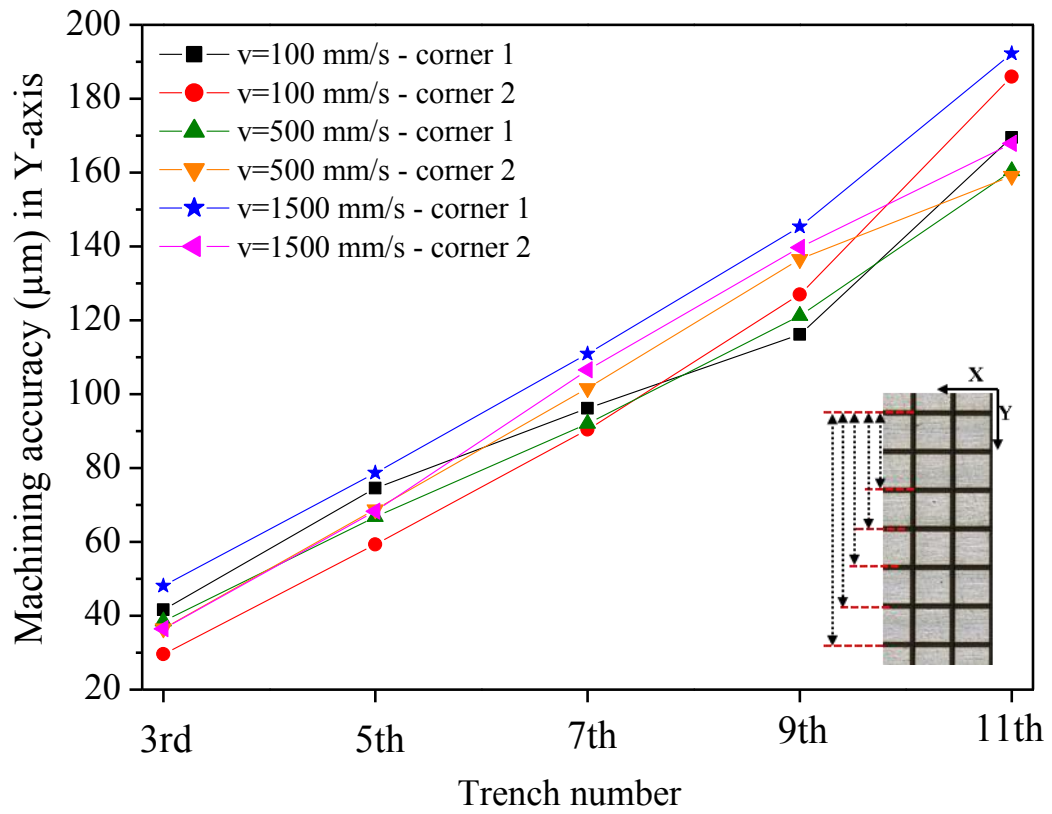
Figure 4.19 Machining accuracies along Y-axis in Test 5 (workpiece inclined along Y-axis)
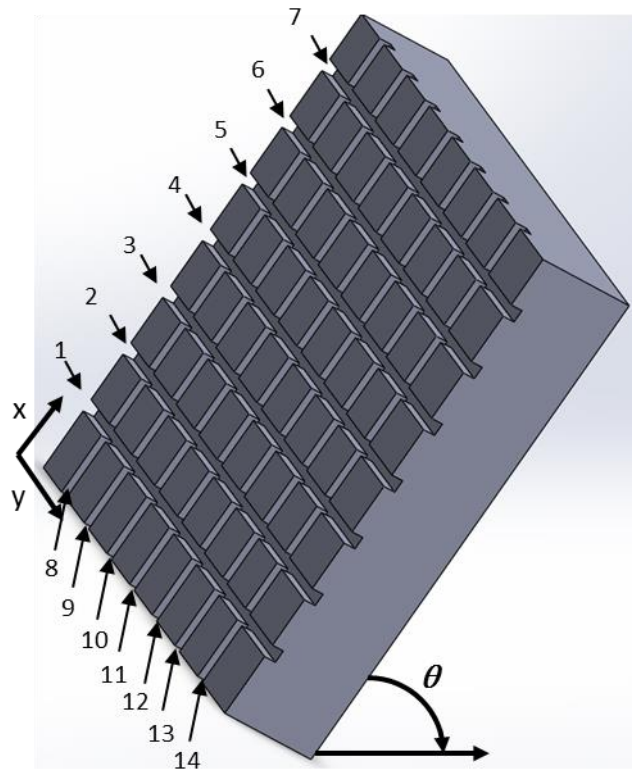
Figure 4.20 Graphical representation of trenches produced along the inclined X-axis

Note to Figure 4.20: when producing the trenches normal to the X-axis, the Z-module is fixed at a certain Z setting throughout the machining of the trenchs, while the Y beam deflector executes the machining movements. In contrast, when producing the trenches normal to the Y-axis both the X beam deflector and the Z-module simultenioursly execute the machining movements.

The depths and diameters of the dimples produced on surfaces normal and inclined to the incident beam are shown in Figures 4.21 and 4.22, respectively. With the increase of the scanning speed, dimple depths remained typically consistent within the range of 27 to 29 μm on the sample normal to the incident beam. Similar results were also obtained on the sample when inclined at 5° and 10⁰. However with the increase of the inclination angle (greater than 10°), the dimple depths decreased gradually with the increase of the scanning speed. This could be attributed to the lower Z-module dynamic that led to a lag in executing the programmed focusing movements along the Z-axis and consequently affected the machining results. The negative effects were more pronounced at the higher inclination angles, i.e. 15° and 20° where the depth of the focus (approximately 2.45 mm with the used beam delivery configuration) could not compensate the inferior dynamic of the Z-module compared with that of the X and Y beam deflectors. In particular, these negative effects on the dimple depths are clearly observed at scanning speeds higher than 1 m/s when the samples were inclined at 15° and 20° (see Figure 4.21). For example, the dimple depths at a scanning speed of 2 m/s have been reduced to 25.5 μm and 19.5 μm at the inclination angles of 15° and 20°, respectively.
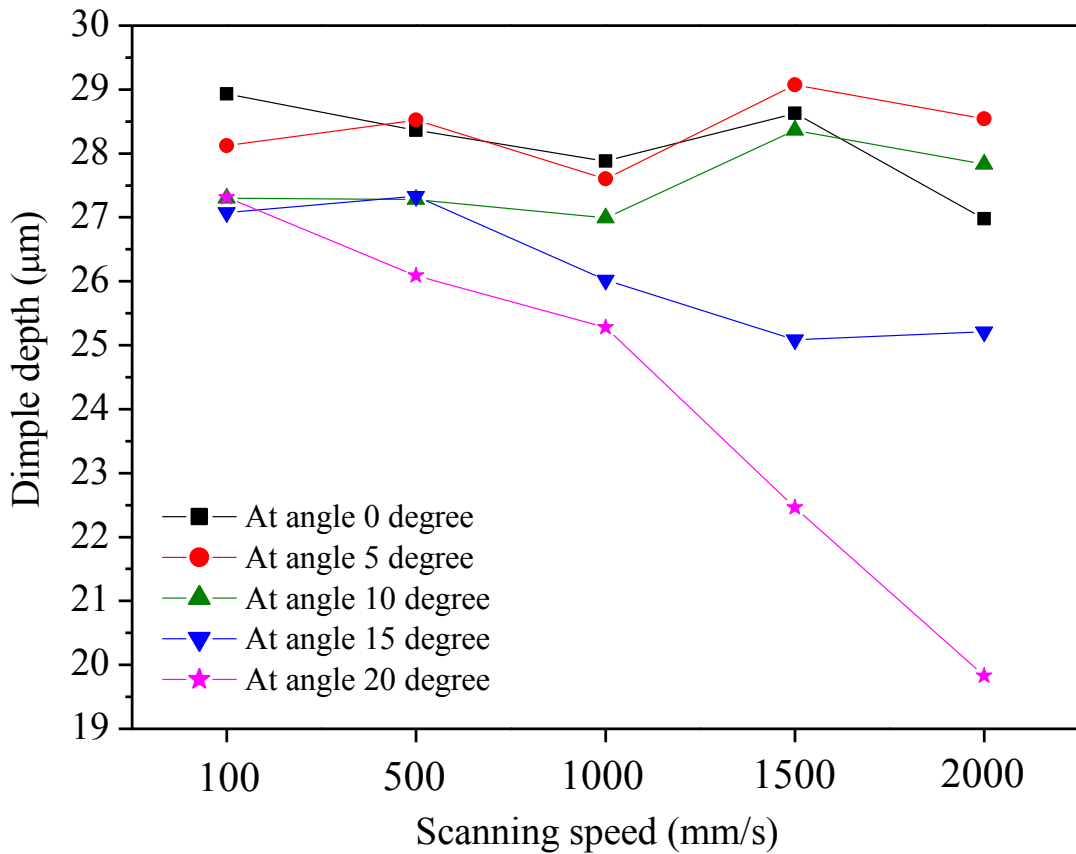
Figure 4.21 The plot of dimple depths produced on normal and inclined surfaces to the incident beams at various scanning speeds in Test 6

The diameters of the dimples, as shown in Figure 4.22, gradually increased with the increase of scanning speed at all investigated inclination angles. Conversely, dimple diameters decreased with the increase of the angle at the lower processing speeds, i.e. 100 mm/s and 500 mm/s, however such a trend was not apparent at the higher scanning speeds, i.e. 1 m/s and 1.5 m/s. The increase of dimple diameter with the increase of processing speed is also clearly depicted in Figures 4.23 and 4.24. This can be explained with the deterioration of dimples' machining accuracy due to the lower Z-module dynamic compared with the X and Y beam deflectors. Especially, this results in shifting of pulses' incident positions that leads to an increase of the dimple diameters.
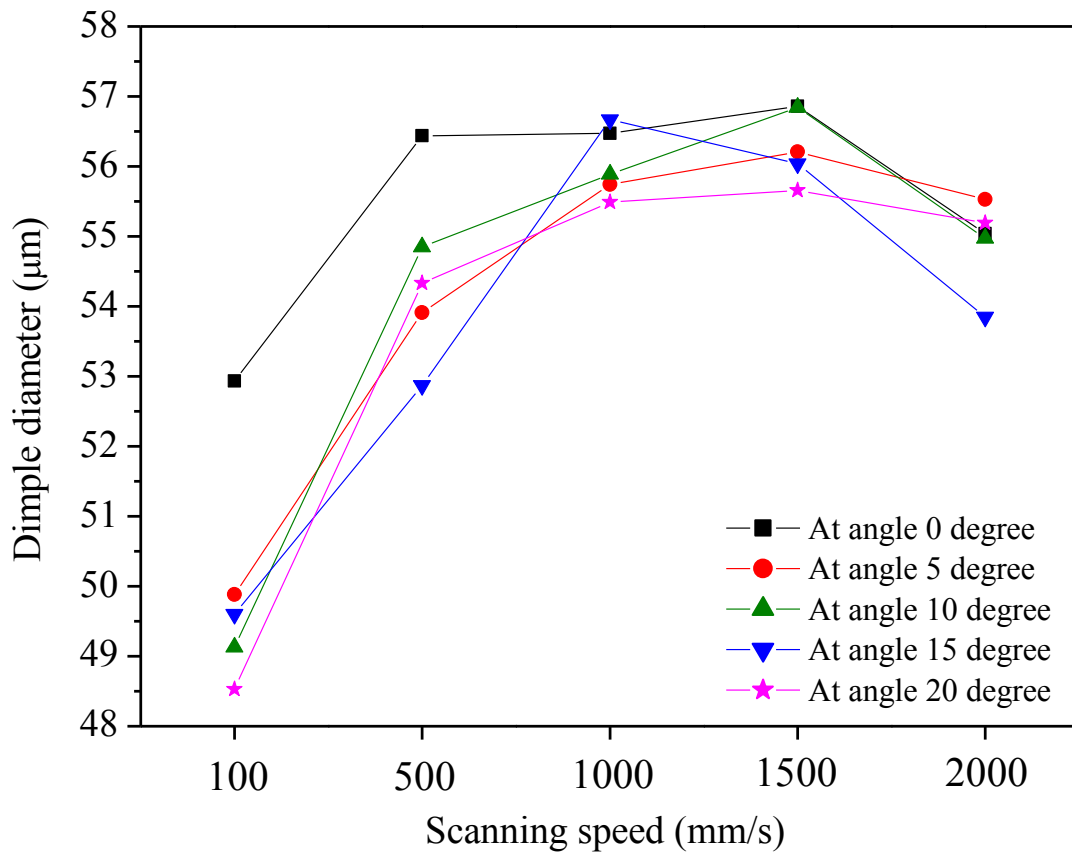
Figure 4.22 The plot of dimple diameters produced on normal and inclined samples to the incident beam at various scanning speeds in Test 6

Based on the results for dimple diameters and depths in Test 6, it can be stated that the depth of focus could not compensate completely the inferior Z-module dynamic at higher inclination angles and scanning speeds. Thus, it is necessary to investigate the Z-modules' dynamic performance and its potential negative impact on 3D laser machining results. A specialized experimental technique to conduct such quantitative investigation of the dynamic limitations of Z-module is proposed in the next section of this Chapter (Section 4.4).
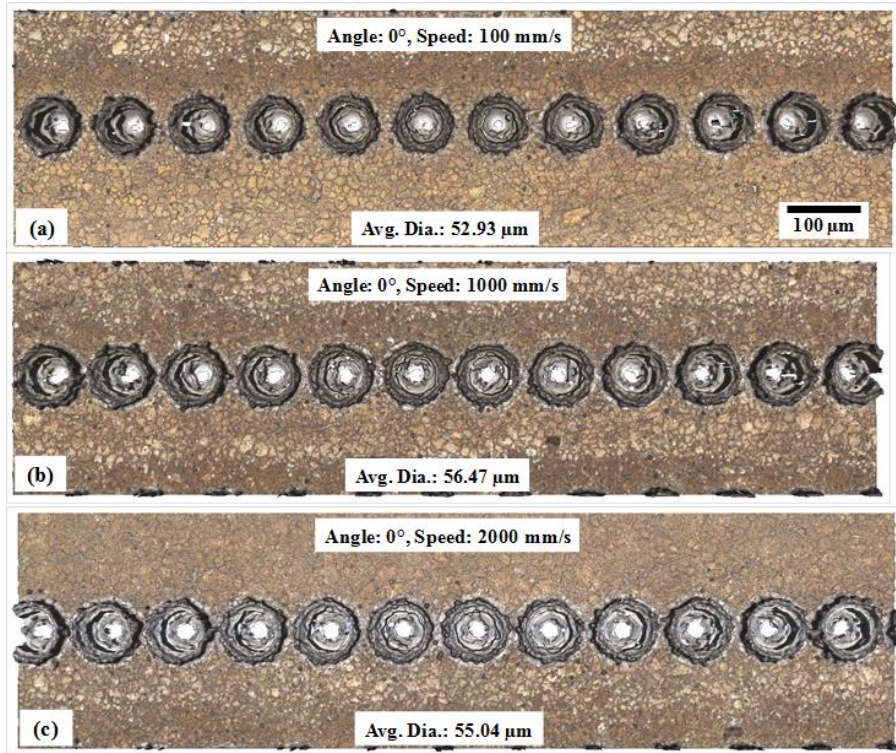
Figure 4.23 Scanned images of dimples produced on a surface normal to the incident beam at three different scanning speeds: (a) 100, (b) 500 and (c) 1500 mm/s
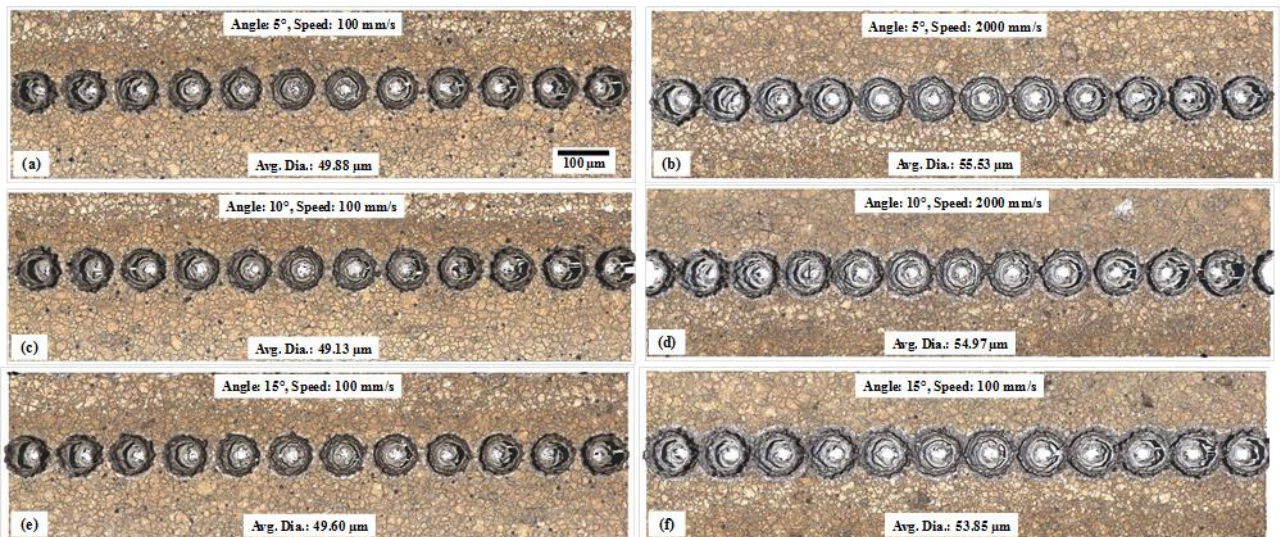
Figure 4.24 The dimples produced with two scanning speeds on the samples inclined to the incident beam at four different angles

4.3.5 Machining repeatability and reproducibility

Pseudo-repeatability data of Systems A, C and D are presented in Table 4-6. It compares the distance between 1st and 2nd trenches within the laser structured Fields 1 and 2 in Test 3. Systems A and C exhibited a pseudo-repeatability in the range of 6.18 to 13.34 μm at the two corners of the machined fields. However, pseudo-repeatability of the System D was much

worse (in the range of 39.96 to 41.60 µm), although the results within each field (Corners 1 and 2) were comparable.

Table 4-6 Pseudo-repeatability data of different laser systems

| Systems | Regions | Test 3 | | Repeatability (µm) |
| | | Field 1 | Field 2 | |
		Accuracy (µm)	Accuracy (µm)	
A	Corner 1	-4.74	3.17	8.44
	Corner 2	-5.81	2.84	8.65
C	Corner 1	63.74	69.92	6.18
	Corner 2	58.62	71.96	13.34
D	Corner 1	12.46	54.06	41.60
	Corner 2	11.78	51.74	39.96

The reproducibility of the optical axes of Systems A, C and D was determined by comparing the distance between 1st and 3rd trenches in Tests 1 and 3 as shown in Table 4-7. The results obtained solely with the scan heads were reproducible and ranged from 1 to 6 µm with only two exceptions.

Table 4-7 Laser scanheads' reproducibility of Systems A, C and D

| Systems | Regions | Test 1 | Test 3 | Reproducibility (Precision) (µm) |
		Deviation from the nominal (µm)	Deviation from the nominal (µm)	
A	Corner 1	0.76	-4.74	5.50
	Corner 2	6.94	-5.81	12.75
C	Corner 1	22.20	63.74	41.54
	Corner 2	64.48	58.62	-5.86
D	Corner 1	11.31	12.46	1.15
	Corner 2	9.13	11.78	2.65

The deterioration of machining repeatability and reproducibility in the comparative study could be mainly attributed to the utilization of not sufficiently adequate handling techniques for the workpieces in the laser systems. In particular, systems C and D did not provide

sufficient tools and techniques for precise positioning and alignment of the workpiece in the laser systems prior to the machining operations.

4.4 Experimental methodology for investigating the dynamic capabilities of dynamic focussing modules

4.4.1 Introduction

Results from Test 6 in Section 4.3.4 above revealed that the dynamic limitations of z-modules can significantly impair machining results. Therefore, the aim of this section is to design an experimental technique that can clearly quantify the dynamic capabilities of z-modules and thus to judge about their negative effects in laser micro-processing of complex free-form (3D) surfaces. Z-modules, also called Dynamic Focusing Modules (DFMs), are built in two different configurations, which are schematically presented in Figure 4.25. Figure 4.25(a) shows a beam expander DFM configuration, which consists of a diverging optic that can be translated coaxially along the optical beam path via a linear motor, and a stationary focusing optic. In contrast, Figure 4.25(b) shows a beam condenser DFM configuration, which includes a converging optic and a stationary focusing optic. Choice of a suitable DFM configuration for a particular laser system is dependent on the laser beam characteristics of the used laser source such as beam waist diameter and collimation, because DFM optics are selected to give minimum laser beam aberrations. Examples of laser beam aberrations caused by a lens that have to be taken into account when selecting a DFM configuration include spherical aberrations, chromatic aberrations and aperture diffraction [192]. Even though, DFMs are supplied in two different configurations, their working principles are the same. In particular, movements of the diverging or converging optics during a laser processing operation changes the relative distance between the moveable and the stationary optics, which causes changes in laser system's focal length and thus the laser beam spot can be focussed at different planes along its propagation axis (z axis) [193].
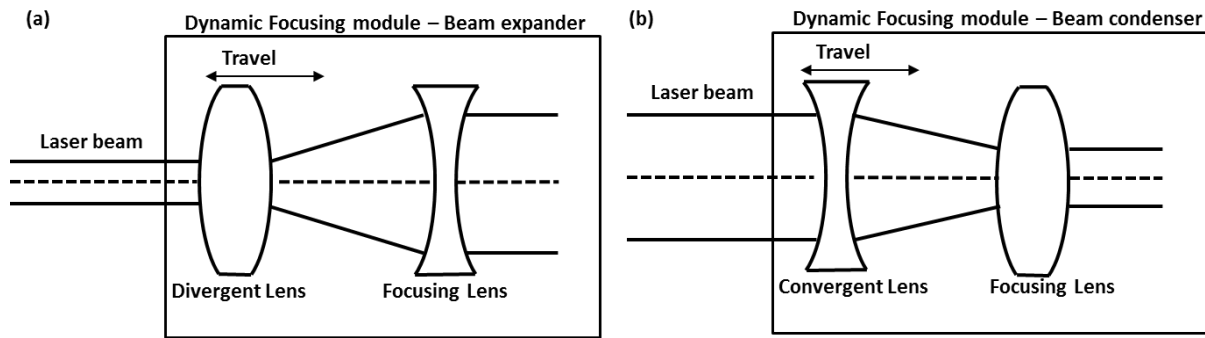
Figure 4.25 DFM configurations: (a) beam expander DFM and (b) beam condenser DFM

4.4.2 Methodology

Figure 4.26 presents the test sample used to evaluate the DFM dynamic capabilities. In particular, the experiments involved the machining of 30 mm long tracks with dimples produced on two SS 316 samples with different scanning speeds, V_1, V_2 …V_n, one sample is normal and the other is tilted at 15^0 in regards to the incident beam. Table 4-8 provides the laser parameters utilized to machine the laser tracks. Twelve laser tracks were produced at different scanning speeds, but it should be noted that each laser track is produced with constant scanning speed. The title angle of 15° was selected in order to fit the machined area on the sample within the focusing envelop of the used 3D scanner and focusing lens, in particular within the enveloped defined by the DFM Z range (7.7 mm) and the focusing lens's field of view (35 x 35 mm). The sample was tilted by employing the rotary stage, which rotates the sample about the x axis of the workpiece and thus the tilt is along its y axis as shown in Figure 2. Thus, the laser tracks on the tilted sample were produced along its y axis, because the movements along the tilted axis have components both along the y and z axes and thus DFM has to be utilized in combination with the X-Y optical beam deflector system. The steps between the dimples along the laser tracks are 100 μm, while the step-over distance between the laser tracks was set to 150 μm. Furthermore, the dimple diameter was determined by the laser beam spot diameter, because there was no overlapping of pulses in each laser scan. The tracks were produced by 15 repeated scans and thus each dimple was created by a sequence of 15 laser pulses. In this way the target dimple depth of 12 μm was achieved. Also, it should be noted that the laser tracks both on the tilted and the normal samples were produced with an offset from the focal plane that is equal to the Rayleigh length (z_R), where z_R can be calculated using Equation 3.7 from Section 3.2.1. Furthermore, to account for any laser beam focus aberrations caused by the optics, the offset from the focal plane was also experimentally determined by measuring the distance at which the beam spot diameter is

equal to sqrt(2)*w_0 (Rayleigh length criterion) by utilizing the beam analyser (presented in Chapter 3).

The DFM dynamic capabilities were assessed by analysing the depth profiles' differences of the dimples produced on the tilted and the normal plates to the incident beam.
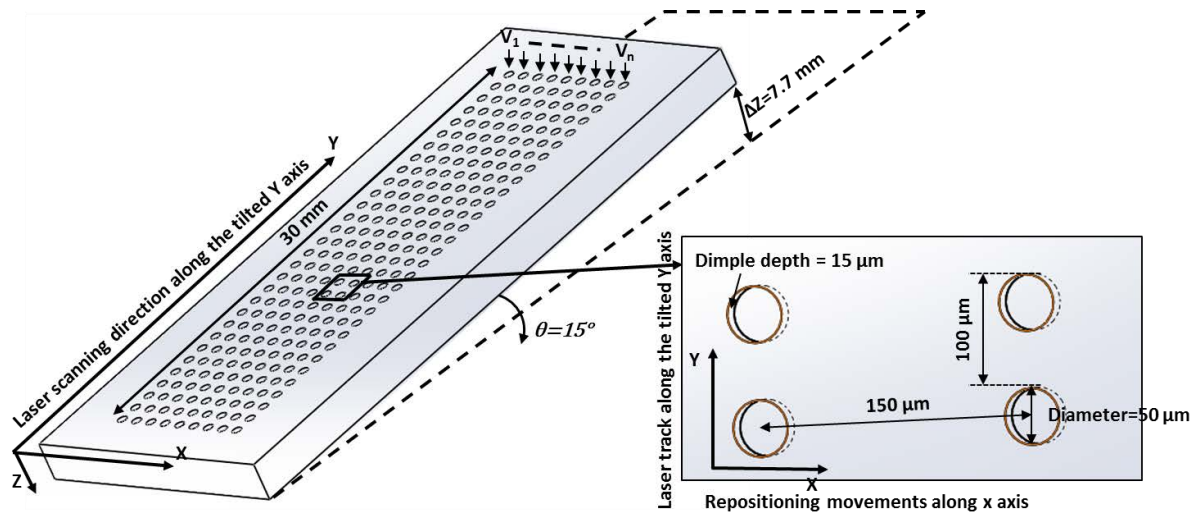
Figure 4.26 The test sample used to evaluate the DFM dynamic capabilities

Note to Figure 4.26: The laser tracks are produced along the tilted Y axis of the workpiece, while laser repositioning movements before the machining of each laser tracks (non-machining movements) are executed along the x-axis of the workpiece.

Table 4-8 Laser parameters for the experimental tests

Laser track	1	2	3	4	5	6	7	8	9	10	11	12
Average Power [W]	40											
Pulse duration [ns]	220											
Beam diameter at focus [μm]	63											
Frequency [kHz]	1	5	10	12	13	14	15	16	17	18	19	20
Scanning Speed [m/s]	0.1	0.5	1.0	1.2	1.3	1.4	1.5	1.6	1.7	1.8	1.9	2.0

4.4.3 Results and discussions

Figure 4.27 shows that the laser beam spot diameter at the focal plane and at an offset distance equal to the Rayleigh length above the focal plane are 63 μm and 89 μm, respectively. The offset distance calculated using Equation 3.7 from Section 3.2.1 in Chapter 3 was 2.45 mm and it resulted in a laser beam Depth of Focus (DOF) of 5.9 mm, twice the Rayleigh range. Since, DoF is comparable to the working Z range of the DFM , it greatly impairs the deterministic evaluation of the DFM dynamic capability. This is because DOF compensates the "lagging" of the laser beam movement along the z-axis that is due to the

DFM insufficient dynamic capability. Thus, the depth profiles of the produced dimples will be similar, because the changes of energy density (fluence) can be considered negligible within the beam DOF. Therefore, it is necessary to reduce substantially and even to eliminate the DOF compensation effects on dimples' depth profiles. This can be achieved by producing the laser tracks at an offset distance equal to Rayleigh length, 2.45 mm in our case, and thus any further displacements of the laser beam from the focal plane due to insufficient DFM dynamic capabilities to lead to a significant difference of energy densities and as a consequence of this to dimples' depth profiles.

Figure 4.28a shows a 3D view of all produced laser tracks on the sample normal to the incident beam (no movements with DFM along the Z axis), while Figure 4.28b provides a magnified top view of the area at the end of the tracks. It can be judged visually in Figure 4.28b that the dimples have very similar profiles regardless of the scanning speeds. In addition, Figure 4.28c provides the depths of the dimples produced at all processing speeds and they are very similar, approximately 12 μm. Table A3.1 in Appendix 3 provides detailed measurement results for the depths of dimples that are produced at the different speeds on the flat sample (tilt angle of 0^0). Also, it can be seen in Figure 4.28b that there are small errors/differences in the laser tracks produced at different scanning speeds. They can be explained with the fact that any small variations of the scanning speeds caused by torsional resonance, heat dissipation, drift, nonlinearities, noise and calibration routines [192], are amplified since the there is no pulse overlapping and each dimple is the results of 15 pulses. Thus, even small beam machining errors are revealed and accumulated along the 30 mm long tracks even though they do not affect the overall accuracy of the 3D scanhead in executing the machining vectors. In particular, if there is a pulse overlap any small variations of scanning speeds in producing the dimples will not be noticeable at the end of the tracks.

Figure 4.29 depicts the carried out measurements of the dimples produced on the tilted sample. It can be clearly seen in Figure 4.29b that the topography of the dimples changes with the increase of the scanning speed. For example, the dimples are barely visible at a speed of 2 m/s (the rightmost laser track in Figure 4.29b). Furthermore, Figure 4.29c provides the depth profiles of the dimples produced at all processing speeds. It can be clearly seen that at processing speeds above 1500 mm/s, the dimples do not have the expected depth of 12 μm. Table A3.2 in Appendix 3 provides detailed measurement results for the depths of dimples that are produced at the different speeds on the tilted sample (tilt angle of 15^0).This should be

attributed to the DFM inability to follow closely the surface that is not normal to the incident beam along the z axis with the required dynamic. A comparison of the results in Figure 4.28 and Figure 4.29 reveals that the DFM dynamic is sufficient only up to a scanning speed of 1500 mm/s. In particular, DFM can execute beam movements along the Z axis without lags, synchronously with X and Y movements, only if the required speed does not exceed 388 mm/s (sin θ * V) and thus it is less than 10 % of the maximum V achievable with the X and Y beam deflectors of the investigated system in this research, in particular 4 m/s.
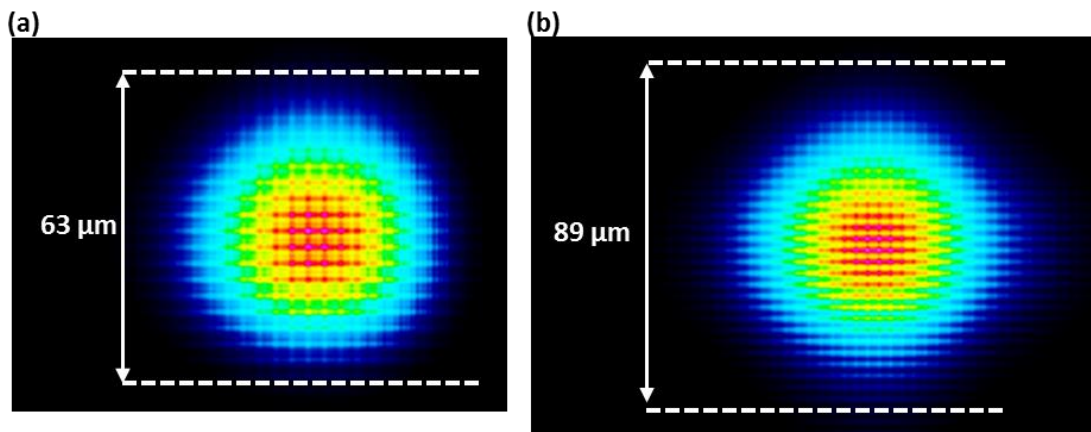
Figure 4.27 Laser beam energy profiles (a) at the focal plane (z=0) and at an offset distance of 2.45 mm above the focal plane (z=+2.45 mm)
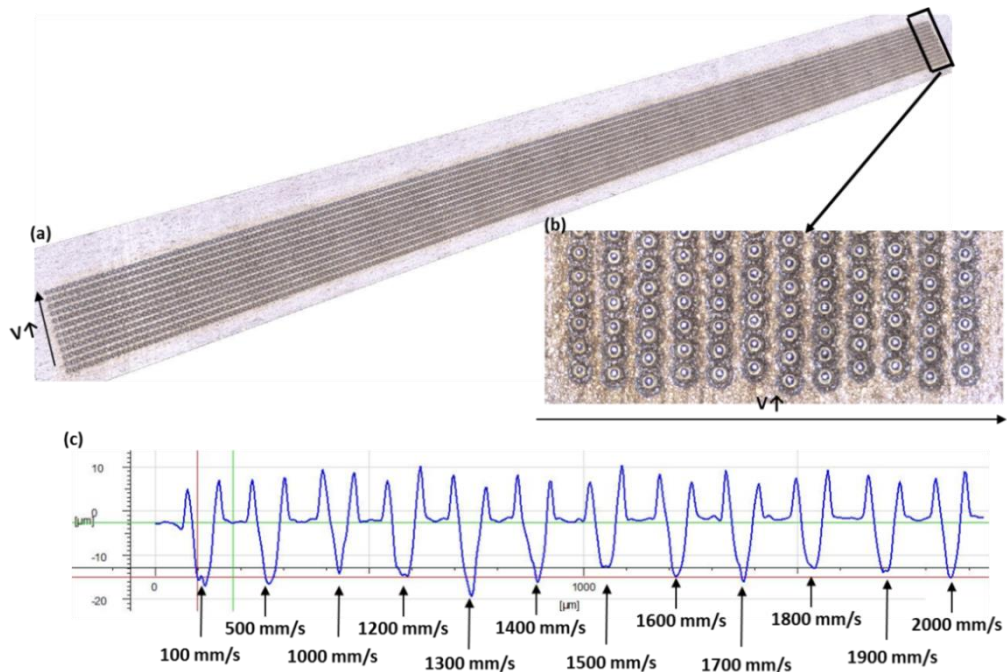
Figure 4.28 Laser tracks produced at different scanning speeds on the SS 316 sample when it is normal to the incident beam: (a) 3D view of the produced laser tracks; (b) magnified view of the area at the end of the laser tracks; (c) depth profile of dimples at the end of the laser tracks
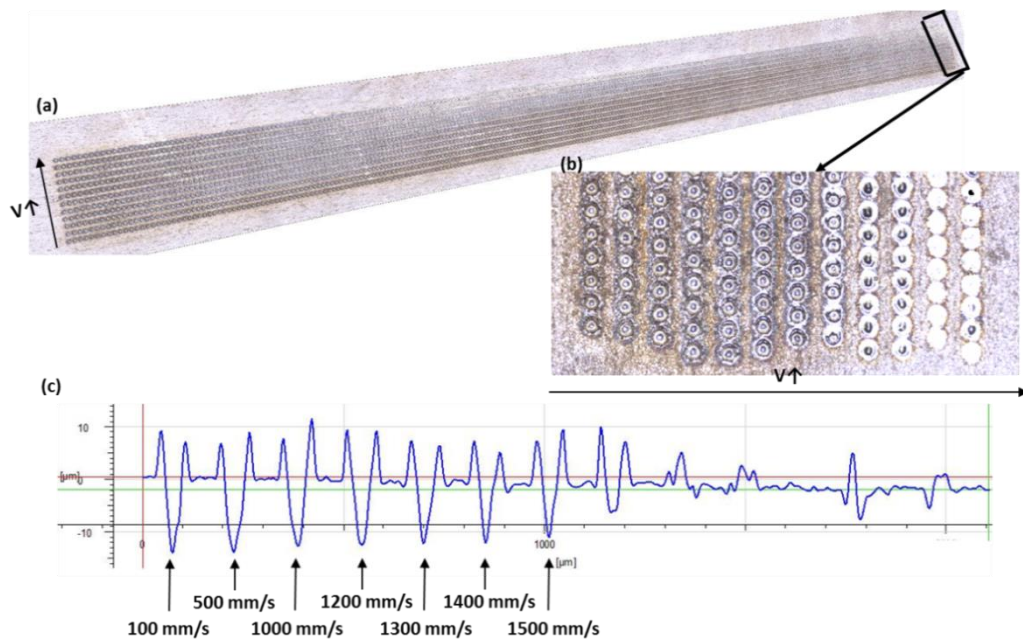
Figure 4.29 Laser Tracks produced at different scanning speeds on the SS 316 sample at $\Theta=15^0$ to the incident beam: (a) 3D view of the produced laser tracks; (b) magnified view of the area at the end of the laser tracks; (c) depth profile of dimples at the end of the laser tracks

4.4.4 Effects of DFM's dynamic limitations on the laser processing of 3D surfaces

This section aims to highlight that the clear understanding of DFMs dynamic limitations is a very important factor in obtaining uniform and consistent machining results on complex 3D surfaces. In particular, the results from laser polishing trials of 3D printed stainless steel workpiece (SS 316L) are shown in Figure 4.30. Fig 4.30a shows the 3D printed SS316L cube that was manufactured employing the Digital Metal® technology [194] and Figure 4.30b shows the workpiece surface roughness prior to the laser polishing experiments. It can be seen from Figure 4.30a that the workpiece incorporates complex 3D geometries and thus the laser polishing operation of the cube would require the utilization of the Z-module in order to efficiently follow the contours of the workpiece and to achieve uniform laser polishing results. Figure 4.30c and Figure 4.30d depict the resulting surface roughness after the laser polishing trials without and with optimization of the toolpath to take into account the DFM dynamic limitations. It should be mentioned that the laser polishing parameters were kept the same in both machining trials with the exception of scanning speed, which was optimized in accordance to the DFM max achievable speed in Figure 4.30d. Specifically, the laser settings were as follows: pulse energy - 0.52 mJ; hatch direction along the tilt (vertical direction); hatch spacing - 4 μm and pulse distance also kept to 4 μm. It can be clearly seen from Figure 4.30 c and Figure 4.30d that DFM dynamic limitations can have a very detrimental effect on

the machining results if they are not taken into account when generating the Part NC programme (G code).
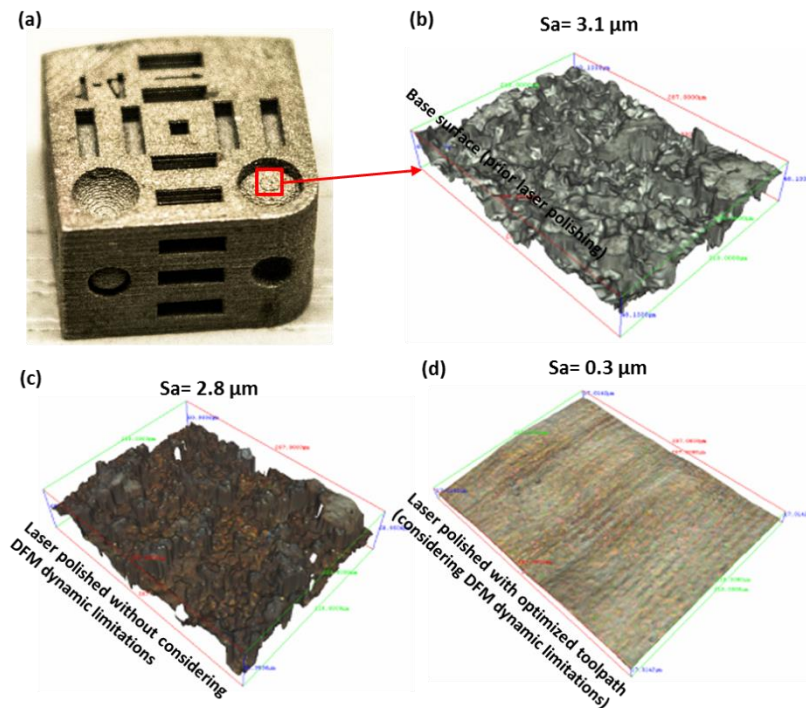
Figure 4.30 Laser polishing trials: (a) 3D Printed cube with different geometrical features; (b) surface roughness measurements prior to laser polishing; (c) surface roughness after laser polishing, but without optimized toolpath; (d) surface roughness after laser polishing with optimized toolpath (considering the DFM limitations)

4.5   Conclusions

This chapter reported a systematic quantitative study for investigating the ARR capabilities of state-of-art LMM systems. The following conclusions could be drawn based on the results from the carried out research in this Chapter:

- The machining accuracy with the optical axes typically decreased with the increase of nominal dimensions of the geometries to be produced, which suggests that the best machining accuracy could be obtained at the centre of the laser machining field of view defined by the integrated focusing lens. System A exhibited the best machining accuracy level of the optical axes amongst all systems both along horizontal and vertical directions with the majority of data lying within the machining accuracy tolerance of ±10 μm. However, the rest of the investigated laser exhibited much higher machining errors, in particular, the accuracy of systems B, C and D was 120 μm, 433 μm and 85 μm, respectively. The deteriorated machining accuracy in systems B, C and D can be mostly

attributed to laser system calibration errors, which exemplifies that the calibration of scan heads is very critical for obtaining the desired level of machining accuracy. This was also demonstrated by the significant improvements of the machining accuracy following calibration of the laser systems, i.e. system D exhibited a ~80% improvement in the accuracy level after its calibration.

- The accuracy of the mechanical axes was much better, generally in the range of ±2 μm to 4 μm, compared to that of the optical axes. This could be partially attributed to the much lower processing speed of the mechanical stages, typically less than 100 mm/s, in contrast to that of the scan heads, greater than 500 mm/s. Other factors, which contribute to the better machining accuracy with mechanical axes is their better closed-loop control than that of optical axes.

- Although two of the systems produced repeatable and reproducible machining results, this was not the case for all systems analysed in this study. Import factors which could contribute to the observed deteriorations of machining repeatability and reproducibility in some of the investigated systems include utilization of not sufficiently adequate tools and techniques which can provide the required level of precise positioning and alignment of workpieces prior to the laser machining operations.

- The lower dynamic of Z-module affected the machining accuracies of the beam delivery system when processing inclined surfaces at different scanning speeds. The deviation from the nominal value increases with the increase of scanning speeds. Only at relatively lower scanning speeds, the depth of focus can compensate the inferior dynamic of Z-module to some extent, in comparison to those of X and Y beam deflectors.

- A specialized experimental technique for quantifying the dynamic capabilities of Z modules is also proposed in this research. The results showed that the DFM dynamic capabilities are substantially inferior to those of X and Y beam deflectors, in particular the maximum speed of the Z module is less than 10% of the maximum speeds achievable with X and Y optical axes of the scanhead. This suggests that at high speeds of the X and Y beam deflectors the depth of focus of the laser micro processing setups may not be sufficient to compensate the lag in executing the necessary Z movements when processing free form surfaces. Thus, in such cases, it will be necessary to reduce the X and Y beam deflectors' speeds of the 3D scanheads and thus to operate below the max speeds achievable by any given z-module when performing laser structuring or texturing operation

on free form surfaces in order to achieve the required accuracy and repeatability.

The evaluations of the ARR capabilities of LMM systems' key component technologies highlight that state-of-art LMM systems do not have the technology maturity level of well-established micromachining processes like milling. Finally, the research in this Chapter provides quantitative evidences that further system-level developments are required in order to improve the overall machining ARR of LMM platforms, especially when optical axes are employed during the laser processing operations.

CHAPTER 5

DEVELOPMENT OF GENERIC INTEGRATION TOOLS FOR RECONFIGURABLE LASER MICROMACHINING SYSTEMS

Outline of the chapter

This chapter is dedicated to the development of generic integration tools, which address system-level issues in LMM platforms that has negative impact on laser systems performance in terms of machining ARR. In particular, the chapter reports on the design of a modular workpiece holding system, which increases the flexibility of LMM platforms to realize different machining configurations and also supports the integration of LMM with other complimentary micromachining processes in multi-process manufacturing systems. Furthermore, the chapter proposes an automated workpieces' setting up routine which substantially reduces the time and manual efforts required to register workpieces in the LMM systems prior to the machining routines, while it also increases the alignment ARR of the workpieces and thus to create the necessary pre-requisites for achieving robust and repeatable machining results.

The research reported in this Chapter refers to Publication 4 from the List of Publications.

5.1 System-level performance issues of LMM platforms

5.1.1 Component technologies' requirements

A reconfigurable LMM platform should have sufficient flexibility to realise different processing operations, e.g. structuring of parts that incorporate functional features with varying sizes and geometrical complexity, polishing of free-form parts, capability to process different materials, e.g. metals, polymers and glasses, while satisfying specific requirements in regards to ARR, surface integrity and processing efficiency. Such concentration of operations in a single machining setup requires system-level functionalities that are determined both by the component technologies employed for their realisation and also by a

range of integration tools and techniques used to assure their functional operability within predefined ARR constraints.

Chapter 4 introduced four different reconfigurable LMM platforms. A system-level analysis of those four laser systems was conducted to identify the common component technologies that were necessary for their implementation. It is important to note that the four investigated LMM systems integrate similar and in some case identical state-of-art representative component technologies and they are built by different system integrators. In this way an attempt was made to identify and assess objectively the system-level integration issues in implementing LMM systems. The results of this analysis are provided in Table 5-1, where their component technologies are split into two categories, in particular main component technologies, which were available across all LMM configurations and auxiliary ones, whose implementation and functionality varied between the platforms but were required to fulfil common requirements in regards to systems' operability, stability, flexibility and safety.

Table 5-1 Functional specification of component technologies for LMM

Main Component Technologies
• Short/ultra-short pulsed laser source(s) with capabilities to vary the average power, repetition rates, wavelengths and laser spot characteristics for realising different material processing mechanism
• 3D optical beam deflection system with high dynamic capabilities
• Focusing telecentric lens for a consistent beam incident angles within the field of view
• Linear mechanical stages with high positioning accuracy and precision to realise Infinite Field of View (IFV) processing
• Rotary mechanical stages for realizing different manufacturing configurations
• Measurement probes for inline inspection and alignment of parts
• Optical beam delivery path with capabilities to vary the beam spatial profile
Auxiliary Component Technologies
• Machine frame structure to minimise any disturbances from the surrounding environment
• Enclosure for Class 1 laser processing [195]
• Laser fume extractor
• Inline energy/power measurement device
• Laser beam profiler for setting up optimal laser machining parameters
• Modular workpiece holding for realising different machining configurations and robust integration into multi-process manufacturing systems
• Workpiece's setting up routines
• PC-based control system with specialised Graphical User Interface (GUI)

5.1.2 System-level integration issues

To conduct a critical analysis of integration issues in designing and implementing LMM platforms, it is very important to study laser systems with almost identical or comparable hardware configurations. Thus, any discrepancy in their LMM capabilities can be attributed mostly to system-level integration issues associated with their component technologies and to much less extend to their technical specifications. Therefore, three of the four state-of-the-art LMM systems presented in Chapter 4 were selected to carry out this critical analysis. Key capabilities expected and also representative of those already available in reconfigurable LMM platforms were analysed. In particular, a comparative study to quantify the machining ARR of the three systems was firstly conducted to identify significant discrepancies in their LMM capabilities, as discussed in Chapter 4. In addition, other important key manufacturing capabilities that were considered are provided in Table 5-2 together with the results of the analysis of the three platforms, denoted as A, B and C.

Table 5-2 System-level capabilities of the three reconfigurable LMM platforms

System	Description
Flexible workholding solutions for realising different machining configurations, i.e. for laser processing of axis-symmetric parts and multi-sides laser machining, and for seamless integration of LMM into mutli-stage manufacturing platforms	
A	Custom-made workholding devices for positioning parts (individual solutions for different machining configurations/operations). No integration of LMM into a multi-process manufacturing system is envisaged.
B	In-house workholding devices are produced to meet different application requirements.
C	No special workholding devices. Mechanical stages are used to place samples in the laser system.
Automated routines/strategies for executing complex machining operations that require the utilization of both linear and rotary mechanical axes	
A	Not available and a custom-made solution under development.
B	Manual methods to utilize rotary and linear stages simultaneously.
C	No automated strategies are available.
Workpiece's setting up routines with pre-defined ARR	
A	Optical camera for lateral alignment and a confocal probe for setting up the machining surface. Accuracy and repeatability within +/-10 μm.
B	Alignment solution employing a confocal probe. Accuracy and repeatability better than 20 μm.
C	Manual alignment employing a high resolution optical camera. Accuracy and repeatability better than 50 μm.
Control system with specialised LMM GUI	
A	A system/tool with specialised GUI realised in commercially available CAD software for entering different laser machining parameters and also for handling

	different input file formats.
B	A system with GUI for controlling laser machining parameters.
C	Several GUIs for different component technologies that run simultaneously to control laser machining parameters.
ARR achievable in different LMM operations	
A	ARR better than +/- 10 μm.
B	Accuracy within +/- 60 μm while repeatability and reproducibility are better than 20 μm.
C	ARR better than +/- 150 μm.

There are some other commercially available laser machining systems [196-198] that are designed for specific applications, in particular for producing cooling holes on aerospace components or structuring/texturing free-form surfaces of moulding tools. They are based on conventional machine tool platforms and thus their frame structures, PC-based control systems and workpiece setting up routines and equipment are the same as those used in multi-axis machining centres, e.g. high precision milling machines. Such systems cannot be considered LMM platforms as they represent standalone system implementations designed for handling relatively big components, e.g. turbine blades and mould tools, while the laser machining system that are the focus of the research in this chapter are for machining relatively small components, e.g. usually fitting within a working envelop of mm 65 x 65 mm x 10 mm and weight less than 1 kg. Therefore, such commercially available laser machining implementations were not considered in the system-level analysis carried out in this research.

It is apparent from the system level analysis in Table 5-2 that even though all three LMM systems can provide extensive manufacturing capabilities, their available tools are not generic and far from what should be expected from machine tools for realising complex micromachining operations. Furthermore, the results of the comparative study in Chapter 4 also revealed substantial discrepancies in terms of ARR capabilities of the analysed three systems. For example, the performance of System A was assessed to deliver ARR capabilities better than +/- 10 μm, while System B and C had ARR of +/- 60 μm and +/- 150 μm, respectively. Since, the hardware configurations of the three systems are comparable, the discrepancies in terms of LMM systems performance clearly demonstrate the existence of system-level integration issues. In particular, the system-level issues that were identified as critical for improving the reliability, robustness and interoperability of LMM platforms and also to achieve the necessary machining ARR for their broader use are: the development of modular workpiece holding device, automated workpiece setting up routines and automated multi-axis machining strategies. The importance of these system-level integration solutions

for achieving ARR that are commonly required across different application areas is further reinforced by the work reported by other researchers [199]. In particular, in a study reporting the application of LMM for producing a ceramic microsurgical tool with features on two opposite sides of the component, a sequence of manual operations (fixing, repositioning and alignment in a single machining setup) were performed to manufacture the tool [101]. The system-level issues in this machine-fixture-component configuration had detrimental effects on the overall machining results; i.e accuracy of produced components was within +/- 70 μm while reproducibility was less 100 μm. Even though, the reported machining errors of the produced components were not critical for the parts' functionality, this case study points at some typical requirements that modular workpiece holding devices and automated workpiece setting up routines should fulfil to deliver higher ARR. In another case study on LMM of rollers, a rotary stage is used in a LMM platform [200]. It is stated that new software solutions were developed to achieve the required ARR in the used LMM configuration. Especially, these tools made possible the use of the rotary stages but they were only applicable for the processing of axis-symmetric parts, where the laser beam is fixed and thus the high dynamic of optical beam deflectors could not be used [200]. Again, this case study demonstrates how system-level limitations on the simultaneous use of optical and mechanical beam movements affect the capabilities of the LMM platforms, especially where high ARR are required.

5.2 Developments of system-level integration tools and techniques for LMM

5.2.1 Design and implementation of modular workpiece holding system

Based on the analysis of LMM industrial applications, where features with dimensions of less than 100 μm and accuracy better than 10 μm are required [201], the following generic considerations were identified that were taken into account when designing modular workpiece holding devices:

- High ARR achievable in positioning parts in LMM platforms;
- a modular design for realising different LMM configurations;
- designs based on standardized components for cost effective and robust implementation in different LMM configurations;
- compactness and minimal weight to minimise the negative dynamic effects on machining results;

- the necessity for common unifying solutions for integrating different modular technologies, e.g. machining, material processing, inspection and alignment, in multi-process manufacturing platforms;
- interchangeability for realising different LMM configurations and also to support both manual and automated workpiece setting up routines;

The workpiece holding device that was designed is schematically presented in Figure 5.1. It consists of standardized commercially available components that are well proven in different machining applications and at the same time do not require frequent maintenance [202]. In particular, the workpiece holding device consists of main and secondary assembly units. The main assembly unit incorporates a "macro" receiver that can be precisely fixed and referenced either to a mechanical stage (rotary or linear) or to any other surface of the machine frame structure and a drawbar that provides means to attach precisely various workpiece holding adapters/extensions to the receiver. The secondary assembly unit incorporates workpiece holding extensions that can ensure the necessary flexibility to meet the requirements for various laser machining operations. As shown in Figure 5.1, examples of workpiece holding extensions include:

- pallets - interface plate assemblies for holding prismatic parts in machining operations requiring only linear movements of mechanical stages,
- L-shaped brackets assembly for holding prismatic parts in machining operations requiring both linear and rotary movements of mechanical stages;
- chucks for holding axis-symmetric parts.

Another workpiece holding extension that was designed and implemented in this research to enable two-side laser micro-processing routines is also provided in Appendix 4. Thus, the modular design of the proposed workpiece holding device provides the flexibility and the robustness necessary to realize various LMM configurations. Figure 5.2 shows examples of manufacturing configurations that were implemented to test the proposed design. In particular, workpiece holding devices to carry out one-side processing of a single part or an array of parts, multi-side machining of parts, and processing of axis-symmetric parts. Since the different manufacturing extensions are accurately referenced via a system of datum points in the macro receiver and the pallet by applying a consistent force through the drawbar, different extensions can be easily integrated into the LMM platforms without the need for any manual setting up operations. This leads both to significant reduction in setting up time and

also reduces uncertainty associated with workpieces' positioning in LMM platforms. Figure 5.1 also provides details about the masses of both the main assembly unit and also of each of the proposed workpiece holding extensions. Taking into account the capabilities of mechanical stages [163] and stacks of them in LMM platforms it can be concluded that the proposed workpiece holding device with a mass not exceeding 3.5 kg will have minimal negative dynamic effects on LMM operations. The modular design will also facilitate the integration of LMM operations in multi-process manufacturing systems. In particular, an installation of the main assembly units in each of the integrated processing steps in a multi-process manufacturing system allows workpieces to be mounted on a common holding extension and subsequently to be carried throughout all processing and/or inspection steps. This can lead to significant reduction in alignment efforts in each of the integrated processing setups and also in a significant reduction of uncertainties associated with the entire multi-process manufacturing sequence. The positioning ARR of the proposed workpiece holding device are carefully assessed in the later sections of this chapter.

Component	Mass (kg)
Main assembly	0.83
Extension 1	0.34
Extension 2	2.48
Extension 3	1.12

1	Macro reciever
2	Drawbar
3	Pallet
4	Interface plate
5	L-shaped bracket
6	Axis-symmetric chuck
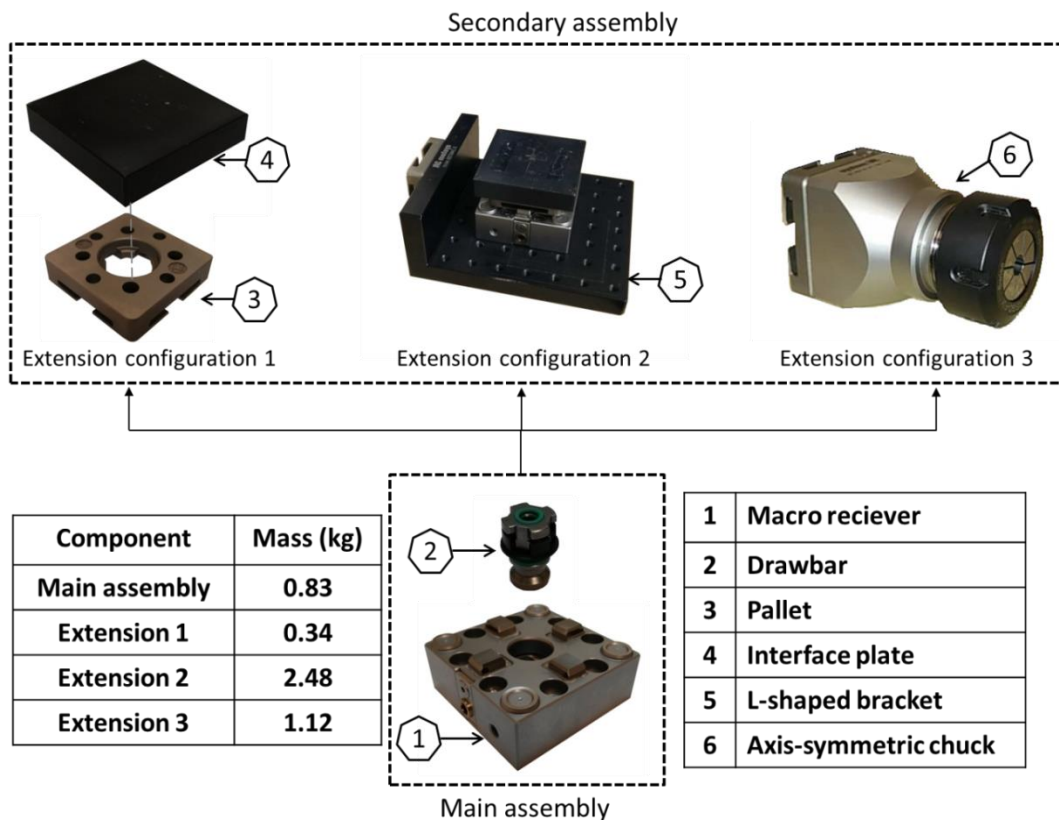
Figure 5.1 The modular design of the proposed workpiece holding device
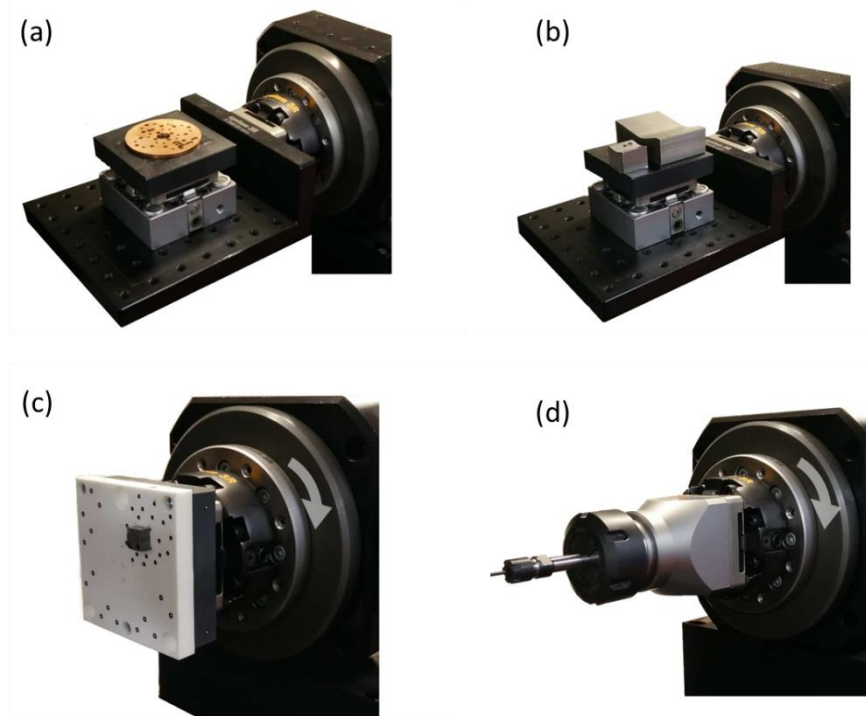
Figure 5.2 Workpiece holding extensions to realize: (a) one-side processing of a single part; (b) one-side processing of an array of parts; (c) multi-side processing of a single part; (d) machining of axis symmetric parts

5.2.2   Design and implementation of an automated workpiece's setting up routine

The geometrical registration of a workpiece in the machine coordinate system (MCS) prior to executing LMM operations is of critical importance in achieving the required level of machining ARR. The common workpieces' settings up routines used in LMM platforms cannot be considered adequate due to their high level of uncertainty in the registration of components in the laser systems [203]. Important factors that contribute to the high level of uncertainty associated with the widely used workpieces' settings up routines include: the reliance on operators' experience to perform the alignment procedures, the utilization of different component technologies for alignment, such as cameras, confocal probes, and mechanical contact probes [204]. These factors affect the achievable ARR in correlating the workpiece coordinate system (WCS) to MCS and are a major contributor to the overall ARR in LMM operations. Thus, to minimise the uncertainty associated with the workpieces' settings up routines new tools have to be developed that can address the following requirements:

- flexibly to align work pieces with various geometries;

- minimising/eliminating the influence of workpiece's imperfections, e.g. edge definition and surface integrity, on the alignment results;

- capabilities to link WCS to MCS without the need for pre-existing alignment marks;

- capabilities to perform non-contact alignment of workpieces and thus to avoid damaging processed surfaces and hence additional uncertainty in executing such routines, especially when polymers are machined or pre-existing micro features that can be easily damaged are used as datum points;

- minimising the influence of the human factor and the need to use experienced operators in conducting the alignment routines.

An automated workpiece's setting up routine is proposed to address these requirements. A schematic representation of this routine is given in Figure 5.3. It utilizes the FV technology [176] and the modular workpiece holding system presented in Section 5.2.1. The installation of the modular workpiece holding device both in a FV system and in the LMM platform establishes the physical link between them and thus the coordinate systems of the FV system (FCS) and MCS can be correlated with a repeatability better then +/- 1 μm (see the experimental validation section of the modular workpiece holding device – Section 5.4.1) and thus can be considered as a single coordinate system of the holding device (HCS). Therefore, through the use of the FV system the geometrical correlation of WCS to HCS can be established that consecutively links WCS to MCS automatically because the correlation between HCS and MCS is already established. The proposed alignment routine is fully automated and this is illustrated in Figure 5.3. Since the FV system creates a 3D representation of the workpiece as a cloud of points with uncertainty less than 0.12 μm (when 5x magnification is used) [176], it is possible to capture workpiece imperfections and thus to eliminate their negative effects in linking WCS to MCS. Furthermore, the alignment routine is non-contact and pre-existing micro features can be used without damaging them, and thus eliminates the need for alignment marks on the workpiece. The proposed alignment routine can also increase significantly the throughput of LMM platforms, because the idle times associated with in-situ alignment routines are eliminated. In addition, it is important to stress that the same alignment routine can be used if a FV probe is integrated in the LMM platforms as shown in Figure 5.4. In this way the uncertainty associated with the routine can be further reduced in expense of the LMM platforms' throughput. Finally, it should be also noted that in-line inspection routines similar to the workpiece's setting up one can be developed for

implementing rest-volume machining strategies on LMM platforms [205] and also for generating "customized" toolpaths for adaptive machining [206]. In particular, the adaptive machining approach allows form variations of a workpiece in comparison to its CAD model to be compensated and thus to improve the overall machining ARR [207].
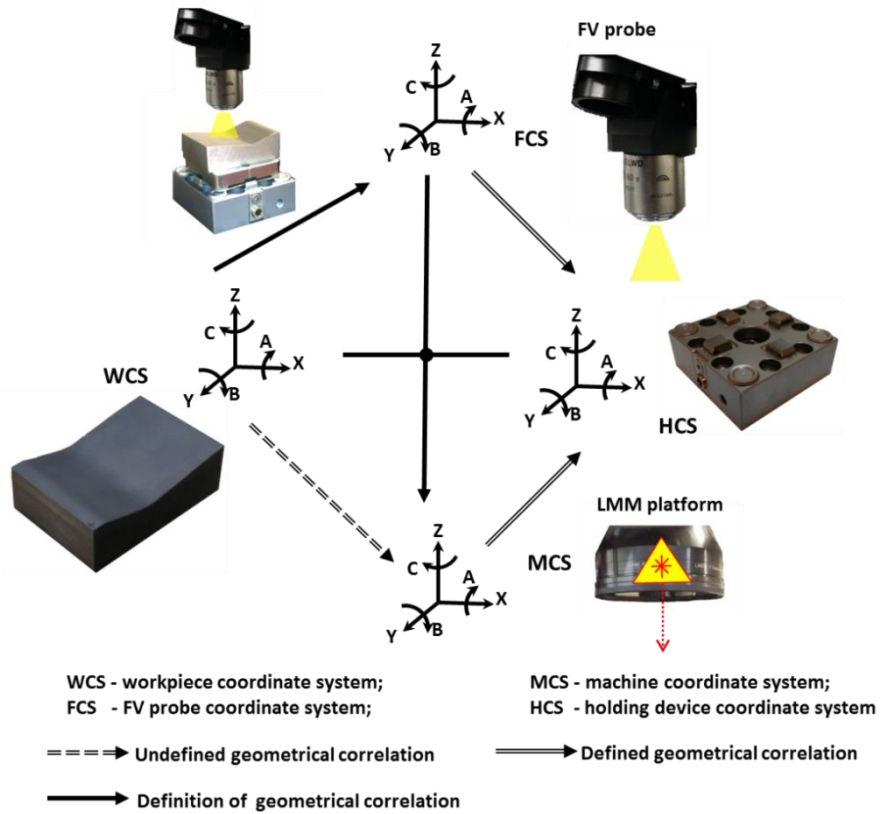
Figure 5.3 Schematic representation of proposed workpiece's setting up routine

Note to Figure 5.3: The Right-hand rule notations are used.
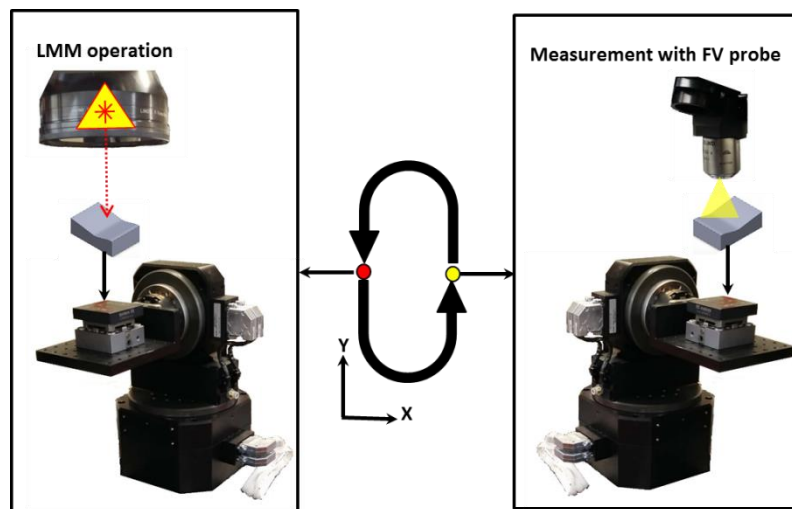
Figure 5.4 Workpiece's setting up routine with a FV probe integrated into a LMM platform with C rotary stage to swivel between machining and inspection positions

5.3   Experimental evaluation of the proposed integration tools and techniques

5.3.1   Modular workpiece holding device

The positioning ARR of the proposed modular workpiece holding device are validated with the test part shown Figure 5.5. In particular, four equidistantly patterns are produced on an interface plate of the modular workpiece holding device with a spacing between them equal to 50 mm. The pattern consists of five 0.5 mm long crosses, which are positioned along the x and y axes of the LMM platform with the nominal distance between them of 0.6 mm. The relative positioning movements between the crosses were performed with the mechanical stages due to their higher accuracy and repeatability than the optical scanning head. After the laser machining of each cross in the four patterns the pallet was dismounted from the holding device and then mounted back in order to investigate the ARR achievable with the proposed workpiece holding device. The test structures in Figure 5.5 were machined on one more interface plate in order to evaluate the positioning reproducibility of the proposed modular workpiece holding device. The positioning accuracy was evaluated based on the maximum deviations of the distances between the crosses in comparison to their nominal values of 600 µm. The positional repeatability and reproducibility of the holding device were evaluated by comparing the measured distances between the crosses with the average distances between them that were obtained from the four patterns on one plate and on the two plates, respectively. Thus, positional repeatability and reproducibility of the modular workpiece holding device are evaluated based on results obtained from 40 repositionings of the two plates in the LMM setup (20 repositionings per sample).
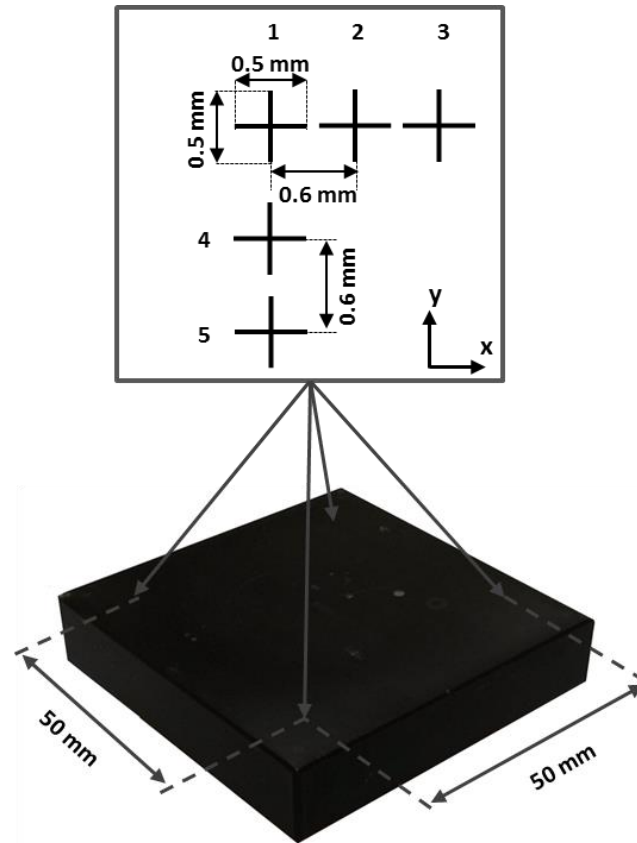
Figure 5.5 The test plate used to validate positioning ARR of the proposed modular workpiece holding device

5.3.2 Automated workpieces' setting up routine

Experimental evaluation of the alignment ARR of the proposed automated setting up routine is performed on a 3D surface of a stainless steel workpiece shown in Figure 5.6. The overall size of the sample is 60 x 40 mm and LMM is used to texture the 3D surface of the sample with 0.04 mm wide and 0.02 mm deep intersecting trenches, which are 1mm apart and run along the x and y axes of the workpiece. In the absence of pre-existing alignment marks on the wokrpiece, one of the sample corners is used as a WCS origin as shown in Figure 5.6. The laser machining of each trench on the sample is performed after the workpiece has been dismounted and aligned again with the proposed setting up routine and thus to assess its alignment capabilities. In total, 98 trenches were machined, 59 and 39 along x and y axes, respectively. The processing speed was reduced to 10 mm/s in order to improve the quality of the produced trenches, i.e. their edge definition. The LMM operation was performed on two different workpieces. Since LMM is very sensitive to focal point changes along z axis, the beam propagation direction, any depth and width deviations of the trenches along the 3D surface were used to judge about the alignment capabilities of the proposed routine along the

z axis. At the same time, the lateral (X-Y plane) alignment accuracy was assessed based on the overall deviations of the relative distances between trenches in comparison to the nominal value of 1 mm. The lateral repeatability and reproducibility of the proposed alignment routine were evaluated by comparing the measured distances between trenches to their average values obtained from the inspected regions on one sample and on the two samples, respectively. Thus, the repeatability and reproducibility of the proposed automated workpiece's setting up routine are evaluated based on results obtained from 196 repetitions of the alignment strategy (98 alignments per sample).
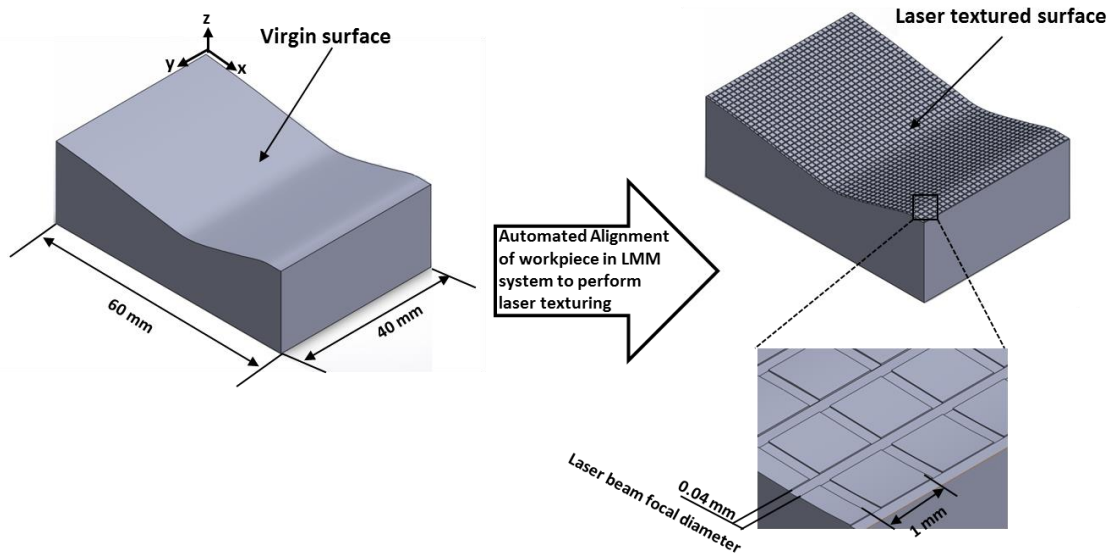
Figure 5.6 Laser textured test part used to validate the proposed workpiece's setting up routine

5.4 Results and Discussions

5.4.1 Modular workpiece holding system

Figure 5.7a shows one of the laser produced patterns on the interface plate of the workpiece holding device and also the measurements carried out to assess the positioning ARR of the device. In particular, D_1, D_2, D_3, and D4 are the relative distances between crosses 1 and 2, 2 and 3, 1 and 4, and 4 and 5, respectively. Also, Figure 5.7b shows how one single measurement of the relative distance between crosses 1 and 2 (D_1) is completed using the Parallel Line Automatic tool of the Alicona G5 2DImageMerasurment module [178]. The automatic tool was used due to the high accuracy and repeatability of the carried out measurements. Table 5-3 provides the results for the four patterns on the two interface plates and each of them is the average value of five measurements as prescribed in the guidelines for

assessing machine tools uncertainty budgets [208]. In particular, Table 5-3 provides the measured distances together with their corresponding deviations from the nominal value of 600 μm and the calculated average values calculated based on the results from each sample and from both together. The positioning ARR capabilities of the proposed workpiece holding device are assessed based on the analytical procedure provided in Section 5.3.1. It can be seen in Table 5-3 that the positioning accuracy of the proposed workpiece holding device is 0.85 μm, 0.75 μm, 0.75 μm and 0.95 μm and 0.90 μm, 1.00 μm, 0.55 μm and 0.75 μm for Patterns 1, 2, 3 and 4 on the two plates, respectively. Thus, it can be stated that the positional accuracy of the proposed modular wokrpiece holding device is better than 1.00 μm. The positional repeatability based on the average measured distances calculated from Sample 1 and 2, 599.55 μm and 599.95 μm, is 1.2 μm and 1.05 μm, respectively, and thus it is better than 1.2 μm. At the same time, the average measured distance value for the two plates is 599.87 and therefore the positioning reproducibility of the proposed workpiece holding device is better than 1.1 μm. Since the mechanical stages are used to execute repositioning movements between the crosses, their positional resolution should be also included in the uncertainty calculations when quantifying the ARR capabilities of the workholding device. In particular, by taking into account the uncertainty related to the stages' movements of 0.25 μm, the total uncertainty is 0.3 μm at the 95% confidence level (calculated based on the uncertainty procedure provided in Chapter 2). Overall, it can be stated that the positioning ARR of the proposed workpiece holding device including the expanded uncertainty are better than +/- 1.0 μm.

Table 5-3 Results from experimental testing of the modular workpiece holding device

Plate 1 – Pattern 1 (bottom left)				
	D_1	D_2	D_3	D_4
Nominal distance (μm)	600			
Measured distance (μm)	599.35	599.15	600.35	599.45
Deviation (μm)	-0.65	-0.85	0.35	-0.55
Plate 1 – Pattern 2 (bottom right)				
Nominal distance (μm)	600			
Measured distance (μm)	600.50	600.15	600.75	599.35
Deviation (μm)	0.50	0.15	0.75	-0.65
Plate 1 – Pattern 3 (top left)				
Nominal distance (μm)	600			
Measured distance (μm)	599.30	599.25	600.35	600.45
Deviation (μm)	-0.70	-0.75	0.35	0.45
Plate 1 – Pattern 4 (top right)				
Nominal distance (μm)	600			
Measured distance (μm)	599.50	599.65	600.15	599.05

Deviation (µm)	-0.50	-0.35	0.15	-0.95
Average measured distance for Sample 1 (µm)		599.55		
Plate 2 – Pattern 1 (bottom left)				
	D_1	D_2	D_3	D_4
Nominal distance (µm)	600			
Measured distance (µm)	599.10	599.25	599.35	599.95
Deviation (µm)	-0.90	-0.75	-0.65	-0.05
Plate 2 – Pattern 2 (bottom right)				
Nominal distance (µm)	600			
Measured distance (µm)	601.00	600.15	600.45	599.85
Deviation (µm)	1.00	0.15	0.45	-0.15
Plate 2 – Pattern 3 (top left)				
Nominal distance (µm)	600			
Measured distance (µm)	600.50	599.45	600.05	599.75
Deviation (µm)	0.50	-0.55	0.05	-0.25
Plate 2 – Pattern 4 (top right)				
Nominal distance (µm)	600			
Measured distance (µm)	600.20	600.65	600.25	599.25
Deviation (µm)	0.20	0.65	0.25	-0.75
Average measured distance for Sample 2 (µm)		599.95		
Average measured distance for the two plates (µm)		599.90		
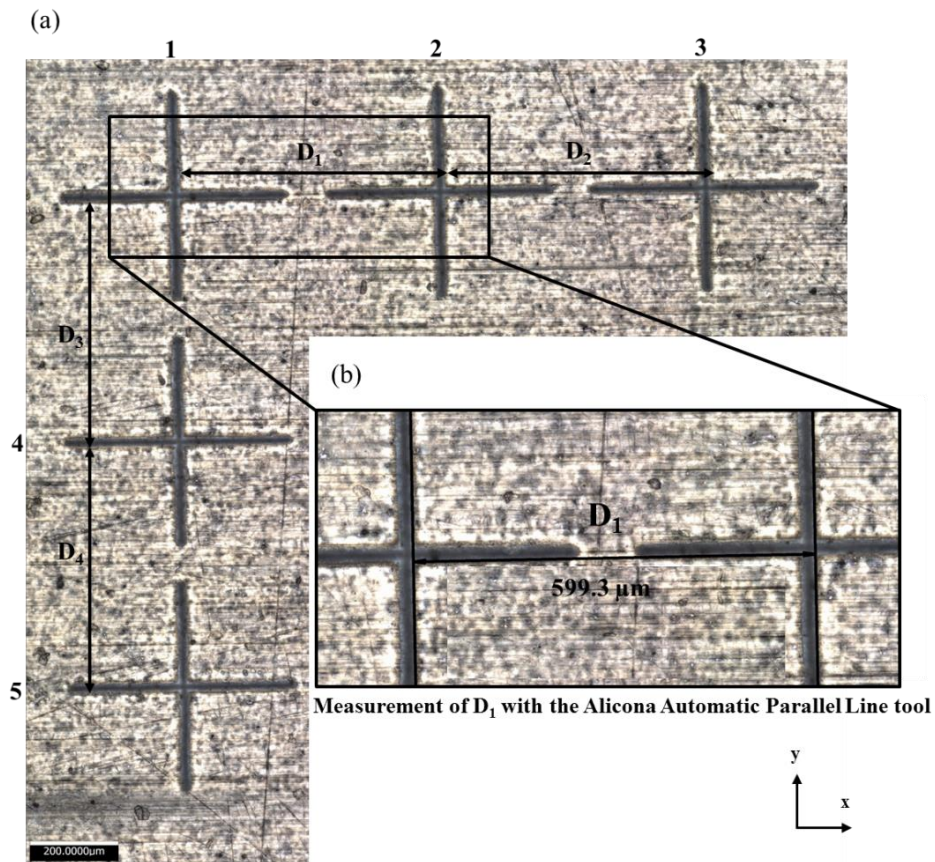
Figure 5.7 Laser machined Pattern 1 on the first interface plate: (a) a view of the complete pattern and (b) close view of two crosses from the machined pattern

5.4.2 Automated workpiece's setting up routine

Figure 5.8a shows a cloud of points representing the 3D surface of a sample prior to the laser texturing operation, while Figure 5.8b provides a close view of one of the sample edges, where workpiece imperfections such as roughness, waviness and edge definition are clearly visible. Such workpiece imperfections affect the achievable alignment accuracy with manually executed setting up routines when high resolution optical cameras are employed. In contrast, the proposed alignment routine scans the complete sample and thus takes into account the wokrpiece imperfections and minimises their effects on alignment accuracy and precision. Figure 5.9 shows a scan field of the laser textured 3D surface, where the test procedure applied to validate the proposed workpiece setting up routine is also depicted. In particular, P_i represents the points at which the depth and width profiles of the trenches are analysed, while I_i represents the intersection points between the trenches used to evaluate the lateral alignment accuracy. An example of the carried out profile analysis is given in Figure 5.10 where the width and depth of a single trench at three P_i are provided. LMM operations are very sensitive to any offsets of the focal points from the workpiece surface which results in variations of the depth and width of the trenches along the 3D surface. There are two main factors contributing to this offset, in particular the alignment accuracy and the dynamic of the Z optical axis, especially the moving lens used to realise it. The scanning speed during the laser texturing operation in this test was reduced to 10mm/s to minimise the effects of this factor. Consequently, the good profile uniformity of the trenches along the 3D surface can be attributed mostly to the capability of the proposed setting up routine. The total number of analysed trenches is six, three along the x and y axes, and thus the total number of P_i inspected is 18. Figure 5.11 provides a plot with the performed analysis of all 12 trenches machined on the two samples. Based on these results it can be stated that the maximum deviation of the widths and the depths of the trenches on the two samples do not exceed +/- 5 μm and thus this demonstrates the accurate and repeatable alignment along the z axis of the LMM platform.

Furthermore, a quantitative evaluation of the lateral alignment ARR achieved with the proposed setting up routine is also performed by measuring the distances between individual trenches at the intersection points, I_i, as shown in Figure 5.12. In particular, the relative distance between the trenches is measured and then compared with their nominal values to judge about the alignment accuracy of the proposed setting up routine. For example, the

alignment accuracy shown in Figure 5.12 is 5.3 μm and 2.5 μm along the y and x axes, respectively. The total number of intersection points investigated per sample is four and the results are provided in Table 5-4. The maximum overall deviation of the relative distances between the trenches for the two machined samples is 7.4 μm and thus it can be stated that the lateral alignment accuracy is better than 7.4 μm. Thus, taking into account the average values in Table 5-4 the lateral alignment repeatability achieved for Sample 1 and 2 are 5.8 μm and 7.3 μm, respectively, while the lateral alignment reproducibility is better than 6.9 μm. The total uncertainty of the alignment routine is 0.7 μm at the 95% confidence level (refer to Chapter 3 for detailed explanation of the uncertainty procedure). Based on these results, it can be stated that the lateral alignment ARR achievable with the proposed workpiece setting up routine including the expanded uncertainty are better than +/-4.0 μm.
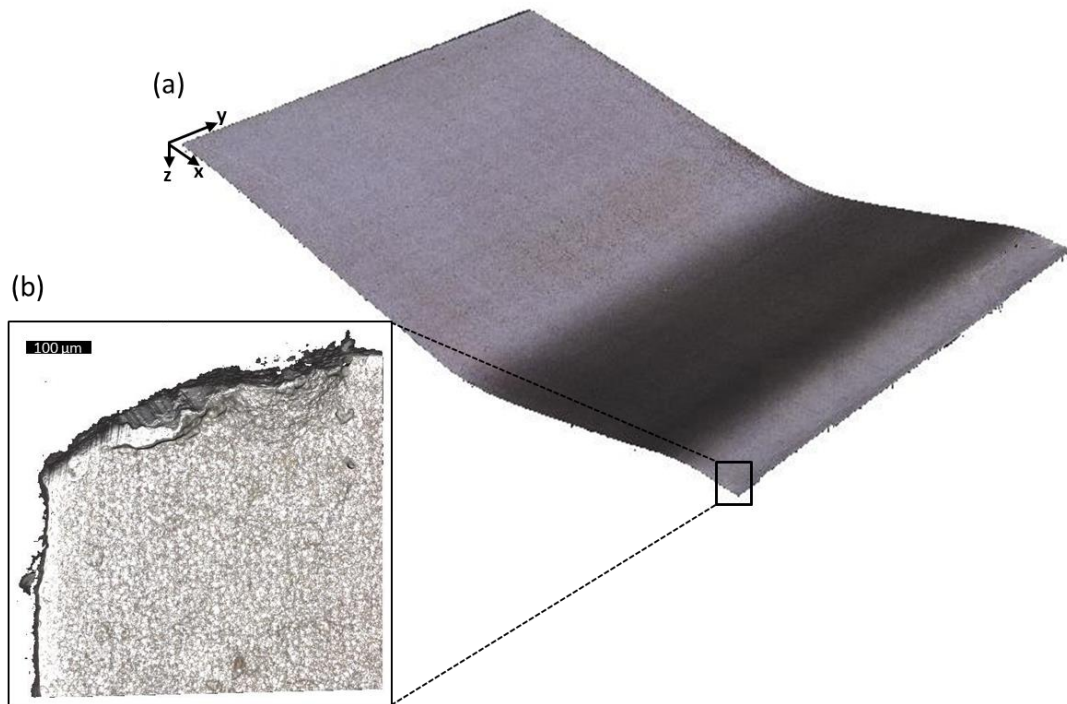
Figure 5.8 The scan results obtained with the FV system: (a) 3D surface of the sample workpiece represented as a cloud of pints and (b) a close view of a sample edge
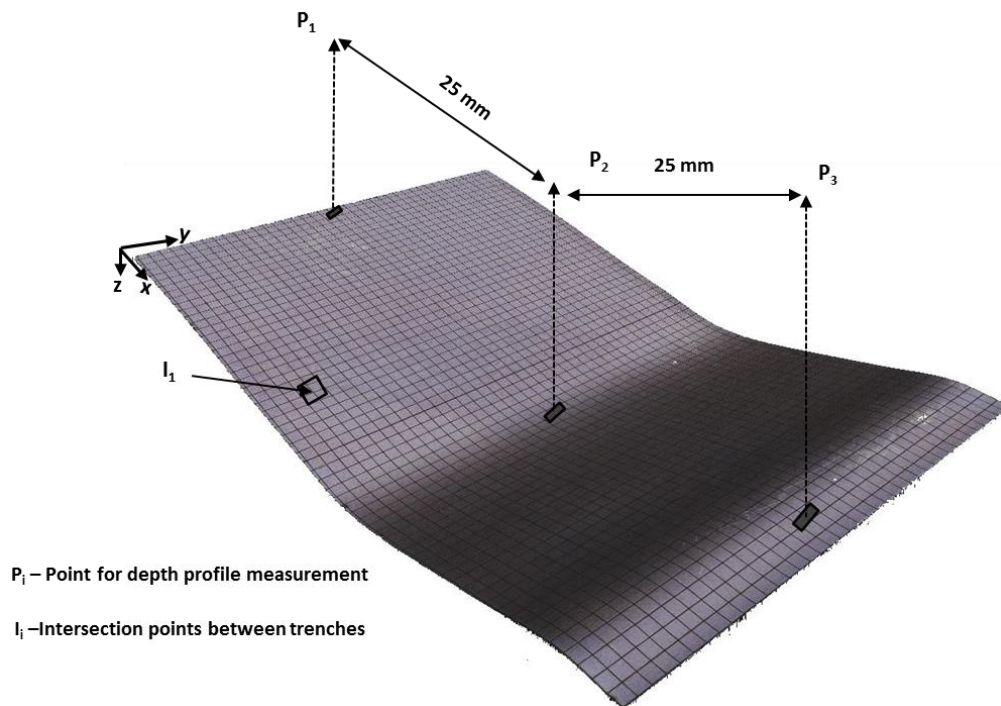
Figure 5.9 Laser textured surface represented as a cloud of points acquired with the FV system
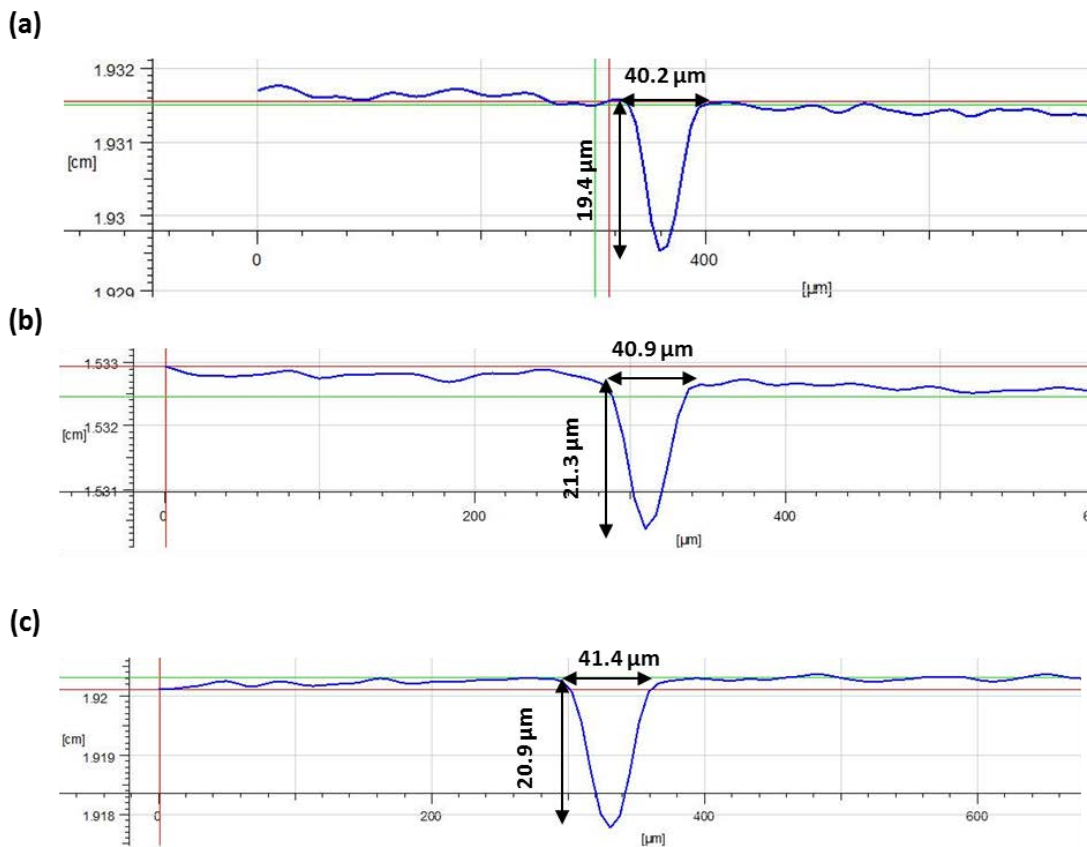
Figure 5.10 Depth and width profiles at three different points on a single trench: (a) point 1 (P1), (b) point 2 (P2) and (c) point 3 (P3)
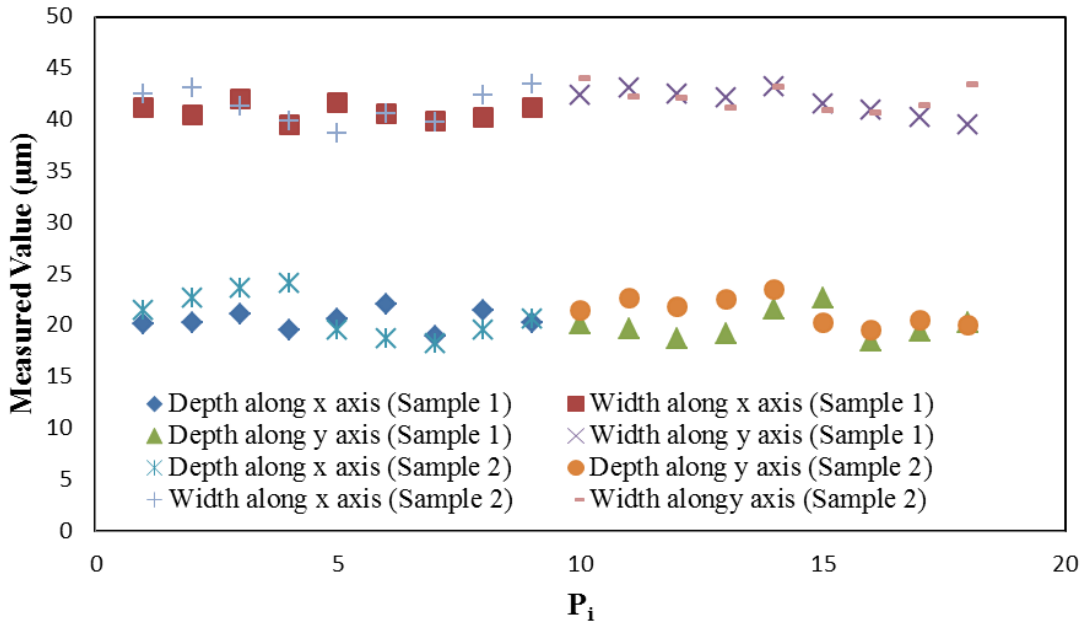
Figure 5.11 Results for the six trenches per sample analysed on the two samples
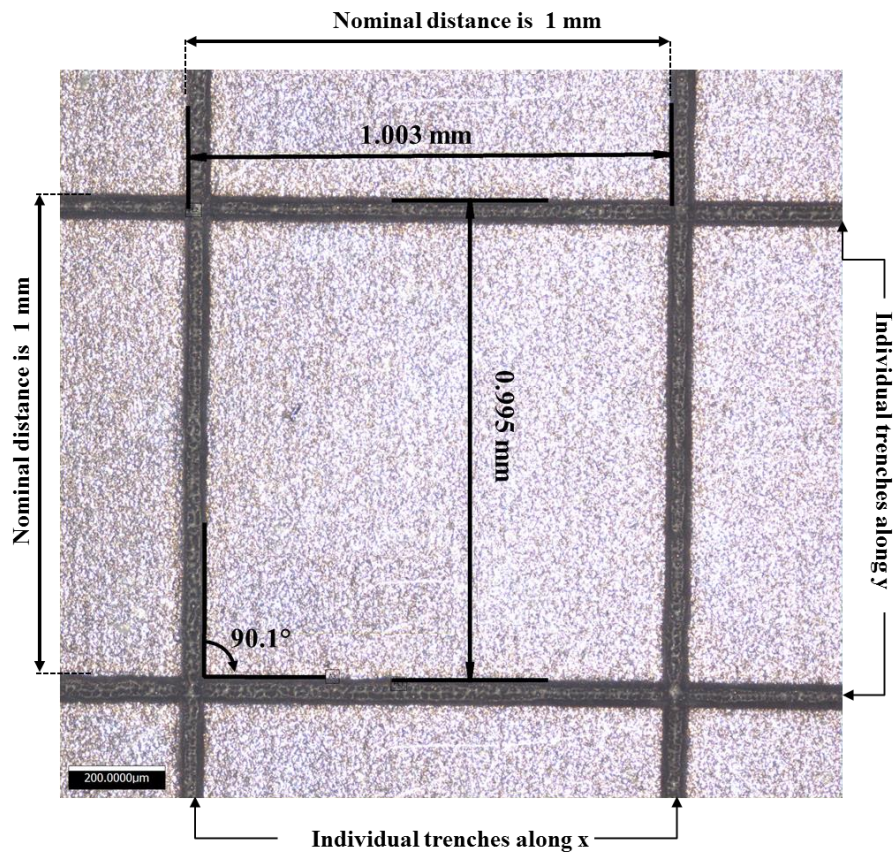
Figure 5.12 The measurements of distances between the trenches at an intersection point

Table 5-4 Measurements of relative distances between the trenches in regards to their nominal values

Parameter	Sample 1				Sample 2			
Intersection Point	I_1	I_2	I_3	I_4	I_1	I_2	I_3	I_4
Nominal Length (x-axis) (μm)	1000							
Measured Length (x-axis)(μm)	1002.5	1001.6	998.2	1003.2	1003.1	1004.2	997.6	1006.1
Deviation-x axis (μm)	2.5	1.6	-1.8	3.2	3.1	4.2	-2.4	6.1
Nominal Length (y-axis) (mm)	1000							
Measured Length (y-axis)(μm	994.6	996.5	1001.4	1005.1	993.9	996.4	1004.1	1004.2
Deviation-y axis (μm)	-5.4	-3.5	1.4	5.1	-6.1	-3.6	4.1	4.2
Overall absolute deviation (μm)	6.0	3.8	2.3	6.0	6.8	5.5	4.8	7.4
Average Measured Length (μm)	1000.4				1001.2			
Average Measured Length from the two samples (μm)	1000.8							

5.5   Conclusions

This chapter presents two generic integration tools for improving the system-level performance of reconfigurable LMM platforms. The tools offer sufficient flexibility, robustness and operability to address important system-level issues in LMM and create the necessary pre-requisites for improving machining ARR of LMM platforms. In particular, the research reports the design and implementation of modular workpiece holding device and automated workpiece setting up routine that have a significant influence on the machining capabilities of LMM platforms. The following conclusions can be made:

- System-level integration issues in LMM systems have been identified that limit their manufacturing capabilities and are important factors affecting their machining performance and also their broader use in various application areas.

- Existing LMM systems can provide extensive manufacturing capabilities but their available system-level integration tools are not generic and far from what should be expected from machine tools for realising complex machining operations. Especially, the system-level component technologies that were identified as critical for improving the reliability, robustness and interoperability of LMM platforms and also to achieve the necessary machining ARR for their broader use are: modular workpiece holding device and automated workpiece setting up tool.

- The modular workpiece holding device allows different LMM configurations to be realised, e.g. the machining of complex prismatic and axis-symmetric parts, while delivering positional ARR better than +/- 1 μm, respectively. The design is based on the use of standardised commercially available components that can be used for manual or

automated positioning of the parts on LMM platforms. Furthermore, the modular design facilitates the integration of LMM systems into multi-process manufacturing platforms.

- The proposed automated workpiece setting up routine can be applied for LMM of complex free-from parts without the use of alignment marks. The routine is fully automated while delivering alignment ARR better than +/- 4 μm, respectively, by employing the proposed workpiece holding device and an FV probe. Due to the low resolution required to execute the setting up routine, a very good balance between its ARR and the time necessary to complete it can be achieved. It should be noted that the same alignment routine can be used if a FV probe is integrated in the LMM platforms and in this way the uncertainty associated with the routine can be reduced but in expense of the LMM platforms' throughput. In addition, in-line inspection routines similar to the workpiece's setting up one can be developed for implementing rest-volume machining strategies on LMM platforms and also for generating "customized" toolpaths for adaptive machining.

CHAPTER 6

GENERIC SOFTWARE TOOLS TO EXTEND THE MANUFACTURING CAPABILITIES OF RECONFIGURABLE LASER MICROMACHINING SYSTEMS

Outline of the chapter

This chapter is dedicated to the development of generic software tools, which can substantially improve the manufacturing capabilities of reconfigurable LMM systems in terms of machining throughput and complexity of the laser manufacturing operations. In particular two generic software solutions are proposed and validated:

- A software tool to counteract the negative dynamic effects of optical scanning head systems, caused by beam deflectors' inertia. In particular, a detailed characterization of the speed dependent performance of state-of-art beam deflector system is carried out and based on the revealed dynamic deficiencies of the scanning head, the proposed software tool introduces machine specific compensations in machining vectors to counteract the negative dynamic effects of scan heads and thus to improve significantly the laser machining performance across the full range of available processing speeds. Hence, the machining throughput can be increased, while at the same time machining quality is substantially improved by maintaining a constant pulse distance throughout the machining operations.

- An automated software routine for multi-axis LMM employing rotary stages. In particular, the proposed techniques maps the displacement vectors between the coordinate systems of the optical axes (defined by the scan head) and the mechanical axes (defined by the mechanical stages) when the rotary stage(s) is(are) utilized to execute arbitrary angular movements. Thus, the software tool predict translational errors between the two coordinate systems when arbitrary angular rotations are performed and accordingly introduces corrective commands in the machine routines in order to maintain the established relative geometrical correlation between the coordinate systems of the scan

head and the stack of mechanical stages. Hence, the manufacturing capability of the LMM platform to perform demanding complex machining routines, which require accurate and precise repositioning of workpieces during the machining operations, has been substantially increased.

The research reported in this Chapter refers to Publication 4 and 6 from the List of Publications.

6.1 Generic software tool for counteracting the negative dynamic effects of optical scan heads

6.1.1 Introduction

The comparative study presented in Chapter 4 revealed that achievable machining accuracy with optical beam deflection systems is worse than that achievable with mechanical axes. In addition, processing capabilities of optical laser beam deflection systems were also investigated by a number of research groups and their common conclusion is that they are not sufficiently mature [209-211]. A general misconception for their capabilities is the presumption that the scanner movement ARR stated in equipment manufacturers' specifications is an absolute parameter. For example, in an experimental study focused on evaluating ARR of LMM systems, it was concluded that their performance was far away from their stated specifications [209]. Thus, it should be noted that the beam movement accuracy is a relative parameter that depends highly on the operating parameters of the beam deflection system, such as the movement mode and the used scanning speed and machining strategies. Therefore, a deterministic evaluation of the system performance can only be accomplished if the processing framework is pre-defined. Thus, any investigations of LMM systems' performance should be carried out within a pre-defined processing framework, for example by employing the vector movement mode and by utilising the full field of view of the used focusing lens.

Optimizations of beam deflection systems to improve machining results were also reported in a number of publications. In particular, the proposed approaches apply "a drive signal digital pre-filtering" techniques to improve the dynamic performance of optical beam deflection systems by performing a real-time Fourier analysis of the raw command signals [110, 111, 212]. However, this techniques are not sufficiently effective when it is required micro-engineering components to be produced with high ARR [7,213] and therefore other MMPs

have to be employed together with specially developed software tools to compensate process limitations [214, 215]. Such software tool for layer-based micromachining was also reported to improve the resulting surface topography following laser-milling [116] by optimising the slicing procedure and vector orientations in each layer for 3D geometries. However, the proposed software tool does not address ARR issues associated with the negative dynamic effects of the optical beam deflection systems. A commercial beam deflection system that was introduced recently offers a ''sky-writing'' function for applications requiring a higher accuracy, where each "mark" vector is precisely executed at a constant processing speed over the entire vector length [216]. However, an important shortcoming of this function is that users still need to manually define a set of functional parameters by conducting time consuming optimization experiments. Furthermore, the ''sky-writing'' functionality is available only to customers of this commercially available system and thus it cannot be considered a generic solution.

6.1.2 Main components and working principle of optical beam deflection systems

Optical beam deflection systems are closed-loop dynamic systems that consist of reflective mirrors mounted on highly precise galvanometer motors with servo control systems [217]. The galvanometer has two main parts: an actuator that produces a rotary beam deflection in response to electric current and an integral position detector for a closed loop control. The closed loop servo system controls the movement of the laser beam by comparing the position detector's current output signal with the reference input signal, the commanded position, and then drives the actuators to the desired position by introducing the necessary corrective action [218]. Furthermore, the controller also synchronizes the laser triggering in accordance to the laser beam movement in order to produce the desired machining patterns [216].

The optical laser beam deflection systems are component technologies in LMM systems that are controlled through discrete numerical control (NC) commands to deliver the required machining movements. Their operation can be customized through a list of user-defined parameters, such as laser delays, scanner delays and processing speeds, which can be set to fulfil specific machining requirements. The optical beam deflection systems support three types of vectors, namely jump, arc and scan vectors [216]. In essence, jump vectors command rapid beam positioning movements with the laser shatter on, whilst scan and arc vectors execute machining movements with predefined laser processing settings. Throughout the execution of a given machining path, the closed loop servo system feeds corrective actions

into the controller and thus to guarantee the precise rotary movements of the beam deflectors. However, even with the implementation of such Proportional Integral Derivative (PID) control loop, the corrective actions cannot offset fully the system inaccuracies due to the existence of inertia and damping [111]. Other factors, which limit the performance of optical beam deflection systems, include torsional resonance, heat dissipation, drift, nonlinearities, and noise [110]. The dynamic effects due to the system's inertia increase with the increase of the beam deflectors' rotary speed that ultimately affects the machining results. The dynamic effects have a direct impact on the resulting machining accuracy and quality and they are discussed in the two sub-sections below.
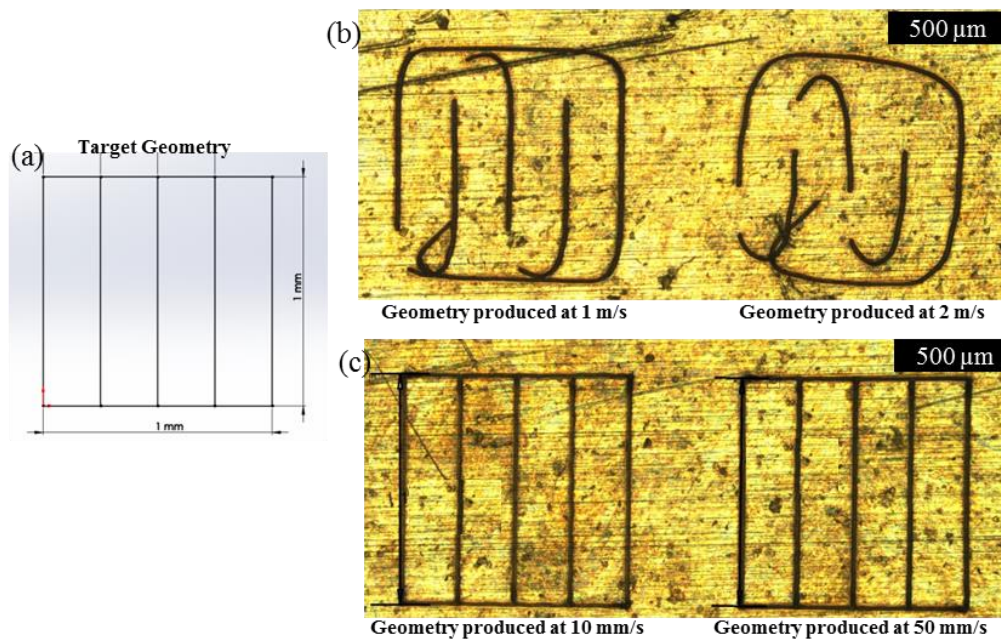
Figure 6.1 Dynamic effects of an optical beam deflection system on the dimensional accuracy during the laser machining of (a) target geometry (b) with deactivated scanner and laser delays and (c) with activated scanner and laser delays

6.1.2.1 Machining accuracy

Figure 6.1b gives a simple example of the beam deflection system effects on dimensional accuracy of the laser machining results. It can be clearly seen by referring to Figure 6.1a that the system does not perform the machining movements as intended and there is a speed dependent discrepancy between the programmed and the actual beam movements. In particular, the machining vectors do not reach the programmed position and "tails" are formed along the beam path both at the beginning and at end of each vector. Also, these errors increase with the increase of the processing speed as it can be seen by comparing Figure 6.1b,

where the geometry is produced at the high scan speeds (1-2 m/s), and Figure 6.1c, where the geometry produced is produced at significantly lower scan speeds (10-50 mm/s).
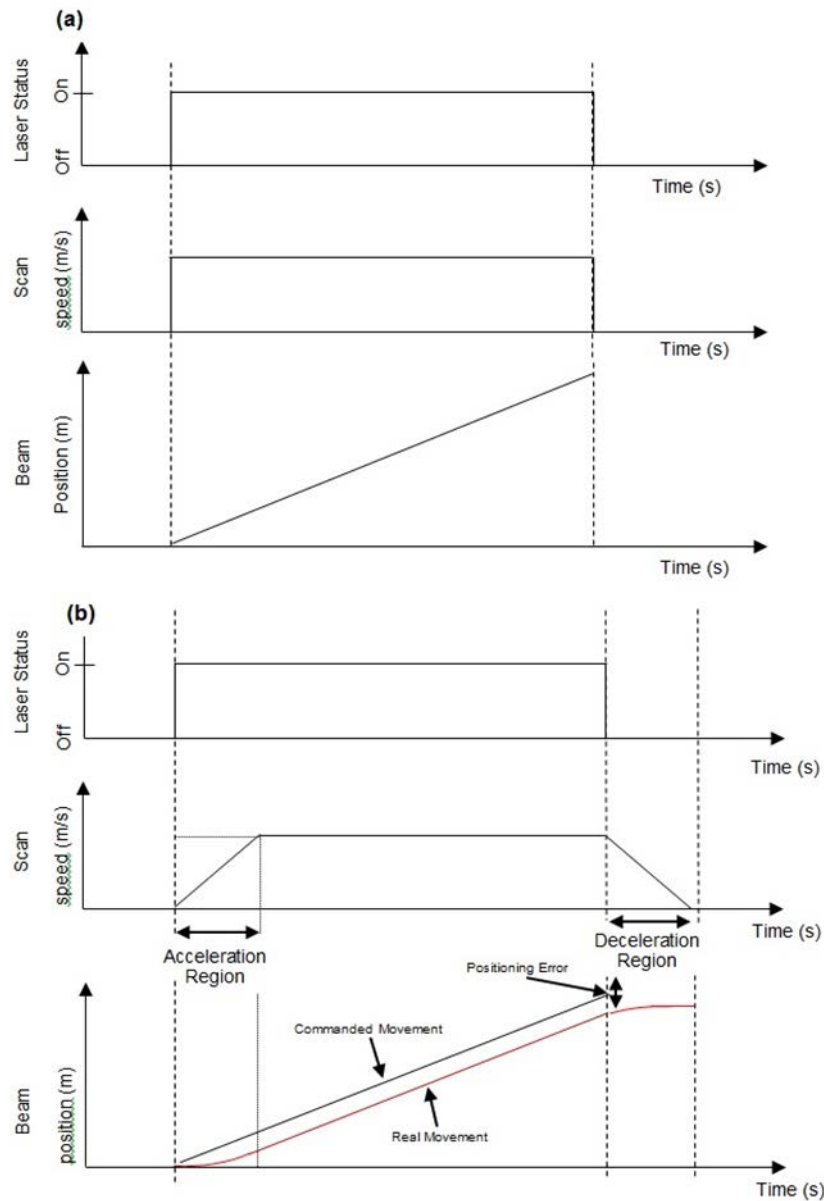
Figure 6.2 An example of (a) programmed machining vector and (b) executed machining vector

Figure 6.2a shows an example of a machining vector that was programmed for execution by the beam deflection system while Figure 6.2b depicts the actual response of the mirror galvanometers to the programmed movement command. It can be clearly seen that there is a discrepancy between the programmed and actual machining paths that results from the existence of acceleration and deceleration regions at the start and end of each machining vector, respectively. These machining errors occur because the programmed path and the set

107

scan speed only without the dynamic of the beam deflection system were taken into account when generating the control signal for the galvanometers' rotary movement. In particular, the errors represent the difference between the programmed movement with a constant scan speed and the actual path without the effects of the galvanometers' dynamic, especially a shorter travel than intended.

The state-of-the-art optical laser beam deflection systems have the capabilities to compensate the dynamic effects by introducing delays in the galvanometer rotary movements and also in triggering the lasers [111, 216]. There are three types of scanner delays, namely jump, mark and polygon delays that have to be included after each jump or scan command, and effectively give more time to the mirror galvanometers to complete the programmed movements. Additionally, there are two types of laser delays, namely laser on and laser off delays, which adjust the triggering of the laser to the amended laser beam movement with the incorporated time compensations for the galvanometers' acceleration and deceleration regions. Furthermore, laser delays are also used to compensate the response time of the employed laser source. In particular, the lag between the executed and the programmed movements is compensated with a mark delay as shown in Figure 6.3, which gives the mirror galvanometers more time to complete a machining command while the laser on and off delays are adjusted in accordance to the beam deflectors' real movement. The introduction of scanner and laser delays can improve significantly the dimensional accuracy of produced components and thus to minimise and even to eliminate the scanners' machining errors by providing enough time for the scanners to complete the programmed movements as exemplified in Figure 6.3. However, it should be also noted that the introduction of scanner and laser delays can be very time consuming and tedious task because the delays need to be optimised for different processing speeds and also for different machining geometries [110]. Furthermore, the introduction of scanner delays does no eliminate the varying pulse distances at the start and the end of each machining vector (see Figure 5.3) with its negative side effects (see Section 6.1.2.2 below) and also increases the machining time.
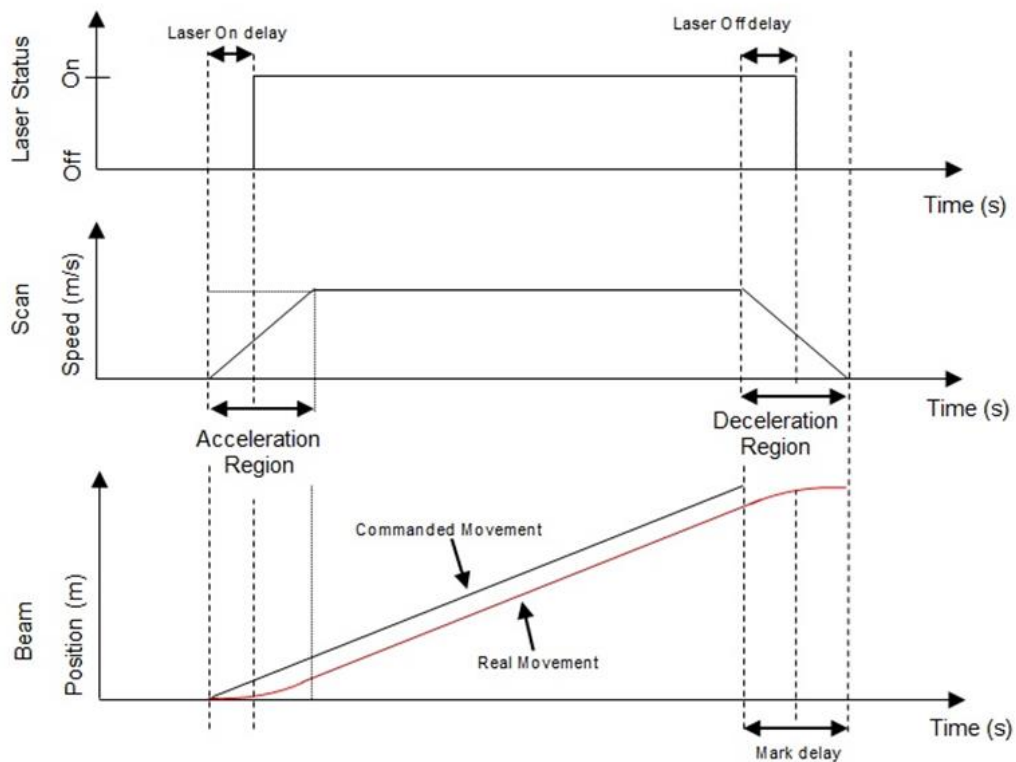
Figure 6.3 Introduction of scanner and laser delays to improve machining accuracy by eliminating positioning errors of scanner systems

6.1.2.2 Machining quality

The negative scanner dynamic effects also affect the machining quality, especially the uniform ablation of material across the whole processing area. This is the result of the varying pulse distance, $PD = V_{scan} / f_p$, where V_s and f_p are the beam scan speed and pulse frequency, respectively. In particular, since f_p is constant across any laser machined area, the changes of V_s in the acceleration and deceleration regions leads to variations of the pulse distance at the beginning and the end of every scan/machining vector. Thus, more laser pulses are irradiated in these regions as shown in Figure 6.4, which is the reason for not having a uniform material ablation along the beam path.

Even though, fine tuning of scanner and laser delays could lead to marginal improvements of machining quality, they are not sufficient to achieve optimum machining results, because the acceleration and deceleration regions are still present even after the introduction of delays. This is due to limitations in integration architectures of laser sources and scanner systems, especially the limited capabilities of scanner drivers to vary the laser processing parameters "on the fly". Especially, the main components of LMM systems, e.g. laser sources, scanner systems and mechanical stages, are controlled independently with limited exchange of control

data, and thus their operations cannot be fully synchronized when executing machining vectors. An evidence of this not fully synchronized control of LMM component technologies is non uniformed material ablation across the laser processed areas. Figure 6.5 depicts the accumulated result of this non uniform processing after layer-based LMM of a pocket, in particular after ablating five layers (five repetitive scans of machining vectors) on a stainless steel specimen.
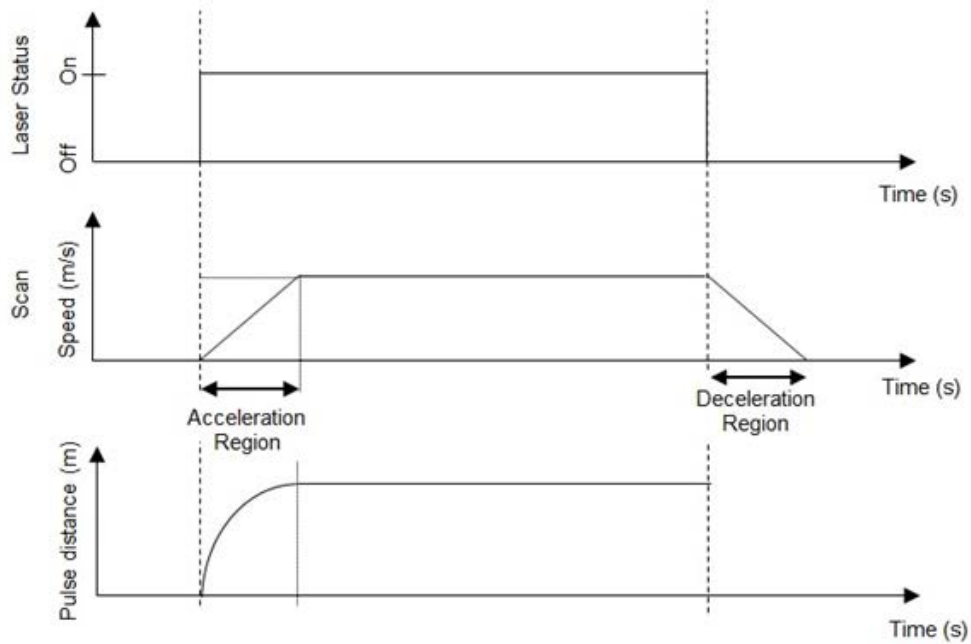
Figure 6.4 Pulse distance variations with the increase of the scan speed in the acceleration region of a machining vector
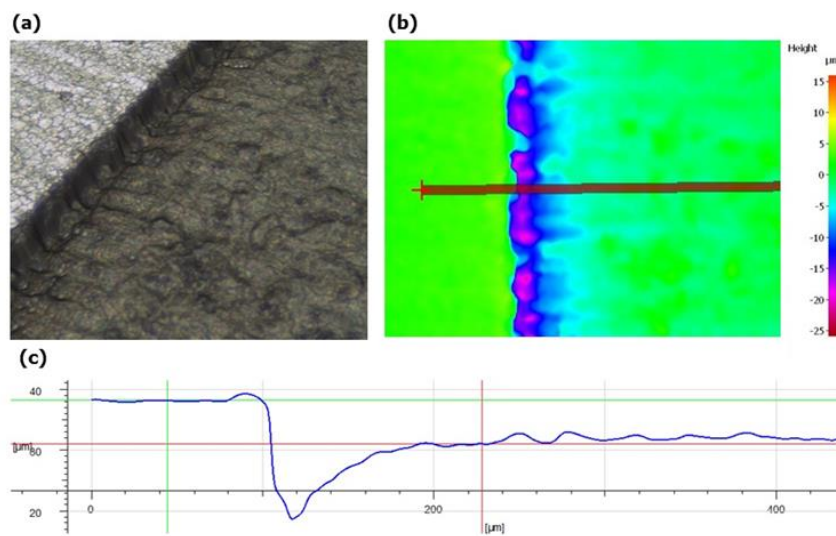
Figure 6.5 The non-uniform ablation after processing five layers of material: (a) 3D view; (b) contour plot; (c) profile cross section on the ablated region

6.1.3 Design considerations

Taking into account the limitations of currently available control architectures for integrating laser sources with beam deflection systems, especially in context of Configuration B and C LMM (presented in Chapter 2), a software solution to improve both dimensional accuracy and machining quality is proposed. This is achieved by developing an adaptive CAD/CAM postprocessor that minimises the negative dynamic effects of beam deflection system on the LMM systems' ARR. This adaptive solution supplements a conventional postprocessor that only translates the beam path created based on the CAD data into a NC part-program for a given LMM system configuration. In particular, this adaptive postprocessor includes the capabilities of the conventional postprocessor for translating the beam movements into machine executable commands in addition to the capabilities for introducing systematic changes, in particular compensations for the beam deflectors acceleration and deceleration regions, into the machining vectors. Thus, it becomes an "active layer" between the standard CAD/CAM process and LMM systems. Its functionality includes apart from translating jump and machining vectors into machine executable commands, the introduction of machine and process settings' dependent compensations in order to offset the specific negative dynamic effects of the used beam deflectors.

The proposed adaptive postprocessor minimises and even eliminates the discrepancies between the programmed and actual beam movements in the acceleration and deceleration regions of machining vectors by introducing beam path adjustments while improving the machining quality by maintaining a constant pulse distance during all machining commands. This is achieved by calculating machine specific compensation values based on the used beam scanning speed that equal the necessary acceleration and deceleration distances to reach the set scanning speed. The system architecture of this adaptive postprocessor is schematically presented in Figure 6.6. The postprocessor is initiated with the input of a Cutter Location (CL) data file, which represents the laser beam path generated directly from the part CAD model for a selected laser machining strategy [116]. Such CL data files can be generated by most commercially available CAM software tools and a detailed description of the CL data generation for layer based machining is reported by other researchers. Following input of the CL data, it is necessary to enter laser machining parameters, namely scanning speed and laser beam diameter. Then, the postprocessor introduces systematic changes to the beam path that are compensations for laser delays and laser beam diameter in machining vectors. Finally, the

postprocessor outputs a NC file that contains machine executable commands to realise the beam path by taking into account the NC technology language of a given LMM system and also includes a text header with the optimised laser delays.
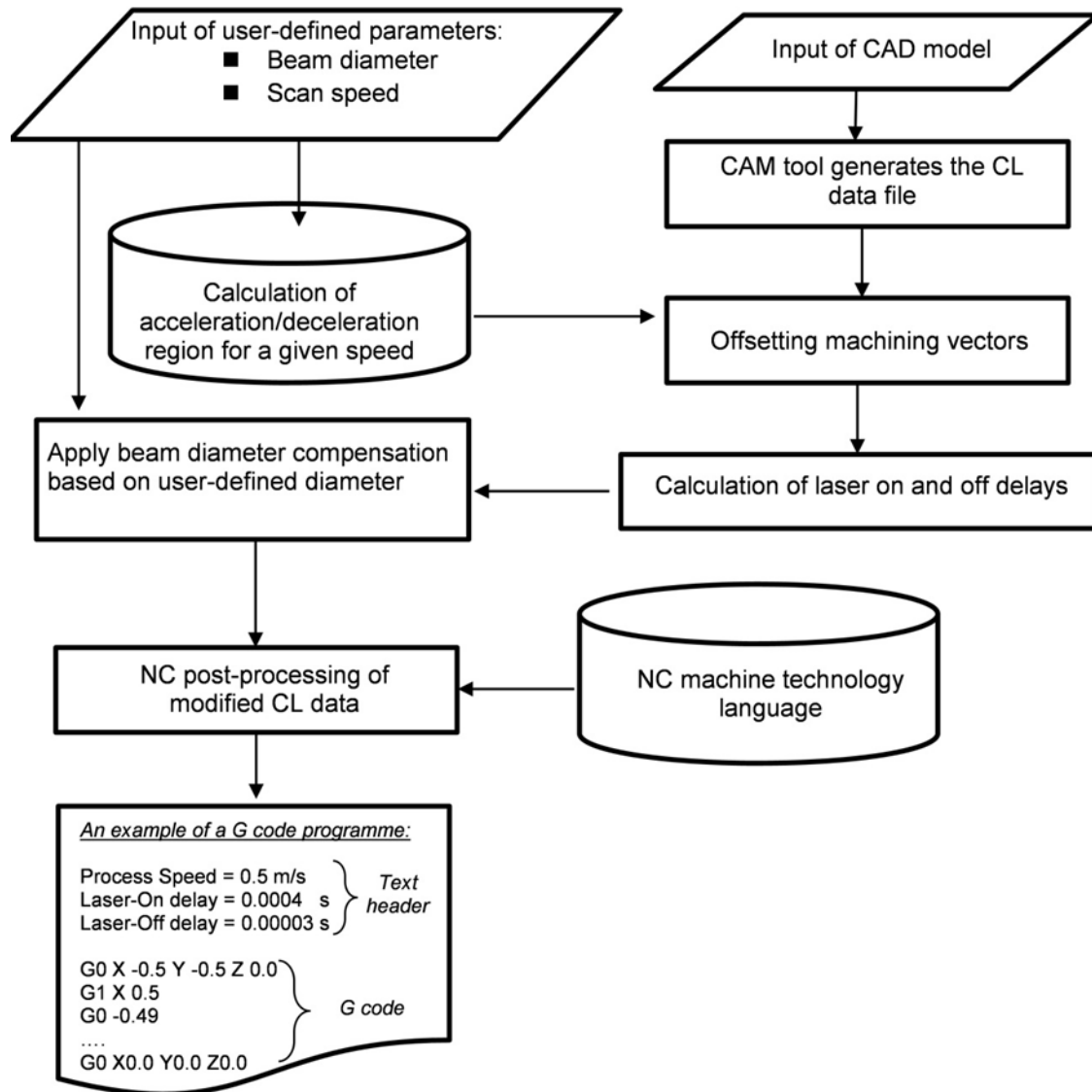
Figure 6.6 The architecture of the adaptive postprocessor

The implementation of the proposed adaptive postprocessor, especially its ''active layer'', includes the following two steps:

Step 1: Offsetting of machining vectors

It is necessary to obtain experimentally information about the dynamics of the beam deflection system used in any given LMM system. Especially, an empirical model has to be created that characterizes the actual dynamic response of the beam deflection system when executing machining vectors across the full range of accessible processing speeds.

Experimental tests have to be conducted that include the machining of single lines with different processing speeds and thus to obtain information about the acceleration and deceleration regions at different scanning speeds. Based on the collected data for the dynamic performance of the beam deflection system, a regression model can be created to determine l_a ≈ $f (V, \beta)$, where: V is the scan speed, l_a - the acceleration region length and β – regression parameters.

Such empirical models can be used also to predict deceleration region lengths (l_d) at different scan speeds by assuming a symmetrical dynamic performance of the beam deflection system at the end of each machining vector. By applying these models, scanning speed dependent compensations to each machining vector can be introduced that in practice represent offsetting values of the vectors' start and end points with l_a and l_d, *respectively*.

Step 2: Application of laser delays

Following the offsetting step, the laser on and off time events should be adjusted to maintain constant pulse distances when executing laser machining commands and thus to have an uniform laser ablation over the processed areas. Thus, it is necessary to find the time that the beam deflection system needs to travel through the acceleration region and thus to calculate the laser on delay. Since laser on time events are triggered by the laser source controller, they can be calculated based on the assumption that the beam deflectors travel with a constant speed throughout the full length of a given machining vector. Consequently, the time (t_a) required by the beam deflection system to cover an acceleration region at a certain speed can be calculated as follows:

$$t_a = \frac{L}{V} - \frac{(L - \Delta L) - l_a}{V} + \frac{d}{2V}$$
(Equation 6.1)

where: L is the nominal length of a machining vector; ΔL - the deviation (machining error) between the nominal and the actual lengths of the vector; V – the programmed scan speed; and d – laser beam diameter.

Since ΔL is a speed dependent parameter, experimental tests have to be performed in order to derive their interdependence empirically. Again, based on such experimental data, a regression model can be created, in particular: $\Delta L \approx f (V, \beta)$.

Thus, to minimise the machining errors and achieve laser processing with a constant pulse distance it is necessary to apply a laser-on delay (t_{on}) at the start of each machining vector that is equal to t_a at the set scan speed for a given beam deflection system. At the same time, laser-off delay (t_{off}) is calculated as follows:

$$t_{off} = \frac{L}{V} - \frac{(L+l_a+l_a)- \Delta L - l_a}{V} - \frac{d}{2V} = \frac{\Delta L - l_a}{V} - \frac{d}{2V} \qquad \text{(Equation 6.2)}$$

In addition, a compensation for the laser beam diameter is introduced in this step. This is achieved by adding and subtracting a time constant $(d/2V)$ from t_{on} and t_{off}, respectively.
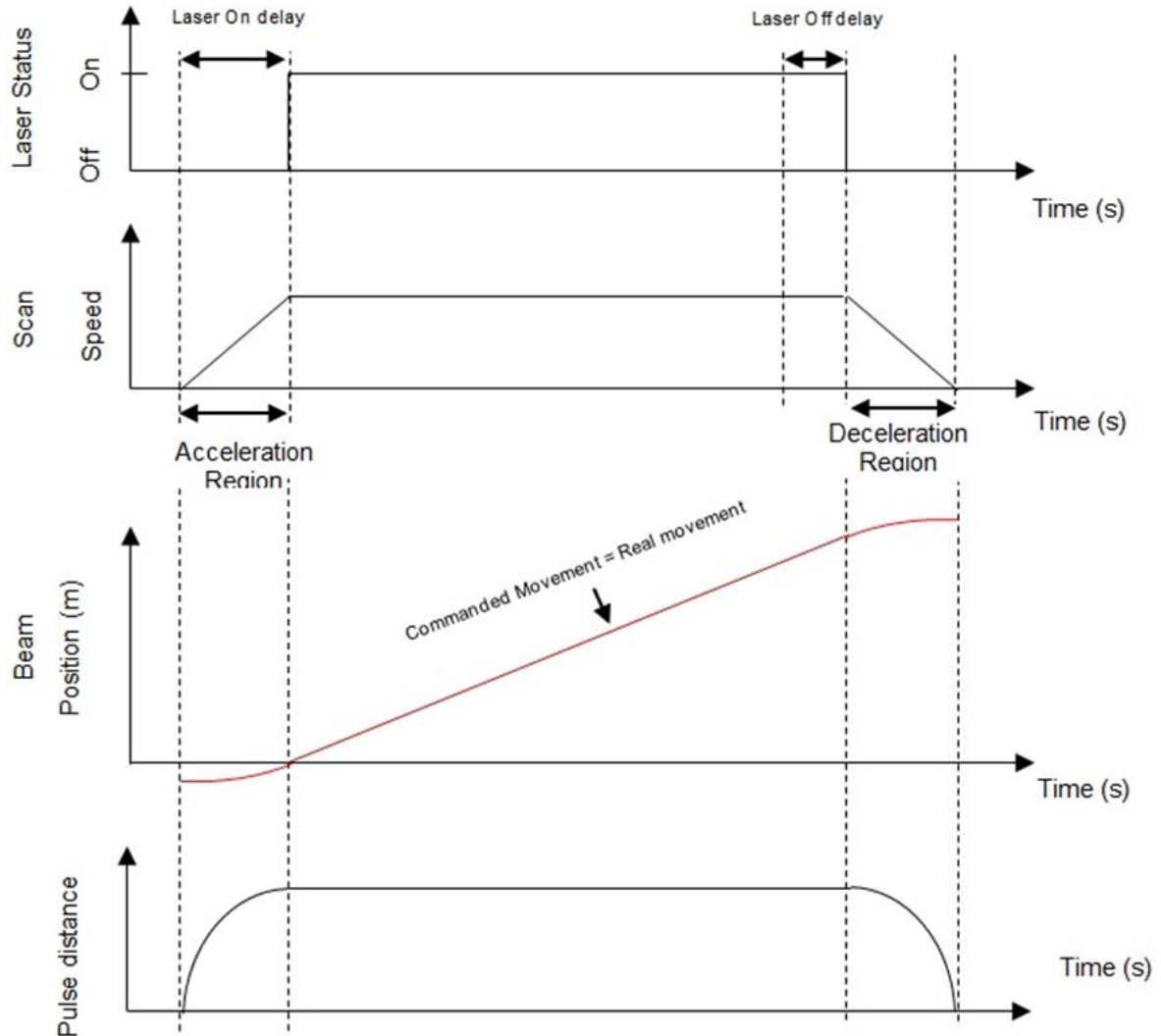
Figure 6.7 The combined effects of applying the adaptive post-processor on machining accuracy and machining quality

Figure 6.7 exemplifies how such systematic compensations for the dynamics of the beam delivery system can be used to "adapt" machining vectors to the set scanning speeds and then by applying the necessary laser on and off delays to obtain a constant pulse distance when executing machining commands. Thus, it is ensured that the real movements of the laser beam are executed with no discrepancy from the laser beam movement commands. Furthermore, the use of such a postprocessor also eliminates the need to apply laser beam diameter offsets, because they are already included into the generated machine executable commands and no

further changes into the CAD and/or CAM models are needed in order to achieve machining accuracy and machining quality improvements on LMM platforms.

The proposed adaptive postprocessor was implemented using a commercially available software tool for creating postprocessors, in particular DELCAM PostProcessor and then integrated into commercial CAD/CAM systems, in particular ArtCam and PowerMill, to validate its performance. Since dynamic behaviour of beam delivery systems is already taken into account by this postprocessor, the generation of beam paths and then machine executable part programs is fully automated. Thus, users can benefit from this software solution regardless of their knowledge and experience with the used specific LMM systems. Appendix 5 provides in-depth description of the implementation of the proposed postprocessor as a stand-alone software tool by utilizing the DELCAM Postprocessor, while Appendix 6 demonstrates integration of the implemented adaptive postprocessor in DELCAM ''ArtCam'' software and provides an example of its application for the laser machining of complex 3D geometries.

6.1.4 Experimental Validation

6.1.4.1 Experimental acquisition of the dynamic response of the beam deflection system

Experimental tests were performed on a Configuration B LMM platform that is equipped with a state-of-art beam deflection system and two laser sources - a SPI redENERGY G4 S-type 50 W fibre laser and an Amplitude Systemes Satsuma 5W ultrafast fibre (the detailed description of the laser system could be found in Chapter 3).

Experimental tests were conducted on the state-of-art LMM platform to determine the dynamic effects of the optical beam deflection system integrated in it. As it was explained in Section 6.1.3, these experiments were necessary to obtain the machine specific information that is required to implement the proposed software tool. In particular, the experiments included the machining of single lines with different processing speeds and thus to obtain information about the acceleration and deceleration regions at different scan speeds. Figure 6.8 depicts the interdependences between acceleration region lengths and scan speeds for the used beam deflection system. Based on this result an empirical model is generated to determine the acceleration region length, in particular:

$$l_a = 0.1772V + 2.0451 \qquad \text{(Equation 6.3)}$$
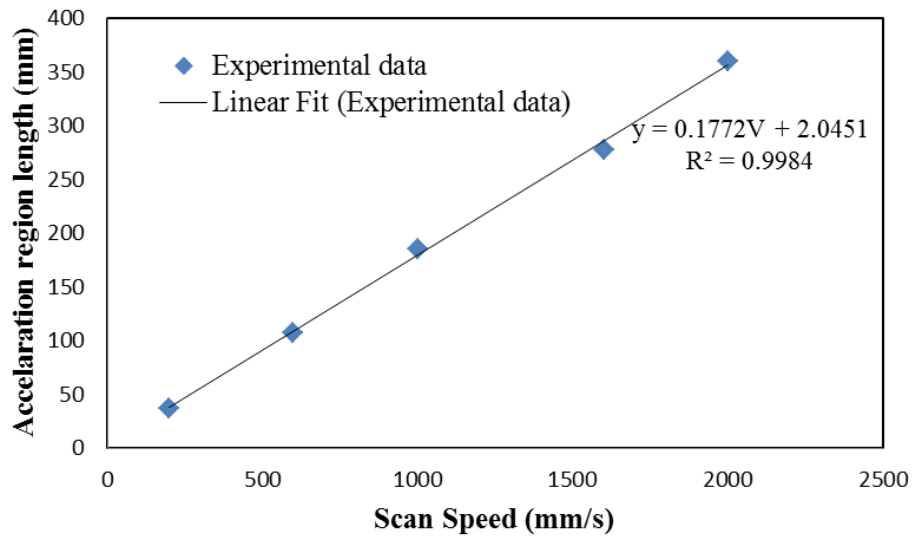
Figure 6.8 Interdependences between acceleration region lengths and scan speeds

In addition, further experiments were conducted to determine the machining error (ΔL) dependence on the scan speed on this LMM platform. Again, this is necessary in order to implement the proposed software tool. Especially, Figure 6.9 shows the interdependence between the machining errors and the set scan speeds for the used LMM platform. Based on these experimental results the following empirical model is created:

$$\Delta L = 0.2177\,V - 1.3233 \qquad\qquad \text{(Equation 6.4)}$$
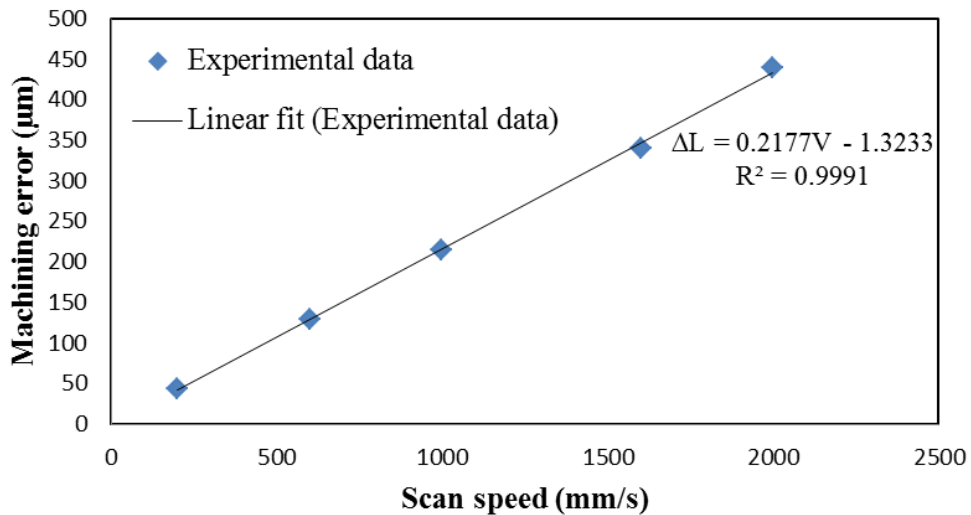
Figure 6.9 Interdependences between the machining errors and the set scan speed

Measurements and analyses of experimental results were performed on an optical 3D microscope, namely Alicona Infinite focus G5 (further technical information for the system could be found in Chapter 3).

6.1.4.2 Experiments' design

6.1.4.2.1 Lines' machining

The experimental validation of the proposed software solution for offsetting the dynamic effects of the scan heads included the machining of simple lines on the sample surface and thus to demonstrate clearly the benefits of the proposed tool for improving the ARR capabilities of the optical beam deflection systems. The lengths of the lines were set to 2 mm in order to perform high resolution measurement of the produced geometries. In addition, lines were produced along X and Y axes of the optical beam deflection system and thus to demonstrate the effectiveness of the proposed software solution regardless of machining vectors' directions. This simple test structures were produced both before and after applying the proposed software tools in order to assess their effectiveness in improving the machining results. Especially, to validate both the proposed adaptive postprocessor under different dynamic conditions, four processing speeds were investigated. Furthermore, each line was scanned ten times and thus to draw conclusions about the effects of the proposed tool on ARR capabilities of the used LMM platform. The machining of the lines was carried out on Stainless Steel (SS316) specimens by employing the SPI laser source. The laser machining parameters used are provided in Table 6-1. The laser frequency was varied with the increase of the scan speed in order to obtain single pulse craters. The appropriate laser delays were calculated for the respective process speed by using Equations 6.1 and 6.2. Using these process settings the following three machining trials were conducted:

- Trial 1: machining of lines without applying the software tool;
- Trial 2: machining of lines without applying the postprocessor, but with optimized scanner and laser delays;
- Trial 3: machining of lines after applying the stand-alone adaptive postprocessor both along the X and Y axes of the beam deflector system.

Table 6-1 Process settings used in the lines' machining

	Simple lines – Trial 1,2, and 3			
	Line 1	Line 2	Line 3	Line 4
Laser Source	SPI			
Material	Stainless Steel(SS316)			
Average Power [W]	40			
Frequency [kHz]	5	10	15	20
Pulse duration [ns]	220			
Beam Diameter [µm]	30	30	30	30
Scanning Speed [m/s]	0.5	1	1.5	2
Layers	10	10	10	10

6.1.4.2.2 Machining of passive waveguide filters

The experimental validation of the adaptive postprocessor is also performed on an intricate 3D geometry with a micro engineering application. The component is a passive waveguide filter [219], which was selected due to its complex geometry, which includes micro- and meso- scale functional features. Thus, the effectiveness of the proposed software tools was evaluated both across the full field of view of the used focusing lens system and also for machining micro-scale structures. Figure 6.10 shows the CAD model of the waveguide filter with its nominal dimensions. The machining of the waveguide structure was carried out on a brass specimen by employing the Satsuma laser source. The machining strategy employed in the trials generated machining vectors that are normal across the waveguide length and layer-based processing was used to produce the 3D structures.

Nominal dimensions of the microwave component

	Width (mm)	Height (mm)	Thickness (mm)
Microwave filter	0.432	25	0.035
Feature 1 & 6	0.17	0.10	0.035
Feature 2 & 5	0.29	0.15	0.035
Feature 3 & 4	0.34	0.15	0.035
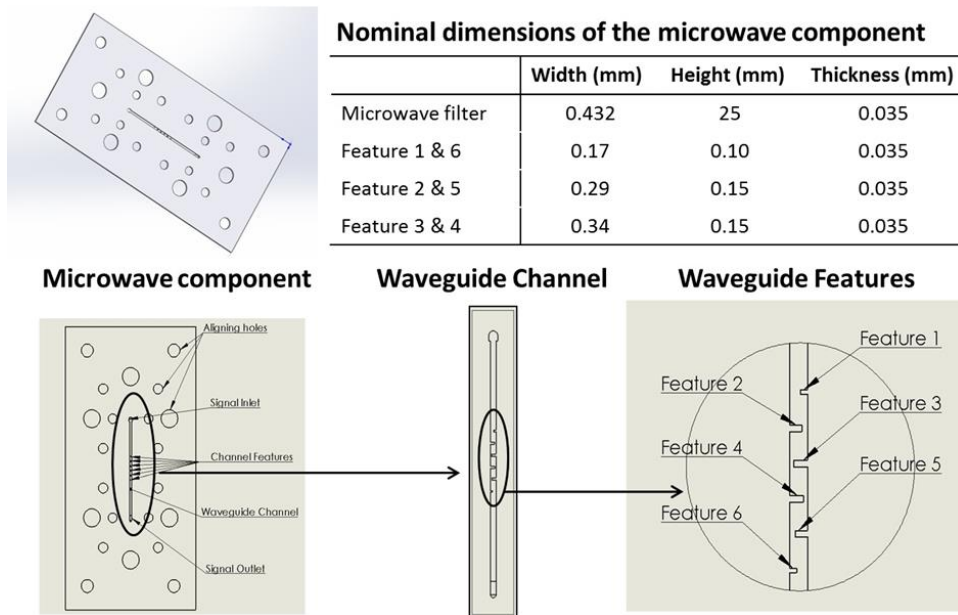
Figure 6.10 The design of the microwave filter together with its important nominal dimensions

The used laser machining parameters are provided in Table 6-2. The laser processing settings were optimised to meet the technical requirements for this passive waveguide filter, in particular a surface roughness (Ra) better than 300 nm. The laser delays are again calculated by applying Equations 6.1 and 6.2. The impact of the proposed adaptive postprocessor on laser machining time and thus the machining effectiveness was also assessed. It is important to note that the machining without applying the adaptive postprocessor required a substantial lowering of the scan speed in order to obtain comparable machining results from the both tests. Thus, a total number of four machining trials were conducted, in particular:

- *Trial 1:* machining of the microwave filter without applying the postprocessor at a high scan speed;

- *Trial 2:* it is the same as Trial 1, but with optimised beam deflection system and laser delays;

- *Trial 3:* machining after applying the adaptive postprocessor and by using the same scan speed as in Trial 1;

- *Trial 4:* machining without applying the postprocessor but with the optimised (reduced) scan speed (calculated using Equation 6.4) in order to obtain similar machining results to those in Trial 3.

Table 6-2 Process settings used for the machining of passive waveguide filters

	Microwave Component	
	Trial 1, 2 and 3	Trial 4
Laser Source	Satsuma	
Material	Brass	
Average Power [W]	4.2	4.2
Frequency [kHz]	500	12.5
Pulse duration [fs]	310	310
Beam Diameter [μm]	30	30
Scanning Speed [m/s]	2	0.050
Layers	15	15

6.1.5 Results and Discussions

6.1.5.1 Single pulse craters' lines

The results from the machining of single craters' lines to validate the proposed adaptive postprocessor are shown in Figure 6.11, while Table 6-3 provides machining errors and acceleration region lengths at the applied scan speeds in the three trials. The total measurement uncertainty at the 95% confidence level, provided in Table 6-3, was calculated based on the uncertainty procedure provided in Chapter 3. Figure 6.11a shows the results

from the machining of the horizontal lines without applying the proposed postprocessor. It can be seen that each of the lines is shorter than the programmed length of 2 mm and the machining accuracy decreases with the increase of the scan speed. For example, at 0.5 m/s, the machining error is 107.3 μm, while at 2 m/s it is 431.9 μm. Furthermore, the machining quality at the beginning of the lines is much worse in comparison to their middle sections, which is due to the increasing scan speed and changing pulse distance in the acceleration regions as shown in Figure 6.12. In addition, Figure 6.12 shows that the acceleration region length increases with the increase of process speed. Once, the beam deflector system reaches its set scan speed, the pulse distance becomes constant and as a consequence the distance between the pulse craters become uniform as this can be clearly seen in Figure 6.11a. Figure 6.11b shows the results of the machined horizontal lines without applying the proposed postprocessor, but with optimized scanner and laser delays. Even though the introduction of the appropriate scanner and laser delays can significantly improve the dimensional accuracy of the laser processed simple lines, in particular the deviation was reduced to +/- 10 μm, the machining quality of the lines is not acceptable, because the pulse distance is not kept constant along the laser machining path. In addition, the laser processing of short vectors with lengths comparable to the sum of acceleration and deceleration lengths can be difficult to realise without reducing substantially the scanning speed and thus sacrificing the machining efficiency. Figure 6.11c shows the results of the machined horizontal lines after applying the proposed adaptive postprocessor. The machining errors were reduced and the process ARR was improved dramatically and thus to be able to produce lines with deviations less than +/- 10 μm from their nominal dimensions regardless of the set scan speed. Furthermore, the quality of produced lines in Trial 3 is also improved, because the pulse distance is maintained constant throughout the whole length of the lines, which results in uniform distances between the pulse craters. This allows laser processing of different size features regardless of the set scan speed, even if the machining vectors are much smaller than the respective acceleration and deceleration lengths. Table 6-3 summarizes the results from the machining of X and Y lines with the proposed adaptive postprocessor and they are comparable along the both axes. Thus, this demonstrates that the performance of the proposed software tool does not depend on the direction of the machining vectors. Also, Trial 3 demonstrates that machining results with pseudo-repeatability of less than 1.5 μm at different scan speeds can be achieved by maintaining the pulse distance constant when executing the machining vectors. In addition,

based on the results from Trial 3 it can be stated that a reproducibility of less than 7 μm was achieved regardless of the set scan speed.

Table 6-3 The results from the single pulse craters' lines

	Trial 1 (without the postprocessor)				
	Line 1	Line 2	Line 3	Line 4	U_T
Machining error [μm]	104.6	217.4	323.0	425.0	+/- 1.1
Acceleration region length [μm]	89.9	187.7	292.6	349.6	+/- 1.2
	Trial 2 (without the postprocessor, but with delays)				
	Line 1	Line 2	Line 3	Line 4	SD
Machining Error [μm]	4.2	2.3	8.0	9.9	+/- 0.9
Acceleration region length [μm]	89.9	187.7	292.6	329.6	+/- 0.8
	Trial 3 (with postprocessor, X)				
	Line 1	Line 2	Line 3	Line 4	U_T
Machining Error [μm]	3.1	2.2	7.4	5.8	+/- 0.9
Acceleration region length [μm]	0	0	0	0	+/- 0.9
	Trial 3 (with postprocessor, Y)				
	Line 1	Line 2	Line 3	Line 4	U_T
Machining Error [μm]	2.8	2.1	5.4	4.1	+/- 1.4
Acceleration region length [μm]	0	0	0	0	+/- 1.4
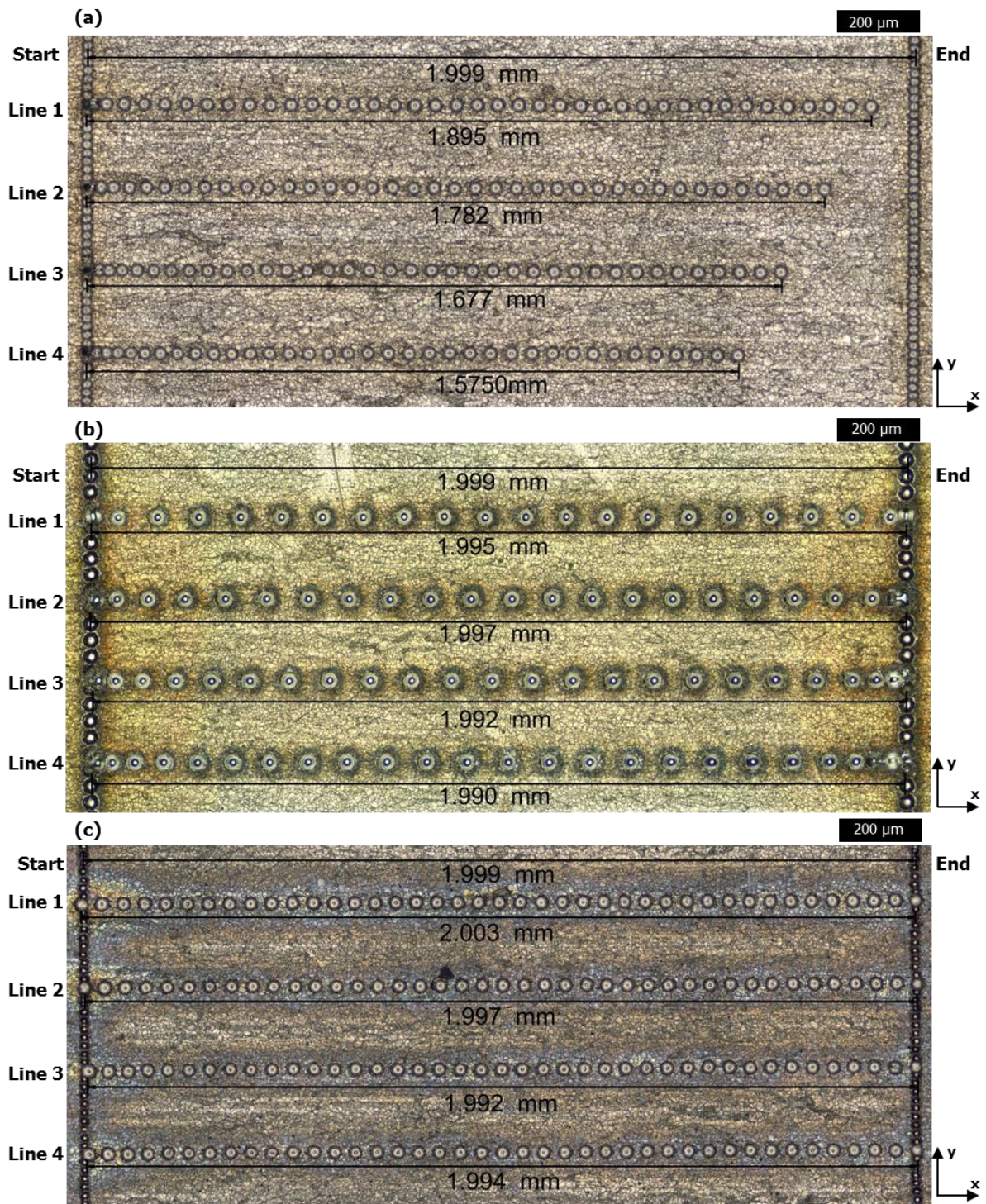
Figure 6.11 Validation tests with single pulse craters' lines: (a) Trial 1 – machined lines along x-axis without the postprocessor, (b) Trial 2 - machined lines along x-axis without the postprocessor, but with optimized scanner and laser delays (c) Trial 3 – machined lines along x-axis after applying the postprocessor
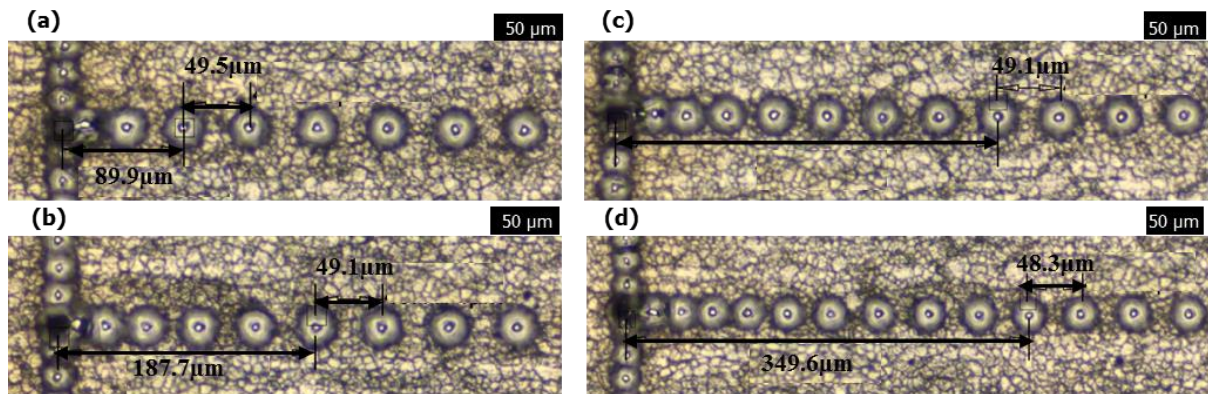
Figure 6.12 Acceleration region lengths in Trial 1 and Trial 2 produced at scan speeds of: (a) 0.5 m/s, (b) 1 m/s, (c) 1.5 m/s, (d) 2 m/s

6.1.5.2 Passive microwave filter

The laser machining results of the waveguide are shown in Figure 6.13, while Table 6-4 summarizes the accuracy achieved in Trials 2, 3 and 4. The total measurement uncertainty at the 95% confidence level is calculated to be less than +/-1 μm. The structure produced in Trial 1 demonstrates the inability of the laser machining process to deliver the required level of dimensional accuracy at high processing speeds. This is due to the negative dynamic effects of the used beam deflection system that result in waveguide channels that are significantly narrower than the programmed nominal dimensions and also important functional features are not produced (see the CAD model in Figure 6.10 for reference). In particular, the necessity to execute machining vectors with micro scale lengths (up to 80 μm), while the acceleration length is more than 4 times longer (~ 350 μm at the set scan speed of 2 m/s) is the reason for inability of the laser machining process to deliver the required level of processing resolution and dimensional accuracy. Trial 2 demonstrates that through optimisations of beam deflection system and laser delays, the machining error can be reduced to obtain a satisfactory dimensional accuracy. For example, Figures 6.14a and 6.14b, which depict Feature 1 of the waveguide, show that the deviation of the produced structure is within +/- 10 μm from its nominal dimensions. However, the machining quality in Trial 2 is still not satisfactory even after the introduction of the delays due to varying pulse distances and hence non-uniform ablation rates in the acceleration and deceleration regions of the machining vectors. Thus, the depth profile of the produced structures has a convex shape as shown in Figures 6.14c and 6.14d. The effects from accumulation of laser pulses at the beginning and end of each machining vector after the applied 15 machining layers and the normal orientation of the machining vectors to the waveguide length result in a four times higher depth along the

123

edges of the structure in comparison to that in its centre. Thus, even after optimising the delays in Trial 2, it is not possible to address the quality requirements for the manufacturing of the waveguide filter.
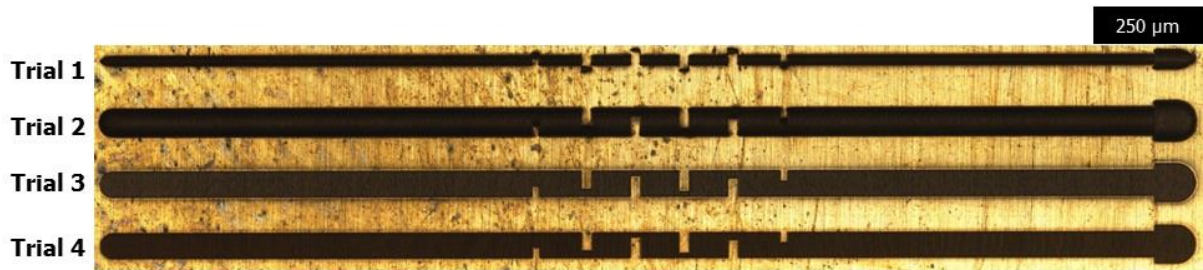
Figure 6.13 The waveguide structures produced in the four laser machining trials
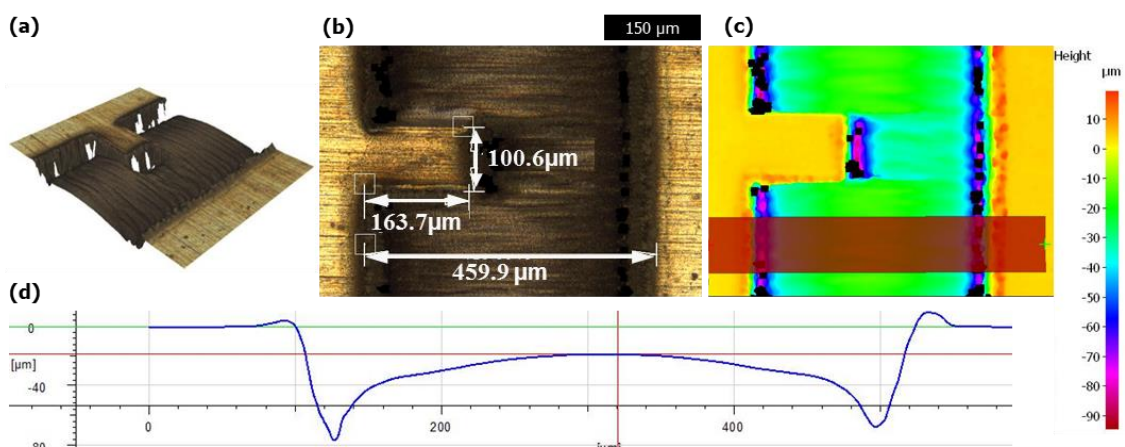
Figure 6.14 Feature 1 of the produced waveguide channel in Trial 2: (a) 3D view of the feature, (b) top view of the Feature with some measurements, (c) and (d) the depth profile of the produced waveguide channel

In Trial 3, the laser machining of the waveguide was carried out after applying the adaptive postprocessor. The machining results clearly demonstrate the postprocessor capabilities to offset the negative dynamic effects of the beam deflection system and thus to improve both dimensional accuracy and quality of the machined structure at high scan speeds. Figures 6.15a and 6.15b, which show Feature 1 of the microwave filter, clearly demonstrate that the deviation of the waveguide dimensions from their nominal values is within the target dimensional tolerance of +/- 10 μm. Furthermore, the machining quality is improved dramatically by maintaining the pulse distance constant throughout the full length of the machining vectors and thus uniform material ablation is achieved across the waveguide channel as shown in Figures 6.15c and 6.15d.
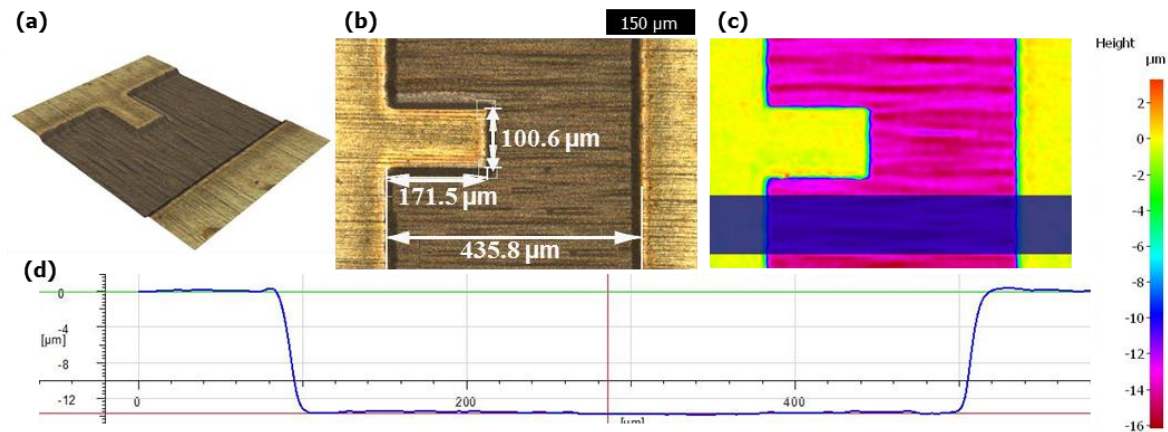
Figure 6.15 Feature 1 of the produced waveguide channel in Trial 3: (a) 3D view of the feature, (b) top view of the feature with some measurements, (c) and (d) the depth profiles of the produced waveguide channel

The machining accuracy and quality achieved in Trial 4 was almost the same as in Trial 3 but the laser machining efficiency in Trial 3 was significantly better in comparison to Trial 4. In particular, the machining time for the fabrication of the waveguide in Trial 3 and Trial 4 was 102 and 391 seconds, respectively (see Table 6-4). Thus, an almost fourfold efficiency improvement can be achieved if the adaptive postprocessor is utilised due to the capabilities to perform the processing operations with much higher scan speeds. Furthermore, beam diameter compensations in Trial 4 were manually introduced to the CAD model in order to achieve the required machining accuracy that had time implications in generating the beam-path.

Finally, it should be noted that the two different experimental validation tests demonstrate that the proposed software tools for offsetting the negative effects of the beam deflection system dynamic can be implemented with laser sources that have different control architectures, e.g. MOPA, Q-switching and mode-locking.

Table 6-4 The results from the machining of the waveguide structures

Waveguide filter Trial 2							
Filter Feature	1	2	3	4	5	6	Channel
Width [µm]	100.8	153.1	148.8	148.7	153.3	101.1	463.4
Height [µm]	175.1	296.5	346.3	346.5	296.8	175.7	NA
Total machining time [s]	99						
Waveguide filter Trial 3							
Feature [µm]	1	2	3	4	5	6	Channel
Width [µm]	100.6	153.2	152.1	151.9	152.8	100.4	435.8
Height [µm]	171.5	293.6	339.6	339.8	293.8	171.5	NA
Total machining time [s]	102						
Waveguide filter Trial 4							
Feature [µm]	1	2	3	4	5	6	Channel
Width [µm]	104.1	158.1	157.2	157.6	158.8	104.3	428.4
Height [µm]	173.5	290.1	343.4	339.9	290.8	173.7	NA
Total machining time [s]	391						

6.2 An automated software routine for multi-axis LMM employing rotary stages

6.2.1 Introduction

The implementation of automated multi-axis strategies with rotary stages can broaden significantly the manufacturing capabilities of LMM platforms. For example, such automated strategies are critical for laser polishing of free-form surfaces in order to keep the beam normal to the workpiece and to accurately follow the contours of the processed surfaces, and thus to ensure a consistent laser irradiation for uniform polishing results. Furthermore, such an automated tool can also offer an effective solution to address an important intrinsic LMM limitation, namely the side walls tapering of laser machined structures [220], which can affect adversely the parts' functionality. Other applications of such automated strategies include multi-side laser processing of parts (see Figure 5.2c in Chapter 5) and laser processing of axis-symmetric parts (see Figure 5.2d in Chapter 5). The requirements that such automated multi-axis LMM strategies should fulfil are:

- to be easily adaptable to the specific requirements of different LMM operations, in particular for machining structures with user-defined side walls taper angle, axis-symmetric parts (Figure 5.2d) and also parts requiring a multiple-side processing (Figure 5.2c);
- to provide high machining ARR;

- to take into account changes of the laser beam position in LMM platform coordinate system due to potential laser beam thermal drifts and alignment and calibration issues associated with the beam delivery components.

Machine tools standard PD ISO/TR 16907:2015 provides a general outline of machine tool configurations, where machine assembly components are physically linked to the frame of the machine tools through mechanical joints and thus all machine components such as tool spindle and mechanical axes have absolute topologies, determined by the tolerances of the employed mechanical joints, in the machine coordinate system (MCS) [221]. For example, the representation of the kinematic chain diagrams of five-axis milling machines demonstrates that the absolute topological structure of the systems' components in MCS allows the establishment of a structural loop , which maintains the relative positions between a cutting tool and a workpiece throughout the NC machining commands [222]. Thus, to realise any machining process it is necessary to establish a single geometrical correlation between the MCS and the workpiece coordinate system (WCS) [223]. However, this is not valid in state-of-art LMM machine tool configurations, because they employ both mechanical and optical axes, which are not physically linked and thus possess independent coordinates systems. This is demonstrated in a study where simultaneous utilization of optical axes and a linear stage was only possible after the development of synchronization algorithm, which relies on real time signal transfer between the employed linear stage and the galvanometer scanner [112]. Furthermore, LMM systems incorporate complex beam delivery sub-systems whose component technologies require frequent alignments and calibrations due to the extreme sensitivity of the laser beam pointing stability to environmentally related factors, e.g. temperature, humidity and vibrations [224]. Such beam positional instabilities lead to beam spot (the laser material interaction area) shifts in the MCS and thus do not allow an absolute topology to be established for the laser system component technologies. Therefore, the LMM machine tool configurations should be represented by two coordinate systems, in particular MCS that describes the working volume of the integrated mechanical axes and a beam coordinate system (BCS) that defines the focusing volume covered by the integrated optical axes . Thus, it is necessary to correlate BCS geometrically to the MCS in order to achieve the desired topological laser irradiation of a workpiece. Figure 6.16 provides a graphical representation of the necessary geometrical correlations between WCS, BCS and MCS that are necessary for executing different LMM operations. In particular, machining results are

determined by the geometrical correlation between WCS and BCS that is achieved by referencing both WCS in MCS and BCS in MCS. Since the workpiece is physically attached to the mechanical stages of LMM platforms, WCS is dynamically referenced in MCS and thus any linear or rotary motions of the mechanical stages would maintain the established geometrical correlation of WCS in MCS within the uncertainties associated with the component technologies used to realise the relative movements. However, this is not the case for the geometrical correlation of BCS in MCS because it is assumed to be static due to the absence of a physical link between the laser beam and the mechanical stages. Thus, the execution of any rotary motions will lead to translational errors in the geometrical correlation of BCS in MCS. These errors after any rotational movements also lead to geometrical misalignments of WCS in BCS and thus to formation of machining errors on the processed workpieces. Therefore, an effective automated strategy for the utilization of rotary stages in LMM platforms ought to include:

- techniques for correlating BCS to MCS, in particular to link BCS to the stages axes of rotations;

- tools for predicting the translational errors in correlating geometrically BCS to MCS after any arbitrary rotary movements;

- corrective commands in the machining routines to compensate the translational errors of BCS in MCS after the execution of rotary movements and thus to ensure high machining ARR.
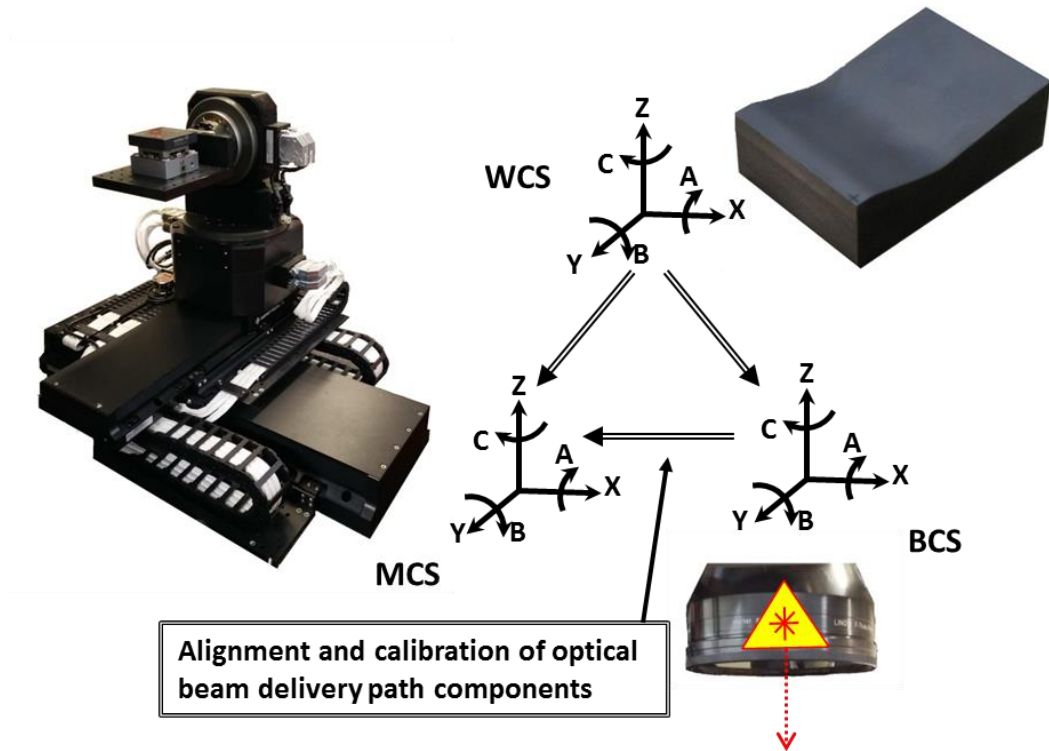
WCS- workpiece coordinate system; BCS- laser beam coordinate system; MCS- machine coordinate system

Figure 6.16 Geometrical correlations between MCS, BCS and WCS in executing LMM operations

Note to Figure 6.16: The Right-hand rule notations are used.

6.2.2 Design considerations

6.2.2.1 Geometrical correlation between BCS and the stages' axes of rotation

Figure 6.17a and Figure 6.17b depict a method for establishing the geometrical correlation of BCS in relation to the axis of the rotary stages along x and y axes and z axis of a LMM platform, respectively. Points A_0, A_1, A_2,….A_n and Δd_1,…. Δd_n represent the locations of the beam spot in the working plane of the rotary stage and the corresponding distances to its axis of rotation at arbitrary angles, θ_0, θ_1, θ_2,… θ_n, respectively. Thus, the geometrical correlation of BCS in regards to the axes of the integrated rotary stages can be defined using Equation 6.5.

$$D_0 = \frac{\sum_{i=0}^{n} \frac{\Delta d_i}{\sin \theta_i}}{n+1}$$

(Equation 6.5)

It should be noted that the uncertainty of the proposed correlation method reduces with the increase of the number of rotational angles.
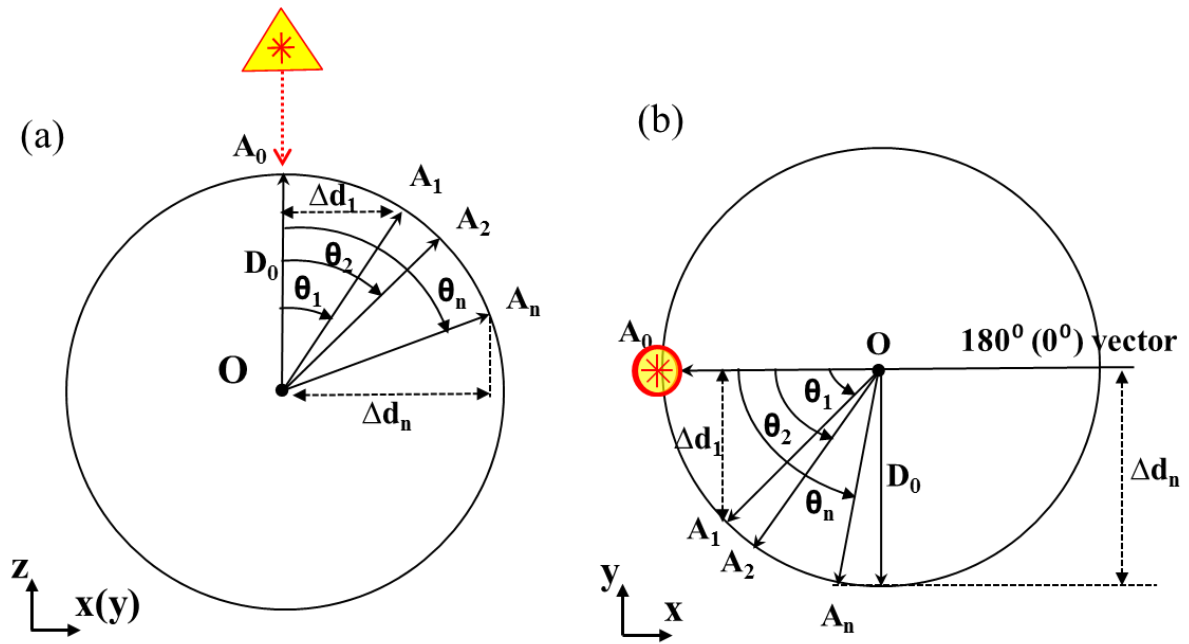
Figure 6.17 A method for establishing a geometrical correlation between BCS and the axis of a rotary stage about (a) x and y axes and (b) z axis of a LMM platform

6.2.2.2 Prediction of translational errors

Figure 6.18 exemplifies the formation of translational errors in correlating geometrically BCS to MCS after any arbitrary rotary movement (θ) about x and y axes of a LMM platform. Equations 6.6 and 6.7 can be used to calculate translational errors, $\Delta y(\Delta x)$ and Δz, respectively.

$$\Delta y(\Delta x) = \frac{D_\gamma}{\cos \gamma} \times \sin(\theta - \gamma) + a \qquad \text{(Equation 6.6)}$$

$$\Delta z = D_1 - (\frac{D_1}{\cos \gamma} \times \cos(\theta - \gamma)) \qquad \text{(Equation 6.7)}$$
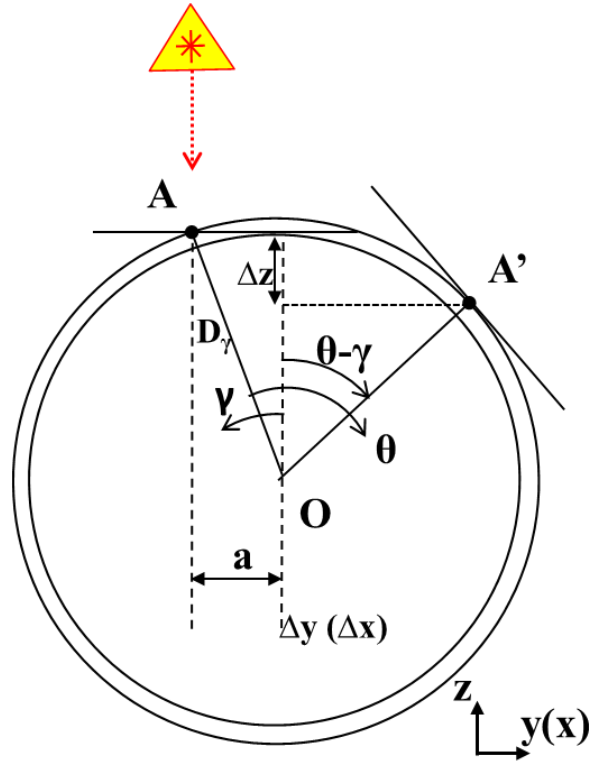
Figure 6.18 Translation errors in correlating geometrically BCS to MCS after any arbitrary rotary movement about the x and y axes of a LMM platform

Notes to Figure 6.18: (i) points A and A' represent the initial position (prior to the rotation) and the final position (after the rotation) of the beam spot in MCS, respectively; (ii) point **O** is the centre of rotation of the rotary stage; (iii) **θ** is the arbitrary angle of rotation; (iv) **a** is the offset distance of beam spot in regards to the axis of rotation along y and x; (v) **γ** is the angle between A and O due to a; (vi) **Dγ** is the distance of point A to the axis of rotation; and (vii) Δy (Δx) and Δz represent the translational errors of the beam spot in MCS due to the rotation along the y(x) axis of the LMM platform.

Figure 6.19 describes the formation of translational errors in correlating geometrically BCS to MCS after any arbitrary rotary movement (θ) about the z axis of the LMM platform. Equations 6.8 and 6.9 can be used to calculate translational errors Δx and Δy, respectively.

$$\Delta x = \cos(\Omega) \times \frac{b}{\tan(\Omega)} - \cos(\theta + \Omega) \times D_\Omega \qquad \text{(Equation 6.8)}$$

$$\Delta y = \sin(\theta + \Omega) \times D_\Omega - b \qquad \text{(Equation 6.9)}$$
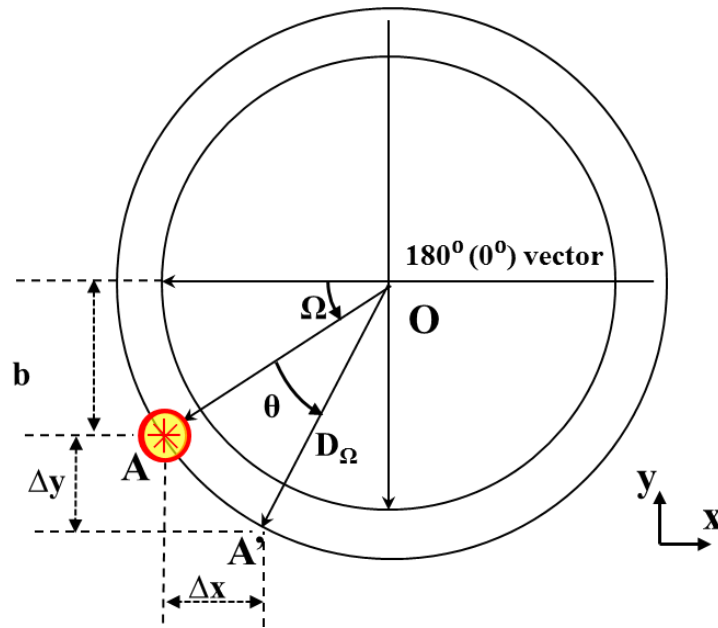
Figure 6.19 Translation errors in correlating geometrically BCS to MCS after any arbitrary rotary movement (a) about the x and y axes and (b) about the z axis of the LMM platform

Notes to Figure 6.19: (i) **b** is the offset distance of beam spot in regards to the 0^0 (180^0) vector; (ii) Ω is the angle between 0^0 (180^0) vector and vector OA; and Δx and Δy represent the translational errors of the beam spot in MCS due to the performed rotation along the z axis of the LMM platform.

6.2.2.3 Corrective commands

Figure 6.20 provides a schematics representation of the algorithm used to implement a routine for performing laser multi-axis machining with rotary stages. The proposed algorithm is fully automated and introduces corrective commands in the machining routines based on given rotational angles. Furthermore, the algorithm can account for geometrical errors in correlating BCS to MCS caused by alignments and calibrations of optical components in the beam delivery system and thus to improve the machining ARR.
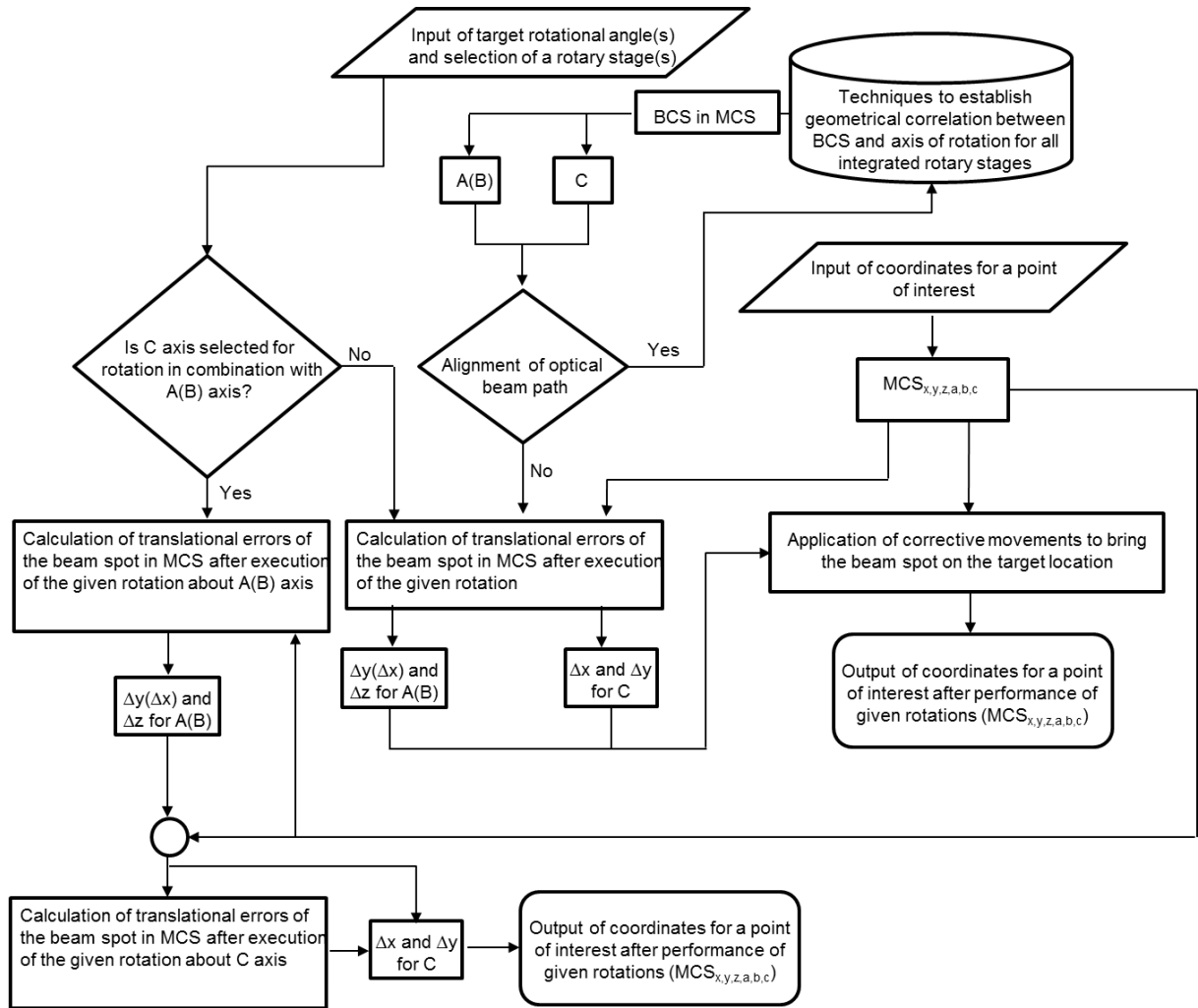
Figure 6.20 Implementation algorithm for performing laser machining with rotary stages

6.2.3 Experimental Validation

Experimental evaluation of the machining ARR of the proposed automated strategy for multi-axis LMM using rotary stages is performed using the test procedure in Figure 6.21. The machining ARR achievable when the A and C axes are employed individually are evaluated first with the test procedure in Figure 6.21a. In particular, a pattern consisting of seven 0.5 mm long crosses that are 0.55 mm apart is machined after pre-defined rotations of both stages. The rotational angles used in the tests are 0^0, +/- 5^0, +/- 10^0 and +/- 15^0 for both A and C axes, respectively. The pattern in Figure 6.21a was produced twice per sample and on two samples in order to assess the repeatability and the reproducibility of the proposed strategy for a single rotary stage. The machining accuracy achievable with either of the two rotary stages (A and C) was assessed based on the maximum displacement of the produced crosses at the pre-defined rotary angles in regards to the reference crosses produced at the home position of

the A or C axes ($\theta=0^0$), respectively. At the same time, the repeatability and reproducibility were evaluated by comparing the displacements of the produced crosses to their average values calculated based on the results from one sample and the two samples, respectively.

The machining ARR when A and C axes are simultaneously utilized, are evaluated by laser machining the pattern in Figure 6.21b. It consists of five concentric circles whose radiuses increase with an incremental step of 0.1 mm from the innermost circle with a radius 0.25 mm to the outermost circle with a radius of 0.65 mm. Each of the circles is produced after pre-defined simultaneous rotations of both A and C axes. The rotational angles used in the experimental tests are +/-10^0 and +/- 2^0 for both axes. The pattern from Figure 6.21b was produced twice per sample and on two samples in order to assess the repeatability and the reproducibility of the proposed strategy for simultaneous utilization of two rotary stages. The machining accuracy achievable with the proposed automated strategy is evaluated by measuring the concentricity of the circles in regards to the reference circle produced at the home position of A and C rotary stages ($\theta=0^0$). The repeatability and reproducibility were assessed by comparing the concentricity of the circles to their average concentricity values calculated based on the results from one sample and the two samples, respectively. Thus, the repeatability and reproducibility of the proposed automated strategy for multi-axis LMM are evaluated based on 40 test structures produced with the proposed strategy (24 are produced with a single rotary axis and 16 with the simultaneous utilization of two rotary axes).
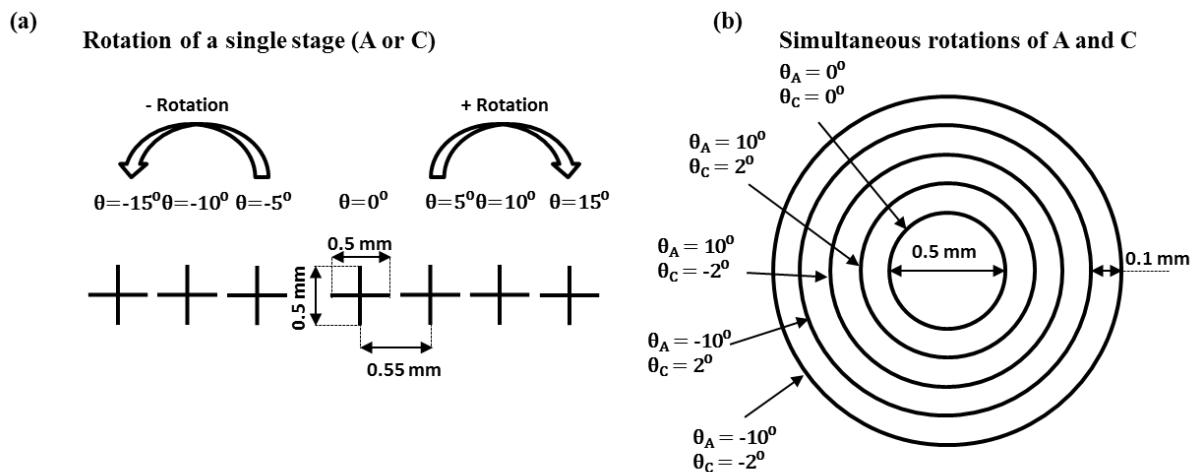
Figure 6.21 The test procedure used to evaluate the automated strategy (a) the use of a single rotary stage and (b) the simultaneous utilization of A and C rotary stages

6.2.4 Results and Discussions

Figure 6.22a shows the top view of the crosses produced after completing the test procedure described in Section 6.2.3 of this chapter. The central cross in Figure 5.22a is produced at $\theta_A = 0^0$ and it is used as a reference to quantify the displacements (Δd) of other crosses produced after executing pre-defined rotations with the A rotary stage. The displacements of the crosses were calculated by using the Alicona Contour tool [178] as shown in Figure 6.22b. In particular, the crosses' contours were extracted and then automatic fitting of parallel lines was applied on the respective edges as shown in Figure 6.22c. In this way, their displacements are quantified to assess the effectiveness of the corrective commands when executing multi-axis machining strategies with a single rotary stage. For example, the measurement procedure used to assess the accuracy of the applied corrective command after a rotation of -5 degrees with the A axis is illustrated in Figure 6.22c. The results from the tests carried out for both A and C axes are provided in Table 6-5. The positioning ARR capabilities of the proposed multi-axis machining strategies with a single rotary stage are assessed based on the analytical procedure provided in Section 6.2.3 of this chapter. It can be seen in Table 6-5 that the maximum displacement of the crosses produced with the A axis are 5.4 μm and 5.3 μm and 4.2 μm and 4.1 μm for Patterns 1 and 2 on the two samples, respectively. At the same time, the maximum overall displacements of the crosses produced with the C axis are 5.7 μm and 4 μm and 4.9 μm and 5.0 μm for Patterns 1 and 2 on the two samples, respectively. Thus, it can be stated that the accuracy achievable with the proposed strategy for multi-axis LMM employing either A or C axes is better than 5.7 μm. The repeatability of the proposed strategy with the A axis is 5.3 μm and 3.8 μm for Samples 1 and 2, respectively, based on average displacements in Table 6-5. Since, the machining of the crosses with the proposed strategy using the C axis required corrective commands with x and y components, the repeatability is assessed taking into account the displacements both along x and y axes. Figure 6.23 shows the distribution of the crosses' displacements in regards to the average displacements for the two samples, respectively, and thus the repeatability of the proposed strategy using the C axis is 6.4 μm and 6.2 μm for Samples 1 and 2, respectively. Based on these results, it can be stated that the repeatability of multi-axis LMM employing either A or C axes is better than 6.4 μm. At the same time, the reproducibility of the proposed strategy is 5.0 and 5.9 μm using the A and C axes, respectively, based on the average displacements of the crosses in Table 6-5 and Figure

6.23. The total uncertainty at the 95% confidence level in quantifying the ARR capabilities of the proposed strategy for multi-axis LMM with either A or C axes is 0.46 µm.
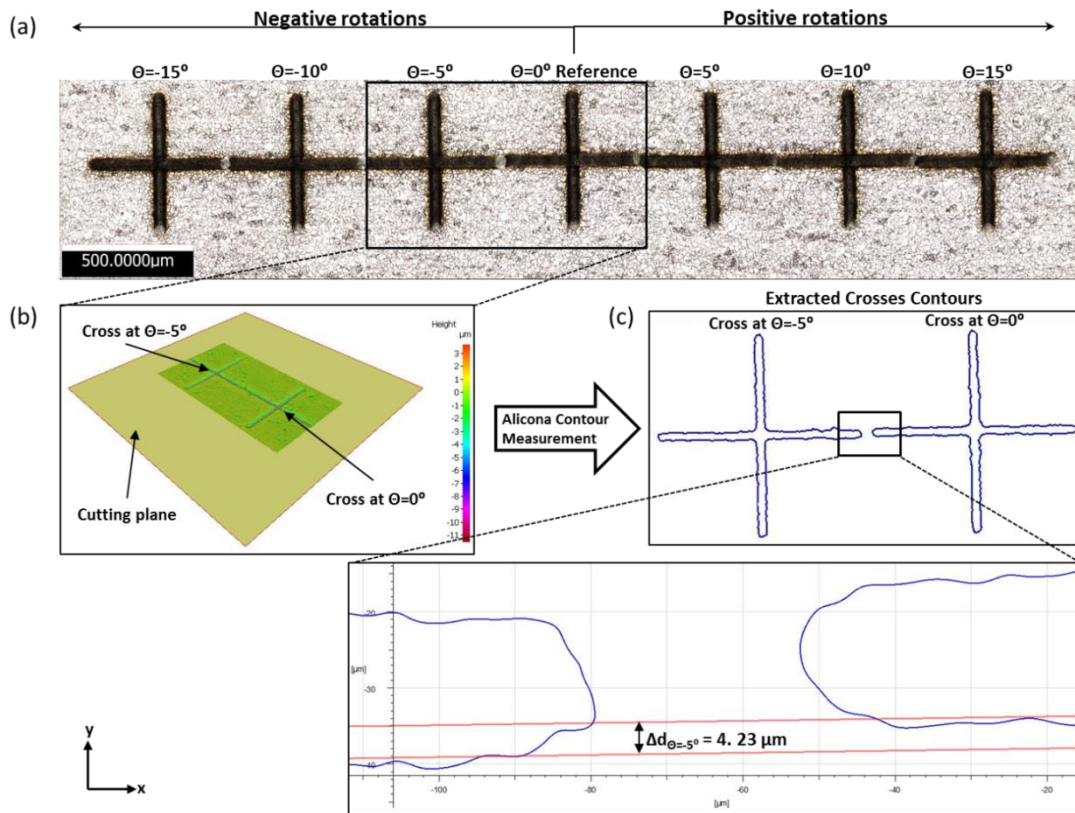
Figure 6.22 Laser machined crosses with the proposed automated strategy when A axis is used only, (a) top view of the crosses for all investigated rotational angles, (b) application of Alicona Contour tool on crosses produced at $\theta_A = 0^0$ and $\theta_A = -5^0$, (c) extracted crosses contours and measurement of the positional deviation of the cross at $\Theta_A = -5^0$ in comparison to the cross at $\theta_A = 0^0$
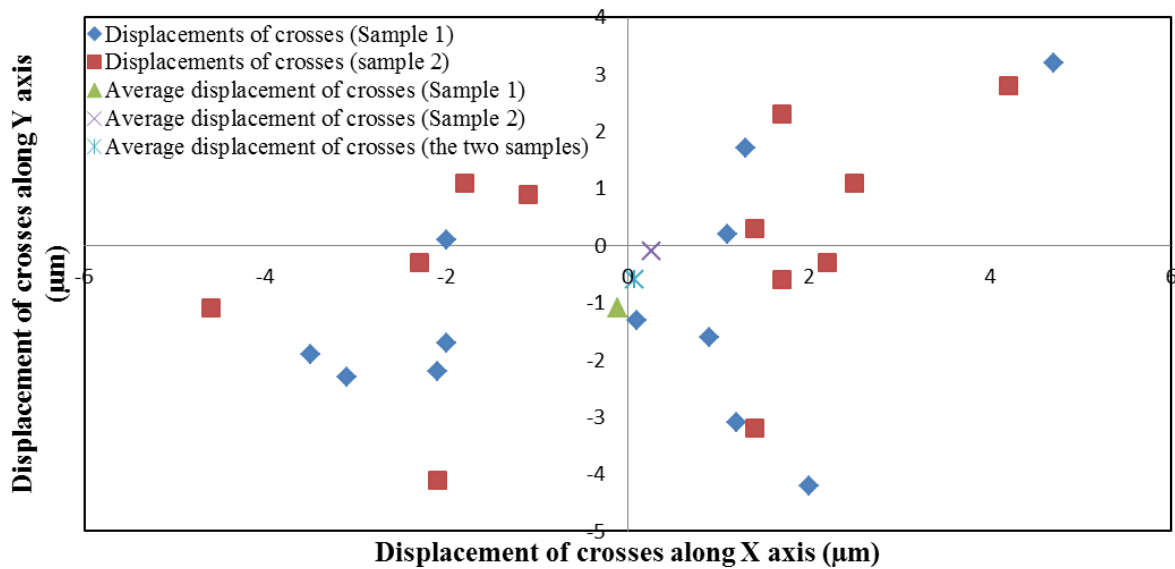
Figure 6.23 Repeatability and reproducibility of the proposed strategy using the C axis

Table 6-5 Test results after using the A and C rotary stages separately

Parameter	Sample 1 – Pattern 1 - A axis						Sample 1 – Pattern 2 - A axis					
Rotary angle (^{0})	5	10	15	-5	-10	-15	5	10	15	-5	-10	-15
Displacement-x axis (µm)	-	-	-	-	-	-	-	-	-	-	-	-
Displacement-y axis (µm)	5.4	5.1	-2.7	-4.2	-1.9	5.1	5.3	4.1	0.5	-2.6	-4.2	3.7
Average displacement for Sample 1- A axis (µm)							1.1					
Parameter	Sample 2 – Pattern 1 - A axis						Sample 2 – Pattern 2 - A axis					
Rotary angle (^{0})	5	10	15	-5	-10	-15	5	10	15	-5	-10	-15
Displacement-x axis (µm)	-	-	-	-	-	-	-	-	-	-	-	-
Displacement-y axis (µm)	-2.1	3.7	-2.3	-1.2	4.2	2.1	1.1	4.1	-1.3	-1.6	-2.2	0.7
Average displacement for Sample 2 – A axis (µm)							0.4					
Average deviation for the two samples – A axis (µm)							**0.8**					
Parameter	Sample 1 – Pattern 1 - C axis						Sample 1 – Pattern 2 - C axis					
Rotary angle (^{0})	5	10	15	-5	-10	-15	5	10	15	-5	-10	-15
Displacement-x axis (µm)	1.2	-3.1	-2.0	2.0	-3.5	4.7	0.1	-2.0	1.1	0.9	-2.1	1.3
Displacement-y axis (µm)	-3.1	-2.3	-1.7	-4.2	-1.9	3.2	-1.3	0.1	0.2	-1.6	-2.2	1.7
Overall absolute displacement (µm)	3.3	3.9	2.6	4.7	4.0	5.7	1.3	2.0	1.1	1.8	3.0	2.1
Parameter	Sample 2 – Pattern 1 - C axis						Sample 2 – Pattern 2 - C axis					
Rotary angle (^{0})	5	10	15	-5	-10	-15	5	10	15	-5	-10	-15
Displacement-x axis (µm)	2.2	-1.1	-1.8	1.4	-2.3	1.7	1.4	-4.6	2.5	1.7	-2.1	4.2
Displacement -y axis (µm)	-0.3	0.9	1.1	-3.2	-0.3	2.3	0.3	-1.1	1.1	-0.6	-4.1	2.8
Overall absolute displacement (µm)	2.2	1.4	2.1	3.5	2.3	2.9	1.4	4.7	2.7	1.8	4.6	5.0

Figures 6.24a and 6.24b show the top and 3D view of the circles produced with the proposed automated strategy that required the simultaneous utilization of both A and C axes of the LMM platform. The experimental validation of the proposed tool is performed by measuring the concentricity of the circles produced following the test procedure in Section 6.2.3 of this chapter. In particular, the concentricity of C2, C3, C4 and C5 were measured in respect to C1

produced at $\theta_A = \theta_C = 0^0$ as shown in Figure 6.24c. Figure 6.25 provides a plot with the results and it can be stated that accuracy of the proposed strategy with simultaneous utilization of A and C axes is better than 10.6 µm. Furthermore, the repeatability of the proposed strategy is better than 10.9 µm and 10.8 µm for Samples 1 and 2, respectively, while the reproducibility is better than 12.6 µm. The total uncertainty for quantifying the ARR capabilities of the proposed strategy is 0.53 µm. Based on these results, it can be stated that the machining ARR achievable with the proposed multi-axis LMM strategy with the simultaneous use of the A and C rotary stages including the total uncertainty are better than +/-6.5 µm.
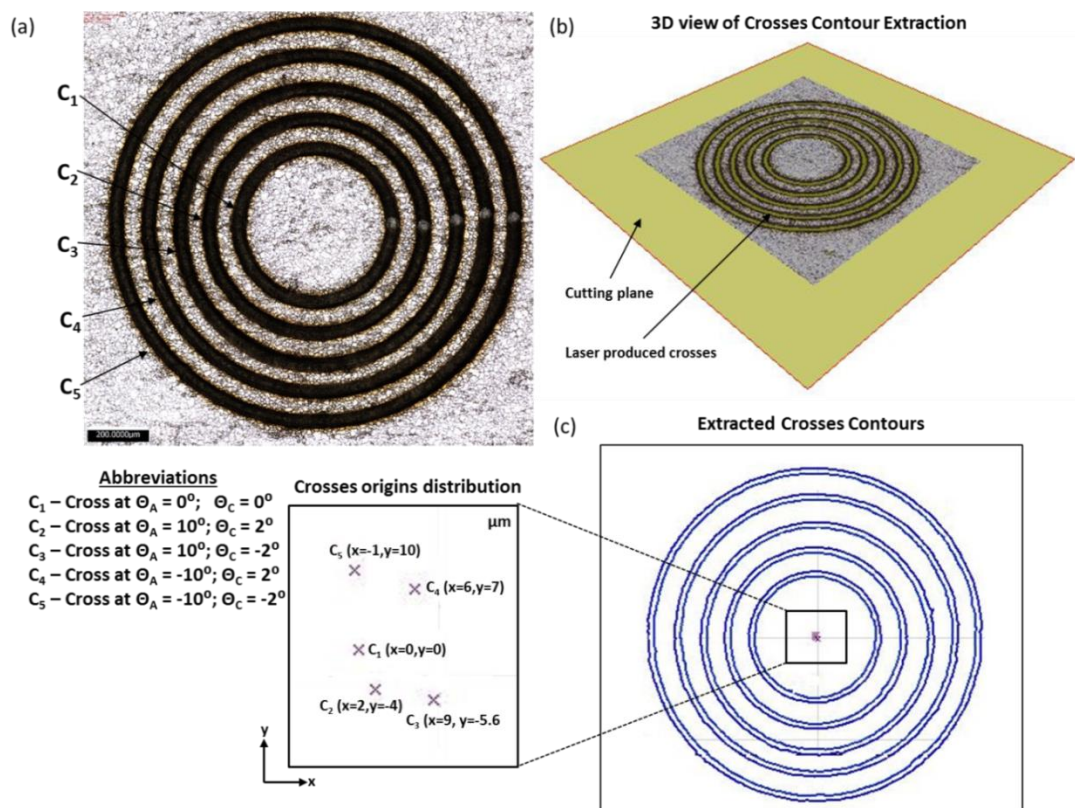
Figure 6.24 The circles machined with the proposed automated strategy with the simultaneous utilization of the A and C axes: (a) Top view of the circles; (b) 3D view of the circles generated with Alicona Contour tool; and (c) extracted circles' contours with the procedure for measuring their concentricity
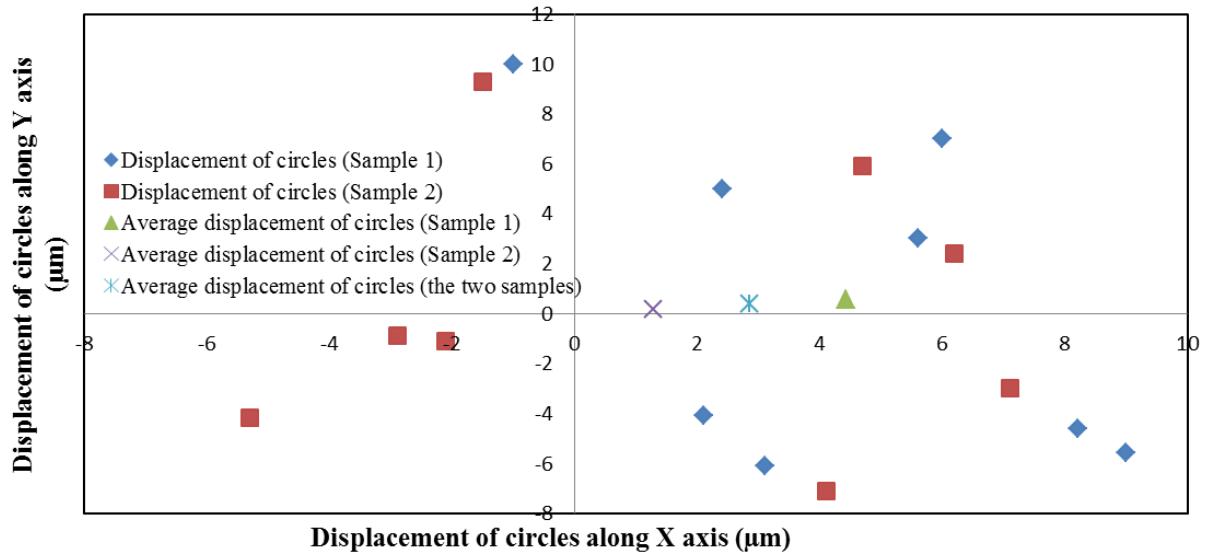
Figure 6.25 Repeatability and reproducibility of the proposed strategy with simultaneous utilization of A and C axes

6.3 Conclusions

This chapter presents two generic software tools, which can substantially improve the manufacturing capabilities of reconfigurable LMM systems in terms of machining throughput and complexity of the laser manufacturing operations. In particular, the proposed two generic software solutions are: (i) a software tool to counteract the negative dynamic effects of optical scanning head systems and thus to improve significantly the laser machining accuracy, quality and efficiency of LMM platforms and (ii) an automated strategy for multi-axis LMM with rotary stages for performing demanding complex machining routines. The achieved manufacturing improvements with the proposed software tools are achieved by implementing ''adaptive'' postprocessors as stand-alone software solutions. In this way, the generation of machine executable part programs is fully automated and users can benefit from these software tools regardless of their knowledge and experience with any given LMM systems. The following conclusions could be drawn from this research:

- The dynamic effects of beam deflection systems integrated into LMM systems lead to significant machining errors and have a detrimental effect on the quality of produced structures and this negative impact increases with the increase of the scan speed.

- Such dynamic effects can be minimised by introducing machine specific compensations in machining vectors to counteract their acceleration and deceleration regions regardless of

their directions, length and set scan speed. Thus, laser machining with micro scale machining vectors can be performed while maintaining a higher ARR.

- The proposed software tool, which counteracts the negative dynamic effects of optical beam deflection systems, leads to substantial improvements of machining quality because uniform ablation rates can be maintained throughout the full length of machining vectors. In addition, the use of the proposed software tool increases the laser machining efficiency substantially by allowing much higher scan speeds to be applied without any detrimental effects on ARR and machining quality.

- The developed automated strategy for multi-axis LMM employing rotary stages allows machining operations to be carried out with ARR better than +/- 6.5 µm, respectively.

CHAPTER 7

NOVEL LASER-BASED MULTI-PROCESS MANUFACTURING SOLUTION FOR THE SCALE UP PRODUCTION OF TERAHERTZ TECHNOLOGY DEVICES

Outline of the chapter

The research work in this chapter aims at demonstrating the laser micro-processing as a modular manufacturing technology that can be seamlessly integrated in multi-process manufacturing solutions, i.e. process chains, for extending the capabilities of well proven conventional manufacturing routes, i.e. mechanical machining, and thus to provide the required manufacturing capabilities for the cost effective fabrication of complex products with multi-length scale (micro-and meso-scale) functional features. In particular, this chapter investigates a laser-enabled manufacturing route that combines LMM with mechanical machining for the scale up production of complex miniaturised products. Terahertz (THz) technology devices were selected as a representative example of such miniaturized products in this research because they are difficult to manufacture due to the following two reasons: (i) the highly complex 3D geometrical designs of the THz devices with meso- and micro- scale functional structures, which necessitate requirements for extreme manufacturing reconfigurability and flexibility; (ii) the challenging technological requirements, driven by the high functional performance sensitivity of the THz devices on their dimensional accuracy and surface integrity, which necessitate very high process reliability and robust machine tool performance for obtaining the required level of manufacturing ARR. To fulfil these requirements, the generic system-level tools and techniques presented in Chapters 4 and 5 are deployed into a LMM system to machine the waveguide structures of THz devices with required ARR and also to integrate it with a precision milling system for cost effective manufacturing of components with multi-scale functional features. The proposed laser-enabled manufacturing route for producing miniaturised products is validated on three

industrially representative THz devices and thus to demonstrate the LMM capabilities achieved with the system-level tools developed in this research.

The research reported in this Chapter refers to Publication 2 from the List of Publications.

7.1 Introduction

7.1.1 Terahertz technology

Terahertz (THz) technology encompasses devices that harness the Terahertz electromagnetic radiation (from 100 GHz to 10 THz) that lies in the boundary region between light and radio waves [225]. Thus, THz technology fills the ''transition region'' between Electronics and Photonics [226]. The THz range of the electromagnetic spectrum was called until recently the THz ''gap'', because it has not been practically used with the exception of a number of limited applications in high-resolution spectroscopy and remote sensing areas [227]. However, new advances in different technologies, such as the advent of time-domain spectroscopy (TDS) with ultrashort-pulse laser sources, have made in the recent years the previously unused terahertz frequency extremely attractive to researchers due to its ability to achieve innovative sensing systems [228]. Some of the very appealing characteristics of Terahertz waves include: they can handle ultra-broad band signals, have very large absorption due to water or water vapor, and are transparent through many materials (e.g., plastic, paper, cloth, and oil) that are opaque in visible and IR light [225, 229]. Thus, the list of possible applications of THz technology is extremely extensive and innovative. Application examples of THz technology are shown in Figure 7.1 and are reported in the field of biomedical engineering, safety monitoring, product quality control, non-destructive testing in materials science and engineering, astrophysics, atmospheric research, short distance communications and networking, spectroscopy and imaging technology, remote sensing safety applications and military sector [229-238].
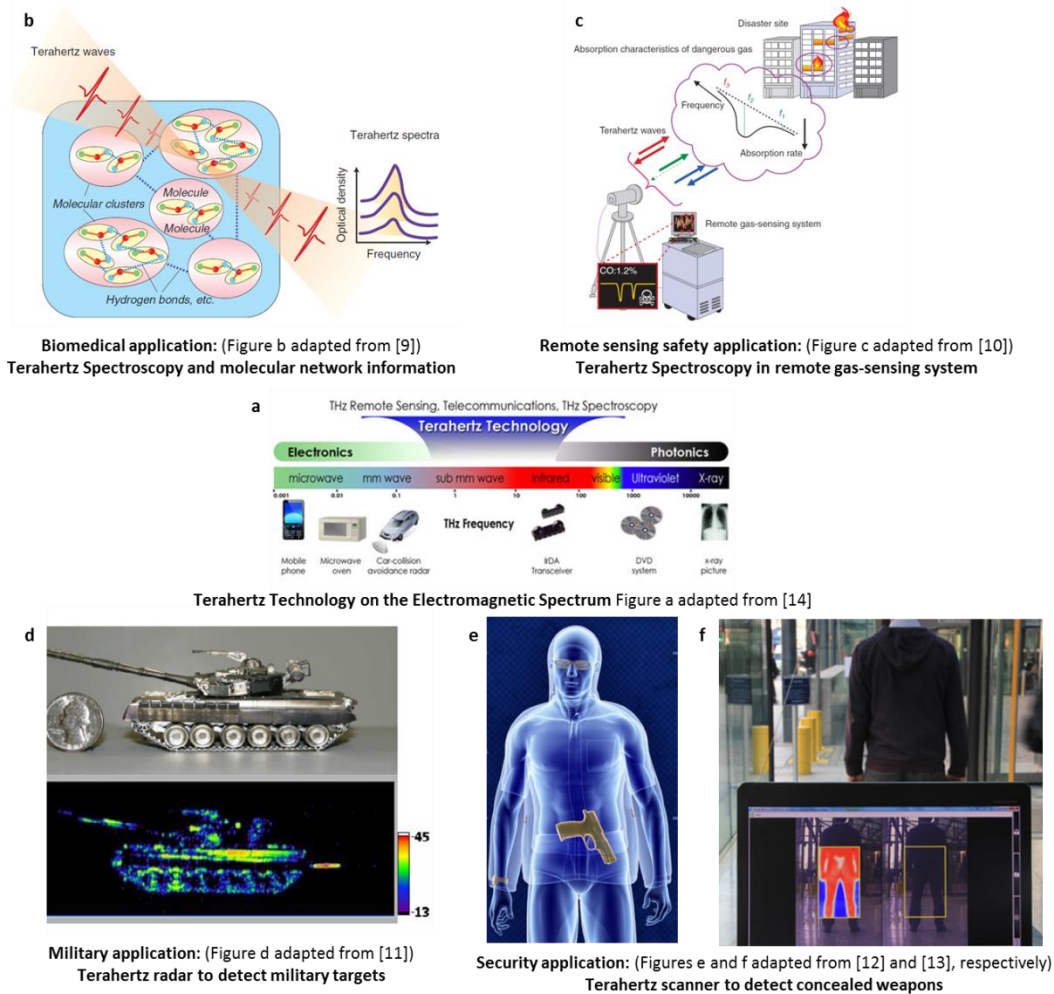
Figure 7.1 Applications of Terahertz Technology: (a) Terahertz technology on the electromagnetic spectrum (Figure adapted from [238]), (b) Biomedical (Figure adapted from [233]), (c) Remote sensing application (Figure adapted from [234]), military application (Figure adapted from [234]), (e) security application (figure adapted from [236]) and (f) security application (figure adapted from [237])

7.1.2 Current manufacturing technologies for producing Terahertz technology devices

The drive for THz, also called sub-millimetre, waveguide instruments at the high end of the electromagnetic spectrum (90-500 GHz) has experienced considerable growth in the past few years because these devices enable the development of highly innovative sensing systems for diverse application areas, which were discussed in Section 7.1.1 of this chapter. Figure 7.2a shows an example of a family of Terahertz technology devices that operate at the high end of the electromagnetic spectrum [239]. A critical component of a Terahertz technology device is the waveguide , exemplified in Figure 6.2b, which is usually a hollow air-filled structure used to confine and propagate electromagnetic waves, and is widely used at THz frequencies [240].

This is mainly due to its low microwave loss characteristic, i.e. a high transmission rate at the THz frequencies.
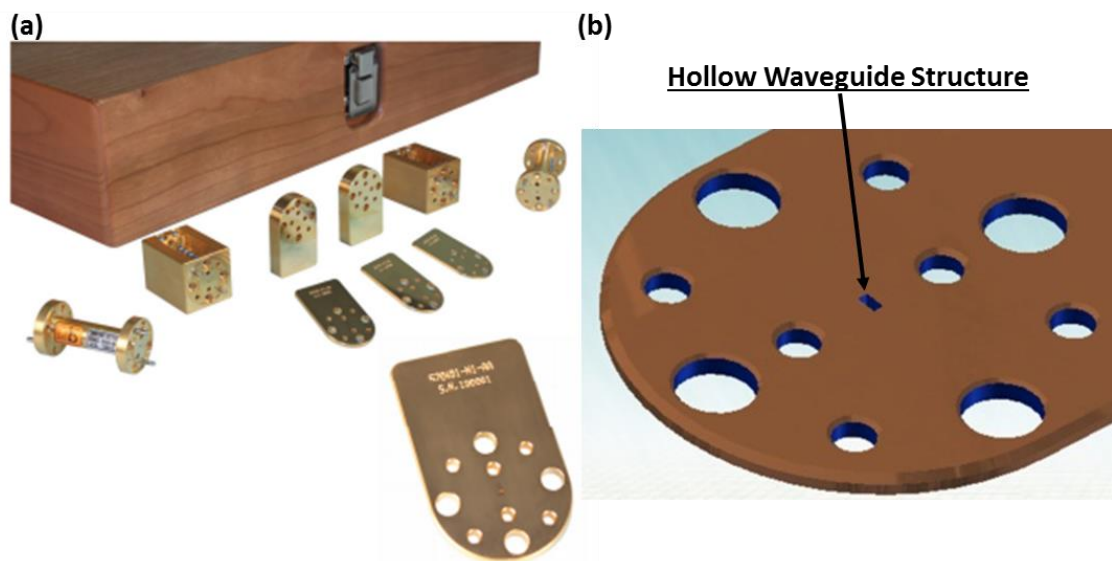
Figure 7.2 (a) A family of Terahertz technology devices that operate at the high end of the electromagnetic spectrum (frequency range: 90-500 GHz); (b) An Example of a waveguide hollow structure (Figures adapted from [239])

Due to the 2.5D design and micro-scales required at these frequencies, waveguide fabrication methods have mainly been based on photoresist micro-manufacturing techniques. Among them three techniques were identified as the most suitable, in particular Silicon Deep Reactive Ion Etching (DRIE) [241-243], LIGA-based thick layer electroplating [244, 245] and SU8 or KMPR photoresist based fabrication [246- 248], due to their capabilities to produce high aspect ratio structures both across meso- and micro- length scales [219]. However, such fabrication routes are extremely complex and their manufacturing capabilities are characterized with a high level of fabrication uncertainty, because they require multi-step processing and clean room technologies. In addition, these manufacturing technologies have intrinsic limitations regarding the materials that can be processed and thus used in designing THz devices; also, they introduce constraints regarding the devices' design, especially the necessity to split the designs into structured Si or SU8 layers that have to be metalized before integrating them with high precision into the 2.5D devices' geometry [249]. These limitations make the photoresist-based fabrication approaches capital intensive and thus potentially viable only for relatively high batch sizes while the unit costs are still relatively high due to the use of clean room manufacturing technologies and the required high precision alignment and packaging operations.

To address the limitations of photoresist-based manufacturing technologies, researchers have also explored alternative fabrication solutions such as direct machining of waveguide components on metallic substrates employing high precision CNC micro-milling [250]. Waveguide components fabricated by CNC milling with good functional performance have been demonstrated, such as the work reported at W-band (75-110 GHz frequency range) (e.g. [251, 252]), WR-4 band (170-260GHz) [253] and WR-3 band (220-325GHz) [254]. However, such a manufacturing solution can be only implemented in economically viable manner for structures with features sizes bigger than 200 μm [250] due to the CNC machining process repeatability and reliabilities issues in regards to available cutter sizes, the wear or breakage of cutters, generation of defects and cracks due to mechanical stresses, and achievable aspect ratios [255, 256]. Another very important limitation of CNC micro-milling for the production of THz devices is the existence of waveguide cavities corner radius due to the size and shape of the cutting tools, which affects the geometrical accuracy of the produced waveguides and impairs their functionalities. At the same time, as the frequencies continue to increase (above 325 GHz) waveguide inner dimensions are getting even smaller, e.g. functional features in the order of 50 μm and less are required, which are clearly outside the capabilities of the CNC micro-milling process. Thus, in order to overcome aforementioned limitations of CNC micromachining, waveguides which operate at high frequencies, i.e. WR-2 (325-500 GHz), WR-1.5 (500-750 GHz) and WR-1 (750-1100 GHz), are also manufactured in a two-stage process chain, which combines electroforming and CNC milling [257]. However, an important limitation of such a process chain, which significantly increases the cost of fabrication and machining time, is the requirement for a sacrificial mandrel in the electroforming process that can be used only once [258].

7.1.3 LMM enabled fabrication of Terahertz technology devices

LMM is becoming a very attractive manufacturing technology for the fabrication of a wide range of micro-components and has some very appealing advantages over other micro machining processes (MMPs) as it was discussed in Chapter 2. Especially, LMM offers manufacturing capabilities that make it a very attractive solution for the fabrication of THz technology devices and thus to become an alternative route for their small to medium batch production. This can lead to significant reductions in production times and cost while it can also increase the accuracy of the THz devices due to the LMM capabilities to produce complex 3D structures without assembly operations in a single machining step. However, the

current application of LMM for the production of Terahertz devices has been only limited for the fabrication of various optical or quasi-optical components such as metal mesh filters [259]. In particular, literature review shows that the laser technology has not been utilized yet for the fabrication of submillimeter-wave waveguide components with the exception of one research that reports on the laser production of a 2 THz horn antenna cut from silicon [260]. The limited utilization of LMM for the manufacturing of THz devices can be explained mainly with their demanding ARR requirements that are difficult to achieve due to the process reliability and machine tool control issues in state-of-art LMM implementations (discussed in Chapter 2).

Compared with SU8 or silicon based processes used for the fabrication of waveguides, LMM has the following manufacturing advantages:

- It allows all functional features of the waveguide devices to be directly fabricated on metal (copper) substrates and thus to accommodate challenging application scenarios where a higher thermal stability of the devices is required;

- It is capable of producing 3D waveguide structures with varying depths (or heights) from one workpiece and thus eliminates the need for splitting the device into several layers and then assembling them with a high accuracy. This could yield an improved insertion loss and ultimately a better microwave performance.

- It is a ''direct write'' approach and thus has the capabilities to produce cost effectively small to medium batches of devices while it also offers a higher flexibility to introduce modification in the waveguide designs.

In addition, in comparison to CNC milling, LMM can achieve smaller feature sizes with similar and even greater dimensional and geometrical accuracy if system-level integration tools and techniques are incorporated in the laser systems to enhance their machine tool performance, as demonstrated in Chapters 5 and 6. Also, there is no tool-wear or machine vibration due to cutting forces, as LMM is a non-contact process.

7.2   Terahertz demonstrators design and manufacturing requirements

7.2.1   Design of the Terahertz devices

The LMM enabled process chain is validated on three industrially representative THz devices, which operate at different frequency bands at the high end of the electromagnetic spectrum, encompassing the frequency range from 75-325 GHz. In particular the three demonstrators are:

- Demonstrator 1 - Straight through waveguide section, shown in Figure 7.3;

- Demonstrator 2 – 4th order WR3-band waveguide (220-325 GHz), shown in Figure 7.4;

- Demonstrator 3 – 4th order W-band waveguide (75-110 GHz), shown in Figure 7.5.

Appendix 1 also provides detailed engineering drawings of the demonstrators. The three demonstrators were selected, because they fulfil the requirements of a microwave system for industrial applications where they are used to remove any interference by transmitting only certain band of frequencies and rejecting others. Some applications of such waveguide filters are THz transmitters and receivers in communications systems, measurement instruments and other applications which demand frequency selectivity. It can be seen from Figures 7.3, 7.4 and 7.5 that the three components consists of both functional structures that perform microwave filtering and alignment and fixing holes that are used for the precise mounting of the waveguide in a microwave system. The CAD model of the WR-3 waveguide through section is shown in Figure 7.3a. Its functional structure represents a rectangular 864 x 432 μm through hole that is located in the centre of a workpiece with a thickness of 800 μm. The positions of alignment and fixing holes together with their nominal dimensions are provided in Figure 7.3a, while the relative positions of the holes in respect to the centre of the component are also depicted in Figure 7.3b. It should be noted that since all three components were integrated to a standard self-aligning UG-387 flange (including pins and screws) for quick and reliable connections [261], their assembly holes are identical. The CAD model of the 4th order WR-3 band waveguide filter is shown in Figure 7.4 together with a close view of its functional feature on one side of the filter. In particular, the full waveguide device consists of two 432 μm deep functional features on the two opposite sides of the sample that are mirrored about the centre of the sample with an offset of 320 μm and 180 μm in x and y directions, respectively. These two functional features are connected via 50 μm deep rectangle hole as shown in Figure 7.4. The CAD model of the 4th order W waveguide filter is shown in Figure 7.5a. Figure 7.5b also depicts the air volume, which is confined by the complex geometrical design of the functional structure of the waveguide. In particular, the waveguide functional structure consist of two 1.27 mm deep symmetrical features on the two opposite sides of the workpiece, connected via 0.1 mm deep rectangular hole. The lateral nominal dimensions of the functional feature are provided in Figure 7.5c, which also shows the relative alignment between the two features on the workpiece.
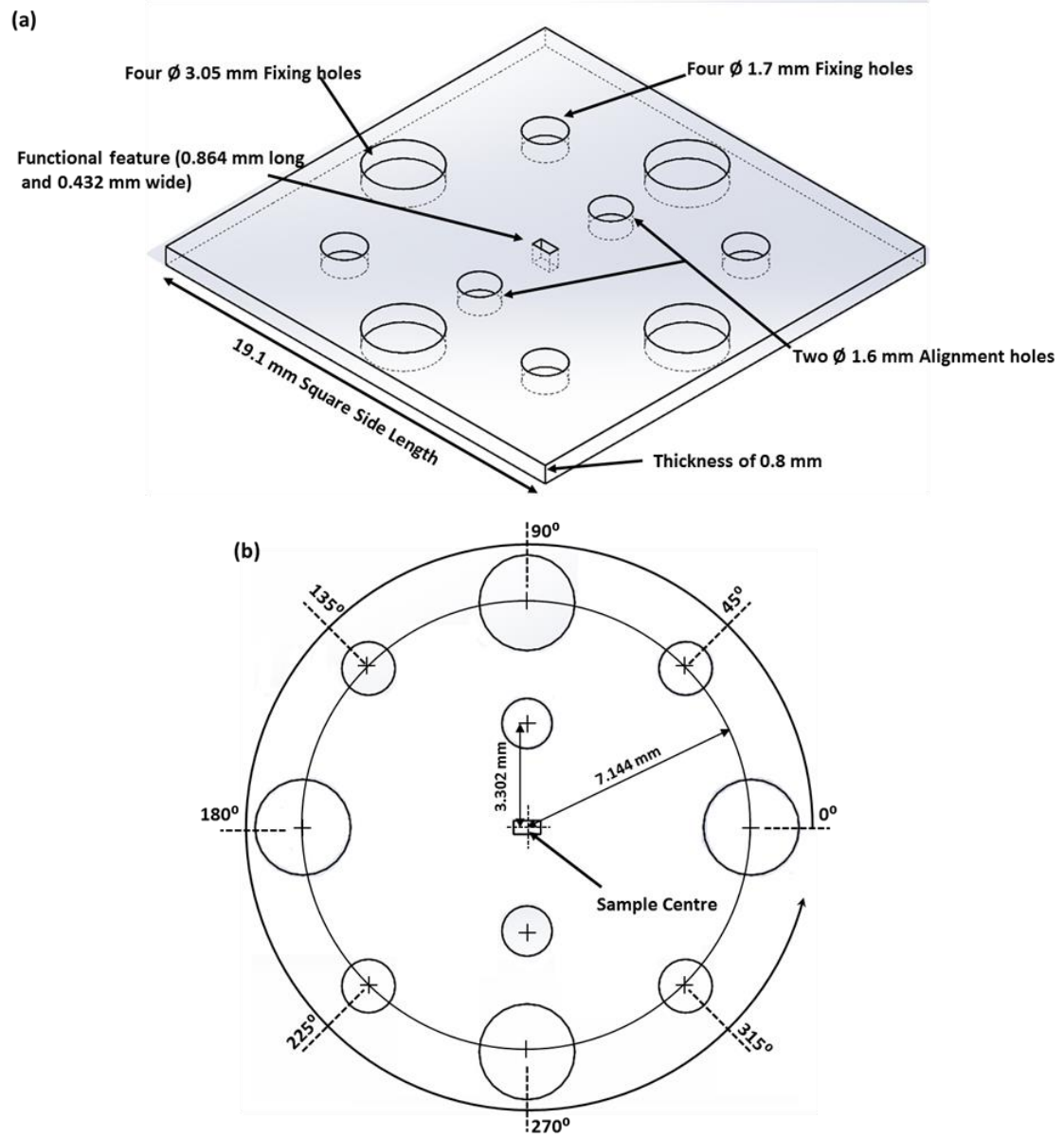
Figure 7.3 (a) The CAD model of the straight through waveguide section and (b) the relative positions of holes in respect to the centre of the sample
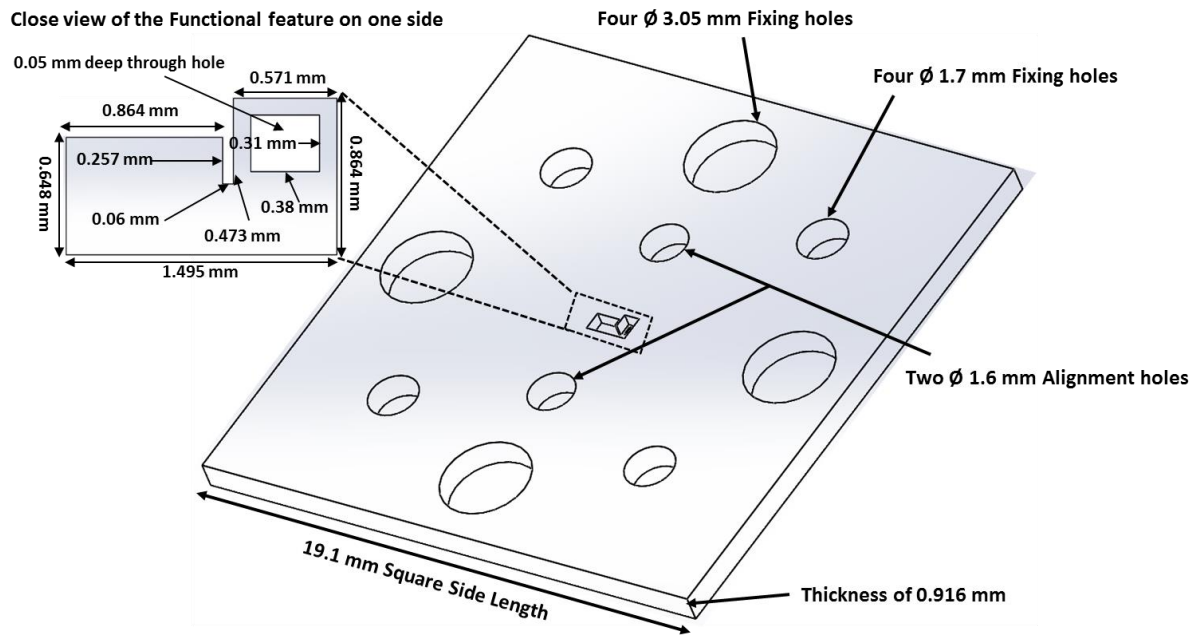
Figure 7.4 The CAD model of the 4th order WR3 waveguide filter that operates at the 220-350 GHz range of the electromagnetic spectrum
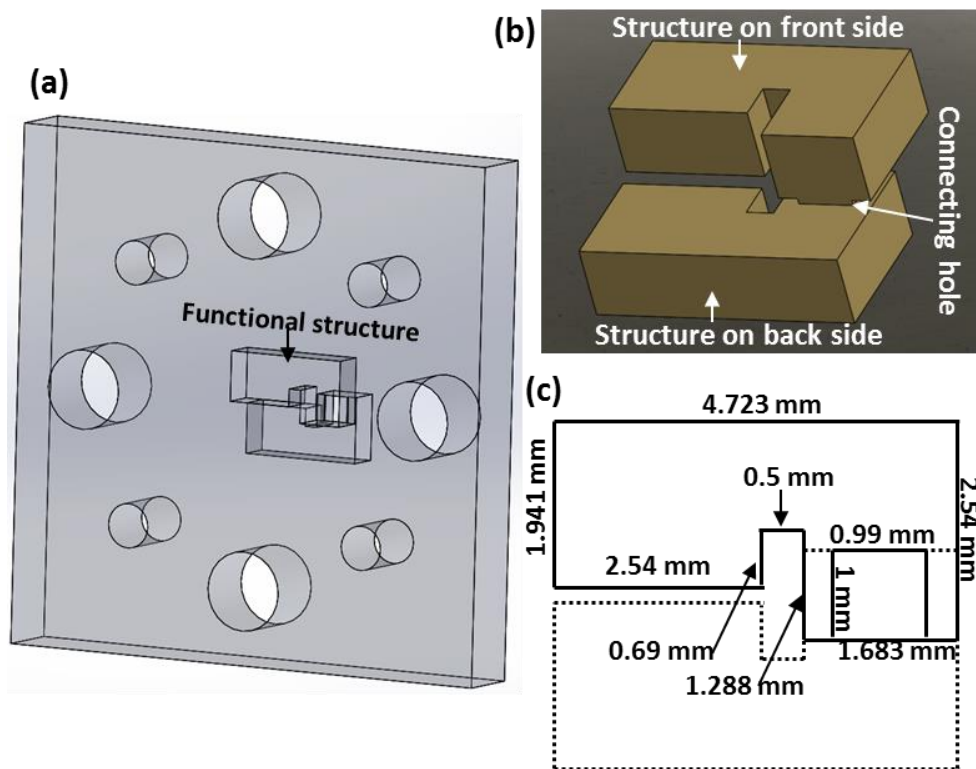
Figure 7.5 (a) The CAD model of the 4th order W-band waveguide filter that operates at the 75-110 GHz range of the electromagnetic spectrum; (b) Air volume of defined by the functional feature of the waveguide functional feature; (c) lateral nominal dimensions of the functional feature on one side of the component (solid black line) and relative position of the functional feature on the opposite side of the component (dotted black line)

7.2.2 Critical technical requirements of the THz devices

A clear understanding of THz devices' requirements is critical in designing and implementing a LMM enabled process chain for their scale-up manufacture. Therefore, it is necessary to study the effects of some key technical requirements, in particular the dimensional and geometrical accuracy and surface quality, on THz devices' performance, and thus to define them objectively, and also to design viable manufacturing solutions.

The effects of dimensional and alignment accuracy on THz devices' functional performance were modelled in an EM simulator [262]. The results showed that the tolerances should be within 10 µm of the calculated nominal dimensions. In addition, their performance depends greatly upon the joining quality between the THz device and the measurement setup. In particular, the flatness of copper workpieces used to produce the THz waveguides affects the interface quality and can lead to air gaps, and ultimately yields energy leakages. The carried our EM simulations showed that the flatness deviations of copper workpieces should not exceed 1 µm. All the EM simulations were carried out using CST Microwave Studio [262]. Also, the waveguides in this research were designed with vertical side walls and without any side wall taper angles. The carried out preliminary tests showed that the tolerance on the 90 degrees' side walls should not exceed 1 degree in order to avoid filtering performance deterioration, which is exemplified by significant operating frequency shift. Surface roughness is an important factor affecting the signal loss of THz waveguide components. The loss is due to scattering of electrons, and can be quantified analytically [246]. For the filter presented in this work, a surface roughness better than 1.5 µm is sufficient to fulfil the signal loss requirement of the final devices. Preliminary experimental tests, which were also carried out in order to empirically relate the machining results of produced waveguides with their microwave functionalities allowed the explicit determination of the manufacturing requirements for the successful fabrication of the waveguides and those requirements can be summarized as follows:

- Lateral (x-y plane) geometrical accuracy better than 10 µm;
- Vertical (z axis) accuracy better than 2 µm;
- Side wall taper angle deviation from vertical (90^0) less than 1^0 deviation;
- Waveguide cavities corner radius less than 15 µm;
- Surface roughness Sa better than 1.5 µm;

- Flatness better than 5 μm on an area of 5 mm x 5 mm surrounding the waveguide functional structures;

- Alignment accuracy between functional structures better than 10 μm.

Furthermore, based on the results from the preliminary experimental trials, in particular the characterization of resulting functionalities with specific waveguide dimensional and geometrical attributes, the physical trade-offs for the fabrication of this class of waveguide filters could be summarized as follows: geometrical deviations of the produced waveguides from their nominal designs are responsible for the overall shape, centre frequency and bandwidth of the transmitted terahertz signal curve, while surface roughness is responsible for the filter loss, i.e. the reduction of the terahertz signal at the output of the filter.

It should be noted that these requirements can be considered typical in designing THz waveguides and thus represent important design for manufacture considerations. At the same time, the actual requirements vary between THz designs and are determined based on their intrinsic performance specifications. Nevertheless, as the frequency of the waveguides increases, their performance sensitivity to dimensional and geometrical errors also increases and thus the manufacturing requirements are becoming even more demanding.

7.3 Process chain design and implementation

7.3.1 Critical limitations of LMM for the fabrication of THz devices

Since LMM is employed to machine the functional structures of the THz waveguide devices in the proposed process chain, it is important to consider any critical LMM limitations that can significantly impair the microwave functional performance of the THz demonstrators. In particular, taking into account such limitations, tools should be developed and implemented to minimize or in some cases even to eliminate their negative effects on the performance of the produced devices. Considering the key technical requirements discussed in Section 7.2.2, it is very important to address two main LMM inherent process-related limitations, the tapering of the THz waveguides' side walls and also machining ARR achievable with the LMM process. They are briefly discussed below in the following two sub-sections.

7.3.1.1 Side walls' tapering

The side walls' tapering in laser machined structures was observed by a number of researches when developing LMM solutions for different applications, e.g. the generation of preferentially oriented diamond micro-arrays for superabrasive grinding wheels [263],

manufacture of ceramic components for micro-surgical tools [101] and micro tool-making [264]. Important factors that contribute to the formation of side walls tapering include the used laser fluence (laser energy intensity), machining strategy, beam delivery optics, laser beam spatial geometrical characteristics and laser beam polarization [101, 265, 266]. Significant reductions of side wall's tapering had already been reported and it was achieved through the utilization of specialized machining routines and laser cutting heads for performing trepanning and helical drilling [265]. In particular, the use of micro-cutting head with a co-axial assist gas helps the debris removal from the laser-material interaction zone and thus to achieve structures with up to 20:1 aspect ratios [266]. However, an important disadvantage of those specialized machining routines is that they do not allow high dynamic beam deflectors to be utilised due to the restrictive size of the head nozzle tip, and therefore all relative beam-workpiece movements have to be performed with mechanical stages, which greatly reduces the machining throughput. In other recent studies, the use of optical helical drilling allowed holes with aspect ratio of more than 8:1 in different materials to be produced [267, 268]. Unfortunately, this technology can be applied only for reducing the taper angles in laser drilling and cutting operations and not in LMM of components with complex geometries such as THz waveguide structures. Therefore, it is necessary to develop and implement appropriate LMM routines for manufacturing micro structures with controlled side wall taper angles.

7.3.1.2 LMM accuracy, repeatability and reproducibility

Chapter 3 presented a comprehensive comparative study to quantify the machining ARR of state-of-art laser systems and the results from the study quantitatively identified substantial discrepancies in the manufacturing performances of the investigated systems in terms of their ARR capabilities. Thus, LMM platforms cannot be considered as robust machine tools in regards to their manufacturing predictability and reliability. Taking into account the technical requirements for the manufacture of THz devices that were introduced in Section 7.2.2 of this chapter, it is necessary to improve the LMM process reliability in order to allow the machining of waveguides with ARR better than 10 μm.

7.3.2 Process integration issues

The carried on literature review in Chapter 2 revealed that in the context of process chains that integrate LMM systems, critical interface requirements are the needs for accurate and precise repositioning and referencing of the workpiece in the different machine set-ups of the

process chain as this has a direct impact on the overall products' ARR. Thus, process integration issues should also be addressed in the implementation of the proposed process chain, because they contribute to the final ARR of the produced THz devices. In particular, the overall alignment of the functional structures of the waveguide in regards to the assembly holes is determined by the accuracy of the waveguide registering routines in the LMM system prior to the laser manufacturing operations. Thus, the design and implementation of the process chain should incorporate adequate tools and techniques for precise repositioning and alignment of workpieces in the different processing steps of the proposed chain in order to ensure that the alignment accuracy between the functional structures of the filters is better than 10 μm.

7.3.3 Manufacturing platform design

Taking into account the technical requirements outlined in Section 7.2.2 and the issues related both to LMM (Section 7.3.1) and the integration of machining technologies into multi-process manufacturing platforms (Section 7.3.2), the following generic considerations were identified as critical when designing and implementing laser-based manufacturing solutions for the fabrication of THz devices:

- High ARR achievable in registering workpieces in different machining setups;

- A modular workpiece holding device with capabilities to support different machining configurations for the fabrication of devices with different designs, e.g. structuring on one, two and three sides of the workpiece;

- Minimising/eliminating the influence of workpiece's imperfections, e.g. edge definition and surface integrity, when implementing alignment routines for the constituent machining setups;

- Minimising the influence of the human factor and the need to use experienced operators in conducting the repositioning and alignment routines;

- Capabilities to perform non-contact registering of workpieces and also without the need for pre-existing reference marks in the different machining setups;

- Capabilities to realize complex two-side LMM without the need for manual repositioning the workpieces;

- Capabilities to control the side walls' tapering of laser machined structures.

The generic tools and techniques, described in Chapters 5 and 6, were employed to address these critical manufacturing requirements and thus to achieve the required level of machining ARR in producing THz devices.

The proposed multi-process manufacturing route for the scale up production of THz devices is presented in Figure 7.6a, while Figure 7.6b also provides a detailed graphical description of all processing step. In Step 1, the fabrication process starts with the mounting of a copper bar into a CNC turning system where the machining of meso-scale features of the THz device, e.g. alignment and fixing holes, are carried out together with the parting-off of the workpiece to the desired thickness. In Step 2, the cut-off workpiece is fixed onto the interface plate of a pallet (modular workpiece holding system described in Chapter 5) that is then placed under a FV probe to register the CNC machined alignment holes produced in Step 3. This is done by utilizing the automated workpiece setting up routine (described in Chapter 5) and thus to establish a physical link between the FV and LMM systems with the use of the modular workpiece holding device. In this way, their coordinate systems, FCS and MCS, are correlated with a repeatability better then +/- 1 µm (refer to results from Chapter 4) into the single coordinate system of the holding device (HCS) as shown in Figure 7.6b. Through the use of the FV probe the geometrical correlation of the workpiece coordinate system (WCS) to HCS is established automatically and thus a link of WCS to MCS. In Steps 4 and 5 of the proposed manufacturing route, the THz waveguide structures on the two opposite sides of the workpiece are produced by the LMM in one machining setup. In particular, once the structure is produced on one side of the workpiece (Step 4), the rotary stage is used to rotate the sample with 180^0 and machine the second functional structure on the opposite side of the workpiece (Step 5). These two LMM operations are carried out in a one-setup machining operation by utilizing the automated strategy for multi-axis LMM (described in Chapter 6) and thus to achieve a machining ARR better than +/- 6.5 µm [28]. Then, the functional features of the THz devices are inspected with the FV probe and compared with the CAD model (Step 6). If there are any deviations further machining is carried out by executing a "rest volume" operation based on the difference between the actual and the CAD data and thus to achieve the required geometrical accuracy of the produced functional features, i.e. to produce side walls with tapering angle less than +/- 1^0. Such further laser processing operations for minimising any deviations from the CAD model require additional rotations of the workpiece

employing rotary stages that again are performed with the automated strategy for multi-axis LMM (presented in Chapter 6).

It should be noted here that since LMM is a subtractive process, any improvements of the geometrical ARR are possible only if the dimensions of the components are smaller than their nominal values after the first LMM operation. Therefore, an optimization of laser parameters to provide repeatable laser machining results was critical and thus to reduce the number of sub-standard parts. Such detailed analyses of LMM manufacturing results in terms of ARR have already been performed in Chapters 4, 5 and 6. Therefore, taking into account these results, all dimensions were modified (reduced with a scaling factor that takes into account the achievable LMM ARR) to produce the structures always as desired as or smaller than designed and thus to reduce the number of rejects. Finally, quality assurance techniques that were employed at the end of the manufacturing process included detailed inspection of the produced devices to evaluate the conformity with their technical specifications and geometrical tolerances. Then, the THz devices are dismounted from the interface plate of the modular workpiece holding device for functional performance evaluation tests.
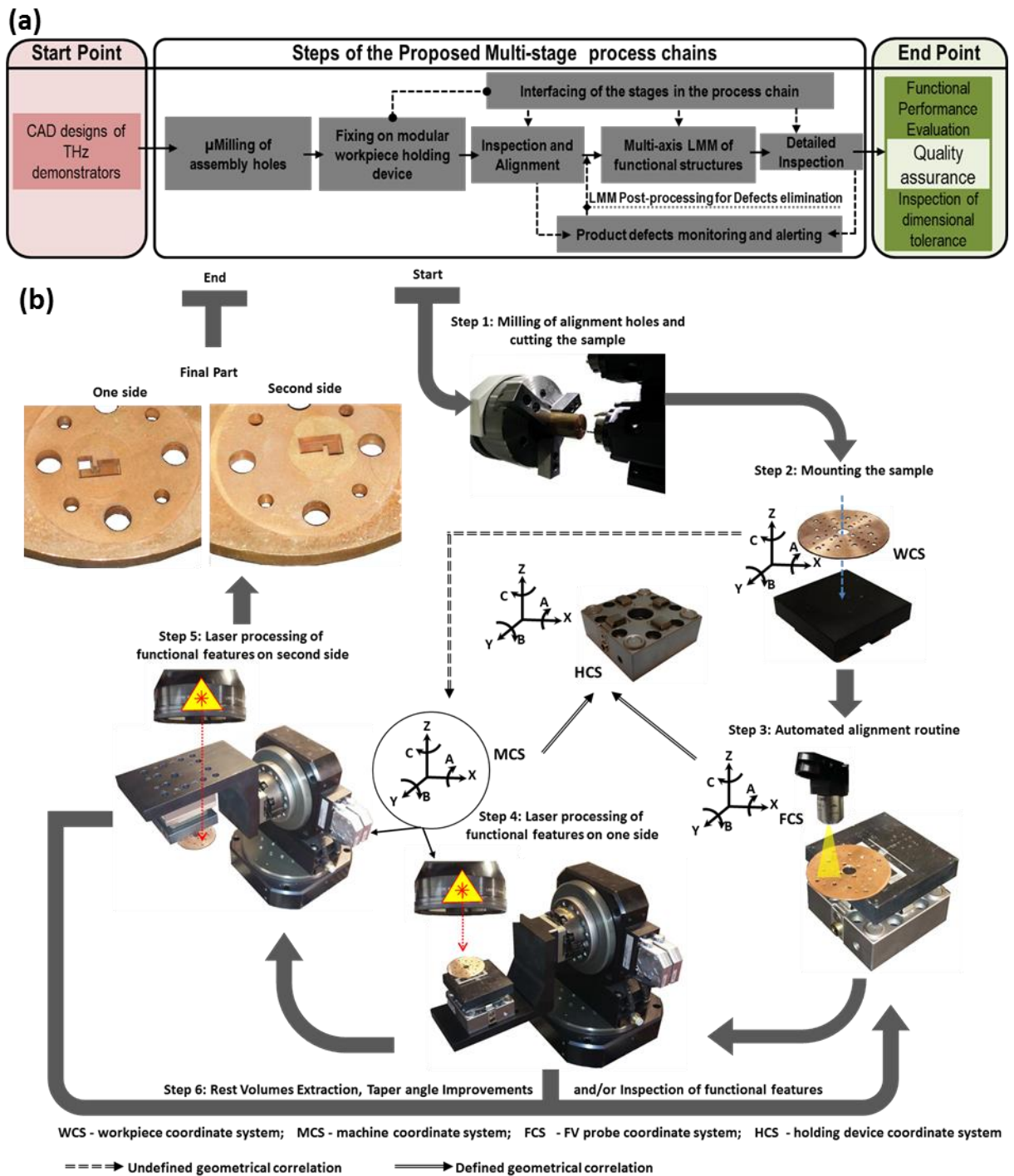
Figure 7.6 (a) Overview of the proposed process chain and (b) Detailed graphical description of the steps in the proposed multi-process manufacturing route for producing THz devices

7.4 Experimental validation

7.4.1 Material

The material used in the experiment validation tests is a special grade of copper bars (Cu99.55S0.45) with a diameter of 50 mm that are commonly used for producing EDM

electrodes. This material was selected due to its improved machinability and thus to achieve the required surface finish during the milling, drilling or turning operations in the first step of the proposed multi-process manufacturing route. Furthermore, the material was also selected due to its excellent electrical conductivity of 58.5 X 10.E6 Siemens/m, which is of critical importance for the functional integrity of the THz technological devices.

7.4.2 Equipment

The CNC precision turning machine that was used in this research was Mazak Quick Turn Smart 200M with a driven tool turret. The maximum rotational speed of the main spindle is 5000 RPM, while the maximum rotational speed of the driven head is 6000 RPM.

The LMM system used in the pilot implementation of the proposed manufacturing platform is described in details in Chapter 3. Experimental tests were conducted employing the Yb-doped sub-pico 5 W laser sources from Amplitude Systemes.

The FV Alicona G5 system, described in Chapter 3, was employed for performing the inspection of the produced components.

The functional performance of produced WR-3 band THz (220-325 GHz frequency range) devices was evaluated by carrying out measurements on Agilent E8361A Network Analyzer with a pair of OML WR-3 extensions (T/R module at test port 1 and a receive-only T module at test port 2), as shown in Figure 7.7. An enhanced calibration, which is effectively a one-port calibration combined with a through calibration, was performed before taking any measurements on the filter performance. During the calibration, the WR-3 waveguide calibration kit (produced by OML Inc) was utilised to accurately calibrate the Network Analyzer to achieve precise S-parameters of the filter. For the measurements, the THz filter is sandwiched between flanges of two test ports. Two alignment pins are carefully pushed through the waveguide filter and the flanges alignment holes to reduce any misalignment between them. Screws attached to the flanges also go through the waveguide device and into the thread holes of the opposite flange to secure the required good connections.

The functional performance of produced W-band THz devices was again evaluated by carrying out measurements on Agilent E8361A Network Analyzer, but the Port 1 and Port 2 were changed to deliver THz signal with a frequency range of 75-100 GHz due to the different operating frequency of the W-band waveguide filters. Figure 7.8 depicts a representative measurement of a W-band filter.
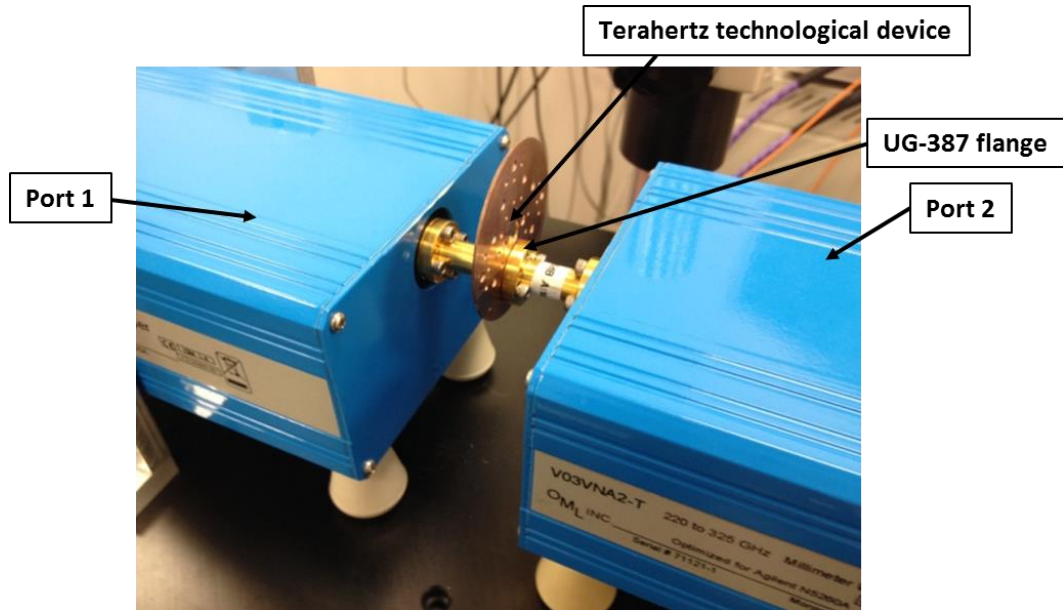
Figure 7.7 The setup used to analyse the performance of WR-3 band THz devices
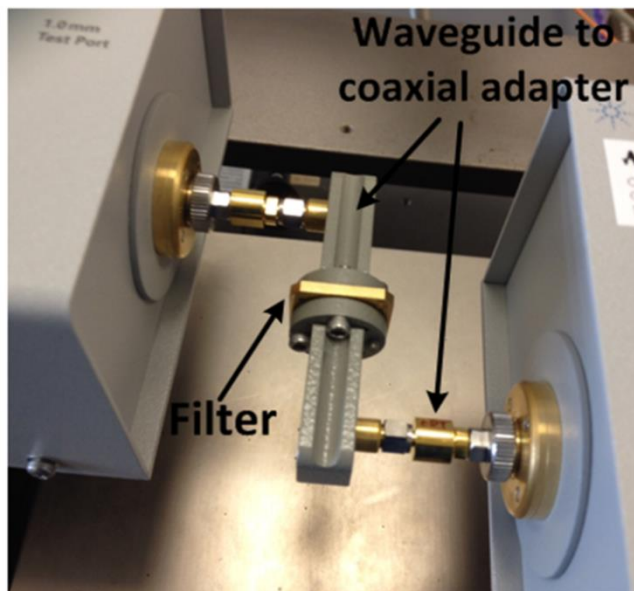
Figure 7.8 The setup used to analyse the performance of W-band THz devices

7.4.3 Planning of validation manufacturing trials

7.4.3.1 WR3-band Straight through waveguide section

The CAD model of WR-3 waveguide straight through section was already introduced in Figure 7.3. The alignment holes were initially machined with self-centred carbide drills and then reamed to produce them with required quality on the CNC turning machine. Then, two laser machining strategies were employed to produce the functional features of the waveguide section. In particular, the through rectangular hole was machined from one side and also from

two opposite sides of the workpiece by employing the rotary stage and thus to compare the capabilities of the two machining approaches. The positional accuracy of the rectangular hole on the two sides of the workpiece was assessed by measuring its deviation in regards to the workpiece's centre while its reproducibility by conducting these measurements on two samples. The centre of the workpiece is calculated by using as references the centres of alignment and fixing holes. The dimensional accuracy of the produced waveguide section was evaluated by analysing the deviations of the actual dimensions from their nominal values. The side walls' tapering of the machined structures was also analysed to determine the level of taper angle formation control that could be achieved when multi-axis LMM with rotary stages was employed. Finally, the functional performance of the waveguide calibration artefact was also assessed.

7.4.3.2 W-band and WR3-band waveguides

The CAD models of WR3-band and W-band filters have been provided in Figure 7.4 and 7.5, respectively. Functional tests of the produced waveguide filters were conducted to assess their microwave functional performance. The dimensional and geometrical accuracy of the filters were also analysed and thus to judge better to what extend their technical requirements were met. The time required for carrying out each machining/inspection step of the proposed manufacturing process chain was recorded in order to assess its throughput capabilities for serial production of THz devices. Finally, 20 waveguide filters both for the WR3 and the W frequency bands were produced and the machining results in regards to the manufacturing requirements (see Section 7.2.2) were analysed in order to assess the part-to-part variations and thus to judge about the reproducibility of the proposed process chain.

7.4.3.3 LMM process settings optimization

The selection of laser machining process parameters was critical for addressing the waveguides manufacturing requirements, which have been defined in Section 7.2.2. Prior to the experimental optimisation of machining parameters, in-depth literature review of reported work on laser processing of copper with ultrafast laser sources was carried out. As a result of this review, the laser parameters with a significant influence on manufacturing results were identified, especially on machining efficiency (ablation rates), surface quality and geometrical accuracy (side wall taper angle formation) [269-273]. Even though the processing with sub-picosecond lasers is characterized with almost negligible heat- and shock-affected zones [274] due to its photochemical processing nature (discussed in details in Chapter 2), laser

processing with high pulse repetition rates, i.e. several hundreds of kilohertz, can lead to heat accumulation and surface temperature rise in the workpiece. This is due to the insufficient time between the impinging pulses to evacuate the heat from the laser-material interaction zone [270]. Such incubation effects can result in a reduction of material ablation threshold and thus to increase material removal rates, but in expense of machining quality, an increased heat-affected area and higher surface roughness [269-274]. Even though particles and /or plasma shielding effects can occur at high laser pulse frequencies, their adverse effects on material removal rates are overbalanced by the heat incubation effects [275]. Also, it is reported by other researchers that heat accumulation and particle shielding effects have only a marginal impact in laser processing of copper, due to its high thermal conductivity and thermal diffusivity, and therefore the frequency increase has a negligible impact on the copper removal rates [276]. Thus, it can be expected that the highest machining efficiency could be obtained by utilizing the maximum pulse energy and pulse repetition rate of the employed laser source.

Taking into account the considerations above, the laser parameter settings were optimised in order to identify a favourable processing window to fulfil the THz waveguides manufacturing requirements, defined in Section 7.2.2. The following laser parameters were optimised in the experimental trials: laser pulse energy, machining strategy (pulse distance, hatch distance, hatch angle between laser machining layers), laser beam polarization and beam spot diameter. In order to evaluate the effects of the laser parameters on a resulting material response, i.e. material removal rates (MRR), surface roughness and taper angle formation, a full factorial Design of Experiments (DoE) was performed. Initial screening tests were firstly performed in order to identify the ranges for laser parameter settings in the DoE optimization trials. Table 7-1 lists the number of levels and their corresponding settings for each of the investigated laser parameters in the DOE optimization tests.

Table 7-1 Number of laser parameters levels and their corresponding value settings in the full-factorial DoE for the final laser parameters optimization tests

Laser parameter	Units	Number of Levels	Level value settings		
Laser Pulse Energy	μJ	3	7.5	5.4	3.2
Beam spot diameter	μm	2	30		60
Polarization state	-	3	p-type	s-type	Circular
Hatching strategy	-	2	One-directional		Random

Figure 7.10 depicts the significant dependences that were observed between machining results and laser parameter settings in regards to material removal rates and surface integrity. It can be seen in Figure 7.10 that by increasing the beam spot diameter from 30 μm to 60 μm, it was possible to improve the resulting surface roughness from Sa= 0.96 to Sa=0.54 μm without sacrificing the material removal rates (MRR) obtained at the maximum pulse energy.
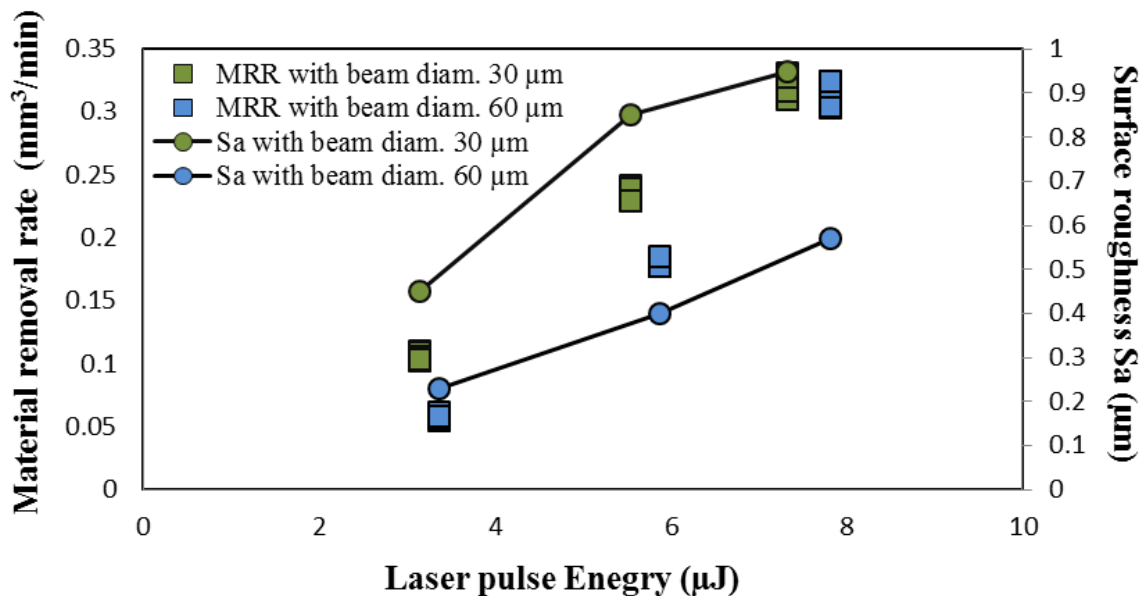
Figure 7.9 Dependences of material removal rates and surface integrity on laser pulse energy and laser beam spot diameter

There are some other important observations about the dependences of machining results on laser parameter settings and they are as follows:

- Laser beam polarisation affects the resulting side wall taper angle formation. Uniform taper angle of 9.5^0 was obtained on all side walls of the laser machined structure with circular laser beam polarization, while the results from the experimental trials with p-type and s-type linear polarizations led to non-symmetrical taper angles, i.e. the angle at the side walls perpendicular to the laser machining vectors was different from the one obtained at the side walls parallel to the vectors. Similar observations are also reported in [101].

- Side wall taper angle decreases with the increase of laser pulse energy.

- Surface roughness could be improved by employing random hatch angle when machining the sequence of layers instead of employing one-directional hatch angle machining

strategy. This is due to uniform irradiation of the laser machined areas that can be achieved with the random hatch angle machining strategy as reported in [16], too.

The optimised laser parameter settings used to produce the THz devices in this research are provided in Table 7-2. The achieved material removal rate, surface roughness (Sa) and side wall taper angle are 0.31 mm^3/min, Sa=0. 75 µm and 9.5^0, respectively.

Table 7-2 Optimized laser parameters for the machining of THz devices

Laser parameter	Units	Value
Power	W	4.2
Frequency	kHz	500
Scanning Speed	m/s	2
Pulse duration	fs	310
Beam diameter	µm	60
Hatch style	-	Random
Hatch Pitch	µm	4
Polarization state	-	Circular

7.5   Results and Discussions

7.5.1   WR3-band Straight through waveguide section

Figure 7.10 shows a representative overview of the samples after drilling of alignment and fixing holes and prior to the laser machining of the functional features of the waveguides. Figure 7.10a provides the dimensions of both fixing and alignment holes. Furthermore, 3D representations of one alignment hole and its measurements are provided in Figures 7.10b and 7.10c, respectively. The holes' diameters were inspected using the Automatic Circle tool of the Alicona G5 2DImageMerasurment module due to the high accuracy and repeatability required in the measurements. Alignment holes' diameters of ten samples were analysed and the results showed that the dimensional accuracy and repeatability achieved with the used drilling sequence were better than 2 µm. The total measurement uncertainty at the 95% confidence level is calculated to be 0.2 µm (based on the uncertainty procedure provided in Chapter 3).
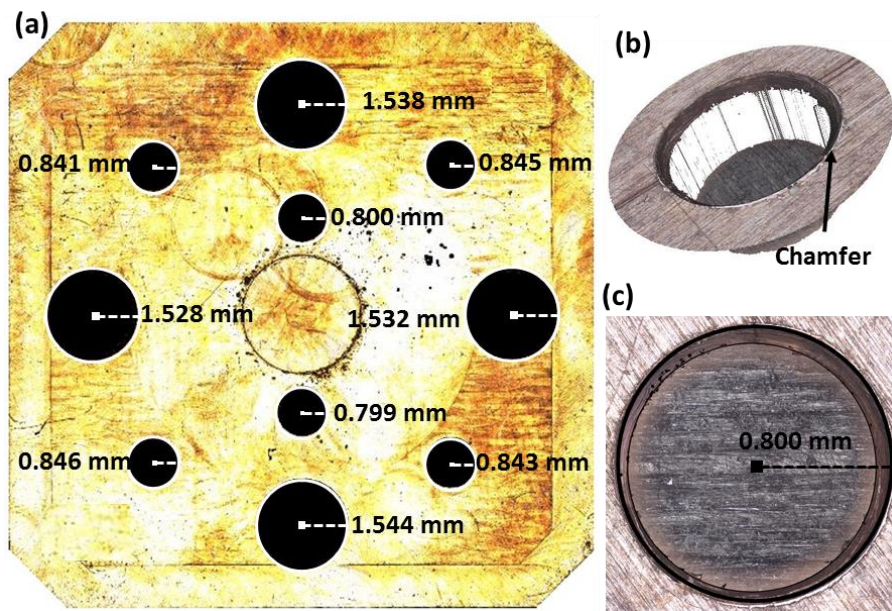
Figure 7.10 A representative sample with drilled alignment and fixing holes prior to the laser machining of the waveguide functional structure: (a) top view of the sample with dimensions of drilled alignment and fixing holes, (b) 3D view of one alignment hole and (c) top view of the alignment hole from (b) with its dimensions

Figures 7.11a and 7.12a and Figures 7.11b and 7.12b show the entrance and exit of the waveguides rectangle holes produced with one- and two- side machining strategies, respectively. The positional and dimensional accuracy of the waveguide feature achieved in the one-side machining is better than 7 μm and 5 μm, respectively, based on the measurement results in Figure 7.11a. However, it can be seen in Figure 7.11b that the edge definition and the machining quality of the rectangular hole exit is not satisfactory. The deterioration of the hole quality at the exit could be mainly attributed to the polarization state of the laser beam, in particular the dependency of material absorption on the laser processing direction. Similar observations at the exit of through structures were reported by other researchers and again they were attributed mainly to the beam polarization [277]. Figure 7.11c depicts the side wall of the waveguide structure, while Figure 7.11d shows the depth profile of the side wall at the specified location from Figure 7.11c. It is evident in Figure 7.11d that the structure side wall is nearly vertical, i.e. the tapering angle is 90.13^{0}.
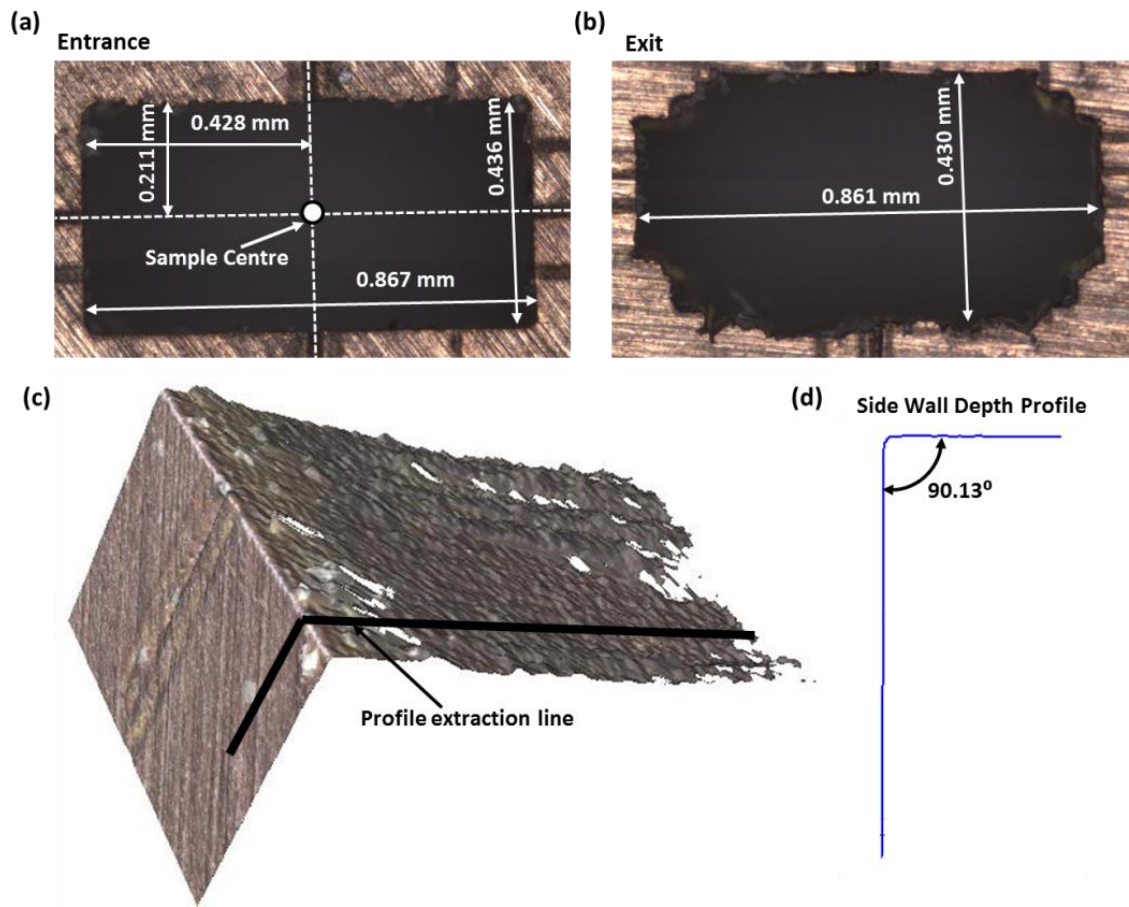
Figure 7.11 WR-3 straight through waveguide section produced with one-side machining strategy: top view of the rectangular through hole at its entrance (a) and at its exit (b), (c) 3D view of side wall after tapering angle improvements and (d) the side wall depth profile at the specified location in (c)

Measurement results in Figure 7.12a and 7.12b depict the accuracy and repeatability achieved with the two-side machining that is better than 10 μm. Furthermore, the quality of the rectangular hole exit is significantly improved in comparison to the machining results achieved with the one-side laser machining approach (compare Figures 7.11b and 7.12b). The positional accuracy of the waveguide feature is better than 5 μm as it can be judged from the measurement results in Figure 7.12a and thus a high machining accuracy can be achieved also by carrying out a multi-axis LMM with the rotary stages. In addition, Figure 7.12c depicts the side wall of the waveguide structure that does not show any misalignment, visible stitching errors, between the two halves of the waveguide structure produced from the two opposite sides of the workpiece, respectively. Finally, it can be seen in Figure 7.12d that the structure side walls are nearly vertical, i.e. the tapering angle is 90.53^0. This confirms again the LMM

164

capabilities and also of the proposed manufacturing process chain for producing THz waveguide structures with nearly vertical side walls.
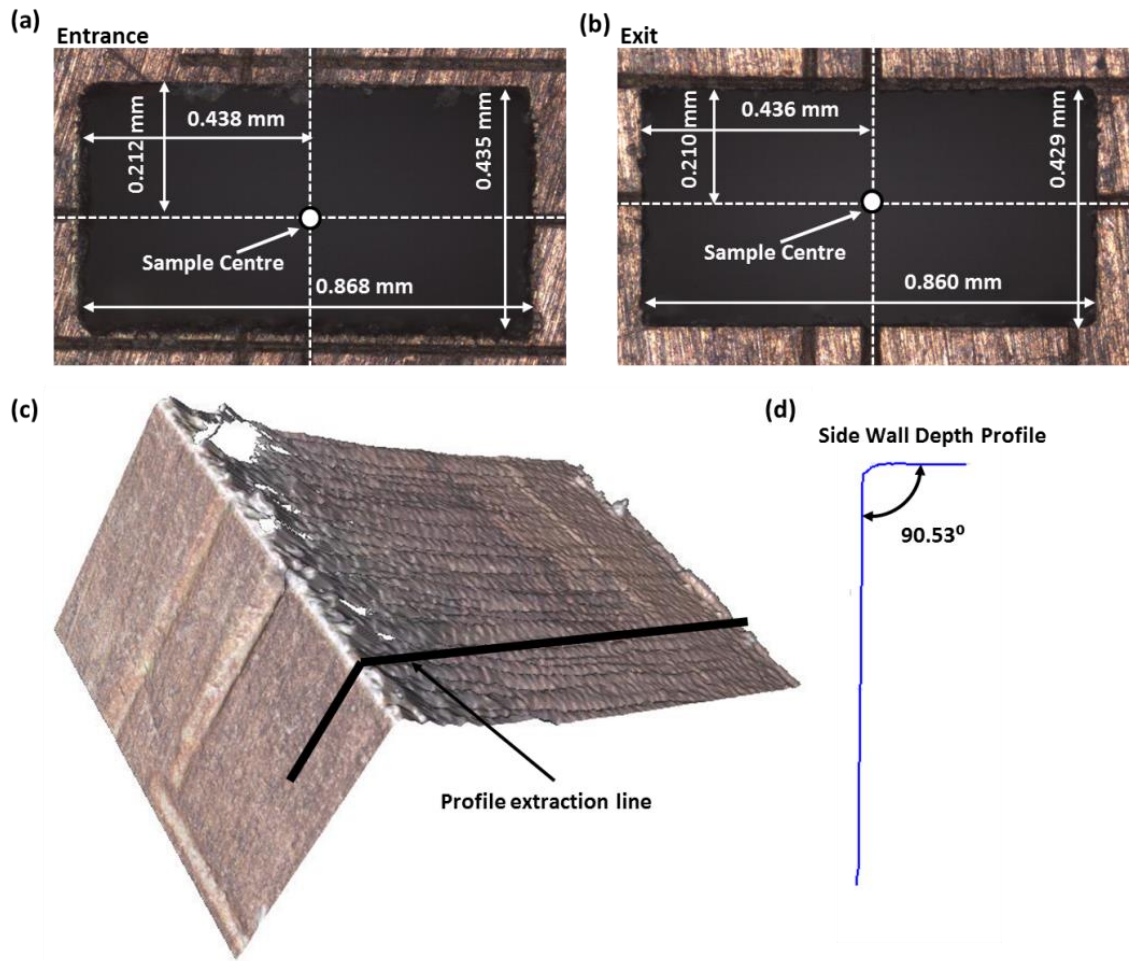
Figure 7.12 WR-3 straight through waveguide section produced with two-side machining strategy: top view of rectangular through hole at its entrance(a) and at (b) exit side of the sample, (c) 3D view of side wall after taper angle improvements and (d) extracted side wall depth profile at the specified location in (c)
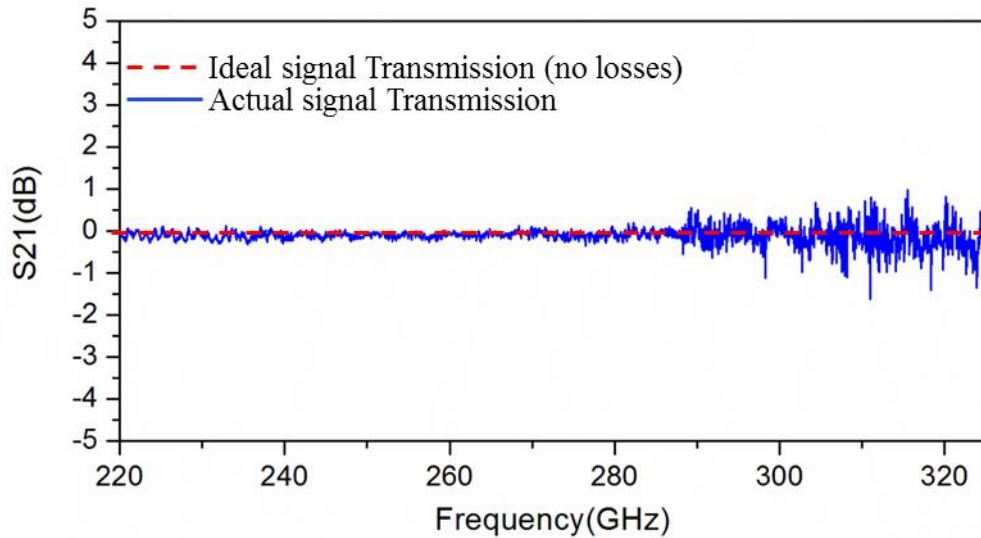
Figure 7.13 . Measured transmission responses of the WR-3 straight through waveguide section produced employing two-side laser machining strategy

S-parameters (scattering parameters) that can be acquired directly from microwave measurements are usually utilised to assess the microwave functional performance characteristics of a waveguide device. In its broadest definition, S-parameters describe the response of an N-port network to voltage signals at each port [241-251]. Detailed explanations for the S-parameters could be found in [241-251]. For a waveguide device with two ports, Ports 1 and 2, S21 is the transmission coefficient of the device from Port 1 to Port 2 and it is usually measured in decibels (dB). Other commonly used S-parameter is the S11, which quantifies the return loss at a signal port [241-251]. More specifically S11 refers to the ratio of signal that reflects from one port for a signal incident on the same port [241-251]. As a straight through waveguide is used to evaluate the capabilities of the proposed manufacturing route, the whole frequency band is expected to be fully transmitted from Port 1 to Port 2, i.e. S21 should be close to 100% or 0 dB. Whereas, only frequencies in the passband are transmitted for a filter and the other frequencies are partially or fully reflected by the device. Figure 7.13 shows the results from the performance evaluation tests obtained for the WR-3 waveguide through section produced using the two-side laser machining strategy, where it can be seen that the average insertion loss is 0.15 dB (0.188 dB/mm).

7.5.2   WR3-band Waveguide filter

Figure 7.14a presents the measurement results of the WR3-band filter functional features on one side of the workpiece. By comparing the measurements with the nominal dimensions in

Figure 7.4 it can be stated that the machining accuracy is better than 5μm. The nearly vertical side walls of the waveguide structure are shown in Figure 7.14b that also depicts the machining quality achieved with the LMM operation. It can be seen in Figure 7.14c that the resulting side wall tapering angle is 90.31^0, which is within the technical requirements for THz devices defined in Section 7.2.2. Once more, the results in Figure 7.15 confirm the capability demonstrated in the LMM-enabled manufacturing of the straight through waveguide section in Section 7.5.1 above. Figure 7.15 also provides measurement results for other machining results, which have been identified as critical for the functional performance of the waveguide in Section 7.2.2. In particular, Figure 7.15a shows the surface roughness (Sa) measurement, Sa = 0.86 μm, of the bottom surface of the waveguide that is within the specified requirement of Sa of less than 1.5 μm. Furthermore, Figure 7.15b depicts a high magnification view of the waveguide bottom surface, where high spatial frequency features such as laser induced periodic self-organized structures (LIPSS) or ripples and micro-holes can be observed. The LIPSS periodicity and orientation are related to the wavelength of the laser source and the beam polarization state, respectively, and are also reported in other detailed investigations into the LIPSS formation mechanisms [32, 55, 56]. In particular, the LIPSS periodicity is ~500nm (half-wavelength of the employed laser source), while their orientation is at 45^0 to the laser beam tracks. Figure 7.15c provides a representative view of one of the corners of the waveguide cavity, where it can be clearly seen that the corner radius of the laser machined filter meets the requirement stated in Section 7.2.2, i.e. the corner radius should be less than 15 μm. Since, the corner radius is determined by the beam spot size at the focal plane, further improvements can be easily achieved by further reductions in the beam spot size. However, such improvements would come in the expense of a reduced machining throughput. It should be noted that such waveguide cavity corner radiuses could not be achieved with conventional micro-milling operations due to cutting tools shape and size limitations and thus this outlines the necessity to employ the LMM for the production of the functional structures of the WR3-band waveguide filter. Table 7-3 also provides information about the machining efficiency of the proposed multi-process manufacturing platform. In particular, the time required for each of fabrication steps was recorded and thus to calculate the overall machining time for the production of one WR3-band waveguide filter. As it can be seen in Table 7-3 the machining time was estimated to be 43 min per one WR3-band filter, which demonstrates the attractiveness of the proposed manufacturing platform for producing

small to medium batches of THz devices. It is worth stressing that this unit manufacturing time includes 100% inspection of produced THz devices. Finally, reproducibility of the proposed process chain is better than 5 μm based on the carried out analyses of the 20 laser machined WR3-band waveguides. Appendix 7 exemplifies detailed measurement results for five of the produced WR3-band waveguide filters.

Table 7-3 The processing times associated with different steps of the proposed manufacturing route

Process chain fabrication step	Time (min)
Drilling of alignment/ fixing holes	10
Fixing a cut-off workpiece on a pallet	2
Automated alignment of cut-off workpiece	3
First laser machining operation (all functional features)	10
Part inspection and rest volumes calculation	7
LMM of rest volumes (tapering angle improvements)	4
Final inspection	7
Total fabrication time per waveguide filter	**43**
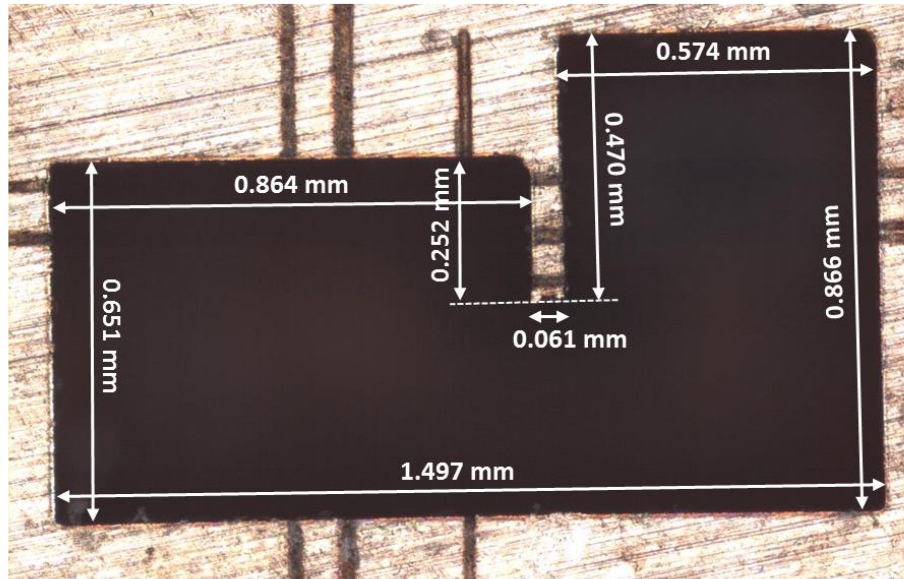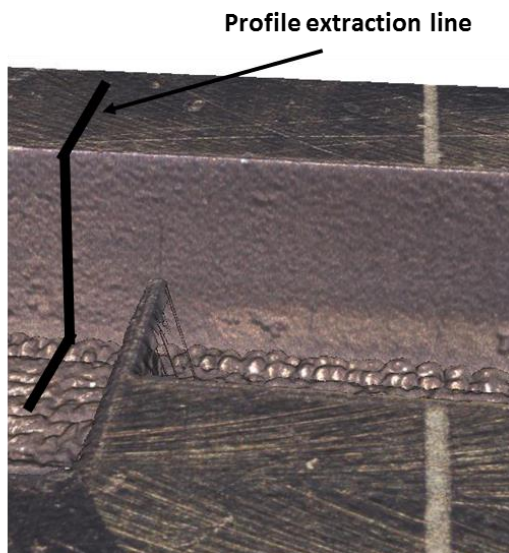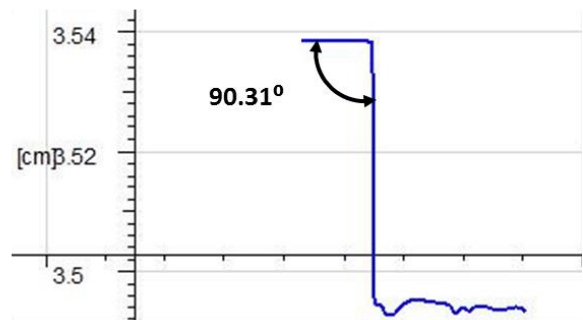
Figure 7.14 A representative laser machined WR3-band waveguide filter: (a) top view with dimensions, (b) 3D view of one side wall and (c) the side wall depth profile at the specified location in (b)
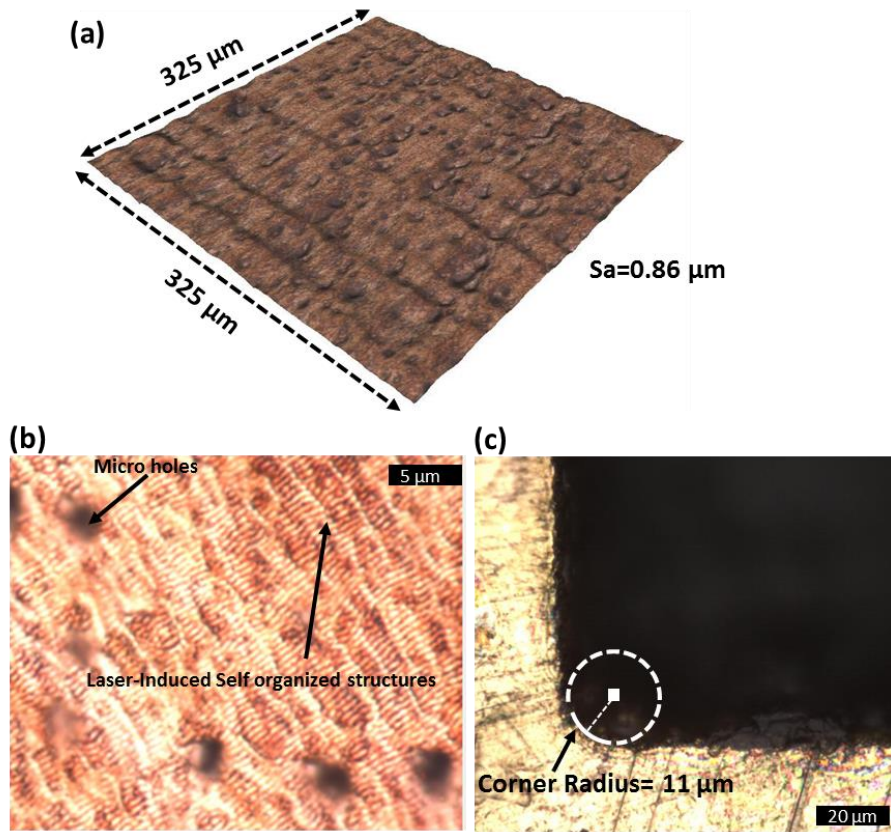
Figure 7.15 Machining results of the produced WR3-band waveguide filter in terms of: (a) Surface roughness (Sa) measurement at the bottom of the produced waveguide, (b) high magnification view of the surface topography at the bottom surface of the waveguide and (c) corner radius measurement
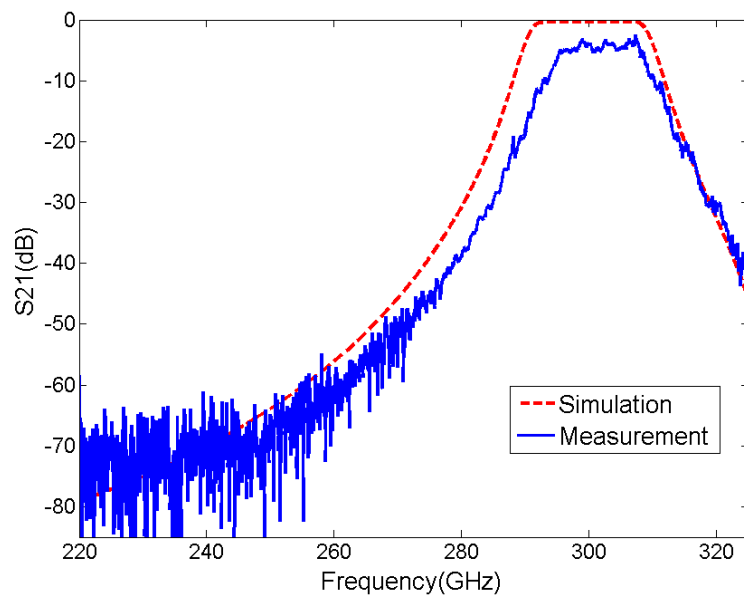
Figure 7.16 Results from the performance evaluation tests of the WR3- band waveguide filter

Figure 7.16 shows the measurement results from the filter performance evaluation tests. The measured average passband insertion loss is around 4.5 dB, which is 4.2 dB higher than the expected value, i.e. 0.3 dB based on the simulation using the copper conductivity. The centre frequency shifts upwards by around 3 GHz (1%) and the bandwidth is narrower in comparison with simulations. This may be attributed to the tapering angle that makes the resonators and coupling slots smaller than designed.

The measured results are in a good agreement with simulations. The insertion loss deviation can be explained mainly with the copper disk flatness. According to simulations carried out with the EM software, a 5 μm air gap at each of two interfaces between filter and measurement equipment contributes to around 3.5 dB additional loss. To reduce this loss that is due to energy leakages, a diamond fly cutting process can be utilised to improve the flatness of the copper workpieces prior to the laser machining operations. THz designs which may tolerate small air gaps at the interface could also be explored to lower the tight requirements on copper workpieces' flatness. Finally, Table 7-4 summarizes the manufacturing capabilities of the proposed process chain in comparison to photoresist-based micro-manufacturing techniques and thus to judge better about the advantages of the proposed process chain for producing THz waveguide filters.

Table 7-4 Comparative analysis of the manufacturing capabilities of the proposed process chain and photoresist-based micro-manufacturing techniques

Manufacturing technology	Photo-resist based [246-249]	Proposed process chain
Geometrical complexity	2D	3D
Requirements for secondary processes	Masks production; Coating	No
Assembly	Required	No
Material Selection	Photoresists	No limitations
Vulnerability to design changes	High	Low
Environmental Impact	Use of chemicals	No
Process chain integration flexibility	Low	High

The qualitative comparative analyses, presented in Table 7-4, clearly demonstrate the manufacturing advantages of the proposed laser-based process chain in comparison to the photo-resist based technologies. It is worth stressing the high flexibility of the proposed process chain to produce various 3D geometries that incorporate different scales' functional features. In contrast, the photo-resist based technologies are considerably more vulnerable and

capital intensive to waveguide design changes, because masks have to be produced for different waveguide designs.

7.5.3 W-band waveguide filter

Figure 7.17a shows a photograph of the produced W-band waveguide, where it can be seen that the overall size of the produced component is similar to a 1-pound coin. Figure 7.17b provides detailed dimensional measurement results of the W-band filter functional features on one side of the component. Comparing the actual dimensions of the functional features with the nominal dimensions in Figure 7.5 reveals that the machining accuracy is better than 5 μm. In addition, the nearly Figure 7.17b shows a 3D view of the produced device, exemplifying the smallest functional feature of the THz device. Figure 7.17c quantifies the resulting side wall tapering angle and it is equal to 90.31^0, which provides further evidence of the capabilities of the LMM for obtaining nearly vertical side walls of the waveguide cavities. Measurements of the produced 20 W-band waveguides reveal that the machining repeatability and reproducibility is better than 5 μm. Appendix 7 exemplifies detailed measurement results for five of the produced W-band waveguide filters. Thus, the dimensional measurement results of the laser produced W-band filters reiterate the high machining reliability and robustness, which was observed during the machining trials of the WR3-band devices (refer to section 7.5.1 and 7.5.2). The S-parameter measurement results from a representative functional performance evaluation test of a W-band filter are shown in Figure 7.18. There is an excellent agreement between the measured performance and simulations. The passband insertion loss is measured to be around 0.65 dB, which is close to the expected value of 0.3 dB obtained from Computer Simulation Technology Microwave Studio (CST MWS) simulations. The maximum passband return loss is measured to be 15 dB, whereas the simulated one is 20 dB. Finally, in order to clearly highlight the capabilities of the proposed multi-process manufacturing solution to produce high quality THz devices, Table 7-5 compares the functional performance characteristic parameters of the produced W-band filter with that of similar W-band components which are commercially available.

Table 7-5 Comparison of the functional performance of the produced W-band waveguides to that of commercially available THz devices

Filter # / Reference	Centre frequency, GHz	Bandwidth, dB	Manufacturing Technique	Insertion Loss, dB	Quality Factor [Q_estimated]
1 [278]	92.6	3.7	CNC milling & then gold-plated	0.3	-
2 [251]	100	10	CNC milling on aluminium	0.6	330.3
3 [279]	92.45	3.2	Silicon DRIE & then copper-plated	1.1	362.3
4 [280]	100	5	SU8 single layer process	1.2	330.3
5 [281]	100	5-10	CNC milling	0.6-0.9	516
6 [This work]	100	5	LMM-enabled process chain	0.7	566.3

It can be seen from Table 7-5 that the Insertion loss of the of the produced W-band waveguide filters in this research is in very comparable to the those obtained by commercially available THz devices. It is worth noting that the insertion loss was obtained without the requirement for a coating operation of the devices after the laser manufacturing step, which significantly reduces manufacturing cost and time with the proposed laser-based manufacturing solution. In addition, Table 7-5 provides an estimated waveguide performance quality factor (Q_estimated) for the investigated filters, where the higher the Q_estimated of a filter the better is its functional performance in terms of a signal loss. It can be clearly seen from Table 7-5 that the quality factor of the produced W-band filters in this research is the highest in comparison to the rest of the filters. This provides quantitative evidences for the manufacturing capabilities of the proposed LMM-enabled process chain to produce high quality THz devices.
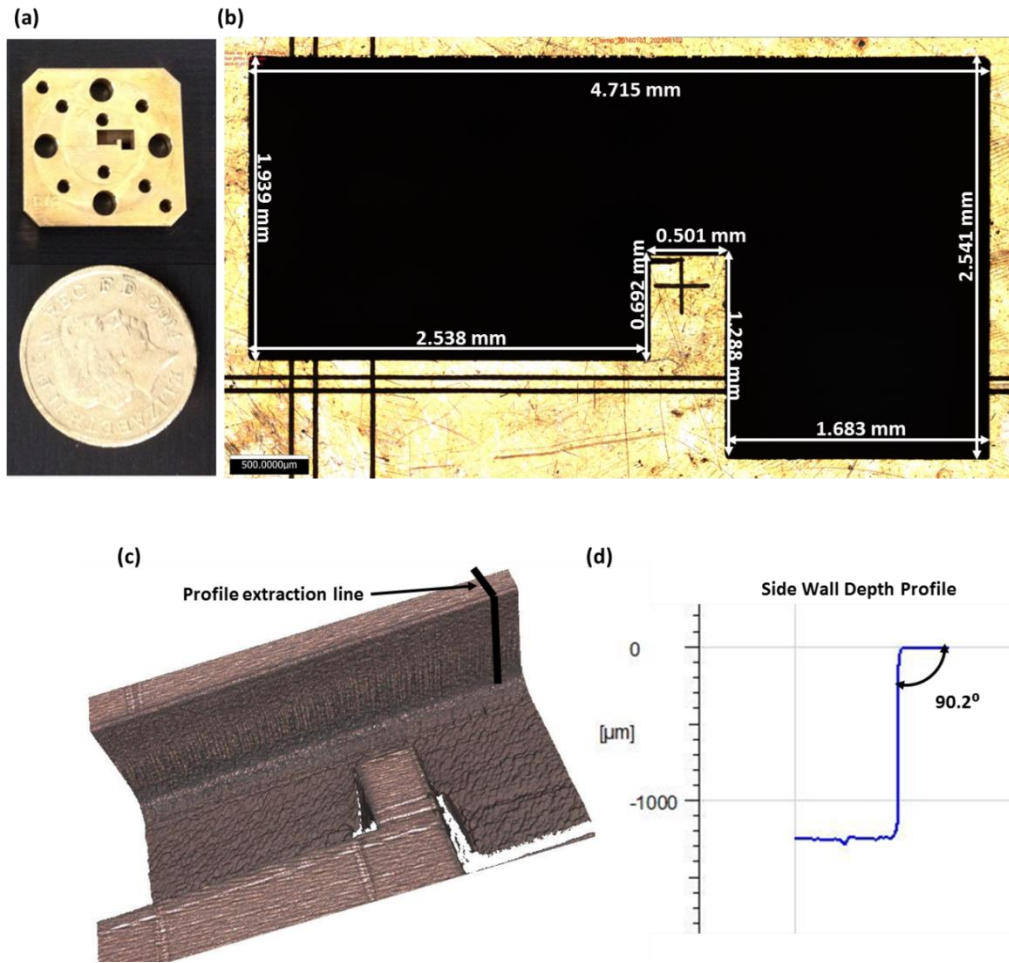
Figure 7.17 (a) A representative laser machined W-band waveguide filter, (b) top view of the filter with dimensions, (c) 3D view of one side wall and (d) the side wall depth profile at the specified location in (c)
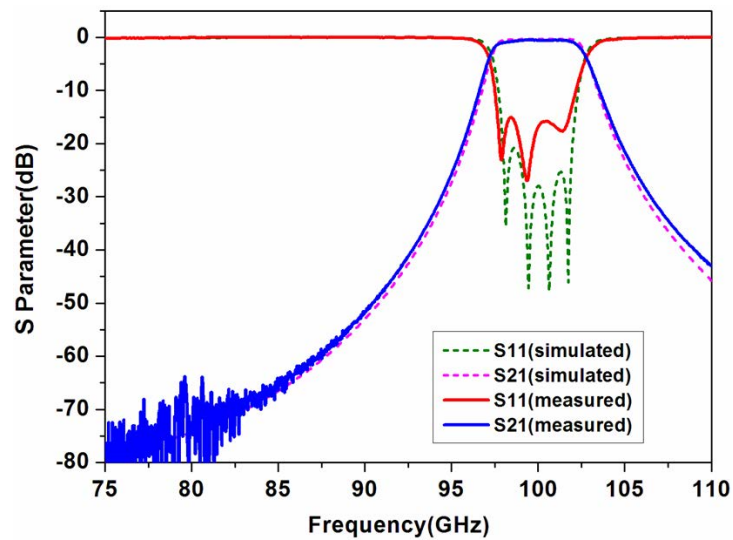
Figure 7.18 Performance evaluation tests results (solid lines) and simulation results (dashed lines) of the laser machined W- band waveguide filter. The simulations are performed in CST [262]

174

7.6 Conclusions

This chapter presents a novel LMM-based process chain for the scale up production of THz technology devices, which operate at the high end of the electromagnetic spectrum. The results demonstrate that the utilization of the system-level tools and techniques developed in this research (Chapters 4 and 5) significantly improves the modularity and reconfigurability of laser micro-processing platforms and thus they facilitate the integrations of LMM in multi-process manufacturing platforms for the fabrication of complex miniaturized products with multi-length scale (micro-and meso-scale) functional features. The following conclusions can be drawn from this research work:

- The overall machining time for producing complex miniaturized products with multi-length scale features, e.g. THz devices, can be significantly reduced by integrating LMM with other manufacturing processes that have complementary cost effective processing windows, e.g. milling.

- Two-side LMM of complex components, e.g. THz waveguide devices, can significantly improve the machining quality of laser machined functional features.

- The side wall tapering of laser machined structures can be controlled to produce them with vertical walls and tolerances within +/- 1^0.

- The cavities corner radius better than 15 µm and surface roughness (Sa) better than 0.9 µm could be achieved;

- Dimensional accuracy of 10 µm can be achieved with the proposed multi-process manufacturing route, while the dimensional repeatability and reproducibility of the produced waveguide structures is better than 5 µm;

- The positional ARR of the laser machined micro-scale waveguide functional features in regards to the milled meso-scale assembly holes are better than 5 µm, which clearly demonstrates the capabilities of the developed system-level tools (Chapters 4 and 5) to enhance the modularity of LMM platforms and to enable their integration in process chains.

The results from the functional evaluations tests of the produced THz devices reveal the capabilities of the proposed LMM-enabled process chain for producing waveguides with exceptional microwave performance, which matches and even exceeds that of commercialized THz passive components. In addition, a comparative qualitative analysis of the manufacturing capabilities of the proposed process chain and the photo-resist based

technologies demonstrate the advantages of the proposed process chain over current waveguide fabrication solutions. Also, it is important to stress that the manufacturing flexibility achieved by deploying the system-level tools and techniques developed in this research allows to fabricate 3D miniaturised components with different length scales functional features in any material and thus to eliminate some additional post-processing steps, i.e. in case of THz devices, fabrication of the complete devices on material substrates with high electrical conductivity (coper) eliminates the requirements for post-processing steps such as coating and assembly operations.

CHAPTER 8

CONTRIBUTIONS, CONCLUSIONS AND FUTURE WORK

Overview

This chapter presents the main contributions and conclusions reached in the research reported in the thesis. Suggestions for future work are also discussed.

8.1   Contributions

The main research findings and contributions to existing knowledge in the laser micro-processing technology are presented in the subsections below.

8.1.1   A systematic approach for quantitative characterization of accuracy, repeatability and reproducibility of state-of-art laser micromachining platforms

A systematic quantitative study for evaluating the accuracy, repeatability and reproducibility (ARR) of state-of-art LMM systems was designed and conducted in this research. The proposed study evaluated the effects of key component technologies on ARR capabilities of laser systems. In particular, the ARR capabilities of the optical and mechanical axes were investigated when they were utilised separately or in combination and thus to clearly quantify the individual contributions of the integrated key component technologies to the observed overall laser machining errors. These are the important generic findings from the performed quantitative study:

- High dynamic optical beam deflection systems are capable of executing laser machining movements with an accuracy of ± 10 μm, but due to their mostly open-loop control, calibration errors have a major impact on the overall performance of LMM systems. Therefore, frequent calibrations of scan heads, i.e. when changes are made in the optical beam delivery paths of laser system, are of critical importance for obtaining consistent machining accuracy. In addition, the machining accuracy with the optical beam deflection systems (optical axes) typically decreases with the increase of nominal dimensions of the

177

geometries to be produced, i.e. the machining accuracy is better at the centre of the field of view defined by the LMM system focusing lens.

- The accuracy of the mechanical axes is much better, generally in the range of ± 2 μm to 4 μm, in comparison to that of the optical axes. This could be partially attributed to the much lower processing speed of the mechanical stages, typically less than 100 mm/s, in contrast to that of the scan heads, greater than 500 mm/s. Other factors, which contribute to the better machining accuracy with mechanical axes is their better closed-loop control than that of optical axes;

- Repeatable and reproducible machining results were not achieved with all investigated systems. Import factors that contributed to the observed deterioration of machining repeatability and reproducibility were the lack of adequate tools and techniques for precise positioning and alignment of workpieces prior to the laser machining operations.

- The dynamic capabilities of Dynamic Focusing Modules (DFM or also called Z-modules) are substantially inferior to those of X and Y optical beam deflectors. In particular the maximum speed of the Z module is less than 10% of the maximum speeds achievable with X and Y optical axes of the 3D scanhead. Thus, the DFM dynamic deficiencies can become a major obstacle for the broader use of high frequency laser sources that necessitate high dynamic 3D scanheads for executing cost effectively free-form surface processing operations.

Finally, the systematic analysis of the ARR capabilities of key component technologies in LMM systems highlighted that state-of-art LMM implementations did not have the technology maturity level of well-established micromachining processes like milling. The analysis provided quantitative evidences that system-level tools and techniques have to be developed for LMM platforms and thus to improve their overall machining ARR, especially when optical axes are employed in the LMM operations.

8.1.2 Generic integration tools for improving the system-level machining performance of reconfigurable LMM platforms

Two generic integration tools, i.e. modular workpiece holding system and an automated workpiece setting-up routine, were developed and validated for improving the system-level performance of reconfigurable laser micro-processing platforms. The proposed tools offer sufficient flexibility, robustness and operability to address important system-level issues in LMM and create the necessary pre-requisites for improving machining ARR of LMM

platforms. In addition, the proposed integration tools improve the machining performance of LMM platforms in terms of manufacturing flexibility and reliability both in stand-alone machine tool configurations and also as constituent manufacturing modules in multi-process manufacturing solutions. These are the important generic findings from the validations of the two developed integration tools:

- The developed modular workpiece holding system and automated workpiece setting up routine improve the reliability, robustness and interoperability of LMM platforms and also the achievable machining ARR.

- The modular workpiece holding system is capable of delivering positional ARR better than +/- 1 μm. At the same time it is a cost effective solution due to the use of mostly standardised and commercially available components and the system can be used both for manual or automated positioning of the workpieces in LMM platforms. These are the main attributes of the system: (i) highly accurate and precise positioning of workpieces in LMM platforms; (ii) flexibility for realizing various laser micromachining configurations, i.e. laser polishing of free-form surfaces, single-side and multi-side laser processing of a single part or an array of parts and laser processing of axis-symmetric parts; (iii) reconfigurability for implementing both manual and automated workpiece setting-up routines and (iv) high level of modularity to enable the integration of LMM systems with other complementary processes.

- The automated workpiece setting up routine reduces significantly the uncertainty in registering parts in LMM platforms. Alignment ARR better than +/- 4 μm is achievable by employing the developed workpiece holding system and an FV probe. These are the main characteristics of the developed automated alignment routine: (i) flexibility for registering workpieces with various geometrical designs; (ii) minimising/eliminating the influence of workpiece's imperfections, i.e. edge definition and surface integrity, on the registration accuracy and precision; (iii) registration of workpiece coordinate systems in LMM setups without pre-existing registration marks; (iv) non-contact registration of workpieces to avoid damaging surfaces, i.e. when polymers are processed or pre-existing micro features are used for alignment; and (v) minimising the influence of the human factor in executing workpieces registration routines.

8.1.3 Generic software tools for extending the manufacturing capabilities of reconfigurable laser micro-processing modules

Generic software tools were developed for improving the manufacturing capabilities of reconfigurable LMM systems in terms of machining throughput and complexity of the laser manufacturing operations that can be realized with them. In particular, the following two generic software solutions were developed and validated: (i) a software tool to counteract the negative dynamic effects of beam deflectors in optical scanning heads and thus to improve significantly the accuracy, quality and efficiency of LMM operations; and (ii) an automated strategy for multi-axis LMM that employ rotary stages for performing complex machining routines. These are the advances in the LMM technology achieved with the developed software tools:

- The negative dynamic effects of optical beam deflection systems are minimised by introducing machine specific compensations in machining vectors to counteract their acceleration and deceleration regions regardless of their directions, length and set scan speed. Such compensations in the machining vectors create capabilities to synchronize ''on-the-fly'' the laser pulse firing with the laser beam movements and thus to improve the LMM accuracy and quality. In addition, the laser machining efficiency is substantially increased through the use of much higher scan speeds without any detrimental effects on ARR and machining quality.

- Capabilities to use rotary stages in conjunction with optical and mechanical axes in LMM platforms for executing automated multi-axis control strategies with high machining ARR. In particular, the developed software tool has in-process synchronization capabilities for: (i) correlating the beam coordinate system (BCS) to the machine coordinate system (MCS); (ii) predicting the translational errors in correlating geometrically BCS to MCS after any arbitrary rotary movements; (iii) executing corrective commands in the machining routines to compensate the translational errors of BCS in MCS after the execution of rotary movements. These tools allow complex machining operations, i.e. laser polishing of free-form surfaces, one-side and multi-side laser processing of a single part or an array of parts and laser processing of axis-symmetric parts, to be carried out with ARR better than +/- 6.5 μm.

8.1.4 LMM enabled multi-process manufacturing solutions for complex miniaturized products

LMM as a constituent technology in process chains that extend the capabilities of well proven conventional manufacturing routes is demonstrated and validated. In particular, the complementary capabilities of LMM and mechanical machining were combined for the fabrication of miniaturised products, i.e. Terahertz technology devices that incorporate multi-length scale (micro-and meso-scale) functional features. The required level of modularity and reconfigurability of the LMM process is achieved through the implementation of the system-level tools and techniques developed in this research (Chapters 4 and 5). These are the generic findings from the deployment of the developed system level tools for integrating LMM with mechanical machining:

- The use of LMM in its complementary cost effective processing window to mechanical machining provides a viable manufacturing route for producing miniaturised products with multi-length scale (micro-and meso-scale) functional features.

- The system-level tools developed in this research improve significantly the ARR and the overall quality of laser machined functional features. In particular, the key improvements achieved with the developed system-level tools are: (i) the side wall tapering of laser machined structures is controlled within +/- 1^0; (ii) complex structures, i.e. the waveguide structures of THz devices, can be produced with corner radius of less than 15 μm and surface roughness (Sa) better than 0.9 μm; (iii) dimensional accuracy of 10 μm can be achieved, while the repeatability and reproducibility is better than 5 μm; and (iv) the positional ARR of the laser machined micro-scale features in regards to the milled meso-scale holes/structures are better than 5 μm.

- The system level tools for carrying out LMM and also for integrating the technology with mechanical machining enable the manufacture of THz devices with required ARR. This is validated by conducting functional tests on the produced THz devices. It was demonstrated that the microwave performance of the waveguides produced with the LMM technology matches and even exceeds that of reference THz passive components produced employing photo-resist based technologies. In addition, the following advantages were identified in a comparative qualitative analysis of the proposed process chain against the photo-resist based technologies that are currently used for producing THz devices: (i) reduction of manufacturing cost and time; (ii) high manufacturing flexibility, capabilities

for producing complex 3D geometries that incorporate different scales' functional features; and (iv) capabilities to structure materials with high electrical conductivity, e.g. copper, brass, etc., that eliminates the requirements for post-processing steps such as coating and assembly operations. The validation research was carried out on three industrially representative THz devices and therefore it can be stated that the proposed manufacturing approach can enable the scaled-up production of a diverse range of THz waveguide devices with the required level of accuracy, precision and surface integrity.

8.2 Conclusions

The overall aim of this research was to improve the system-level performance of reconfigurable LMM platforms and thus to create the necessary pre-requisites for increasing LMM accuracy, repeatability and reproducibility (ARR) in different processing configurations. To accomplish this overall aim the following research were carried out:

- Development and implementation of a systematic approach for quantitative characterization of the manufacturing capabilities of state-of-art LMM platforms in terms of machining ARR **(Chapter 4)**.

- Development, implementation and validation of generic integration tools for reconfigurable LMM platforms which can improve their system-level machining performance in terms of manufacturing flexibility and reliability both in stand-alone machine tool configurations and also as component technologies in multi-process manufacturing solutions **(Chapter 5)**.

- Design, implementation and validation of generic software tools for reconfigurable LMM modules that create capabilities for realizing complex multi-axis laser processing strategies with a high degree of closed-loop manufacturing control and thus to enable a flexible and robust laser micro-processing technology for the fabrication of multi length-scale functional features with the required level of ARR **(Chapter 6)**.

- Development and demonstration of novel multi-process manufacturing platforms that integrate the LMM technology as a key product enabler, and thus to extend the capabilities of industrially proven conventional manufacturing processes such as micro milling for producing emerging high-value miniaturised products. In particular, a multi-process manufacturing solution that combines LMM with mechanical machining is

proposed in this research. It benefits from their complementary cost-effective processing windows for the scale up production of Terahertz technology devices **(Chapter 7)**.

The results from the research provide sufficient evidences that the overall aim of the research was met. In particular, the system-level performance of reconfigurable laser micro-processing platforms has been substantially improved and this provides the necessary pre-requisites for increasing ARR of different LMM operations and processing configurations, i.e. laser polishing of free-form surfaces, one-side and multi-side laser processing of a single part or an array of parts and laser processing of axis-symmetric parts. In addition, the implemented generic integration tools for LMM platforms were demonstrated to create capabilities for increased manufacturing flexibility, operability, reliability and robustness both in stand-alone LMM configurations and also as a constituent technology in multi-process manufacturing solutions.

8.3   Future Work

The following areas for future research were identified:

8.3.1   Further developments of generic system-level tools for achieving mature and reliable laser micro-processing technology

Despite the improved system-level performance of reconfigurable LMM platform investigated in this research, further efforts should be focused on improving the performance of LMM systems from the machine-tool point of view and thus to address other factors contributing to the LMM uncertainty that affect directly the quality of machined structures/components. In particular, the following tools have to be developed:

- *Automated calibration tools for achieving robust LMM results over specified time intervals with pre-defined machining ARR.* Development and implementation of automatic calibration routines should be aimed at creating capabilities for: (i) monitoring the calibration accuracy and precision of LMM systems and thus to alert machine operators or control systems for beam positioning errors, which can deteriorate machining ARR; (ii) fast and efficient self–calibration of LMM systems following changes in the optical beam path configuration, i.e. change in the beam expander factor and changes in the spatial beam profiles (Top-hat, Circular, M-shaped); (iii) automatic recording of alignment and calibration data associated with individual component technologies in the optical beam delivery system and thus to be able to quantify their contributions to the overall LMM

performance; (iv) implementing generic calibration file formats (e.g. .txt, .xml) and thus to be able to access the control boards of optical beam deflection systems from different suppliers.

- *In-process metrology tools and advanced processing control strategies for establishing close-loop LMM control.* Integration of metrology tools for product and process data acquisition with the required level of uncertainty and traceability and thus to enable close-loop LMM control for realising "zero-defect" machining strategies in manufacturing complex miniaturised products. Especially, such tools should enable the execution of advanced process and quality control strategies that employ a wide range of methods, from statistical process control (SPC) to control-chart pattern-recognition and data mining algorithms. Examples of some envisaged key characteristics of such in-process metrology tools and data processing techniques include capabilities for: (i) volumetric error correction to rectify any products deviation from their nominal designs, (ii) in-process laser parameters' optimisation to ensure successful laser processing of products within predefined dimensional and geometrical tolerances, and (iii) model-based inspections to verify dimensional and geometrical compliance of components' key functional features.

8.3.2 LMM enabled multi-process manufacturing solutions for ''zero-defect'' fabrication of diverse miniaturized complex products

Further research efforts should be dedicated to the integration of reconfigurable LMM platforms with other industrially proven manufacturing processes, e.g. injection moulding, powder metallurgy and additive manufacturing, and thus to reduce the cost and industrial risks in developing scale up manufacturing solutions for a range of existing or new emerging miniaturised products. These are two conceptual ideas that exemplify the manufacturing potential of such multi-process manufacturing solutions:

- *Integration of laser micro-processing with additive manufacturing technologies.* The integration of laser micro-processing with different additive manufacturing technologies could result in solutions for batch fabrication of complex miniaturized components with high surface integrity and dimensional ARR while ensuring a sustainable use of advanced materials. Figure 8.1 depicts the envisaged process chain and exemplifies the potential improvements in components' surface integrity following the laser-micro-polishing step.
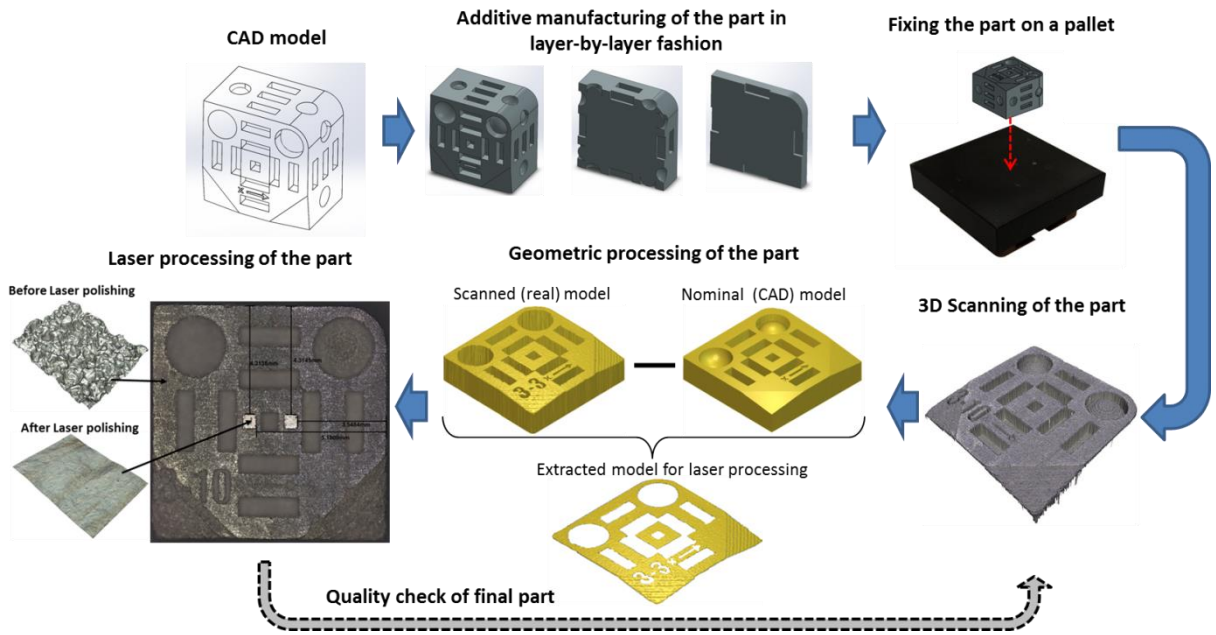
Figure 8.1 A process chain that combines additive manufacturing and laser micro-processing

- *Integration of laser micro-processing with powder metallurgy for novel cutting tools.* Research efforts on the combination of laser micro-processing with powder metallurgy could enable the fabrication of cutting tools with improved designs, i.e. incorporating chip breakers, complex edge radius designs and textured rake and flank surfaces. Such tools could potentially exhibit improved tribological characteristics during machining that could lead to reductions of the cutting forces and tool wear, and also to improvements of the workpiece surface quality/integrity.

APPENDIX 1

DETAILED ENGINEERING DRAWINGS

Appendix 1 provides the detailed engineering drawings of the test geometries, which were machined in the context of the research reported in the thesis.

Figure A1.1 shows the detailed engineering drawing of the test geometry for tests 1, 2, 4 and 5 of the quantitative study in Chapter 4.
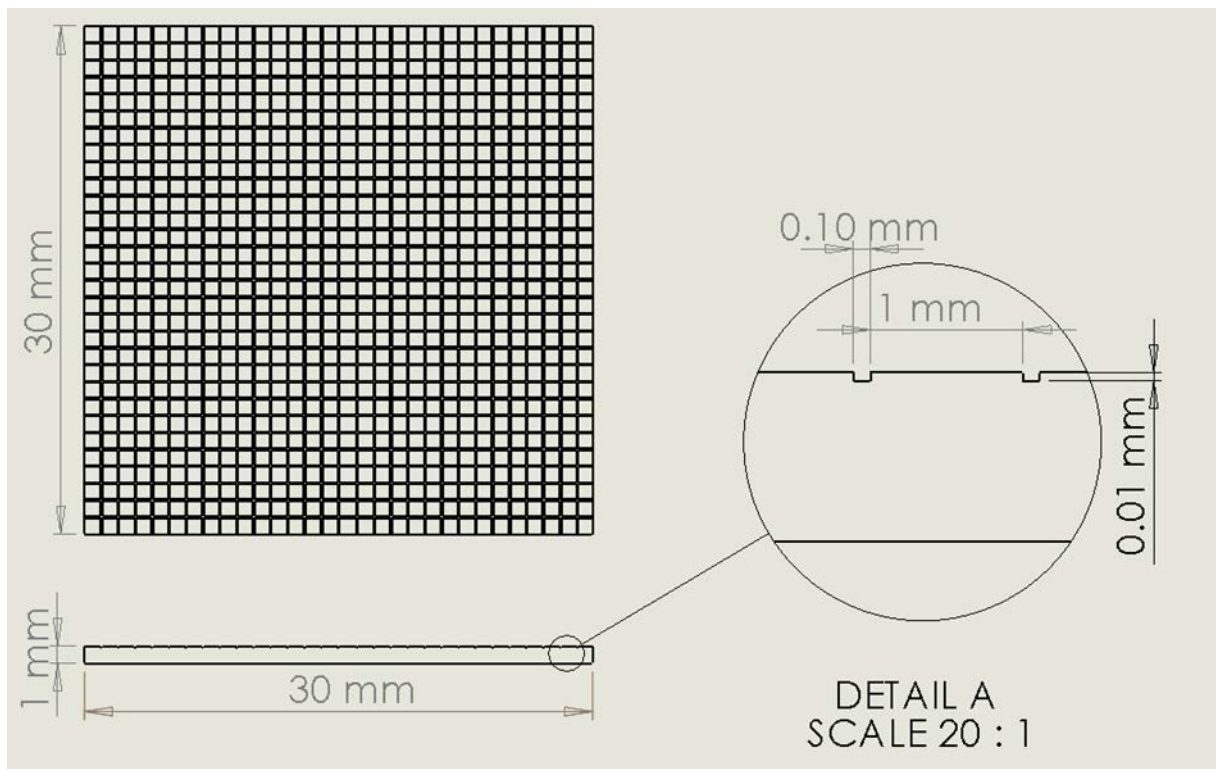
Figure A.1.1. Detailed engineering drawing of the test geometry for tests 1, 2, 4 and 5 of the quantitative study in Chapter 4

Figure A1.2 shows the detailed engineering drawing of the test geometry for test 3 of the quantitative study in Chapter 4.
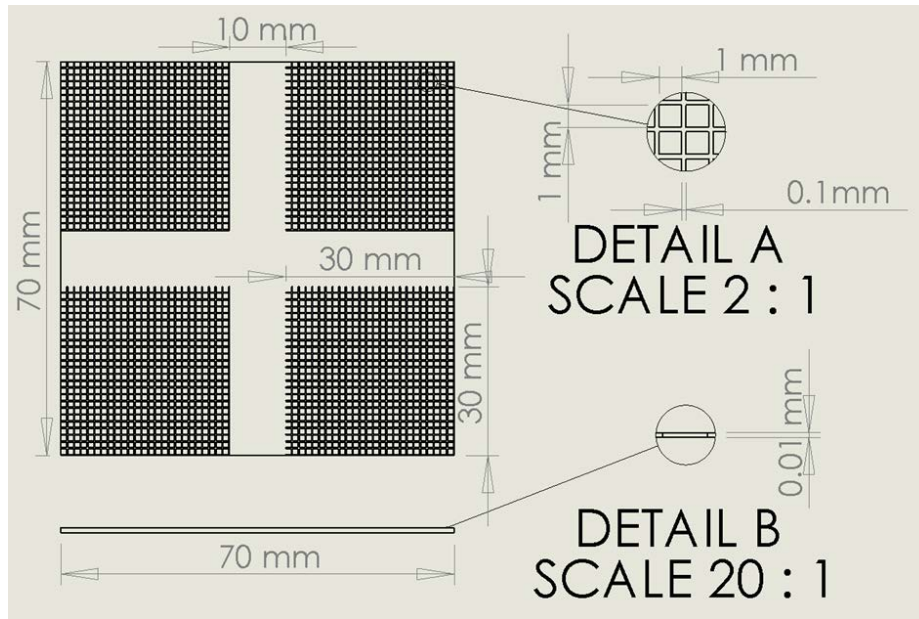
Figure A.1.2. Detailed engineering drawing of the test geometry for test 3 of the quantitative study in Chapter 4

Figure A1.3 shows the detailed engineering drawing of the test geometry for test 6 of the quantitative study in Chapter 4.
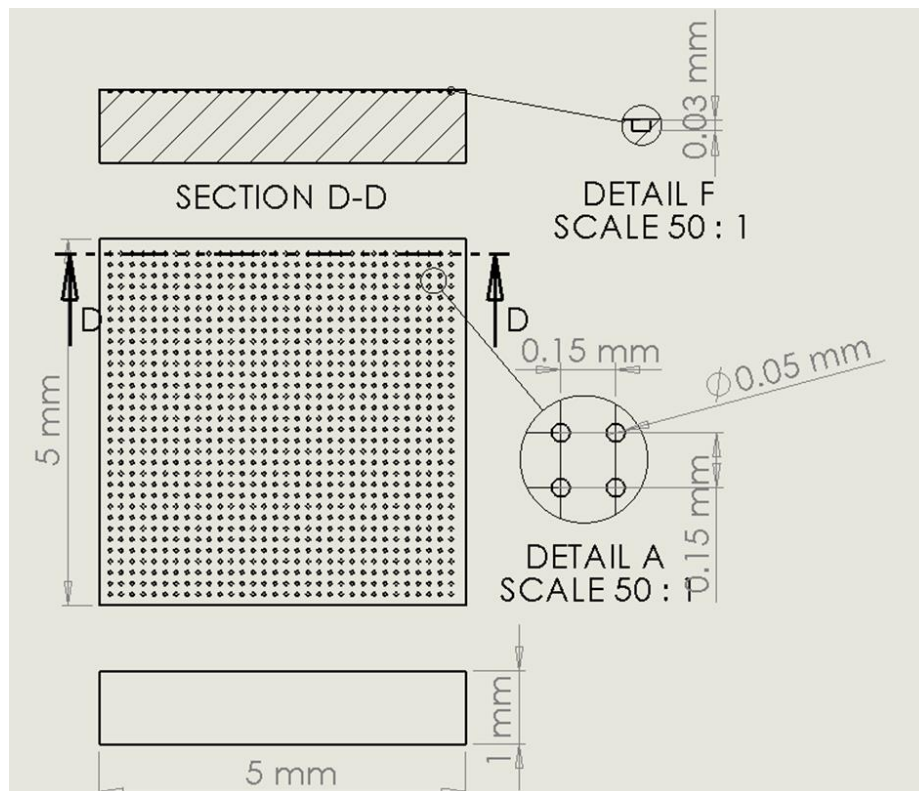
Figure A.1.3. Detailed engineering drawing of the test geometry for test 6 of the quantitative study in Chapter 4

Figure A1.4 shows the detailed engineering drawing of the WR3-band waveguide filter in Chapter 6.
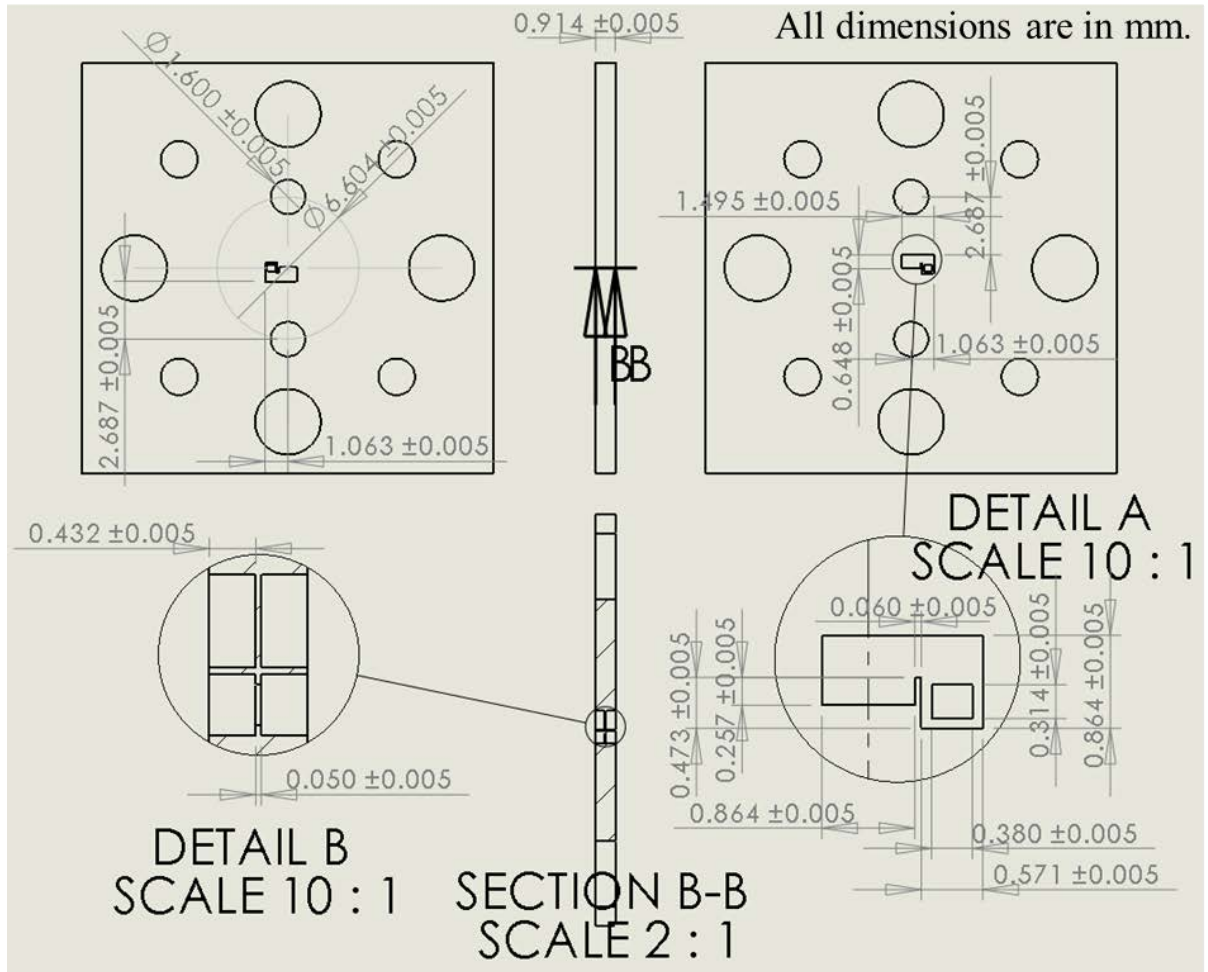
Figure A.1.4. Detailed engineering drawing of the WR3-band waveguide filter in Chapter 7

Figure A1.5 shows the detailed engineering drawing of the W-band waveguide filter in Chapter 6.
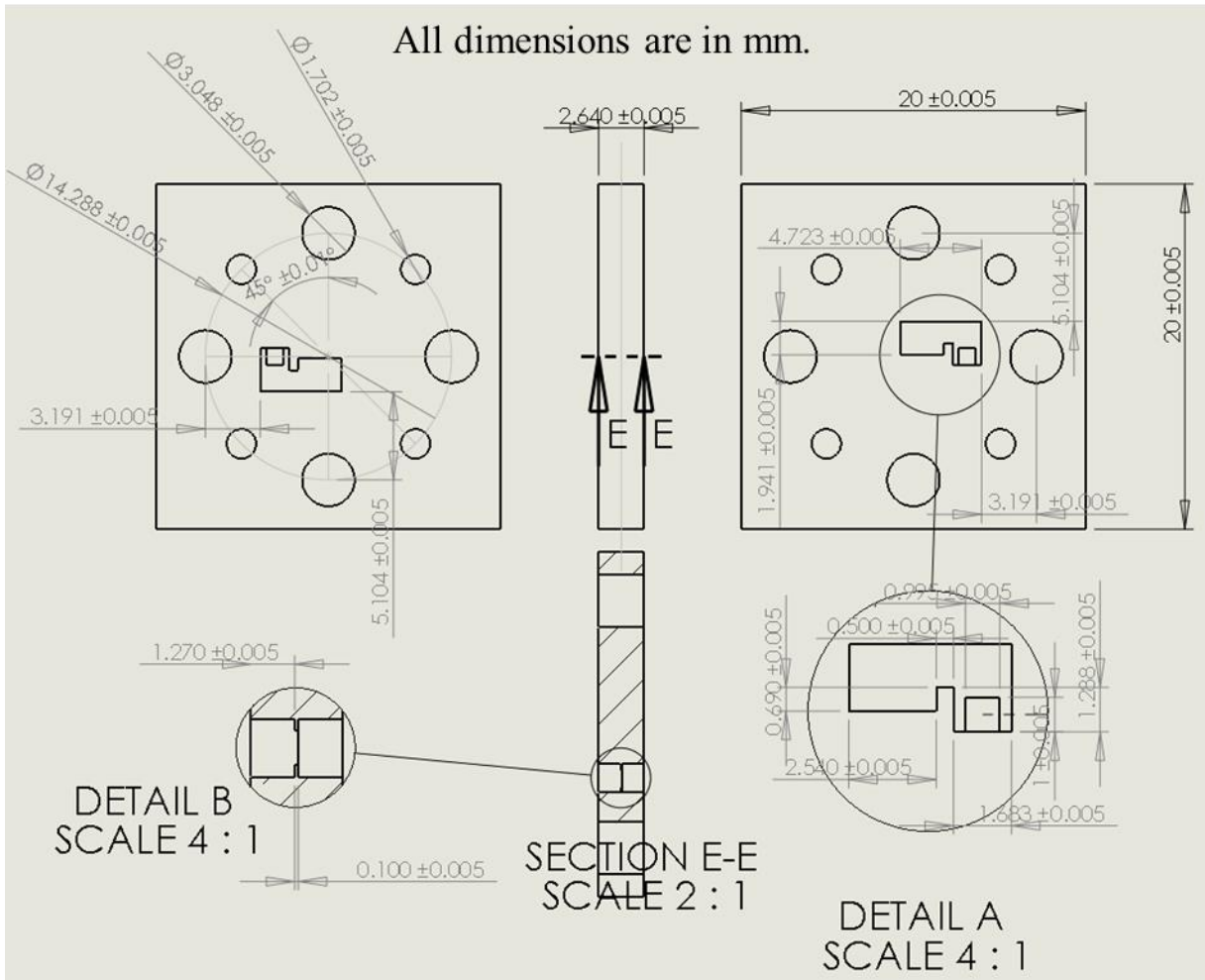
Figure A.1.5. Detailed engineering drawing of the W-band waveguide filter in Chapter 7

APPENDIX 2

CHARACTERIZATION OF THE TOTAL UNCERTAINTY OF THE MEASURMENTS PROCEDURES IN CHAPTER 3

The measurements on laser structured/textured surfaces were carried out using the FV technology, in particular an Alicona G5 InfiniteFocus microscope. Some preliminary measurements of the machined fields were conducted using four different objectives, in particular 5X, 10X, 20X and 50X. The aim of these measurements was to assess the measurement uncertainties associated with these four objective lenses in context of the planned six tests (presented in Chapter 4). A representative test structure, as shown in Figure A2.1, produced with System A was used to carry out this uncertainty assessment. The area enclosed between 1st and 3th trenches was scanned and the corresponding distances between the trenches were measured. To minimise the effect of laser-material interactions on the trench width, the measurements were taken from the edge of 1st trench to the corresponding edge of 3th trench. The '2D measurement' tool provided by the Alicona data analysis software with capabilities for detecting edges automatically was used and the corresponding uncertainties associated with the measurements were calculated. Ten measurements along the edges of 1st and 3th trenches were performed and thus to judge about the total uncertainty of the utilized measurement procedures. Table A 2.1 provides the measurement results with the 5X objective lens. Table A 2.2 provides the measurement results with the 10X objective lens. Table A 2.3 provides the measurement results with the 20X objective lens. Table A 2.4 provides the measurement results with the 50X objective lens.
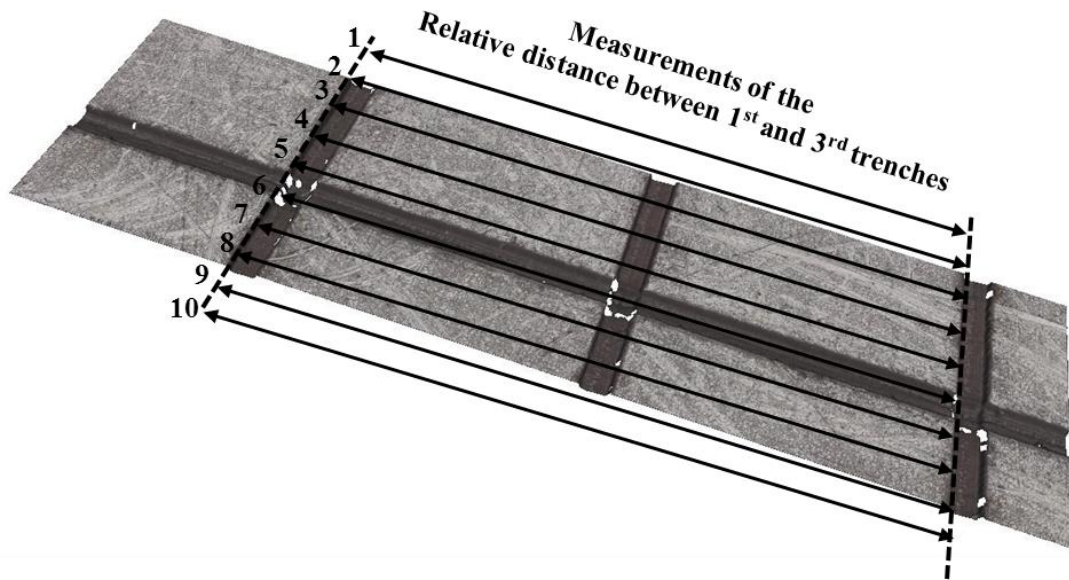
Figure A2.2. Measurements of the relative distance between 1st and 3rd laser produced trenches for characterizing the measurement uncertainty both with x20 and x50 objective lenses

Table A2.1 Measurement results with the 5X objective lens

Measurement [mm]	1	2	3	4	5	6	7	8	9	10
	2.0008	1.9990	2.0012	1.9960	1.9992	2.0001	1.9925	1.9953	1.9914	2.0010
Average [mm]	1.9977									
Standard deviation [μm]	3.62									
Uncertainty [μm]	1.14									
Total Uncertainty 95% level [μm]	2.28									

Table A2.2 Measurement results with the 10X objective lens

Measurement [mm]	1	2	3	4	5	6	7	8	9	10
	1.9956	1.9942	1.9951	1.9956	1.9945	1.9933	2.0005	1.9963	2.0010	1.9935
Average [mm]	1.9959									
Standard deviation [μm]	2.70									
Uncertainty [μm]	0. 85									
Total Uncertainty 95% level [μm]	1.71									

Table A2.3 Measurement results with the 20X objective lens

Measurement [mm]	1	2	3	4	5	6	7	8	9	10
	1.9961	1.9975	1.9955	1.9950	1.9982	1.9970	1.9966	1.9969	1.9990	1.9980
Average [mm]	1.9969									
Standard deviation [μm]	1.24									
Uncertainty [μm]	0. 51									
Total Uncertainty 95% level [μm]	1.02									

Table A2.4 Measurement results with the 50X objective lens

Measurement [mm]	1	2	3	4	5	6	7	8	9	10
	1.9962	1.9959	1.9962	1.996	1.9959	1.9962	1.9963	1.9958	1.9962	1.9963
Average [mm]	1.9961									
Standard deviation [μm]	0. 18									
Uncertainty [μm]	0. 105									
Total Uncertainty 95% level [μm]	0. 21									

Based on the results from Tables A2.1 to A2.4 and taking into account that the expected machining ARR capabilities with optical axes and mechanical axes are +/-10 μm and +/- 2 μm, respectively, 20X objective lens was selected to perform measurements for Tests 1,3, 4,5 and 6, while 50X objective lens was selected to perform measurements for Test 2. In this way, the total measurement uncertainty was less than 10% of the expected ARR tolerance levels.

APPENDIX 3

DEPTH PROFILE MEASURMENT RESULTS OF DIMPLES PRODUCED IN CHAPTER 3 FOR INVESTIGATING THE DYNAMIC CAPABILTIES OF DYNAMIC FOCUSING MODULES

Tables A3.1and A3.2 provide depth profile measurement results of the dimples that were produced in the context of the proposed experimental methodology for investigating the dynamic capabilities of dynamic focussing modules. In particular, Table A3.1 shows the depth of dimples that were produced on the sample normal to the incident laser beam, while Table A3.2 gives information for the depth of dimples that were produced on the sample tilted at 15^0 in regards to the incident beam.

Table A3.1. Depth profile of dimples on flat sample (0° tilt angle)

Speed [mm/s]	Dimple depth [µm] at the bottom section of the produced lines					Average [µm]	Uncertainty 95 % level [µm]	Dimple depth [µm] at the middle section of the produced lines					Average [µm]	Uncertainty 95 % level [µm]	Dimple depth [µm] at the top section of the produced lines					Average [µm]	Uncertainty 95 % level [µm]
100	11.8	12.2	11.9	11.9	12.2	**12.1**	0.2	12.1	12.5	12.8	11.6	11.3	**11.8**	0.4	12.4	12.0	11.9	11.6	11.9	**11.7**	0.4
500	12.1	11.9	11.8	11.9	12.2	**12.0**	0.1	11.8	12.1	12.6	12.5	12.4	**12.2**	0.3	12.6	12.3	11.9	11.8	12.0	**11.9**	0.5
1000	12.4	13.0	12.8	11.9	12.5	**12.5**	0.4	11.9	12.6	12.1	12.4	11.8	**12.1**	0.3	12.9	12.1	12.1	13.1	12.8	**11.9**	0.7
1200	11.9	12.0	12.1	12.5	11.9	**12.1**	0.2	12.0	13.1	12.1	12.1	12.6	**12.4**	0.4	11.8	12.6	11.9	11.7	11.9	**12.2**	0.4
1300	11.6	11.9	12.5	12.5	11.2	**12.1**	0.7	12.6	11.5	12.1	11.5	11.0	**11.9**	0.6	12.7	12.1	12.1	11.0	11.5	**12.1**	0.7
1400	11.2	13.5	11.9	12.4	11.6	**12.1**	0.8	11.2	12.6	12.5	11.9	12.4	**11.8**	0.5	11.5	12.9	12.4	12.0	11.7	**12.0**	0.4
1500	12.5	12.3	11.8	11.1	12.9	**12.1**	0.6	11.9	12.1	13.1	11.6	13.5	**12.6**	0.6	12.5	13.5	12.3	12.4	11.8	**12.2**	0.8
1600	13.2	12.1	12.0	12.0	12.5	**12.3**	0.6	12.4	12.2	12.2	12.4	12.1	**12.0**	0.3	12.6	13.1	12.1	12.0	11.0	**12.2**	0.8
1700	13.5	12.8	11.5	13.1	12.5	**12.6**	0.6	11.7	11.8	12.8	11.5	11.5	**12.1**	0.5	13.2	13.0	11.7	11.7	11.7	**12.2**	0.6
1800	12.7	11.9	12.6	12.7	12.8	**12.5**	0.3	11.8	12.6	13.1	11.8	11.9	**12.2**	0.5	12.6	12.2	12.1	11.5	12.2	**11.9**	0.2
1900	11.8	12.0	11.9	12.7	11.6	**11.9**	0.4	12.3	12.1	11.4	11.8	11.8	**11.9**	0.3	12.0	11.9	11.6	11.6	11.9	**12.1**	0.9
2000	12.6	11.6	12.3	11.8	12.7	**12.2**	0.4	12.1	12.8	11.5	11.9	11.6	**12.0**	0.5	11.8	12.0	12.0	12.0	12.8	**12.1**	0.7

Table A3.2. Depth profile of dimples on the tilted sample (15° tilt angle)

Speed [mm/s]	Dimple depth [µm] at the bottom section of the produced lines					Average [µm]	Uncertainty 95 % level [µm]	Dimple depth [µm] at the middle section of the produced lines					Average [µm]	Uncertainty 95 % level [µm]	Dimple depth [µm] at the top section of the produced lines					Average [µm]	Uncertainty 95 % level [µm]
100	11.3	11.0	11.5	11.2	11.6	**11.3**	0.2	12.1	12.3	11.8	11.6	11.3	**11.8**	0.4	11.2	12.4	11.6	11.6	11.5	**11.7**	0.4
500	11.1	11.3	10.6	11.6	12.1	**11.3**	0.5	11.8	11.7	12.6	12.1	12.5	**12.1**	0.4	12.6	12.1	12.1	11.9	12.0	**11.9**	0.5
1000	12.5	12.8	11.2	11.2	13	**12.2**	0.7	11.9	12.6	11.3	12.4	11.9	**11.9**	0.5	11.8	11.1	11.7	11	11.6	**11.9**	0.7
1200	12.9	11.5	11.9	11.7	11.6	**12.0**	0.5	12.0	13.1	12.6	12.9	11.6	**12.6**	0.7	11.6	11.2	12.7	12.1	12.6	**12.1**	0.6
1300	12.4	11.9	11	10.5	10.9	**11.3**	0.7	12.2	12.1	12.1	12.5	11.1	**12.1**	0.7	11.6	11.9	12.1	11.9	11.5	**11.5**	0.4
1400	12.9	13.1	12	11.5	10.6	**12.0**	0.9	12.4	13.6	13.1	11.9	11.6	**12.6**	0.8	11.5	11.9	12.8	12.8	11.7	**12.1**	0.6
1500	8.9	8.5	10.1	8.7	9.2	**9.1**	0.6	12.6	12.2	11.9	12.7	11	**12.3**	0.8	12.6	13.1	11.7	12.3	11.8	**12.0**	0.6
1600	5.3	4.9	3	4.1	6	**4.7**	1.0	8.9	7.3	10.2	9.9	10.8	**10.7**	0.8	13.2	10.9	12.5	11.7	12	**12.2**	0.8
1700	0.5	0.8	0.9	0.2	0.1	**0.5**	0.3	6.3	7.1	6.9	7	6.2	**6.7**	0.4	12.7	12.2	12.2	10.9	11.5	**11.7**	0.6
1800	0.8	1.2	0.4	0.5	0.4	**0.7**	0.3	5.9	5.7	4.3	3.9	4.9	**4.9**	0.8	12.6	12.6	11.9	11.9	11.3	**11.9**	0.4
1900	0	0.5	1.5	0.8	0.1	**0.6**	0.5	1	1.2	2.1	1.4	1.6	**1.5**	0.4	12	11.3	11.8	11.8	11.1	**11.5**	0.3
2000	1	0.9	0.2	0.1	0.1	**0.5**	0.4	1.1	2	1.3	0.6	0.1	**1.2**	0.6	11.8	12.1	11.6	12	11.5	**11.8**	0.2

APPENDIX 4

WORKPIECE HOLDING EXTENSION FOR ENABLING TWO-SIDE LMM OF WORKPIECES

Figure A4.1(a) provides a graphical overview of a workpiece holding device extension that was designed and implemented to enable two-side laser micro-processing routines. In particular, the proposed workpiece holding extension was designed for accurate and precise fixing of workpieces in the LMM platform as shown in Figure A4.1 In particular, the main components of the workpiece holding device include a main unit, a set of adaptor plates which can hold samples with different sizes and shapes, a spacer which ensures that the sample is hold firmly in the adaptor plate and a holder which keeps the adaptor plate firmly fixed to the main unit body throughout the machining operations. In addition, a standardized high precision pallet is employed to attach the modular workpiece holding extension to the rotary stage of the laser system. Figure A4.1(c) shows an overall view of the produced workpiece holding device that is implemented in the laser system to enable two-side processing operations of samples. The manufacturing benefits of such two-side laser mirco-processing operations include capabilities to (i) increase twofold the aspect ratio of structures produced with LMM in comparison to those resulting from one-sided laser machining and (ii) to improve significantly the exit quality of produced through features and thus to match that of their respective entrances. In order to demonstrate these manufacturing capabilities, some experimental trials were performed and the results were analysed. In particular, the experimental trials, which have been performed to evaluate the proposed two-side laser micromachining strategy included the machining of circular through holes with different dimeters, i.e. 2 mm, 0.8 mm, 0.4 mm, 0.3mm, 0.2 mm, 0.1 mm, both with the two-side strategy and with the conventional one-side laser machining approach. In this way, it was possible to perform a direct comparison of the machining results obtained with the two strategies in terms of critical through holes characteristics, such as quality of the holes both at their entrances and exits and their achievable aspect ratios.
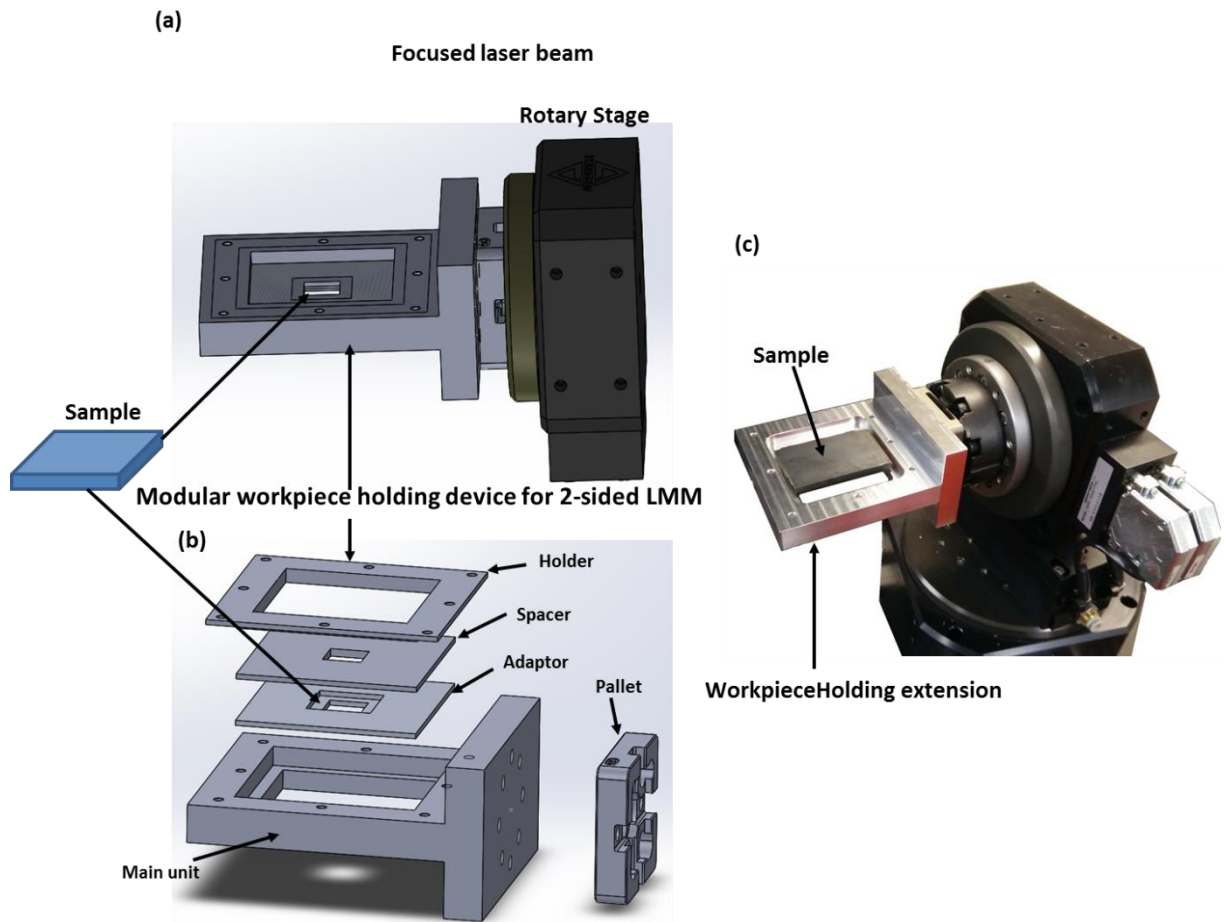
Figure A4.1. (a) The design of a workpiece holding device to enable two-side laser micro-processing operations (b) Exploded view of the proposed workpiece holding extension and (c) An overall view of the produced workpiece holding devices, implemented in the laser system

Figure A4.2(a) and (b) depict the quality at the entrance and exit of 0.2 mm diameter hole produced with the one-side laser machining strategy, respectively. It can be clearly seen that due to the side walls tapering effects, the quality at the hole exit was compromised in comparison to the hole entrance. In contrast, Figure A4.2 (c) and (d) clearly show that the quality of the hole entrance and exit respectively produced with proposed two-side laser micromachining strategy is identical.
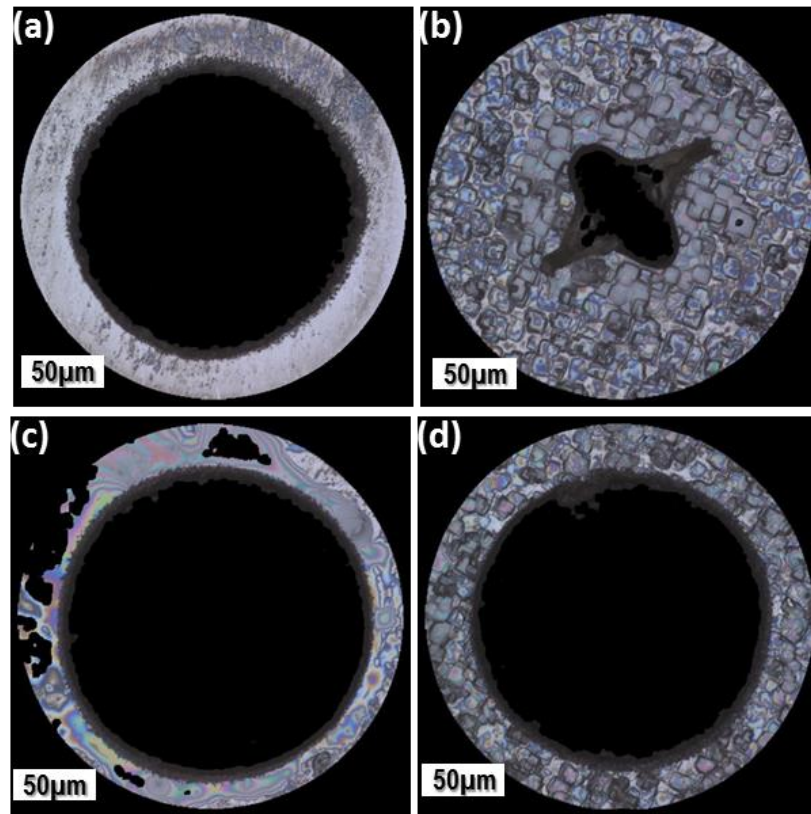
Figure A4.2. (a) entrance and (b) exit of 0.2 mm hole produced with one-side laser machining strategy, (c) entrance and (d) exit of 0.2 mm hole produced with two-side laser machining strategy

Figure A4.3 also depicts a side view (depth profile) of the side wall of a 2 mm diameter hole in order to clearly show the side wall taper angle and depth profile, especially where the holes machined from the two sides meet. It can be also clearly seen in Figure A4.3 that with the automated tool for multi-axis laser machining with rotary stages (presented in Chapter 6), it was possible to compensate any positional errors resulting from the rotary movement of the workpiece and thus to ensure the high accuracy alignment of the laser machining operations executed from the two opposite sides of the substrate (exemplified in Figure A 4.3 by the smooth hole interface region and lack of any height steps that could arise due to inaccurate alignment of the geometries produced from the two opposite sides of a workpiece). The increase of achievable aspect ratio could be explained by the fact that the workpieces can be processed from their two-opposite sides.

197
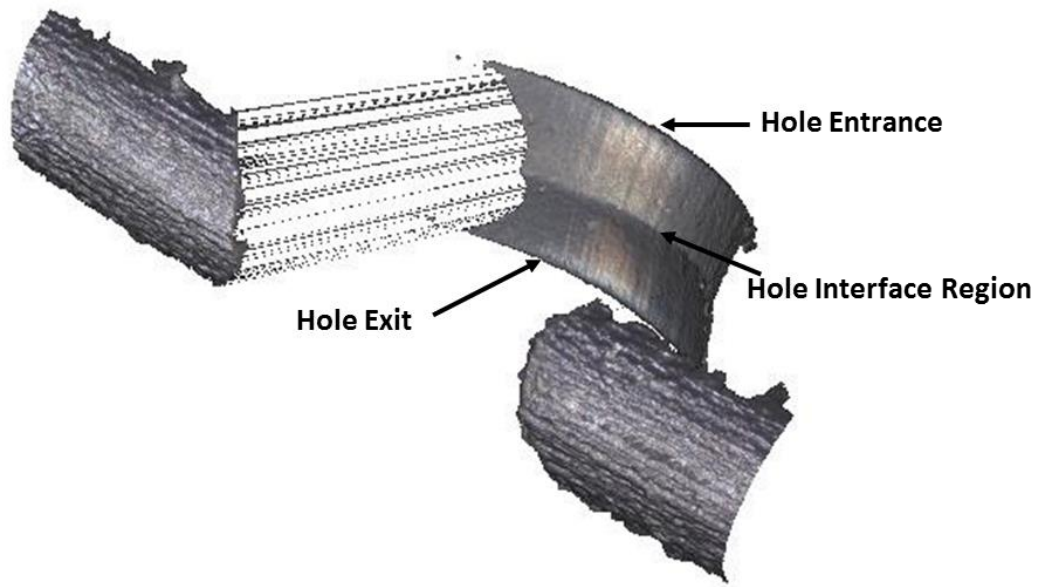
Figure A4.3. The hole side wall profile resulting from the two-side LMM strategy

Note to Figure A4.3: The hole interface region is the region at which the machined holes from the two opposite sides on the sample meet.

Finally, Figure A4.4 shows more holes with different diameters to exemplify the capabilities of the proposed workpiece holding device to enable two-side laser micro-processing operations.
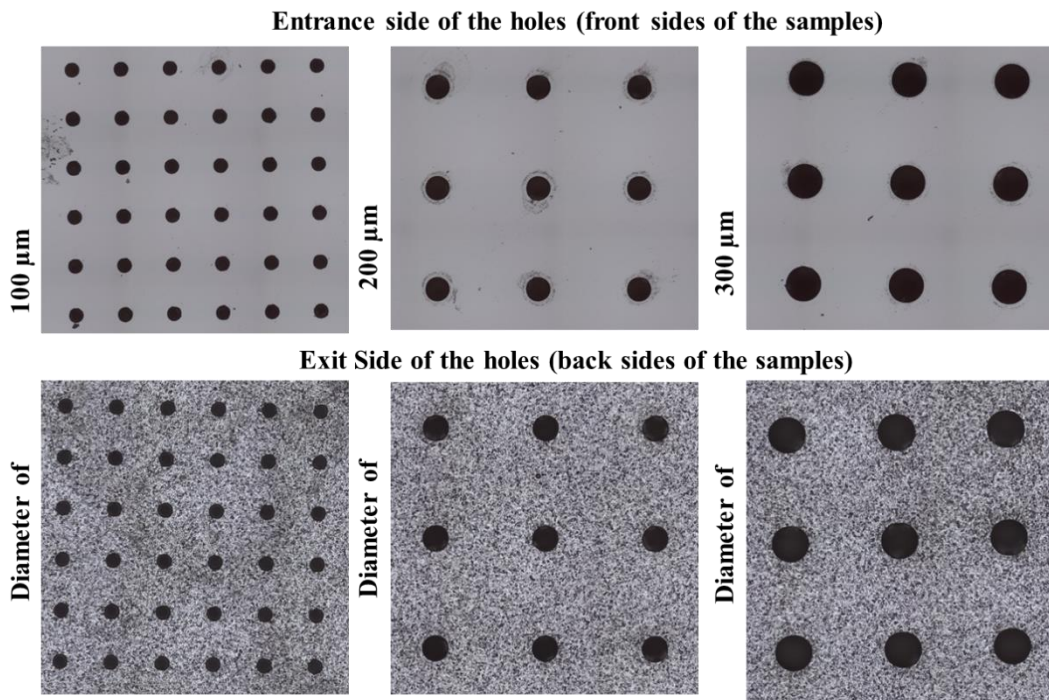
Figure A4.4. Examples of holes with different diameters (100 μm, 200 μm, 300 μm) produced with the proposed workpiece holding extension

APPENDIX 5

IMPLEMENTATION OF THE ADAPTIVE POSTPROCESSOR (CHAPTER 5) AS A STAND-ALONE SOFTWARE TOOL

Definition of program parameters (variables)

In order to successfully implement the adaptive postprocessor as a stand-alone software tool, program parameters (variables) were first created, that were later used for writing the logical instructions of the postprocessor and thus to achieve its targeted functioning in generating machining commands. The following program parameters were created and defined in the DELCAM Postprocessor programming environment:

- Beam_us – Laser beam diameter in microns

- Compare_X_linear – Compares the x coordiantes of the Plunge and Cutting feed rate types from the Move Linear Command. Thus, it shows the length and direction of the machining vector in the x-direction.

- Compare_X_rapid – Compares the x coordiantes of the Retract and Link move types from the Move Rapid Command. Thus, it shows the length and direction of the positioning vector in the x-direction.

- Compare_Y_linear – Same as Compare_X_linear but for the y coordinates.

- Compare_Y_rapid – Same as Compare_X_rapid but for the y coordinates.

- Cutting angle – orientation angle of a machining vector

- Hatch_angle – defined in ArtCam; orientation of machining vectors in a layer in comparison to previous layer

- Hatch_distance – defined in ArtCam; distance between machining vectors

- Laser Off delay_us – Laser off delay in micro seconds

- Laser On delay_us – Laser on delay in micro seconds

- Machining error_mm – The deviation from nominal length of a machining vector (in mm)

- Rapid_angle – the orientation angle of a positioning vector

- Rapid_angle_X – the length in x direction of a positioning vector, where this is calculated by taking the cos of (Cutting vector + 90 degress), because a positioning move should be 90 degrees to a maching move

- Rapid_angle_Y- same as Rapid_angle_X, but for the y-direction

- Scaling_factor_mm- The length at certain speed with which to offset a machining vector

- Scannning Speed_mm/s- the processing speed in mm/s

- X_cutting - X coordinate in Cutting feed rate type

- X_link- the x coordinate when executing a link command (G0 move)

- X_link_pos_max- the distance from the current X coordinate to the maximum X coordinate in a toolpath

- X_link_pos_min- the distance from the current X coordinate to the minimum X coordinate in a toolpath

- X_next_cutting- a scaled X coordinate when executing a G1 move

- X_next_rapid- a scaled X coordinate when executing a G0 move

- X_plunge- X coordinate in Plunge move type

- X_rapid_dir_retract- the length and orientation of retract move in x direction

- X_retract- X coordinate in Retract move type

- Y_cutting- Y coordinate in Cutting feed rate type

- Y_link - the y coordinate when executing a link command (G0 move)

- Y_link_pos_max – same as X_link_pos_max, but for y direction

- Y_link_pos_min – same as X_link_pos_min, but for y direction

- Y_next_cutting- a scaled Y coordinate when executing a G1 move

- Y_next_rapid- a scaled Y coordinate when executing a G0 move

- Y_plunge- Y coordinate in Plunge move type

- Y_rapid_dir_retract- the length and orientation of retract move in y direction

- Y_retract- Y coordinate in Retract move type

Logical steps of the stand-alone postprocessor program

The program is written and complied in DELCAM Postprocessor.The following bullet points describe the building blocks of the stand-alone postprocessor program, that were implemented to achieve its required functionality:

- **Program Start command**

The Program Start command (shown in Figure A5.1) determines the content of the header of the generated g-code file. The command also calls a Script function (Parameters_Input shown in Figure A5.2), which allows defining important parameters for offsetting of machining vectors (Scanning Speed, Beam Diameter, Hatch distance and Hatch angle). Furthermore, machining error is estimated for the respective scanning speed and suitable scaling factor, Laser on delay and Laser off delay are also calculated.

Figure A5.1. Program Start program building blocks

```
//===============================================================
function Parameters_Input()
{
var Scanning_Speed_mms="";
var Beam_us="";
var Hatch_distance="";
var Hatch_angle="";
prompter.AddParam("%p(Scanning_Speed_mms)%");
prompter.AddParam("%p(Beam_us)%");
prompter.AddParam("%p(Hatch_distance)%");
prompter.AddParam("%p(Hatch_angle)%");
prompter.Show();
Scanning_Speed_mms += StandardResponse("");
Beam_us += StandardResponse("");
Hatch_distance += StandardResponse("");
Hatch_angle += StandardResponse("");
return Scanning_Speed_mms;
return Beam_us;
return Hatch_distance;
return Hatch_angle;
}
//---------------------------------------------------------------
```

Figure A5.2. Definition of a script function '' Parameters_Input''

- **First Move After Toolchange command:**

This is the first move in the body of the g-code file. Since the first machining layer is always in the horizontal (along x-axis) direction (0 degrees), the offsetting of machining vectors should be only in the x –direction (as shown in Figure A5.3).

Figure A5.3 First Move After Toolchange program building blocks

- **Move Rapid command:**

This command outputs the positioning moves in the toolpath (G0 moves). In order to effectively offset the positioning vector conditional statements are defined in the body of the command. The length of a positioning vector is determined by subtracting X,Y coordinates of the LINK move type (end coordinates of a positioning vector) from the X,Y coordinates of the RETRACT move type (start coordinates of a positioning vector), while the orientation of the move vector can be found by taking the atan of positing vector length in y/ positioning vector length in x. Before introducing the conditional statements, other parameter which are calculated include Rapid_angle_X and Rapid_angle_Y. Since, cutting angle is a known parameter from the Move Linear command, it is known that the positioning vector should be 90 degrees to the cutting angle and the sum of cos(Cutting angle + 90 degrees) + sin (Cutting angle +90 degrees) should be equal to the predefined hatch distance (as shown in Figure A5.4).

Figure A5.4. Calculation of important conditional parameters in the Move rapid command

The first conditional statement in the Move rapid command building blocks (shown in Figure A5.5) is the main statement that triggers the outputting of the desired (scaled) positioning moves and can be applied regardless of the hatching style and direction.

19	else if ((%p(Rapid_angle_X)%+%p(Rapid_angle_Y)%)==%p(Hatch_distance)% ‖ (%p(Rapid_angle_X)%+%p(Rapid_angle_Y)%)==(%p(Hatch_distance)%*(-1)))							
20	if (%p(X_rapid_dir_retract)%<0)							
21	if (%p(Y_rapid_dir_retract)%<0)							
22	Block Number	Motion Mode	X_next_rapid = %p(X)%-abs(co…	Y_next_rapid = %p(Y)%-abs(si…	Z	Feed Rate Type	Move Type	
23	else if (%p(Y_rapid_dir_retract)%>0)							
24	Block Number	Motion Mode	X_next_rapid = %p(X)%-abs(co…	Y_next_rapid = %p(Y)%+abs(si…	Z	Feed Rate Type	Move Type	
25	end if							
26	else if (%p(X_rapid_dir_retract)%>0)							
27	if (%p(Y_rapid_dir_retract)%<0)							
28	Block Number	Motion Mode	X_next_rapid = %p(X)%+abs(c…	Y_next_rapid = %p(Y)%-abs(si…	Z	Feed Rate Type	Move Type	
29	else if (%p(Y_rapid_dir_retract)%>0)							
30	Block Number	Motion Mode	X_next_rapid = %p(X)%+abs(c…	Y_next_rapid = %p(Y)%+abs(si…	Z	Feed Rate Type	Move Type	
31	end if							
32	end if							

Figure A5.5. First Conditional Statement in the Move rapid command

The sub-conditional statements in the first conditional statement that is shown in Figure A5.5 are inserted in order to apply appropriate scaling of the positioning vector in the correct direction:

(i) The direction of retract move in the negative x direction means the positioning vector should be scaled in the negative x direction.

(ii) The direction of retract move in the positive x direction means the positioning vector should be scaled in the positive x direction.

(iii) The direction of retract move in the negative y direction means the positioning vector should be scaled in the negative y direction.

(iv) The direction of retract move in the positive y direction means the positioning vector should be scaled in the positive y direction.

The second conditional statement in the Move rapid command program building blocks(shown in Figure A5.6) is introduced in order to output accurate positioning vectors when the G0 command is along the same machine track as the previous G0 move (in cases such as machining a donut shape).

Figure A5.6. Second Conditional Statement in the Move rapid command

The third and final conditional statement in the Move rapid command (shown in Figure A5.7) is used to define the G0 commands when switching from one layer to the next and for the homing event at the end of the toolpath. In addition, it also incorporates a special feature that can filter the data and exclude those any zero length (ghost point) vectors from the CLdata files.

		1	2	3	4	5	6	7	8
58		end if							
59		else							
60		Block Number	fff = abs(%p(Cutting...						
61		if (%p(X_link)%==0 & %p(Y_link)%==0)							
62		Block Number	Motion Mode	X	Y	Z	Feed Rate Type	Move Type	'Homing'
63		else if (abs(%p(Rapid_angle_X)%)+abs(%p(Rapid_angle_Y)%)<%p(Hatch_distance)%)							
64		Block Number	'Error'	Motion Mode	X	Y			
65		else							
66		if (%p(X_link_pos_max)%>%p(X_link_pos_min)% & abs(%p(Compare_Y_rapid)%)>0.05)							
67		if (%p(Y_link_pos_max)%>%p(Y_link_pos_min)%)							
68		Block Number	Motion Mode	X_next_rapid = %p(X)%-abs(co...	Y_next_rapid = %p(Y)%-abs(si...				
69		else							
70		Block Number	Motion Mode	X_next_rapid = %p(X)%-abs(co...	Y_next_rapid = %p(Y)%+abs(si...				
71		end if							
72		else if (%p(X_link_pos_max)%<%p(X_link_pos_min)% & abs(%p(Compare_Y_rapid)%)>0.05)							
73		if (%p(Y_link_pos_max)%>%p(Y_link_pos_min)%)							
74		Block Number	Motion Mode	X_next_rapid = %p(X)%+abs(c...	Y_next_rapid = %p(Y)%-abs(si...				
75		else							
76		Block Number	Motion Mode	X_next_rapid = %p(X)%+abs(c...	Y_next_rapid = %p(Y)%+abs(si...				
77		end if							
78		else							
79		Block Number	Motion Mode	X_next_rapid = %p(X)%+abs(c...	Y_next_rapid = %p(Y)%-abs(si...				
80		end if							
81		end if							
82		end if							
83		end if							

Figure A5.7. Third Conditional Statement in the Move rapid command

- **Move Linear command:**

This command outputs the machining moves in the toolpath (G1 moves). In order to effectively offset the positioning vector conditional statements are defined in the body of the command. The length of a positioning vector is determined by subtracting X,Y coordinates of the CUTTING feed rate type (end coordinates of a machining vector) from the X,Y coordinates of the PLUNGE feed rate type (start coordinates of a machining vector), while the orientation of the move vector can be found by taking the atan of machining vector length in y/ machining vector length in x. These important calculations are implemented in the Move linear command of the program as shown in Figure A5.8.

Figure A5.8. Calculation of important conditional parameters in the Move linear command

Four conditional statements are incorporated in the Move linear command building blocks. The first conditional statement is used to filter the data and prevent from outputting 0 length (point) machining vectors. The second and third statements are used when the hatching style is either horizontal or vertical, while the fourth conditional statement is used for any hatching style. Figure A5.9 shows Conditional statements 1,2,3, while Figure A4.10 shows fourth conditional statement.

Figure A5.9 First, Second and Third conditional statements in the Move linear command

22	else if (abs(%p(Cutting angle)%)==(1)*%p(Hatch_angle)%‖abs(%p(Cutting angle)%)==(2)*%p(Hatch_angle)%‖abs(%p(Cutting angle)%)==(3)*%...						
23	if (%p(Compare_X_linear)%<0)						
24	if (%p(Compare_Y_linear)%<0)						
25	Block Number	Motion Mode	X_next_cutting = %p(X)%-abs(co...	Y_next_cutting = %p(Y)%-abs(si...	Z	Feed Rate Type	Move Type
26	else if (%p(Compare_Y_linear)%>0)						
27	Block Number	Motion Mode	X_next_cutting = %p(X)%-abs(co...	Y_next_cutting = %p(Y)%+abs(si...	Z	Feed Rate Type	Move Type
28	end if						
29	else if (%p(Compare_X_linear)%>0)						
30	if (%p(Compare_Y_linear)%<0)						
31	Block Number	Motion Mode	X_next_cutting = %p(X)%+%p(S...	Y_next_cutting = %p(Y)%-abs(si...	Z	Feed Rate Type	Move Type
32	else if (%p(Compare_Y_linear)%>0)						
33	Block Number	Motion Mode	X_next_cutting = %p(X)%+%p(S...	Y_next_cutting = %p(Y)%+abs(si...	Z	Feed Rate Type	Move Type
34	end if						
35	end if						
36	end if						
37	end if						

Figure A5.10. Fourth conditional statement in the Move linear command

APPENDIX 6

INTEGRATION OF THE ADAPTIVE POSTPROCESSOR (CHAPTER 5) IN DELCAM SOFTWARE ''ArtCAM''

This appendix demonstrates the integration of developed stand-alone software tool (the implementation steps of the software are provided in Appendix 4) in ''ArtCAM'' for generating machining code programs for complex laser machining jobs. Figure A6.1 shows the adaptive postprocessor integrated in the ''ArtCAM'' list of machine file formats.
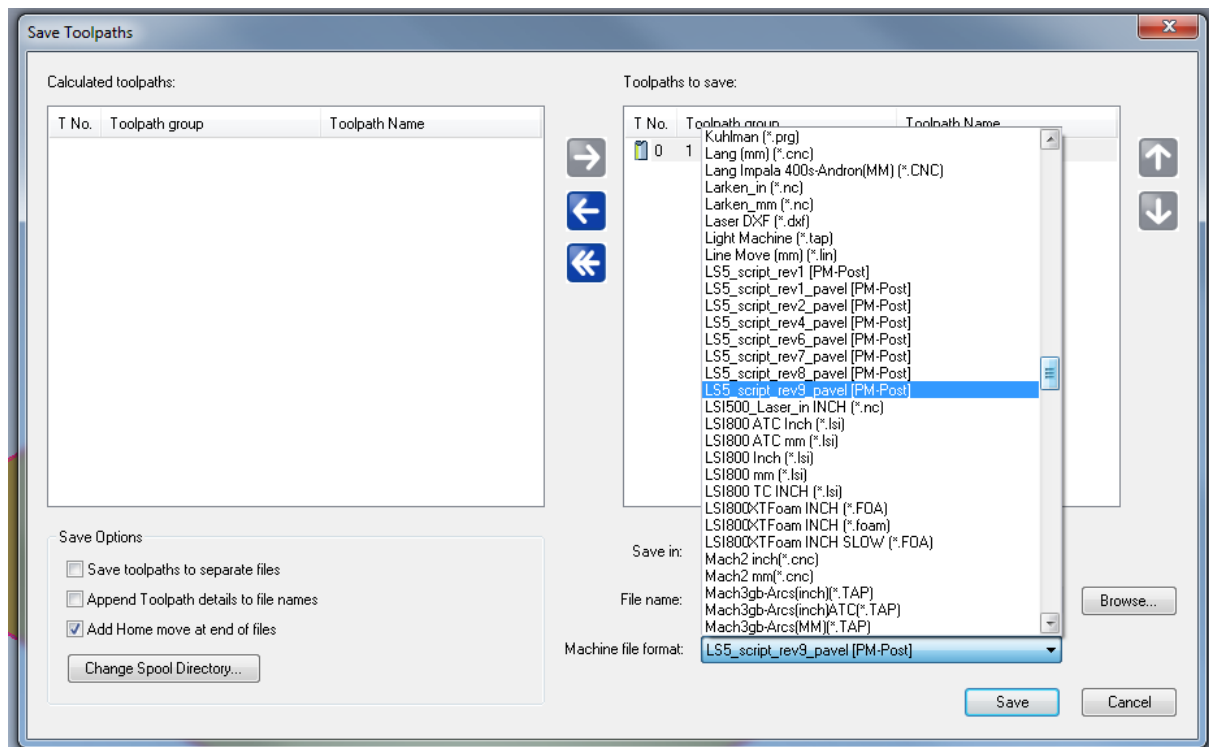
Figure A6.1. The adaptive postprocessor integrated in ''ArtCAM'' list of machine file formats

In order to provide a clear demonstration of the capabilities of the adaptive postprocessor to create machining commands for complex laser machining jobs, an actual machining example is described in details in the following steps below. It should be noted here that in order to provide a clear demonstration of the capabilities of the postprocessor to counteract the negative dynamic effects of the optical beam deflection system and thus to provide

exceptional machining quality and ARR, the maximum processing speed of the integrated scanning system was used in the machining example, in particular 2m/s.

STEP 1: Generating a complex 3D geometrical design

Figure A6.2 shows the generated complex 3D design, which will be used for the machining example. In particular, it incorporates complex geometries and surface textures.
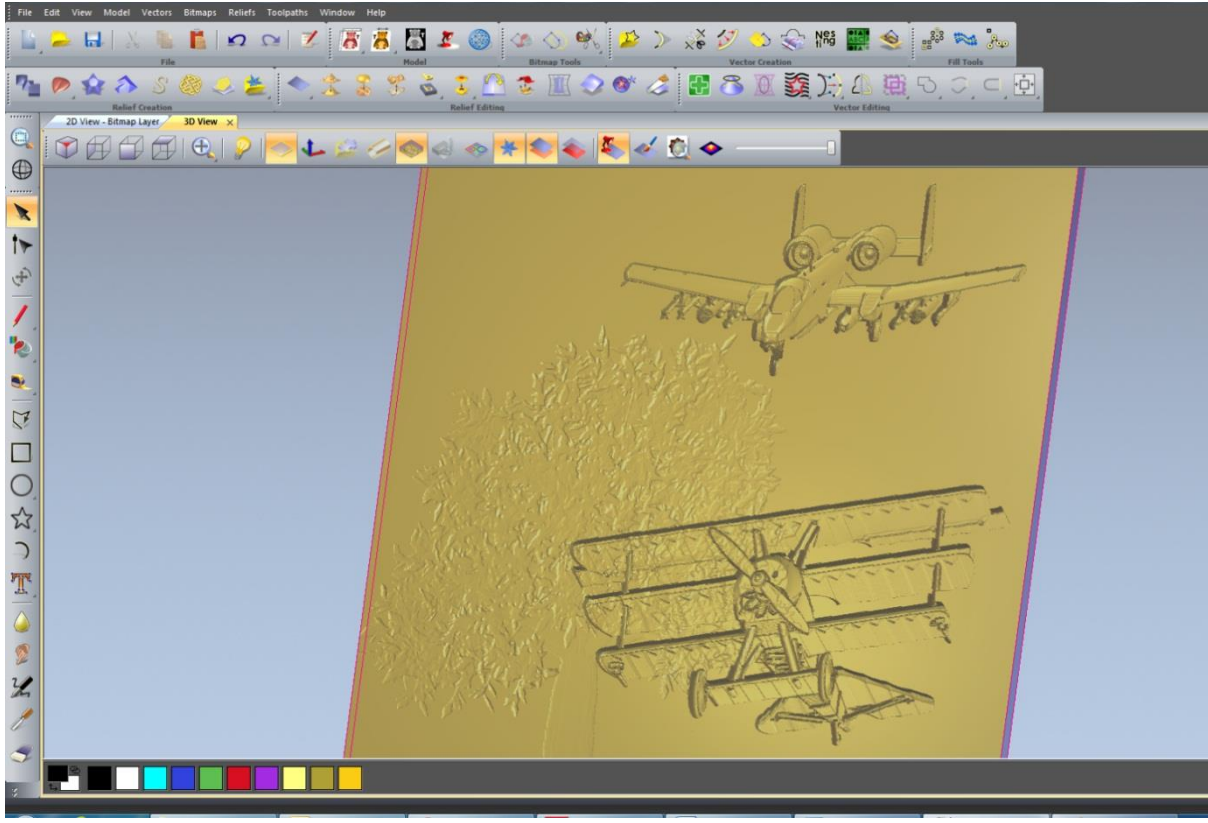
Figure A6.2. Design of the machining example

STEP 2: Generating a laser machining generic toolpath (CL data file)

Figure A6.3 shows the generated generic toolpath (CL data file) that will be processed with the adaptive postprocessor in order to generate machine executable commands program. In particular, the generic toolpath or CL data is represented by the red lines in Figure A6.3.
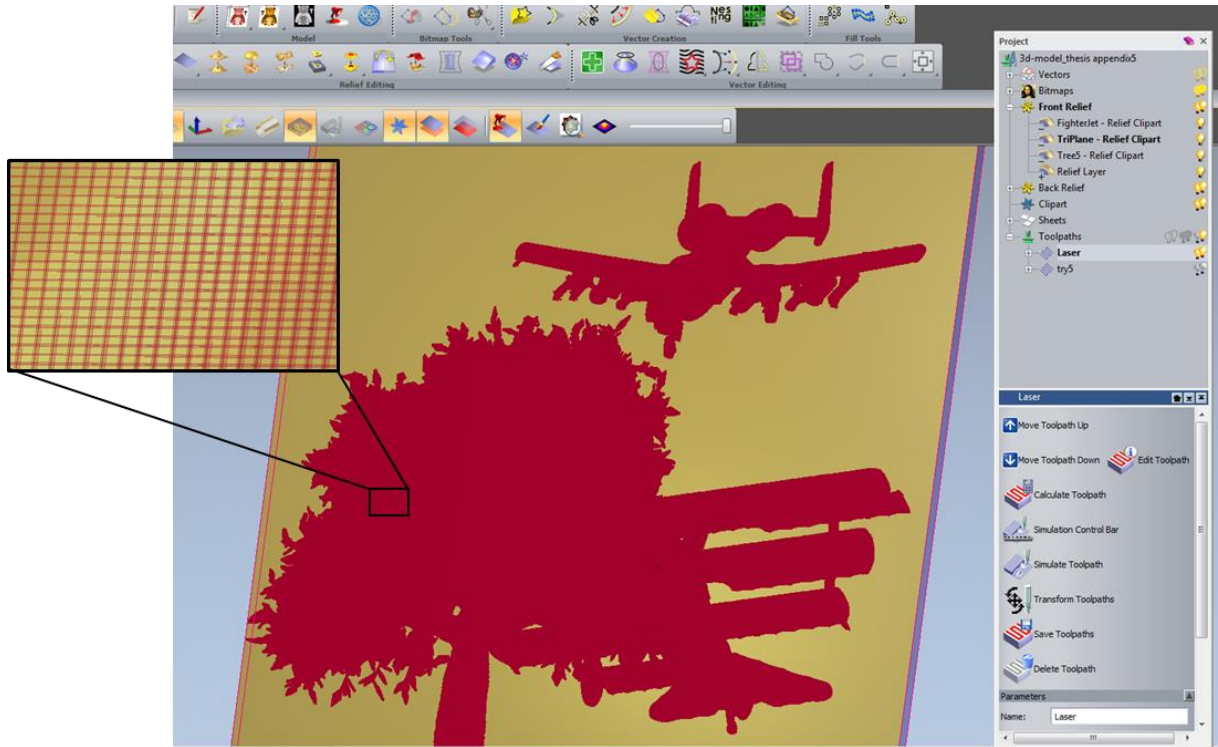
Figure A6.3. Generic toolpath (CL data) represented by the red lines

STEP 3: Utilization of the adaptive postprocessor for generating the machining commands program (G-code file)

Figure A6.4 shows the utilization of the adaptive postprocessor in ''ArtCAM'' for generating the part program G-code file, which will be used for machining the designed complex geometry.
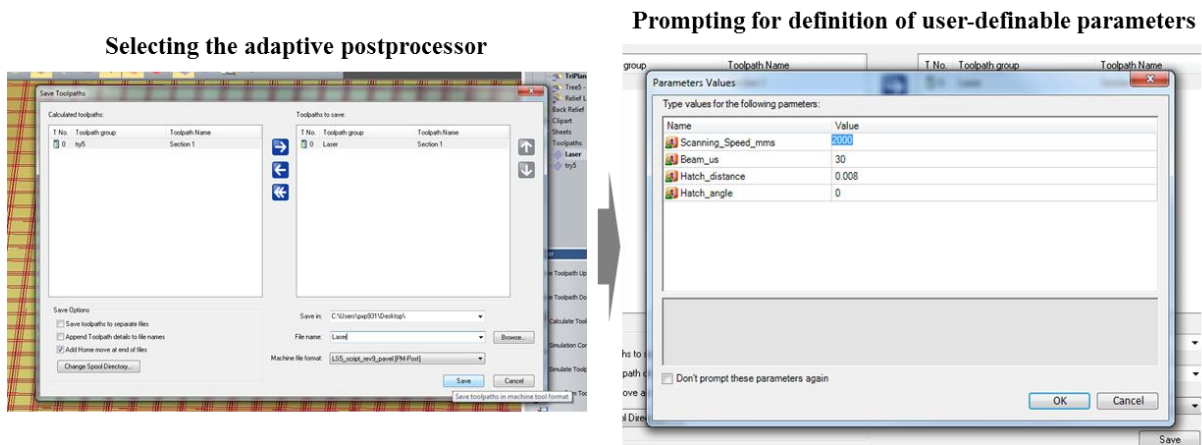
Figure A6.4. Generating the part program G-code file for the machining example

The generated G-code file, which contains all NC commands, is shown in Figure A6.5. Since, the file contained thousands of NC commands, only the begging and end of the G-code file are shown in Figure A6.5.

Begging of NC commands


```
%
0
(pxp931-Pavel Penchev)
(Section 1)
(created on 05/02/2016 at 15:34:33)
Scanning Speed [mm/s] :2000
Beam diameter [us] :30
Scaling factor [mm] :0.356
Machining error [mm]:0.434
Laser on delay [us]:402.5
Laser off delay [us] :31.5
G0 X-10.856 Y-4.753
G0 Z-0.004
G1 X 10.863
G0 X10.863 Y-4.745
G1 X -10.856
G0 X-10.856 Y-4.737
G1 X 10.863
G0 X10.863 Y-4.729
G1 X -10.856
G0 X-10.856 Y-4.721
G1 X 10.863
G0 X10.863 Y-4.713
G1 X -10.856
G0 X-10.856 Y-4.705
G1 X 10.863
G0 X10.863 Y-4.697
G1 X -10.856
G0 X-10.856 Y-4.689
G1 X 10.863
G0 X10.863 Y-4.681
G1 X -10.856
G0 X-10.856 Y-4.673
G1 X 10.863
G0 X10.863 Y-4.665
G1 X -10.856
G0 X-10.856 Y-4.657
G1 X 10.863
G0 X10.863 Y-4.649
G1 X -10.856
G0 X-10.856 Y-4.641
G1 X 10.863
G0 X10.863 Y-4.633
G1 X -10.856
G0 X-10.856 Y-4.625
G1 X 10.863
G0 X10.863 Y-4.617
G1 X -10.856
G0 X-10.856 Y-4.609
G1 X 10.863
G0 X10.863 Y-4.601
G1 X -10.856
G0 X-10.856 Y-4.593
G1 X 10.863
G0 X10.863 Y-4.585
G1 X -10.856
G0 X-10.856 Y-4.577
G1 X 10.863
G0 X10.863 Y-4.569
G1 X -10.856
G0 X-10.856 Y-4.561
G1 X 10.863
G0 X10.863 Y-4.553
G1 X -10.856
G0 X-10.856 Y-4.545
G1 X 10.863
G0 X10.863 Y-4.537
G1 X -10.856
G0 X-10.856 Y-4.529
G1 X 10.863
```

End of NC commands


```
G1 X 10.863
G0 X10.863 Y4.487
G1 X -10.856
G0 X-10.856 Y4.495
G1 X 10.863
G0 X10.863 Y4.503
G1 X -10.856
G0 X-10.856 Y4.511
G1 X 10.863
G0 X10.863 Y4.519
G1 X -10.856
G0 X-10.856 Y4.527
G1 X 10.863
G0 X10.863 Y4.535
G1 X -10.856
G0 X-10.856 Y4.543
G1 X 10.863
G0 X10.863 Y4.551
G1 X -10.856
G0 X-10.856 Y4.559
G1 X 10.863
G0 X10.863 Y4.567
G1 X -10.856
G0 X-10.856 Y4.575
G1 X 10.863
G0 X10.863 Y4.583
G1 X -10.856
G0 X-10.856 Y4.591
G1 X 10.863
G0 X10.863 Y4.599
G1 X -10.856
G0 X-10.856 Y4.607
G1 X 10.863
G0 X10.863 Y4.615
G1 X -10.856
G0 X-10.856 Y4.623
G1 X 10.863
G0 X10.863 Y4.631
G1 X -10.856
G0 X-10.856 Y4.639
G1 X 10.863
G0 X10.863 Y4.647
G1 X -10.856
G0 X-10.856 Y4.655
G1 X 10.863
G0 X10.863 Y4.663
G1 X -10.856
G0 X-10.856 Y4.671
G1 X 10.863
G0 X10.863 Y4.679
G1 X -10.856
G0 X-10.856 Y4.687
G1 X 10.863
G0 X10.863 Y4.695
G1 X -10.856
G0 X-10.856 Y4.703
G1 X 10.863
G0 X10.863 Y4.711
G1 X -10.856
G0 X-10.856 Y4.719
G1 X 10.863
G0 X10.863 Y4.727
G1 X -10.856
G0 X-10.856 Y4.735
G1 X 10.863
G0 X10.863 Y4.743
G1 X -10.856
G0 X-10.856 Y4.751
G1 X 10.863
G0 X0.0 Y0.0
```

G-code program for the part

Figure A6.5. The generated G-code program with the NC commands

STEP 4: Uploading the generated G-code program in the laser system and machining of the designed complex geometry

Following the generation of the G-code program, it is then loaded in the laser system software for performing the laser machining operations (as shown in Figure A6.6).

Loading the generated G-code in the laser system software for executing the laser machining job
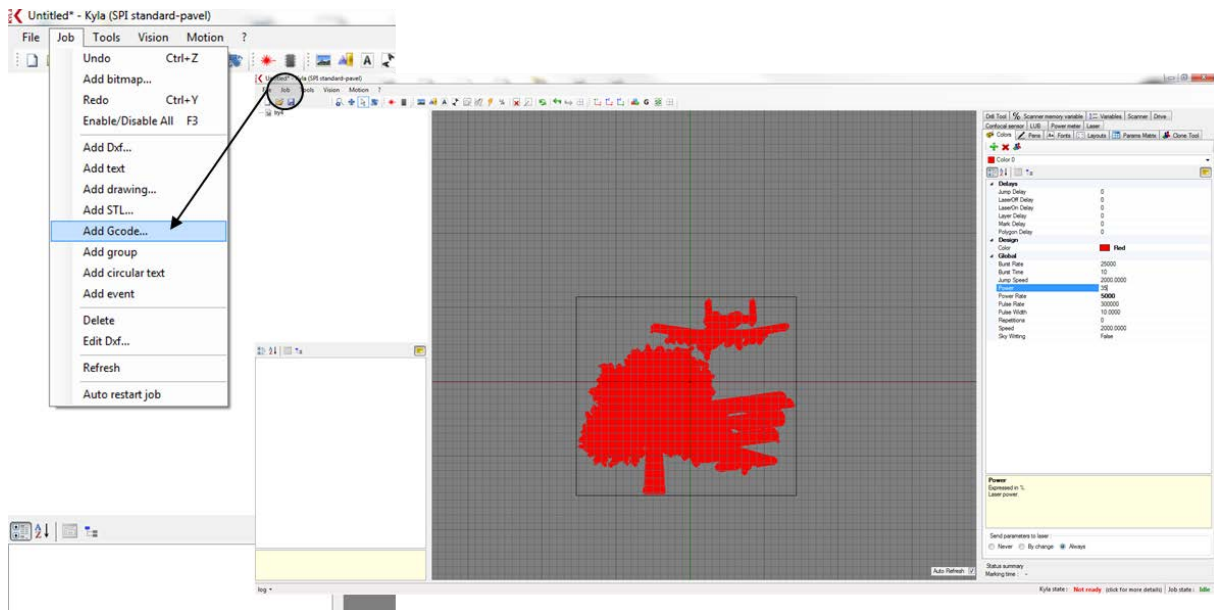
Figure A6.6. Loading of the generated G-code program in the laser system software

Figure A6.7 shows the results of the laser machining operation. In particular Figure A6.7a shows a photograph of the laser machined geometry, while Figure A6.7b shows its pseudo-colour representation. In addition, Figure A6.7c shows a close view of the region identified in Figure A6.7a, where it can be clearly seen that the machining geometry is identical to the designed geometry shown in Figure A6.2 (very high level of processing resolution is achieved and even surface textures with length scale comparable to the laser beam spot diameter (30 μm) are produced as designs) and thus this demonstrates the capabilities of the adaptive postprocessor to enable high speed laser machining without sacrificing machining quality and accuracy. In addition, Figure A6.8 shows more complex 3D geometries that have also been produced as part of the demonstration of the capabilities of the adaptive postprocessor to counteract the dynamic limitations of optical beam deflection system and thus to enable the execution of laser processing operations with the maximum dynamic capabilities of the integrated optical scanning systems without any sacrifices on machining accuracy and quality.
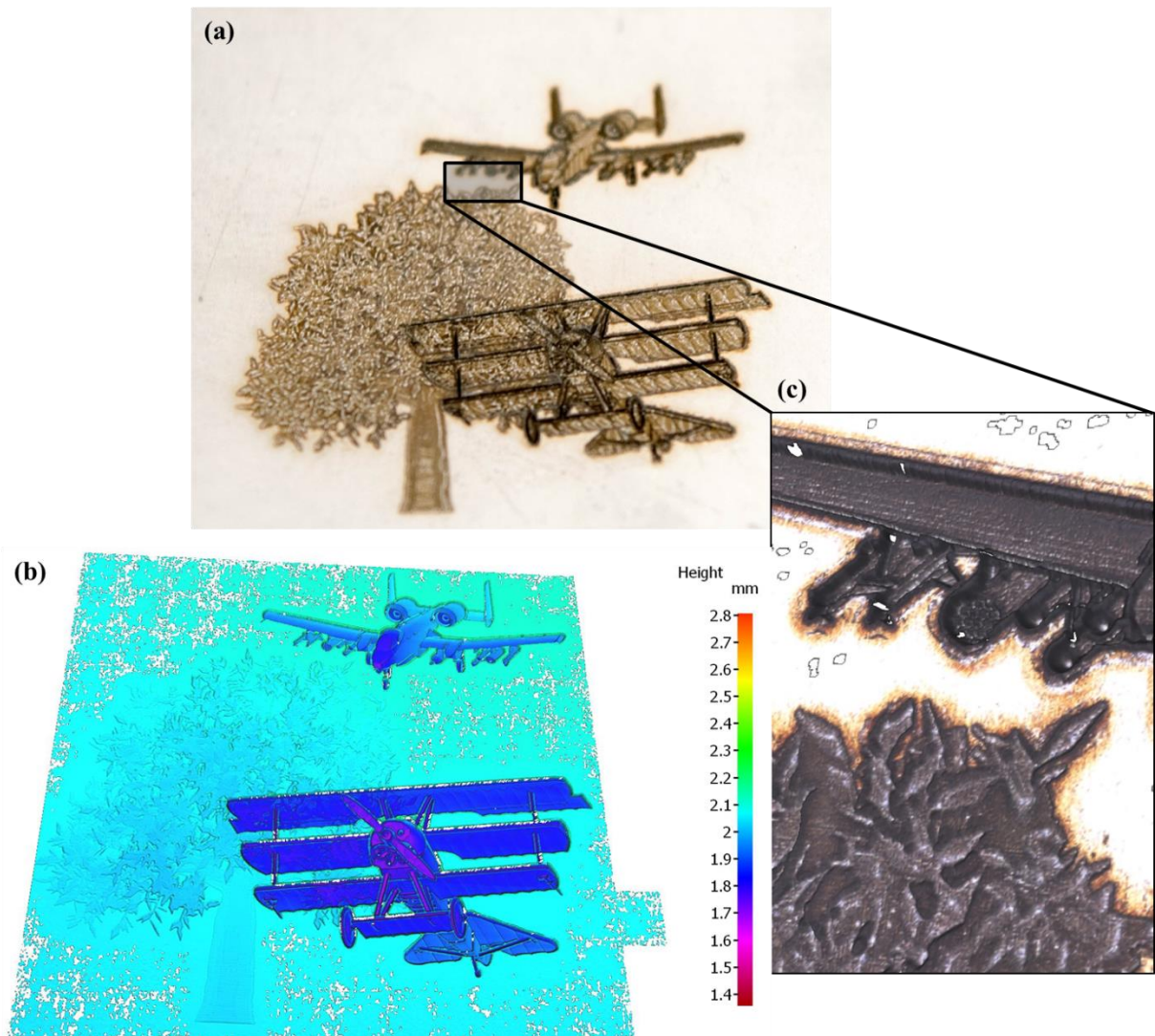
Figure A6.7: (a) A photograph of the laser produced 3D geometry; (b) a close view of the rectangular region identified in (a); (c) a pseudo-colour representation of the laser produced 3D geometry
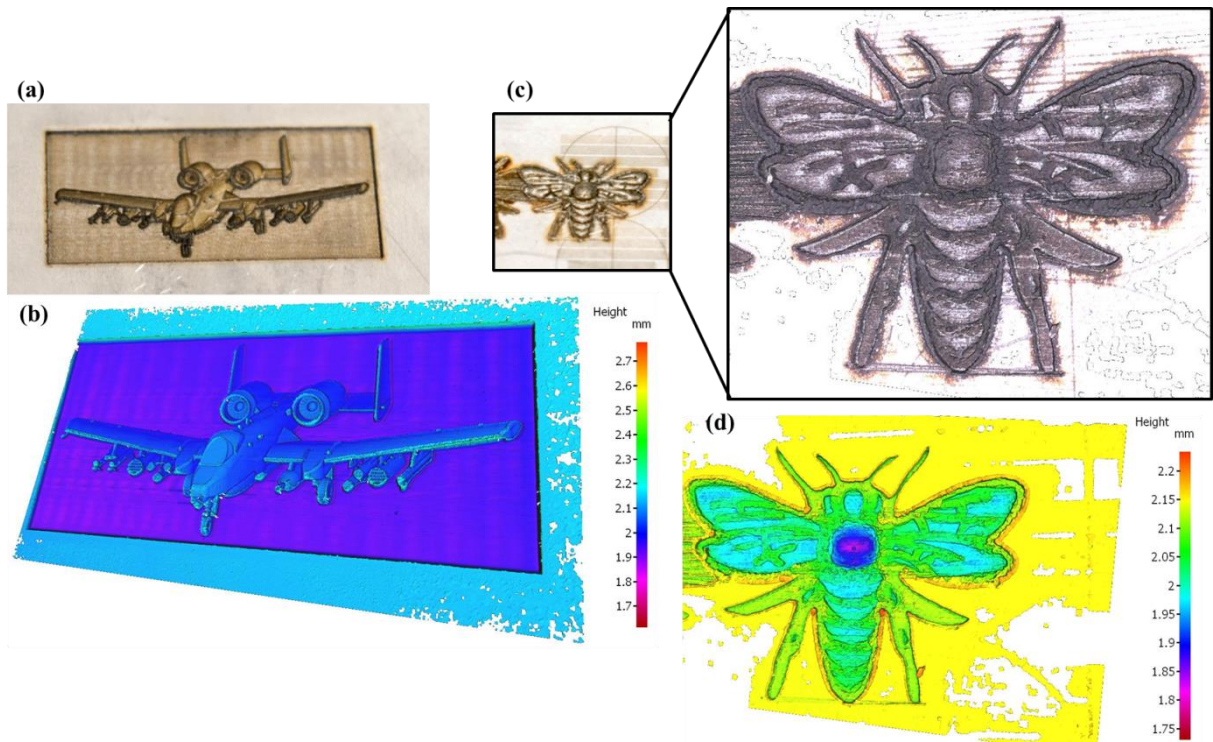
Figure A6.8. More machining examples to demonstrate the capabilities of the adaptive postprocessor: (a) a photograph of a laser produced 3D geometry; (b) a pseudo-colour representation of the laser produced 3D geometry shown in (a); (c) a photograph of a laser produced 3D geometry; (d) a pseudo-colour representation of the laser produced 3D geometry shown in (c)

APPENDIX 7

MEASURMENTS RESULTS FOR THE DIMENSIONAL ACCURACY OF THE PRODUCED W-BAND AND WR3-BAND WAVEGUIDE FILTERS IN CHAPTER 6

WR3-band waveguide filters

A total of 20 WR3-band waveguide filters were produced, some of which are shown in Figure A7.1a. Tables A7.1 to A7.5 summarize the dimensional results from the performed measurements on five produced filters (Figure A7.1b shows the numbering convention for the walls that is used in the Tables).

Figure A7.1. (a) A photograph of some produced WR3-band waveguide filter; (b) a numbering convention for the walls of the waveguide functional feature that is used in the dimensional measurements of the filters

Table A7.1. Dimensional measurements of fabricated WR3-band waveguide 1

Filter Feature	Nominal Dimensions [μm]	Dimensions of Sample 1										
		Actual Dimensional Measurements [μm]										
		Measurements on front filter face					Measurements on back filter face					Average
		1	2	3	4	5	6	7	8	9	10	
Wall 1	1495.0	1497.2	1497.1	1497.5	1497.0	1497.2	1497.4	1497.3	1497.5	1497.6	1497.6	1497.3
Wall 2	864.0	864.5	864.1	864.3	863.8	863.7	864.1	864.2	864.0	864.2	863.9	864.1
Wall 3	60.0	60.5	61.2	61.1	60.2	61.8	62.0	62.1	60.8	61.3	61.7	61.3
Wall 4	571.0	572.5	573.8	573.1	574.5	574.8	575.0	573.8	575.0	572.9	574.5	574.0
Wall 5	648.0	649.5	652.4	654.1	650.3	649.9	652.1	651.5	652.0	651.0	651.2	651.4
Wall 6	473.0	471.5	472.1	469.8	472.5	473.6	469.2	469.1	470.3	469.4	469.8	470.4
Wall 7	257.0	255.1	250.6	251.7	252.4	254.6	251.1	252.7	251.8	253.7	250.9	252.4
Wall 8	864.0	869.1	865.7	864.7	865.2	867.1	866.6	865.1	865.3	867.8	867.5	866.4
Depth	432.0	433.5	440.1	430.2	435.2	432.2	433.9	434.8	436.1	437.5	438.4	435.2

Table A7.2. Dimensional measurements of fabricated WR3-band waveguide 2

Filter Feature	Nominal Dimensions [μm]	Dimensions of Sample 2										
		Actual Dimensional Measurements [μm]										
		Measurements on front filter face					Measurements on back filter face					Average
		1	2	3	4	5	6	7	8	9	10	
Wall 1	1495.0	1496.2	1498.2	1495.3	1499	1492.3	1493.5	1496.6	1498.7	1499.6	1495.6	1496.5
Wall 2	864.0	862.1	863.5	868.1	867.8	863.7	864.8	865.1	862.4	863.9	865.1	865.0
Wall 3	60.0	59.9	58.9	60.9	61.8	62.5	59.9	58.6	61.3	60.6	58.9	60.3
Wall 4	571.0	572.5	571.9	573.8	575.1	576.8	572.6	571.9	572.6	572.6	571.6	573.1
Wall 5	648.0	647.9	649.8	651.6	652.5	651.2	653.2	648.8	650.8	651.2	649.6	650.7
Wall 6	473.0	473.2	477.5	470.6	476.1	469.9	468.8	472.5	468.3	468.1	469.4	471.4
Wall 7	257.0	253.5	254.6	255.8	256.9	252.6	251.9	255.6	251.1	252.6	251.3	253.6
Wall 8	864.0	862.3	863.5	864.7	865.1	865.2	867.5	865.3	867.4	865.6	864.3	865.3
Depth	432.0	438.3	436.8	439.6	432.9	433.5	432.6	437.8	434.5	433.7	438.4	435.8

Table A7.3. Dimensional measurements of fabricated WR3-band waveguide 3

Dimensions of Sample 3

Filter Feature	Nominal Dimensions [μm]	Actual Dimensional Measurements [μm]										Average
		Measurements on front filter face					Measurements on back filter face					
		1	2	3	4	5	6	7	8	9	10	
Wall 1	1495.0	1498.3	1498.6	1492.3	1496.5	1494.8	1498.6	1492.3	1499.5	1498.6	1499.2	1496.9
Wall 2	864.0	866.6	866.2	863.5	865.6	864.4	865.7	866.3	861.1	862.9	861.9	864.4
Wall 3	60.0	62.3	58.6	61.1	61.4	61.9	61.7	59.8	62.7	58.6	58.9	60.7
Wall 4	571.0	576.3	577.8	572.3	575.8	574.9	574.8	572.1	573.6	571.7	571.4	574.1
Wall 5	648.0	654.3	649.3	648.9	653.3	650.6	651.3	649.6	652.3	652.8	648.6	651.1
Wall 6	473.0	472.6	476.9	476.2	469.6	465.3	473.3	469.6	469.7	471.7	468.9	471.4
Wall 7	257.0	255.4	252.3	255.2	250.8	251.7	254.6	256.6	254.8	250.9	251.3	253.4
Wall 8	864.0	864.9	863.1	866.2	866.8	864.9	864.3	867.1	864.3	865.7	867.4	865.5
Depth	432.0	435.8	432.9	432.1	439.8	440.1	436.5	432.9	433.3	435.9	439.7	435.9

Table A7.4. Dimensional measurements of fabricated WR3-band waveguide 4

Dimensions of Sample 4

Filter Feature	Nominal Dimensions [μm]	Actual Dimensional Measurements [μm]										Average
		Measurements on front filter face					Measurements on back filter face					
		1	2	3	4	5	6	7	8	9	10	
Wall 1	1495.0	1499.9	1500.1	1496.9	1495.2	1493.8	1493.6	1498.6	1498.7	1497.9	1496.9	1497.2
Wall 2	864.0	864.7	867.2	862.9	865.8	867.6	867.3	864.2	863.2	862.8	863.4	864.9
Wall 3	60.0	63.1	59.3	62.7	60.5	59.3	62.4	61.9	59.7	59.7	62.6	61.1
Wall 4	571.0	573.9	578.2	572.3	576.3	572.6	576.3	573.2	570.9	571.6	573.4	573.9
Wall 5	648.0	654.2	650.1	652.3	650.9	651.3	651.7	651.4	653.1	652.8	648.6	651.6
Wall 6	473.0	470.5	472.6	469.9	470.9	473.6	472.9	471.8	468.6	470.1	469.3	471.0
Wall 7	257.0	252.9	254.1	255.6	251.9	255.7	252.2	253.7	251.9	250.9	250.6	253.0
Wall 8	864.0	866.2	864.1	867.6	865.4	866.1	865.8	863.9	867.2	867.4	866.7	866.0
Depth	432.0	432.8	433.6	438.7	435.2	437.9	432.4	435.2	437.7	436.9	440.1	436.1

Table A7.5. Dimensional measurements of fabricated WR3-band waveguide 5

Filter Feature	Nominal Dimensions [μm]	Dimensions of Sample 5 — Actual Dimensional Measurements [μm]										Average
		Measurements on front filter face					Measurements on back filter face					
		1	2	3	4	5	6	7	8	9	10	
Wall 1	1495.0	1495.6	1497.7	1496.4	1494.8	1496.5	1497.8	1495.2	1496.8	1494.9	1497.8	1496.4
Wall 2	864.0	864.3	863.7	864.1	864.9	865.9	864.7	862.9	863.1	862.6	862.3	863.9
Wall 3	60.0	62.2	60.3	61.8	59.9	60.8	61.3	60.6	59.6	60.1	58.8	60.5
Wall 4	571.0	573.1	574.8	571.9	575.8	574.9	573.3	572.1	573.6	572.4	571.9	573.4
Wall 5	648.0	652.3	649.8	651.8	651.2	650.7	651.4	650.9	648.9	650.8	651.3	650.9
Wall 6	473.0	471.4	470.9	468.9	472.3	472.9	471.5	470.8	469.1	471.5	473.1	471.2
Wall 7	257.0	250.9	253.1	251.7	254.6	253.6	251.3	254.1	253.8	252.9	255.3	253.1
Wall 8	864.0	865.1	864.9	868.2	864.8	867.2	865.4	864.1	865.3	864.2	867.8	865.7
Depth	432.0	434.8	433.9	438.4	436.3	436.2	435.1	434.5	436.7	433.8	432.9	435.3

W-band waveguide filters

A total of 20 W-band waveguide filters were produced, some of which are shown in Figure A7.2a. Tables A7.6 to A7.10 summarize the dimensional results from the performed measurements on the produced W-band filters (Figure A7.2b shows the numbering convention for the walls that is used in the Tables).
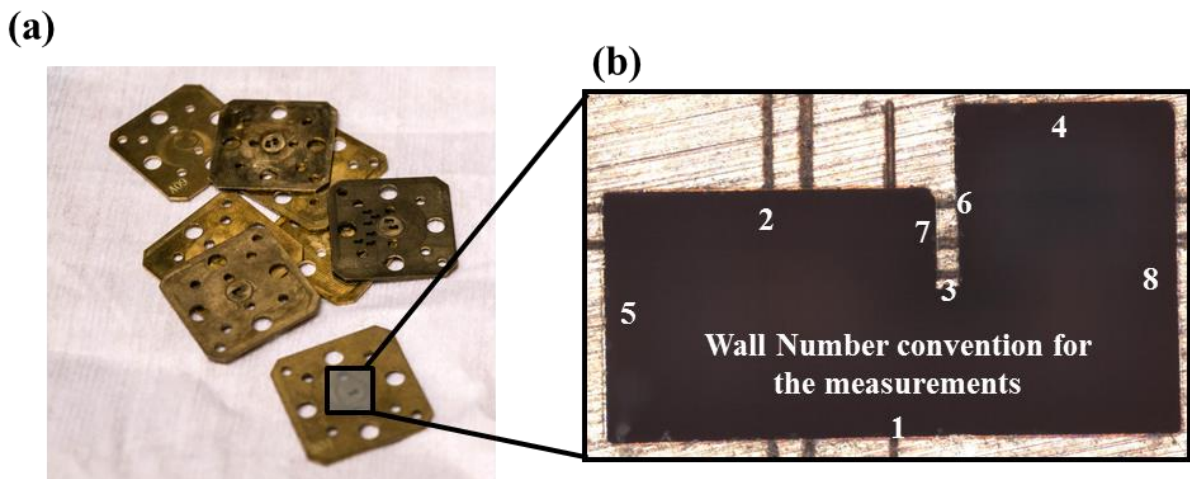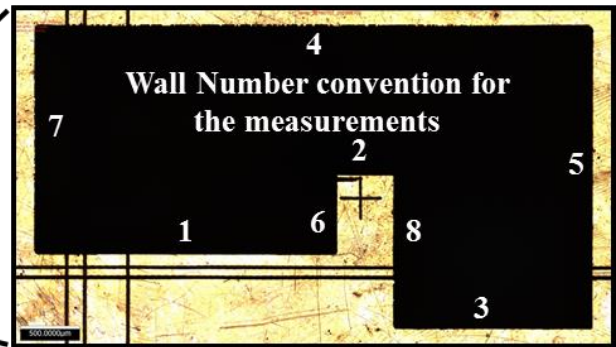

Figure A7.2. (a) A photograph of some produced W-band waveguide filter; (b) a numbering convention for the walls of the waveguide functional features that is used in the dimensional measurements of the filters

Table A7.6. Dimensional measurements of fabricated W-band waveguide 1

		Dimensions of Sample 1										
		Actual Measurements [μm]										
Filter Feature	Nominal Dimensions [μm]	Measurements on front filter face					Measurements on back filter face					Average
		1	2	3	4	5	6	7	8	9	10	
Wall 1	2540.0	2537.8	2537.4	2540.1	2538.5	2541.6	2538.7	2537.2	2537.1	2538.1	2537.6	2538.4
Wall 2	500.0	499.6	498.1	501.6	502.6	500.9	499.8	500.7	502.3	501.9	499.2	500.7
Wall 3	1683.0	1686.8	1685.3	1681.4	1680.9	1684.3	1686.6	1683.1	1684	1683.3	1682.5	1683.8
Wall 4	4723.0	4716.3	4715.7	4713.7	4715.6	4716.5	4717.2	4713.8	4714.1	4715.5	4715.3	4715.4
Wall 5	2540.0	2539.6	2542.3	2541.2	2541.7	2541.8	2542.8	2538.9	2539.9	2541.6	2540.9	2541.1
Wall 6	690.0	694	690.6	690.2	692.1	692.3	693.5	693.7	690.5	693.8	693.2	692.4
Wall 7	1941.0	1939.4	1936.8	1940.8	1938.7	1939.3	1941.2	1940.3	1938.8	1939.6	1939.5	1939.4
Wall 8	1288.0	1285.3	1288.1	1289.8	1284.9	1290.1	1288.6	1289.4	1287.3	1288.1	1289.7	1288.1
Depth	1270.0	1273.1	1271.8	1267.4	1269.1	1270.5	1272.3	1270.9	1271.1	1268.3	1270.2	1270.4

Table A7.7. Dimensional measurements of fabricated W-band waveguide 2

		Dimensions of Sample 2										
		Actual Dimensional Measurements [μm]										
Filter Feature	Nominal Dimensions [μm]	Measurements on front filter face					Measurements on back filter face					Average
		1	2	3	4	5	6	7	8	9	10	
Wall 1	2540.0	2538.1	2539.2	2541.6	2540.3	2541.8	2539.7	2538.9	2539.4	2540.4	2538.7	2539.8
Wall 2	500.0	498.8	501.6	501.7	498.7	502.3	499.7	498.3	501.9	498.4	497.9	499.9
Wall 3	1683.0	1682.4	1685.3	1679.9	1683.4	1684.2	1680.3	1683.3	1684.7	1680.3	1679.9	1682.4
Wall 4	4723.0	4716.8	4720.3	4721.1	4722.2	4716.2	4715.3	4717.6	4718.2	4716.9	4715.4	4718.0
Wall 5	2540.0	2540.9	2543.1	2539.9	2544.4	2544.1	2546.7	2540.7	2541.3	2542.1	2540.8	2542.4
Wall 6	690.0	689.5	690.1	693.7	689.9	691.4	688.9	692.3	692.6	692.4	691.8	691.3
Wall 7	1941.0	1939.6	1938.5	1941.1	1942.3	1939.7	1941.4	1940.9	1941.7	1941.2	1940.6	1940.7
Wall 8	1288.0	1290.3	1289.7	1291.2	1289.9	1291.8	1291.4	1288.9	1290.1	1292.5	1288.6	1290.4
Depth	1270.0	1271.2	1275.1	1276.8	1270.9	1271.1	1273.1	1272.4	1275	1274.3	1272.2	1273.2

Table A7.8. Dimensional measurements of fabricated W-band waveguide 3

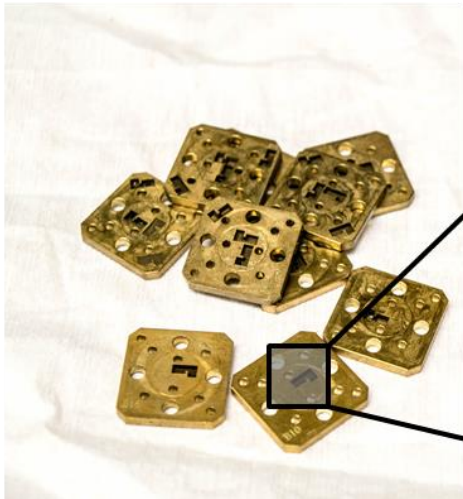| Filter Feature	Nominal Dimensions [μm]	Dimensions of Sample 3 — Actual Dimensional Measurements [μm]										
		Measurements on front filter face					Measurements on back filter face					Average
		1	2	3	4	5	6	7	8	9	10	
Wall 1	2540.0	2540.1	2538.8	2540.6	2540.7	2539.2	2538.9	2539.4	2538.3	2539.1	2538.9	2539.4
Wall 2	500.0	500.2	500.9	499.9	498.7	501.4	500.8	498.5	501.5	502	501.3	500.5
Wall 3	1683.0	1683.5	1687.1	1682.9	1683.8	1684.0	1683.7	1682.8	1681.4	1683.1	1681.5	1683.4
Wall 4	4723.0	4717.4	4718.3	4715.6	4719.8	4716.2	4717.7	4715.3	4715.0	4716.4	4716.8	4716.9
Wall 5	2540.0	2543.6	2541.9	2540.4	2544.7	2546.1	2540.8	2541.7	2542.9	2541.1	2542.1	2542.5
Wall 6	690.0	691.8	690.4	694.7	691.5	693.2	692.7	690.9	691.1	690.6	691.8	691.9
Wall 7	1941.0	1941.5	1943.2	1939.4	1940.0	1938.9	1942.1	1941.7	1939.8	1940.6	1938.7	1940.6
Wall 8	1288.0	1290.7	1289.2	1292.4	1288.7	1288.9	1290.1	1288.6	1290.7	1291.3	1288.5	1289.9
Depth	1270.0	1274.3	1271.6	1270.8	1271.3	1273.5	1272.1	1272.4	1273.9	1271.8	1273.4	1272.5

Table A7.9. Dimensional measurements of fabricated W-band waveguide 4

Filter Feature	Nominal Dimensions [μm]	Dimensions of Sample 4 — Actual Dimensional Measurements [μm]										
		Measurements on front filter face					Measurements on back filter face					Average
		1	2	3	4	5	6	7	8	9	10	
Wall 1	2540.0	2537.9	2540.5	2541.7	2538.8	2538.4	2539.9	2538.1	2539.3	2537.6	2537.4	2539.0
Wall 2	500.0	502.1	501.8	500.7	500.5	501.3	502.2	499.1	501.3	502.4	503.1	501.5
Wall 3	1683.0	1681.4	1684.6	1682.2	1682.9	1685.4	1680.5	1682.5	1681.6	1684.1	1682.2	1682.7
Wall 4	4723.0	4719.8	4718.6	4720.2	4721.5	4719.3	4718.3	4719.3	4718.1	4716.5	4717.1	4718.9
Wall 5	2540.0	2539.9	2541.2	2542.1	2540.8	2542.3	2538.9	2543.1	2538.5	2539.5	2541.7	2540.8
Wall 6	690.0	693.2	689.6	692.8	690.4	693.5	692.8	689.6	693.5	693.2	692.7	692.1
Wall 7	1941.0	1942.5	1940.6	1939.2	1941.5	1939.4	1938.2	1942.3	1942.1	1941.6	1941.7	1940.9
Wall 8	1288.0	1287.3	1288.5	1289.9	1291.4	1292.1	1289.9	1290.7	1291.6	1290.7	1292.4	1290.5
Depth	1270.0	1270.7	1271.4	1272	1273.8	1270.1	1271.6	1274.8	1269.9	1270.7	1271.5	1271.7

Table A7.10. Dimensional measurements of fabricated W-band waveguide 5

Filter Feature	Nominal Dimensions [μm]	Dimensions of Sample 5										
		Actual Dimensional Measurements [μm]										
		Measurements on front filter face					Measurements on back filter face					Average
		1	2	3	4	5	6	7	8	9	10	
Wall 1	2540.0	2541.2	2540.9	2539.9	2538.5	2540.6	2539.4	2541.1	2539.2	2538.1	2539.8	2539.9
Wall 2	500.0	499.6	501.9	501.5	502.2	499.5	503.1	502.7	501.7	502.9	503.5	501.9
Wall 3	1683.0	1680.5	1681.4	1680.9	1682.1	1682.4	1683.5	1681.5	1683.7	1683.5	1681.4	1682.1
Wall 4	4723.0	4721.1	4716.9	4718.8	4719.6	4719.5	4718.2	4717.8	4717.2	4716.8	4717	4718.3
Wall 5	2540.0	2542.7	2542.9	2541.1	2543.9	2540.9	2541.4	2542.5	2541.8	2540.7	2540.5	2541.8
Wall 6	690.0	690.4	692.6	691.5	694.1	694.8	690.2	691.3	690.3	691.1	690.2	691.7
Wall 7	1941.0	1938.8	1940.2	1939.7	1939.6	1941.2	1938.2	1942.1	1939.9	1940.0	1938.8	1939.9
Wall 8	1288.0	1288.9	1291.4	1290.5	1288.7	1287.3	1290.4	1287.8	1288.6	1287.1	1288.3	1288.9
Depth	1270.0	1273.6	1274.1	1270.9	1271	1271.9	1272.4	1272.5	1272.3	1273.5	1273.8	1272.6

REFERENCES

1. Poli C. Manufacturing, design, and design for manufacturing. In: *Design for Manufacturing – A structured approach*, Elsevier Science & Technology Books, 2001, pp. 1-11, IISBN: 0750673419

2. European Comission. Factories of the Future: Multi‑Annual Roadmap for the Contractual PPP under HORIZON 2020. Luxembourg: *Publications Office of the European Union 2013*. ISBN 978-92-79-31238-0.

3. Stieglitz T. Manufacturing, assembling and packaging of miniaturized neural implants. *Microsystem Technologies 2010*; 16:723–734.

4. Lu J-Q. 3-D Hyperintegration and Packaging Technologies for Micro-Nano Systems. *Proceedings of the IEEE 2009*; 97: 18-30.

5. Dubey AK, Yadava V. Laser beam machining—A review. *International Journal of Machine Tools and Manufacture 2008*; 48:609–628.

6. Cheng J et.al. A review of ultrafast laser materials micromachining. *Optics & Laser Technology 2013*; 46: 88–102.

7. Dimov S, Brousseau E, Minev R, et al. Micro- and nano- manufacturing: challenges and opportunities. *Proc IMechE Part C: J Mech Eng Sci 2012*; 226: 3–15.

8. Minev R, Vella P, Brousseau E, Dimov S, Minev E and Matthews C. Methodology for Capability Maturity Assessment of MNT chains. In: *4M conference on multi-material micro manufacture* (ed B Fillon, C Khan-Malek and S Dimov), Bourg en Bresses and Oyonnax, 17-19 November 2010, pp. 249-253. Signpore: Research Publishing Services.

9. El-Hofy H. Nonconventional machining. In: *Fundamentals of machining processes: Conventional and Nonconventional Processes*, USA: Taylor and Francis Group, 2014, pp. 448-459.

10. Chryssolouris G. Overview of machining processes. In: *Laser Machining: Theory and Practice*, New York: Springer Science, 1991, pp. 1-17.

11. Masuzawa T. State of the art of micromachining. *CIRP Annals – Manufacturing Technology 2000*; 49: 473-488.

12. Parandoush P, Hossain A. A review of modeling and simulation of laser beam machining. *International Journal of Machine Tools and Manufacture 2014*; 85: 135-145.

13. Slatineanu L, Coteata M, Besliu I and Dodun O. Thermal Phenomena at the laser beam machining. *Int J Mater Form 2010*; 3:1103 1106.

14. Majumdar J and Manna I. Laser material processing. *International Materials Reviews 2011;* 56 (5–6): 288–341

15. Petkov P. Laser milling: Surface Integrity, Removal strategies and Process accuracy. PhD Thesis, Cardiff University, UK, 2011.

16. Brown M S and Arnold C B. Fundamentals of laser–material interaction and application to multiscale surface modification. In: *Laser Precision Microfabrication*, Berlin: Springer Material Science, 2010, pp. 91-120.

17. Pham DT, Dimov SS, Petkov PV and Dobrev T. Laser milling as a ''rapid'' micromanufactuing process. *Proceedings of the I MECH E Part B: Journal of Engineering Manufacture 2004*; 218(1):1-7.

18. Chichkov BN, Momma C, Nolte S, von Alvensleben, F and Tunnermann A. Femtosecond, picosecond and nanosecond laser ablation of solids. *Applied Physics A 1996*; 63(2): 109–115.

19. Shirk MD and Molian PA. A review of ultrashort pulsed laser ablation of materials. *Journal of Laser Applications 1998*; 10:18-28.

20. Steen W and Mazumder J. Laser ablative processes- Macro- and Micromachining. In: *Laser Material Processing*, New York: Springer, 2010, pp.371-386.

21. Yao YL, Chen H and Zhang W. Time scale effects in laser material removal: a review. *International Journal of Advanced Manufacturing Technology 2005*; 26: 598-608.

22. Bäuerle D.Nanosecond-laser ablation. In: *Laser Processing and Chemistry*, New York: Springer, 2011, pp.235-287.

23. Byskov-Nielsen J, Savolainen J-M, Christensen MS and Balling P. Ultra-short pulse laser ablation of metals: threshold fluence, incubation coefficient and ablation rates. *Applied Physics A 2010*; 101:97-101.

24. Leitza K-H, Redlingshöfera B, Regc Y, Ottoa A, Schmidta M. Metal Ablation with Short and Ultrashort Laser Pulses. *Physics Procedia 2011*; 12: 230–238.

25. Wang DN, Wang Y and Liao CR. Femtosecond laser processing on optical fiber. In: *Laser surface engineering*: Processes and Applications (ed. JR Lawrence and D Waugh), Cambridge: Elsevier, 2015, pp. 359-378.

26. Gamaly EG, Rode AV, Luther-Davies B, and Tikhonchuk VT. Ablation of solids by femtosecond lasers: Ablation mechanism and ablation thresholds for metals and dielectrics. *Physics of Plasmas 2002*; 9: 949-957.

27. Samad R, Machado L, Vieira N and de Rossi W. Ultrashort Laser Pulses Machining. In: *Laser Pulses - Theory, Technology, and Applications* (ed Igor Peshko), InTech, 2012, pp. 143-174.

28. Bloembergen N. A brief history of light breakdown. *Journal of Nonlinear Optical Physics and Materials 1997*; 6: 377–385.

29. Stuart BC, Feit MD, Herman S, Rubenchik AM, Shore BW et al. Nanosecond-to-femtosecond laser-induced breakdown in dielectrics. *Physical Review B 1996*; 53: 1749–1761.

30. Ostendorf A and Konig K. Laser in material nanoprocessing. In: *Optically Induced Nanostructures: Biomedical and Technical Applications*, Berlin: Walter de Gruyter Inc., 2015.

31. Bäuerle D. Ultrashort pulse laser ablation. In: *Laser Processing and Chemistry*, New York: Springer, 2000, pp.259-281.

32. Sugioka K and Cheng Y. Ultrafast lasers—reliable tools for advanced materials processing. *Light: Science & Applications 2014*; 3: 1-12.

33. Sugioka K and Cheng Y. Fundamentals of femtosecond laser processing. In: *Femtosecond Laser 3D Micromachining for Microfluidic and Optofluidic Applications*, New York: Springer, 2014, pp. 19-30.

34. Harzic RL, Huot N, Audouard E, Jonin C, Laporte P and et al. Comparison of heat-affected zones due to nanosecond and femtosecond laser pulses using transmission electronic microscopy. *Applied Physics Letters 2002*; 80: 3886-3888.

35. Overton G, Belforte DA, Nogee A and Holton C. Laser Marketplace 2015: Lasers surround us in the Year of Light, *Laser Focus World magazine*, 2015, http://www.laserfocusworld.com/articles/print/volume-51/issue-01/features/laser-marketplace-2015-lasers-surround-us-in-the-year-of-light.html

36. Mayerhofer R and Geiger S. Status Quo and Perspectives of Laser Micromachining. *Laser Technik Journal 2014*; 11: 30-33.

37. Overton G, Nogee A and Holton C. Laser Marketplace 2014: Lasers forge 21st century innovations, *Laser Focus World magazine*, 2014, http://www.laserfocusworld.com/articles/print/volume-50/issue-01/features/laser-marketplace-2014-lasers-forge-21st-century-innovations.html

38. Belforte DA, 2012 Annual Economic Review and Forecast, *Laser Focus World magazine*, 2013, http://www.industrial-lasers.com/articles/print/volume-28/issue-1/features/2012-annual-economic-review-and-forecast.html

39. Klotzbach U, Lasagni AF, Panzner M and Franke V. Laser Micromachining. In: *Fabrication and Characterization in the Micro-Nano Range* , Berlin: Springer, 2011, pp. 29-46.

40. Zoubir A, Shah I, Richardson K and Richardson M. Practical uses of femtosecond laser micro-materials processing. *Applied Physics A 2003*; 77:311-315.

41. Tünnermann A, Nolte S and Limpert J. Femtosecond vs. Picosecond Laser Material Processing. *Laser Technik Journal 2010*; 7: 34-38.

42. Willenborg E. Polishing with Laser Radiation. In: *Tailored Light 2: Laser Application Technology* (ed. R. Poprawe), Berlin: Springer, 2011, pp. 196-202.

43. Dunn A and et.al. Nanosecond laser texturing for high friction applications. *Optics and Lasers in Engineering 2014*; 62:9-16.

44. Hairaye C, Mermet F, Engel T, Montgomery PC and Fontaine J. Functionalization of surfaces by ultrafast laser micro/nanostructuring. *Journal of Physics: Conference Series 2014*; 558:1-6.

45. Shaoa TM, Huaa M, Tama HY, Cheunga EHM. An approach to modelling of laser polishing of metals. *Surface and Coatings Technology 2005*; 197:77-84.

46. Nüsser C, Wehrmann I and Willenborg E. Influence of Intensity Distribution and Pulse Duration on Laser Micro Polishing. *Physics Procedia 2011*; 12: 462–471.

47. Pfefferkorn FE, Duffie NA, Li X, Vadali M and Ma C. Improving surface finish in pulsed laser micro polishing using thermocapillary flow. *CIRP Annals - Manufacturing Technology 2013*; 62:203-206.

48. Etsion I. Modeling of surface texturing in hydrodynamic lubrication. *Friction 2013*; 1: 195-209.

49. Etsion I and Halperin G. A laser surface textured hydrostatic mechanical seal. *Tribology Transactions 2002*; 45: 430-434.

50. Etsion I and Sher E. Improving fuel efficiency with laser surface textured piston rings. *Tribology International 2009*; 42: 542-547.

51. Ryk G and Etsion I. Testing piston rings with partial laser surface texturing for friction reduction. *Wear 2006*; 261: 792-796.

52. Etsion I. Improving tribological performance of mechanical components by laser surface texturing. *Tribology Letters 2004*; 17: 733-737.

53. Etsion I. State of the art in laser surface textuing. *ASME Journal of Tribology 2005*; 127: 248-253.

54. Kummel J and et.al. Study on micro texturing of uncoated cemented carbide cutting tools for wear improvement and built-up edge stabilisation. *Journal of Materials Processing Technology 2015*; 215: 62-70.

55. Reif J, Costache F, Varlamova O, Jia G, Ratzke M. Self-organized regular surface patterning by pulsed laser ablation. *Phys. Status Solidi C 2009*; 6: 681-686.

56. Bonse J and Kruger J. Pulse number dependence of laser-induced periodic surface structures for femtosecond laser irradiation of silicon. *Journal of Applied Physics 2010*; 108: (034903)1-5.

57. Rohloff M and et.al. Formation of laser-induced periodic surface structures on fused silica upon multiple cross-polarized double-femtosecond-laser-pulse irradiation sequences. *Journal of Applied Physics 2011*; 110: (014910)1-4.

58. Bizi-Bandoki P, Benayoun S, Valette S, Beaugiraud B and Audouard E. Modifications of roughness and wettability properties of metals induced by femtosecond laser treatment. *Applied Surface Science 2011*; 257: 5213-5218.

59. Valette S, Steyer P, Richard L, Forest B, Donnet C and Audouard E. Influence of femtosecond laser marking on the corrosion resistance of stainless steels. *Applied Surface Science 2006*; 252: 4696–4701.

60. Enomoto T and Sugihara T. Improving anti-adhesive properties of cutting tool surfaces by nano-/micro-textures. *CIRP Annals - Manufacturing Technology 2010*; 59: 597-600.

61. Ranella A, Barberoglou MK, Bakogianni S, Fotakis C and Stratakis E. Tuning cell adhesion by controlling the roughness and wettability of 3D micro/nano silicon structures. *Acta Biomaterialia 2010*; 6: 2711-2720.

62. Kohler and et.al. Laser micro-structuring of magnetron-sputtered SnOx thin films as anode material for lithium ion batteries. *Microsyst Technol 2011*; 17:225-232.

63. Vikram V, Iyengar, Barada K, Nayak, Mool C and Gupta. Optical properties of silicon light trapping structures for photovoltaics. *Solar Energy Materials and Solar Cells 2010*; 94:2251-2257.

64. Taylor R, Hnatovsky C and Simova E. Applications of femtosecond laser induced self-organized planar nanocracks inside fused silica glass. *Laser and Photonics Reviews 2008*; 2: 26-46.

65. Doring S and et.al. Hole formation process in ultrashort pulse laser percussion drilling. *Physics Procedia 2013*; 41: 431 – 440.

66. Zhang Y and et.al. Micromachining features of TiCceramic by femtosecond pulsed laser. *Ceramics International 2015*; 41: 6525–6533.

67. Zhao X and Shin YC. Femtosecond laser drilling of high-aspect ratio microchannels in glass. *Appl. Phys. A: Mater. Sci. Process 2011*; 104: 713–719.

68. Kang CL, Xu Y, Yung KL, Chen W and Liu H. Laser drilling on elastomeric polymers. *Advanced Materials Research 2012*; 591: 307-310.

69. Leitz K-H, Redlingshöfer B, Reg Y, Otto A and Schimdt M. Metal Ablation with Short and Ultrashort Laser Pulses. *Physics Procedia 2011*; 12: 230–238.

70. Fornaroli C, Holtkamp J and Gillner A. Laser-beam helical drilling of high quality micro holes. *Physics Procedia 2013*; 41: 661 – 669.

71. Jahns D, Kaszemeikat T, Mueller N, Ashkenasi D, Dietrich R and Eichler HJ. Laser trepanning of stainless steel. *Physics Procedia 2013*; 41: 630 – 635.

72. Huang H, Yang L-M and Liu J. Micro-hole drilling and cutting using femtosecond fiber laser. *Optical Engineering 2014*; 53: (051513) 1-8.

73. Naeem M and Chinn J. Advancement in laser drilling for aerospace gas turbines. *Proceedings of PICALEO*, 2008, pp. 197–202.

74. Hainsey RF, Hooper AE, Swenson EJ and Nashner MS. Recent advances in laser micromachining for semiconductors and microfluidic applications. *Proceedings of ICALEO*,2006, pp.203–212.

75. Gower MC. Industrial applications of laser micromachining. *Optics Express 2000*; 7: 56-67.

76. Ropiak SM. Multiple hole drug delivery balloon. *Patent US5843033 A*, USA, 1998.

77. Ilie M and et. al. Through-transmission laser welding of polymers – temperature field modeling and infrared investigation. *Infrared Physics and Technology 2007*; 51: 73-79.

78. Bag S. Perspective review on laser assisted micro-joining. *Recent Patents on Mechanical Engineering 2011*; 4: 153–167.

79. Tang G. Nanosecond Pulsed Laser Processing of Metals and Welding of Metal-Glass Nanocomposites. *PhD Thesis*, University of Dundee, UK, 2014.

80. Haberstroh E, Hoffmann W-M, Poprawe R and Sari F. Laser transmission joining in microtechnology. *Microsyst Technol 2006*; 12: 632–639.

81. Boglea A, Olowinsky A and Gillner A. Fibre laser welding for packaging of disposable polymeric microfluidic-biochips. *Applied Surface Science 2007*; 254: 1174-1178.

82. Maijer J. Laser beam machining (LBM), state of the art and new opportunities. Journal of *Materials Processing Technology 2004*; 149: 2–17.

83. Rihakova L and Chmelickova H. Laser Micromachining of Glass, Silicon, and Ceramics. *Advances in Materials Science and Engineering 2015*; 2015: (584952) 1-6.

84. Schaeffer R. Laser Theory and Operation. In: *Fundamentals of Laser Micromachining*. USA: Taylor and Francis Group, 2012, pp. 5-31.

85. Matylitksy V, Chui H and Patel R. Spectra-Physics: Ultrashort-PPoliulse Laser Micromachining Advances Implantable Medical Devices. *Biophotonics magazine*, 2014, http://www.photonics.com/Article.aspx?AID=56662

86. Muhammad N, Whitehead D, Boor A, Oppenlander W, Liu Z and Li L. Picosecond laser micromachining of nitinol and platinum–iridium alloy for coronary stent applications. *Applied Physics A 2012*; 106:607–617.

87. Xu L and Knox WH. Lateral gradient index microlenses written in ophthalmic hydrogel polymers by femtosecond laser micromachining. *Optical Materials Express 2011*; 1: 1416-1424.

88. Gittard SD. Light-based Rapid Prototyping of Micro- and Nanoscale Medical Devices for Drug Delivery and Regenerative Medicine. *PhD Thesis*, North Carolina State University, USA, 2011.

89. Oblov K and et.al. Fabrication of Microhotplates Based on Laser Micromachining of Zirconium Oxide. *Physics Procedia 2015*; 72: 485 – 489.

90. Osellame R, Hoekstra H, Cerullo G and Pollnau M. Femtosecond laser microstructuring: an enabling tool for optofluidic lab-on-chips. *Laser Photonics Reviews 2011*; 5: 442–463.

91. Turco SL and et.al. Femtosecond laser micromachining for optofluidic and energy applications. *Optical Materials 2013*; 36: 102-105.

92. Vella PC, Dimov SS, Brousseau E and Whiteside BR. A new process chain for producing bulk metallic glass replication masters with micro- and nano-scale features. *Int J Adv Manuf Technol 2015*; 76:523–543.

93. Scholz SG, Griffiths CA,Dimov SS, Brousseau E, Lalev G and Petkov P. Manufacturing routes for replicating micro and nano surface structures with bio-mimetic applications. *CIRP Journal of Manufacturing Science and Technology 2011*; 4: 347-356.

94. Laser Cheval. An Overview of Laser Micromachining For Industrial Applications. Article in *AZoM*, 2013, http://www.azom.com/article.aspx?ArticleID=8921

95. Joglekar AP and et.al. A study of the deterministic character of optical damage by femtosecond laser pulses and applications to nanomachining. *Applied Physics B 2003*; 77: 25–30.

96. Yu X, Bian Q, Chang Z, Corkum PB and Lei S. Femtosecond laser nanomachining initiated by ultraviolet multiphoton ionization. *Optics Express 2013*; 21: 24185-24190.

97. Lee S. Femtosecond laser nanomachining and applications to micro/nanofluidics for single cell analysis. *PhD Thesis*, University of Michigan, USA, 2008.

98. Ion J. Systems for material processing. In: *Laser processing of engineering materials: Principles*, Procedures and Industrial Application, Oxford: Elsevier's Science and Technology, 2005, pp. 104-139.

99. Qin Y, Brockett A, Ma Y, Razali A, Zhao J, Harrison C, Pan W, Dai X and Loziak D. Micro-manufacturing: research, technology outcomes and development issues. *Int J Adv Manuf Technol 2010*; 47:821–837.

100. Vella P. Micro and nano–manufacturing process chains: maturity assessment and bulk metallic glass enabled manufacturing routes. *PhD thesis*, University of Birmingham, UK, 2015.

101. Pham DT, Dimov SS and Petkov PV. Laser milling of ceramic components. International *Journal of Machine Tools and Manufacture 2007*; 47:618–626.

102. Y. Kwon, T.-L.B. Tseng, Y. Ertekin, Characterization of closed-loop measurement accuracy in precision CNC milling, Robotics and Computer: *Integrated Manufacturing 2006*; 22: 288–296.

103. Chang G, Tu Y. Closed-loop control in ultrafast laser milling process using laser triggered plasma. *International Journal of Machine Tools & Manufacture 2012*; 60: 35–39.

104. Stehr T, Hermsdorf J, Henning T and Kling R. Closed loop control for laser micro spot welding using fast pyrometer systems. *Physics Procedia 2010*; 5: 465–471.

105. Zeng X, Mao XL, Greif R and Russo RE Experimental investigation of ablation efficiency and plasma expansion during femtosecond and nanosecond laser ablation of silicon. *Appl. Phys. A 2005*; 80: 237–241.

106. Zhang Y, Shen Z and Ni X. Modelling and simulation on long pulse laser drilling processing. *International Journal of Heat and Mass Transfer 2014*; 73: 429–437.

107. Venkatesan K, Ramanujam R and Kuppan P. Parametric modelling and optimization of laser scanning parameters during laser assisted machining of Inconel 718. *Optics & Laser Technology 2016*; 78B: 10–18.

108. Williams E and Brousseau EB. Simulation and Experimental Study of Nanosecond Laser Micromachining of Commercially Pure Titanium. *ASME Journal of Micro- and Nano-Manufacturing 2016*; 4:1-9.

109. Aerotech. Integrated Automation Solutions Report: Adavanced control – Position Synchronized Output (PSO), 2013.

110. Mirtchev T, Weeks R, Minko S. Optimizing the feedback control of galvo scanners for laser manufacturing systems. In: *Proceedings of SPIE*: Photonics north. 2010, 77500(T1–T7).

111. Jaeggi B, Neuenschwander B, Hunziker U, Zuercher J, Meier T, Zimmermann M, Selbmann KH and Hennig G. Ultra-high precision surface structuring by synchronizing a galvo scanner with an ultra-short pulsed laser system in MOPA arrangement, In:

Proceedings of SPIE 8243: Laser Applications in Microelectronic and Optoelectronic Manufacturing (LAMOM) XVII. 2012, 82430(K1-K11).

112. Kim K, Yoon K, Suh J and Lee J. Laser Scanner Stage On-The-Fly Method for ultrafast and wide Area Fabrication. *Physics Procedia 2011*; 12: 452–458.

113. Yurevich VI, Grimm VA, Afonyushkin AA, Yudin KV and Gorny SG. Optical design and performance of F-Theta lenses for high-power and high-precision applications. *Proc. SPIE 9626*, Optical Systems Design 2015: Optical Design and Engineering VI.

114. Popov KB, Petkov PV, Layer based micromachining: new approach for tool-path generation. *CIRP Journal of Manufacturing Science and Technology 2011*; 4: 370-375.

115. Pini S, Groppetti R and Senin N. Natural language manual programming for pulsed fiber laser micromachining. *Int J Adv Manuf Technol 2013*; 69:1451–1460.

116. Mutapcic E, Iovenitti P and Hayes JP. A prototyping and microfabrication CAD/CAM tool for the excimer laser micromachining process. *Int J Adv Manuf Technol 2006*; 30: 1076–1083.

117. EU 7th Framework Programme: Call FP7-2011-NMP-ICT-FoF. Minimizing Defects in Micro-Manufacturing Applications (*MIDEMMA*): Project Publishable Summary, 2015, http://www.midemma.eu/

118. Amplitude Systemes, Satsuma HP3 datasheet, 2015, http://www.amplitude-systemes.com/client/document/satsuma_3.pdf

119. Coffey V. Ultrafast and ultrashort: Some recent advances in pulsed lasers. *Optics and Photonic News*, May 2014, pp. 30-35, http://www.osa-opn.org/opn/media/Images/PDF/2014/0514/28-35_PulsedLasers2.pdf?ext=.pdf

120. Arnold C. Ultra-high speed variable focus elements for advance beam delivery. *Industrial Laser Applications Symposium*, 17-18 March 2015, Kenilworth, UK, http://www.ailu.org.uk/assets/document/presentations/15fmmargu17/88.pdf

121. Breit M, Muenzer H. Galvanometer Scanners with Digital PositionSensors Meet Industry's Toughest Challenges. Lasersystems Europe Whitepaper, Feb. 2015, *Europa Science Ltd*, http://www.scanlab.de/en/-/news_events/press/2015_02-LASERSYSTEMS_EUROPE#6713287

122. Aerotech. ADRS Series Stage User's Manual P/N: EDS108 (Revision 1.02.00), 2011.

123. Daemi B. Image analysis for precision metrology: Verification of micromachining systems and aerodynamic surfaces. *PhD Thesis*, KTH Royal Institute of Technology, Sweden, 2014.

124. Helvajian H. 3D Microengineering via Laser Direct-Write Processing Approaches. In: *Direct-Write Technologies for Rapid Prototyping*, San Diego: Academic Press, 2002, pp.415-474.

125. Piqué A, Chrisey DB and Christensen CP. Laser Direct-Write Micromachining. In: *Direct-Write Technologies for Rapid Prototyping*, San Diego: Academic Press, 2002, pp. 385-414.

126. Lasemi A, Xue D and Gu P. Recent development in CNC machining of freeform surfaces: A state-of-the-art review. *Computer-Aided Design 2010*; 42: 641–654.

127. Xu XW and Newman ST. Making CNC machine tools more open, interoperable and intelligent—a review of the technologies. *Computers in Industry 2006*; 57: 141-152.

128. ISO 230-2:2014. Test code for machine tools -- Part 2: Determination of accuracy and repeatability of positioning of numerically controlled axes.

129. Huo D and Cheng K. Design of a 5-axis ultraprecision micro milling machine. *Int. J. Adv. Manuf. Tehchnol. 2009*; 47: 879-890.

130. Park CH, Song CK, Hwang JH and Kim BS. Development of an Ultra Precision Machine Tool for Micromachining on Large Surfaces. *Int. J. Precis. Eng. Manuf. 2009*; 10: 85-91.

131. Scanlab. IntelliSCAN optical scanning heads datasheet, 2015, http://www.scanlab.de/en/products/%E3%82%B9%E3%82%AD%E3%83%A3%E3%83%B3%E3%82%B7%E3%82%B9%E3%83%86%E3%83%A0/intelliscan

132. Camara M, Rubio JCC, Abrao M, Davim JP. State of the Art on Micromilling of Materials, a Review. *J Mater Sci Technol. 2012*; 28:673–685.

133. Razali AR, Qin Y. A Review on Micro-manufacturing, Micro-forming and their Key Issues. *Procedia Engineering 2013*; 53: 665 – 672.

134. Huang SH, Liu P,Mokasdar A and Hou L. Additive manufacturing and its societal impact: a literature review. *Int J Adv Manuf Technol 2013*; 67: 1191–1203.

135. Bigot S, Minev R, Dimov S and Dobrev T. Function and length scale integration in innovative products – technical solutions and new organisational models, *Int. J. Manufacturing Technology and Management 2011*; 23: 157-178.

136. Popov KB, Dimov SS, Pham DT and Ivanov A.New solutions for improving reliability and reducing uncertainty in micro-milling. In: *Proceedings of the 3rd International CIRP High Performance Cutting Conference*, 2008, Dublin, Ireland, pp. 159-168.

137. Quan Z and et.al. Additive manufacturing of multi-directional preforms for composites: opportunities and challenges. *Materials Today 2015*; 18: 503–512.

138. Duflou JR, Callebaut B, Verbert J and De Baerdemaeker H.Laser assisted incremental forming: Formability and accuracy improvement. *CIRP Annals-Manufacturing Technology 2007*; 56: 273-276.

139. Chu WS and et. al. Hybrid Manufacturing in Micro/Nano Scale: A Review, *Int. J.Precis. Eng. Manuf.-Green Tech. 2014*; 1: 75-92.

140. Chavoshi SZ and Luo X. Hybrid micromachining processes: A review. *Precision Engineering 2015*; 41: 1-23.

141. Zhu Z, Dhokia VG, Nassehi A and Newman ST. A Review of Hybrid Manufacturing Processes - State of the Art and Future Perspectives. *International Journal of Computer Integrated Manufacturing 2013*; 26: 596-615.

142. Lauwers B. Surface Integrity in Hybrid Machining Processes. *Procedia Engineering 2011*; 19: 241–251.

143. Lauwers and et.al. Productivity Improvement Through the Application of Hybrid Processes. In: *Advances in Production Technology* (ed. Christian Brecher), Springer, 2015, pp. 101-117.

144. Karunakaran KP, Suryakumar S, Pushpa V and Akula S. Low cost integration of additive and subtractive processes for hybrid layered manufacturing. *Journal of Robotics and Computer-Integrated Manufacturing 2010*; 26: 490-499.

145. Yan J and Tan T-H. Sintered diamond as a hybrid EDM and grinding tool for themicromachining of single-crystal SiC. *CIRP Annals - Manufacturing Technology 2015*; 64: 221–224.

146. Lauwers B and et.al.. Hybrid processes in manufacturing. *CIRP Annals - Manufacturing Technology 2014*; 63: 561–583.

147. Sun S, Brandt M and Dargusch MS. Thermally enhanced machining of hard-to-machine materials—A review. *International Journal of Machine Tools and Manufacture 2010*; 50: 663–680.

148. Schubert A, Gros S, Schulz B and Eckert U. Sequential combination of micro-milling and laser structuring for manufacturing of complex micro-fluidic structures. *Physics Procedia 2011*; 12: 221-229.

149. HaLMMann S, Glockner P, Daniel C, Seyda V and Emmelmann C. Manufacturing of Medical Implants by Combination of Selective Laser Melting and Laser Ablation. *Lasers in Manufacturing and Materials Processing 2015*; 2: 124-134.

150. Li L, Diver C, Atkinson J, Giedl-Wagner R and Helml H J.2007 Sequential laser and EDM micro-drilling for next generation fuel injection nozzle manufacture. *Ann. CIRP 2007*; 55 179–82.

151. Kim S, Kim BH, Chung DK, Shin HS, Chu CN. Hybrid micromachining using a nanosecond pulsed laser and micro EDM.*J Micromech Microeng 2010*; 20:15–37.

152. Zhu Z, Dhokia V, Newman ST and Nassehi A. Application of a hybrid process for high precision manufacture of difficult to machine prismatic parts. *Int J Adv Manuf Technol 2014*; 74:1115–1132.

153. Boivie K, Sorby K, Brotan V and Ystgaard P. Development of a Hybrid Manufacturing Cell: Integration of Additive Manufacturing with CNC Machining, In: *22th Annual International Solid Freeform Fabrication Symposium*, 2011, pp. 153-163.

154. Homar D, Dolinsek S and Boivie K. Optimized manufacturing sequence for hybrid manufacturing. *Journal of Trends in the Development of Machinery and Associated Technology 2012*; 16: 79-82.

155. Bock J, Siegert J, Bauernhansl T and Westkämper E. Interface Requirements and Planning Framework for the Integration of Non-conventional Processes in Production Lines.In: *Leveraging Technology for a Sustainable World* (ed. D. Dornfeld, B. Linke), Springer, 2012, pp.369-373.

156. European Commision. Horizon 2020 Work programme 2016-2017: Cross- Cutting Activities,   2015   ,

https://ec.europa.eu/programmes/horizon2020/sites/horizon2020/files/17.%20CROSS%20CUTTING_2016-2017_pre-publication.pdf

157. The datasheet of redENERGY G4 S-type laser source, SPI Lasers, October 2015, http://www.spilasers.com/Datasheets/redENERGY_G4/S-Type_10W-50W.aspx?#specifications

158. Ball GA, Hull-Allen G and Morey WW. 20-mW single-frequency integrated fiber MOPA with active noise reduction. *Technical Digest OFC 1994*; 4: 22-29.

159. G4 Pulsed Fibre Laser Product Manual- Installation Guide and User Manual, SM-S00245 Rev E, SPI lasers, 2012.

160. Amplitude Systemes, Satsuma HP3 datasheet, 2015, http://www.amplitude-systemes.com/client/document/satsuma_3.pdf

161. Lamb Jr WE. Theory of an optical laser. *Phys. Rev. 1964*; 134 (6A): A1429.

162. Strickland D and Mourou G. Compression of amplified chirped optical pulses. *Optics Communications 1985*; 56: 219-221.

163. Aerotech. PRO165LM Series Stage User's Manual P/N: EDS142 (Revision 1.06.00), 2010.

164. Aerotech. PRO225LM Series Stage User's Manual P/N: EDS143 (Revision 1.01.00), 2010.

165. Aerotech. PRO115LM Series Stage User's Manual P/N: EDS123 (Revision 1.05.00), 2011.

166. Aerotech. ADRS Hardware Manual. P/N: EDS108 (Revision 1.03.00), 2015.

167. Aerotech. High speed and Sub-micron positioning. *Industrial Technology magazine*. http://www.industrialtechnology.co.uk/products--high-speed-sub-micron-positioning.html?thread=No

168. Newson NV. RTA Smart deflector datasheet, A2G_RTA Revision 6.0, 2015, http://www.newson.be/Files/A2G_RTA_060.pdf

169. QiOptiq. Laser material processing brochure, 2013, http://www.qioptiq.com/download/Qioptiq_LaserMaterialProcessing_2013Oct.pdf?inline

170. Throlabs. Nd:YAG Dual Order Laser Mirror (Fundamental and second harmonic) NB1-K13, http://www.thorlabs.de/newgrouppage9.cfm?objectgroup_id=3793

171. Throlabs. Zero-order wave plates, http://www.thorlabs.de/navigation.cfm?guide_ID=2397

172. Special Optics. Variable beam expander 56-302-8x-λ, http://specialoptics.com/products/standard-products/laser-beam-expanders/variable-zoom-beam-expander/

173. BS EN 60825-1 Safety of laser products, Part 1: Equipment classification and requirements.

174. Dino-Lite Digital Microscope. AM7013MT Specifications, http://www.dino-lite.com/products_detail.php?index_m1_id=9&index_m2_id=36&index_id=47

175. Stil SA. CCS Prima - operation and maintenance manual CCS-101-P1 Rev. P, France.

176. Alicona. Alicona Focus Variation magazine: Form and roughness in one system. Edition 5, 2015

177. Semrock. Single edge laser dichroic beam splitter Di02-R1064-25x36, 2015, https://www.semrock.com/FilterDetails.aspx?id=Di02-R1064-25x36

178. Alicona Imaging. IF-Measure Suite manual. Alicona measuring suite manual Version 4.1, 2013.

179. BN ISO 4287/4288. Geometrical Product Specifications (GPS) -- Surface texture: Profile method -- Terms, definitions and surface texture parameters.

180. ISO 1101. Geometrical Product Specifications (GPS)- Geometrical tolerance - Tolerances of form, orientation, location and run-out.

181. Dataray. Scan Slit Beam Profilers User manual REV0805A, 2008,

182. ISO 11146-2:2005.Lasers and laser-related equipment -- Test methods for laser beam widths, divergence angles and beam propagation ratios -- Part 2: General astigmatic beams

183. Meschede D. The Practical Approach to Modern Aspects of Photonics and Laser Physics. *Optics, Light and Lasers 2007*. pp. 46–48. ISBN 3-527-40628-X.

184. Petkov P. Laser milling: surface integrity, removal strategies and process accuracy. *PhD Thesis*, Cardiff University, UK, 2011.

185. Liu JM. Simple technique for measurements of pulsed Gaussian-beam spot sizes. *Opt. Lett. 1982*; 7(5):196.

186. Byskov-Nielsen J. Short-pulse laser ablation of metals: Fundamentals and applications for micro-mechanical interlocking. *PhD Thesis*, University of Aarhus, Denmark, 2010.

187. Nielsen CS and Balling P. Deep drilling of metals with ultrashort laser pulses: A two-stage process. *Journal of Applied Physics 2006;* 99: 093101.

188. ISO, ISO 5725: Accuracy (trueness and precision) of measurement methods and results, ISO, Geneva, 1994.

189. United Kingdom Accreditation Service (UKAS) M3003, The Expression of Uncertainty and Confidence in Measurement, Edition 2, 2007.

190. European co-operation for Accreditation (EA) publication EA-4/02, Expression of the Uncertainty in Measurement and Calibration, 1999.

191. Bell S, National Physical Laboratory Measurement Good Practice Guide No. 11 (Issue 2): A Beginner's Guide to Uncertainty of Measurement, 2001.

192. Siegman A. Defining and measuring laser beam quality. In: *Solid State Lasers: New Developments and Applications* (Eds.: Inguscio M and Wallenstein R). USA: Plenum Press, 1993, pp. 13-29.

193. Scanlab VarioScan brochure.

194. A brochure on Höganäs Digital Metal® 3D Printing Technology.

195. IBS EN 60825-1:1994. Safety of laser products: Equipment classification, requirements and user's guide.

196. Industrial laser solutions for manufacturing. Advanced laser processing systems magazine article, 2010, http://www.industrial-lasers.com/articles/2010/04/advanced-laser_processing.html

197. DMG MORI SEIKI Deutschland GmbH, Design offensive for demanding surface textures in injection moulds, Report, 2015, http://en.dmgmori.com/blob/120168/024215016ecb8aa18301858f9c5f4e09/pl0uk14-lasertec-shape-series-pdf-data.pdf

198. AgieCharmilles, Laser Texturing Solutions, Report, 2013, http://www.gfms.com/content/dam/gfac/proddb/Laser/Laser_EN.pdf

199. Shirinzadeh B. Flexible fixturing for workpiece positioning and constraining. *Assembly Automation 2002*; 22: 112-120.

200. Petkov PV. Development and Implementation of Technology for Laser Micro Structuring of Roller. In: *4M conference on multi-material micro manufacture* (ed B Fillon, C Khan-Malek and S Dimov), Bourg en Bresses and Oyonnax, 17-19 November 2010, pp. 249-253. Signpore: Research Publishing Services.

201. Dausinger F and Sommer S. Ultrafast laser processing: From Micro to Nano scale Industrial applications. In: *Ultrafast Laser Processing* (eds. Sugioka K and Cheng Y). USA: Taylor & Francis Group, 2013, pp.569-586.

202. System 3R. Reference systems for electrode manufacturing & EDMing report, 2012, http://www.system3r.ch/PDF/T-2389-e_edm.pdf

203. Bello SM. New results from the examination of cut-marks using three-dimensional imaging, *Developments In Quaternary Science 2011*; 14: 249-262.

204. Lee N, Joneja A. A methodology to improve manufacturing precision in the presence of workpiece imperfections. *J Manuf Sci and Eng Trans ASEM 1997*; 119(4): 616–622.

205. Carl Zeiss AG. ZEISS Reverse Engineering: From a scan to a model, Product Information brochure, November 2015, http://www.zeiss.co.uk/industrial-metrology/en_gb/products/brochures.html?catalog=reverseengineering.

206. Vijayaraghavan A, Hoover AM, Hartnett J, Dornfeld DA. Improving end milling surface finish by workpiece rotation and adaptive toolpath spacing. *International Journal of Machine Tools and Manufacture 2009*; 49: 89-98.

207. Renishaw, Adaptive machining, 2012, http://resources.renishaw.com/en/details/ap210-productive-process-pattern-adaptive-machining--39412

208. Schwenke H, Knapp W, Haitjema H, Weckenmann A, Schmitt R, Delbressine F. Geometric error measurement and compensation of machines—An update. *CIRP Annals - Manufacturing Technology 2008*; 57: 660–675.

209. Daemi B and Mattson L. Performance evaluation of laser micromachining installations. In: *4M conference on Multi-material micro manufacture* (ed S Azcarate and S Dimov), San Sebastien, Spain, 8-10 October 2013, pp.114-117.

210. Rizvi NH and Apte P. Developments in laser micromachining techniques. *J. Mat. Proc. Tech. 2002*; 127: 206-210.

211. Brousseau E, Barton R, Dimov S and Bigot S. Technology Maturity Assessment of Micro and Nano Manufacturing Processes. In: *4M/ICOMM conference on Micro manufacture* (ed V Saile and S Dimov), Karlsruhe, Germany, 23-25 September 2009, pp. 154-158.

212. Brosens PJ, Scanning speed and accuracy of moving magnet optical scanners. *Opt. Eng. 1995*; 34: 200-207.

213. Wang W, Dong C and Shek C. Bulk metallic glasses. *Material Science and Enginnering R 2004*; 44: 45-89.

214. Dimov S, Pham DT, Ivanov A and et al. Tool-path generation system for micro-electro discharge machining milling. *Proc IMechE Part B:J Engineering Manufacture 2003*; 217: 1633-1637.

215. Nguyen MD, Rahman M, Wong YS. Development of a postprocessing approach for three-dimensional micro-electrical discharge machining milling and application in simultaneous micro-electrical discharge/electrochemical milling. *Proc IMechE Part B:J Engineering Manufacture 2014*; 228: 62-73.

216. ScanLab. Installation and operation manual, The RTC® 5 PC Interface board, February 2014.

217. Engelmayer A. Galvanometer Scanning speeds up laser processing. *Industrial Laser Solutions 2005*.

218. Sabo DA and Engelmayer A. Advantages of digital servos for control optical beam deflection systems. *SPIE Optics and Photonics 2005*.

219. Shang ML, Ke YW, Lancaster MJ. Micromachined WR-3 waveguide filter with embedded bends. *Electronics Letters 2011*; 47: 545-547.

220. Schille J and etc.all. Micro Processing of Metals Using a High Repetition Rate Femtosecond Laser: from Laser Process Parameter Study to Machining Examples. In: *International Congress on Applications of Lasers & Electro-Optics*, Orlando, 23-27 October 2011, pp. 773-782.

221. PD ISO/TR 16907:2015. Machine tools — Numerical compensation of geometric errors.

222. Bohez ELJ. Five-axis milling machine tool kinematic chain design and analysis. *International Journal of Machine Tools and Manufacture 2002*; 42: 505-520.

223. Huang N, Jin Y, Bi Q, Wang Y. Integrated post-processor for 5-axis machine tools with geometric errors compensation. *International Journal of Machine Tools and Manufacture 2015*; 94: 65-73.

224. Shmitt R, MaLMMann G. Process monitoring in laser micromachining. *Manufacturing Technology 2013*, 57-59.

225. Hosako I, Sekine N, Patrashin M, Saito S, Fukunaga K, Kasai Y, Baron P, Seta T, Mendrok J, Ochiai S and Yasuda H. At the dawn of a new era in THz technology. *Proc. IEEE 2007*; 95: 1611–1623.

226. Pawar AY, Sonawane DD, Erande KB, Derle DV. Terahertz technology and its applications, *Drug Invention today 2013*; 5: 157-163.

227. Rostami A, Rasooli H and Baghban H. Terahertz Technology: Fundamentals and Applications. Springer Edition, USA, 2011.

228. X. Yin et al., Terahertz Imaging for Biomedical Applications: Pattern Recognition and Tomographic Reconstruction, DOI 10.1007/978-1-4614-1821-4 2.

229. High Frequency Electronics : Technology Report − Terahertz communications, Imaging and Sensors, February 2008.Pages 38-40.

230. Zhu B, Chen Y, Deng K, Hu W and Yao ZS. Terahertz Science and Technology and Applications, *PIERS Proceedings*, Beijing, China, March 23–27, 2009, pp.1166-1170.

231. Set PK, Mishra PR and Behera S. An Introduction to Terahertz Technology, Its History, Properties and Application. *International conference on computing and communication*, Research Gate Feb 2015

232. Akyildiz IF, Jornet J and Pierobon M. Nanonetworks: a new frontier in communications, *Communications of the ACM 2011*; 54 (11), [doi>10.1145/2018396.2018417]

233. Ajito K and Ueno Y. THz Chemical Imaging for Biological Applications. *IEEE Transactions on Terahertz Science and Technology 2011*; 1(1): 293-300.

234. Shimizu N, Song H-J, Kado Y, Furuta T, Wakatsuki A and Muramoto Y. Special feature: Applied technology for millimetre- Gas Detection Using Terahertz Waves, *NTT Technical Review 2009*; 7(3): 1–5.

235. Danylov AA, Goyette TM, Waldman J, Coulombe MJ, Gatesman AJ, Giles RH, Qian X, Chandrayan N, Vangala S, Termkoa K, Goodhue WD and Nixon WE. Terahertz inverse synthetic aperture radar (ISAR) imaging with a quantum cascade laser transmitter. *Opt. Express 2010*; 18: 16264–72.

236. New tuner could bring terahertz to the masses , June 2012, *Physics World magazine* http://physicsworld.com/cws/article/news/2012/jun/12/new-tuner-could-bring-terahertz-to-the-masses

237. Digital Barriers. Annual Report 2015. Technical Specifications: ThruVision TS4, https://www.digitalbarriers.com/thruvision-ts4/

238. Silicon Radar. Terahertz Imaging, http://www.siliconradar.de/application_2_e.html

239. Flann Microwave Ltd. Product Catlogue: Millimeter & Sub-millimeter Calibration Kits series 704/721/741, 2015, pp.110-115, http://www.flann.com/products/calibration-kits/

240. Woolard DL, Loerop WR and Shur M. Coupling of THz Sensors to Free Space, In: *Terahertz Sensing Technology: Emerging scientific applications and novel device concept*, World Scientific Publishing, UK, 2003, pp.115-134.

241. Li Y, Kirby PL and Papapolymerou J. Silicon micromachined W band folded and straight waveguides using DRIE technique. In: *IEEE MTT-S Int. Microw. Symp. 2006*, pp. 1915–1918.

242. Reck TJ, Jung-Kubiak C, Gill J and Chattopadhyay G. Measurement of silicon micromachined waveguide components at 500–750 GHz. *IEEE Trans. THz Sci. Techn. 2014*; 4(1): 33-38.

243. Liao YS and Chen YT. Precision fabrication of an arrayed micrometal probe by the laser-LIGA process. *J. Micomech. Microeng. 2005*; 15: 2433–2440.

244. Leal-Sevillano CA, Reck TJ, Jung-Kubiak C, Chattopadhyay G, Ruiz-Cruz JA, Montejo-Garai JR and Rebollar JM. Silicon micromachined canonical E-plane and H-plane bandpass filters at the terahertz band. *IEEE Microw. Wireless Compon. Lett. 2013*; 23(6): 288-290.

245. Cullens E, Ranzani L, Vanhille K, Grossman E, Ehsan N and Popovic Z. Micro-fabricated 130–180 GHz frequency scanning waveguide arrays. *IEEE Trans. Antennas Propag. 2012*; 60(8): 3647–3653.

246. Shang X, Ke M, Wang Y and Lancaster MJ. WR-3 band waveguides and filters fabricated using SU8 photoresist micromachining technology. *IEEE Trans. THz Science and Tech. 2012*; 2(6): 629-637.

247. Stanec JR and Barker NS. Fabrication and integration of micro-machined millimeter-wave circuits. *IEEE Microw. and Wireless Component Letters 2011*; 21(8): 409-411.

248. Shang X, Tian Y, Lancaster MJ and Singh S. A SU8 micromachined WR-1.5 band waveguide filter. *IEEE Microw. Wireless Compon. Lett. 2013*; 23(6): 300-302.

249. Lancaster MJ, Zhou J, Ke M, Wang Y and Jiang K. Design and high performance of a micromachined K-band rectangular coaxial cable. *IEEE Trans. Microw. Theory Tech. 2007*; 55: 1548–1553.

250. Lewis SM, Nanni EA and Temkin RJ.Direct Machining of Low-Loss THz Waveguide Components With an RF Choke. *IEEE Microwave and Wireless Components Letters 2014*; 24(12): 842-844.

251. Leal-Sevillano CA, Montejo-Garai JR, Ruiz-Cruz JA and Rebollar JM. Low-Loss Elliptical Response Filter at 100 GHz. *IEEE Microwave and Wireless components Letters 2012*; 22: 459- 461.

252. Liao X, Wan L, Yin Y and Zhang Y. W-band low-loss bandpass filter using rectangular resonant cavities. *IET Microw. Antennas Propag. 2014*; 8(15): 1440-1444.

253. Leal-Sevillano CA, Reck TJ, Chattopadhyay G, Ruiz-Cruz JA, Montejo-Garai JR and Rebollar JM. Development of a wideband compact orthomode transducer for the 180–270 GHz band. *IEEE Trans. THz Sci. Techn. 2014*; 4(5): 634-636.

254. Zhuang JX, Hong W and Hao ZC. Design and analysis of a terahertz bandpass filter.In: *2015 IEEE International Wireless Symposium (IWS*), Shenzhen, China, Mar. 2015, pp.1-4.

255. Popov K, Dimov S, Ivanov A, Pham DT and Gandarias E. New tool-workpiece setting up technology for micro-milling. *Int. J. Advanced Manufacturing Technology 2010*; 47: 21-27.

256. Popov K, Dimov S, Pham DT and Ivanov A. Micromilling strategies for machining thin features. *Proc. Inst. Mechanical Engineers Part C: Journal of Mechanical Engineering Science 2006*; 220: 1677-1784.

257. Leal-Sevillanno CA, Pisano G, Montejo-Garaia JR, Maffei B, Ruiz-Cruzc JA, Ng MW and Rebollar JM. Development of low loss waveguide filters for radio-astronomy applications. *Infrared Physics & Technology 2013*; 61: 224–229.

258. McGeough JA, Leu MC, Rajurkar KP, De Silva AKM and Liu Q. Electroforming process and application to micro/macro manufacturing. *CIRP Ann Manuf Technol 2001*; 50:499–514.

259. Voisiat B, Biciunas A, Kasalynas I and Raciukaitis G. Band-pass filters for THz spectral range fabricated by laser ablation. *Applied Physics A 2011*; 104(3): 953-958.

260. Walker CK, Narayanan G, Knoepfle H, Capara J, Glenn J and Hungerford A. Laser micromachining of silicon: A new technique for fabricating high quality terahertz waveguide components. In: *8th Int. Symp. Space THZ Technol.*, Cambridge, MA, Mar. 1997, pp. 358–376.

261. Millitech, Rectangular waveguide specifications and mil-specification cross reference, http://www.millitech.com/pdfs/recspec.pdf

262. CST Microwave Studio Suite 2015. CST GmbH, Darmstadt, Germany.

263. Butler-Smith PW, Axinte DA and Daine M. Preferentially oriented diamond micro-arrays: A laser patterning technique and preliminary evaluation of their cutting forces and wear characteristics. *Int. J. Machine Tools and Manufac. 2009*; 49: 1175-1184.

264. Pham DT, Dimov SS, Petkov PV, Dobrev T. Laser Milling for Micro–Tooling. *CU IMRC Working Paper Series 2005*, Cardiff University, UK.

265. Webb CE and Jones JDC. *Handbook of Laser Technology and Applications: Applications*, IOP Publishing Ltd. 2005, Bristol, UK, Part D. ISBN: 0 7503 0966 0.

266. Adelmann B and Helmmann R. Rapid micro hole laser drilling in ceramic substrates using single mode fiber laser. *Journal of Material Processing Technology 2015*; 221: 80-86.

267. Zhang Y, Wang Y, Zhang J, Liu Y, Yang X and Zhang Q. Micromachining features of TiC ceramic by femtosecond pulsed laser. *Ceramics International 2015*; 41: 6525-6533.

268. Huang H, Yang LM and Liu J. Micro-hole drilling and cutting using femtosecond fiber laser. *Optical Engineering 2014*; 53: 51513.

269. Vorobyev AY and Guo G. Reflection of femtosecond laser light in multipulse ablation of metals. *Journal of Applied Physics 2011*; 110: 1-9.

270. Schille J, Schneider Luts, Mueller M, Loeschner U, Goddard N, Scully P and Exner H. Highspeed laser micro processing using ultrashort laser pulses. *Journal of Laser Micro/Nanoengineering 2014*; 9: 161-168.

271. Wang SY, Ren Y, Cheng CW, Chen JK and Tzou DY. Micromachining of copper by femtosecond laser pulses. *Applied Surface Science 2013*; 265: 302– 308.

272. Weck A, Crawford TR, Wilkinson DS, Haugen HK and Preston JS. Ripple formation during deep hole drilling in copper with ultrashort laser pulses. *Applied Physics A 2008*; 89: 1001-1003.

273. Byskov-Nielsen J, Savolainen J-M, Christensen MS and Balling P. Ultra-short pulse laser ablation of metals: threshold fluence, incubation coefficient and ablation rates. *Applied Physics A 2010*; 101: 97-101.

274. Petkov PV, Dimov SS, Minev RM and Pham DT. Laser milling: Pulse duration effects on surface integrity. *Proc. of the I MECH E Part B. Journal of Engineering Manufacture 2008*; 222: 35–45.

275. Di Noso F, Gaudiuso C, Sibillano T, Mezzapesa FP, Ancona A and Lugara PM. Role of heat accumulation on the incubation effect in multi-shot laser ablation of stainless steel at high repetition rates. *Optic Express 2014*; 22: 12200-12210.

276. Schille J. Investigation of micromachining using a high repetition rate femtosecond fibre laser. PhD Thesis, The University of Manchester, Manchester, UK, 2013.

277. Kraus M, Ahmed MA, Michalowski A, Voss A, Weber R and Graf T. Microdrilling in steel using ultrashort pulsed laser beams with radial and azimuthal polarization. *Optics Express 2010*; 18: 22305-22313.

278. Liao X, Wan L, Yin Y and Zhang Y. W-band low-loss bandpass filter using rectangular resonant cavities. *IET Microw. Antennas Propag. 2014*; 8: 1440–1444.

279. Li Y, Kirby PL and Papapolymerou J. Silicon Micromachined W-Band Bandpass Filter Using DRIE Technique. In: *Proceedings of the 36th European Microwave Conference*, 2006, Manchester, UK, pp. 1271-1273.

280. Leal-Sevillano CA, Montejo-Garai JR, Ke M, Lancaster MJ, Ruiz-Cruz JA and Rebollar JM. Pseudo-Elliptical Response Filter at W-Band FabricatedWith Thick SU-8 Photo-Resist Technology. *IEEE Microw. Wireless Compon. Lett., 2012*; 22: 105–107.

281. Millitech, Products Catalogue: Passive waveguide components, 2014, pp.33-39, http://www.millitech.com/pdfs/catalog.pdf